Folded Waveguide Resonator Filter for Communication and Radar Systems

Sultan K. Alotaibi

A dissertation submitted for the degree of Doctor of Philosophy

Heriot-Watt University

School of Engineering and Physical Sciences

April 2009

Abstract

In this thesis, a primary investigation into developing a compact and low-loss bandpass filter, using novel folded waveguide resonators with a footprint reduction, has been addressed. A slot coupling between adjacent resonators is introduced, which is characterized by using full-wave EM simulations and verified experimentally. Two designs of 2-pole folded waveguide resonator filters of this type have been considered, fabricated and tested. In this thesis, an even more compact FWG resonator filter using a novel slot technique is reported. The attainable size reduction is about 50%, and the filter design is based on theoretical and full-wave electromagnetic (EM) simulations.

Based on FWG structure, two types of folded waveguide resonators have been studied and considered the half-wavelength resonator and the quarter-wavelength resonator. Moreover, both structures for the realization of microwave cavities with high-Q, with the result of a high spurious free range and reduced footprint, have been evaluated. Furthermore, a novel folded waveguide resonator with about a 75 % reduction of the volume from the conventional size has been described. For comparison, two types of folded waveguide resonators have been studied, i.e. the quarter-wavelength resonator of square shape and the newly proposed triangular shape. In addition, a demonstration of a filter application for miniature triangular folded waveguide resonators has been designed and simulated using an EM simulator.

In addition, numbers of experiments have been conducted to develop cavity FWG and Substrate Integrated folded waveguide SIFW resonator filters using a folded structure, which is the main aim of this thesis. Furthermore, this thesis deals with the simulation and implementation for many designs and topologies of FWG and SIFW resonator filters and their frequency response. Simulation and experimental results were presented to validate the design and to show the advantages of these types of filters. In addition, a new type of filter with a compact multi-layer structure and low loss is attractive for implementation with advanced device technologies, such as micromachining, LTCC and LCP technologies.

Dedication

To

My father Khalid for his love, encouragement and patience.

My mother, Mariam, for her love, support and sacrifice. She continues to be a source of inspiration to me throughout my life.

My sisters and brothers, who are always there to offer a moment of clarity.

&

I must keep special thanks for my wife Badriah and my children Moath, Omar and Maraim for their support and unconditional love, without which I would never have completed this work.

Acknowledgements

I would like to express my gratitude for the guidance provided by my supervisor *Dr Jia-Sheng Hong* and for his excellent supervision, concern and endless support from the first day. He has always been a great source of encouragement. Throughout my doctoral work, he has kept me motivated and given me guidance to develop my research skills.

I would also like to thank *Dr. Young-Hoon Chun* who gave assistance in compiling the test set-up with instructions on the operation of the equipment.

Special thanks go to *Dr. Farid Almalol, Dr. Srikanth Lavu, Dr. Hazem Fayad* and all the Microwave Research Group at Heriot-Watt University for their support, encouragement and assistance along the way.

I would like to extend my gratitude to the mechanical workshop staff, who have been prompt in helping me with my PhD. Thanks are also due to all friends who have encouraged me during my studying, and special thanks are given to *Dr. Fasial AL-Shrif, Dr. Abdullrahman Bagais, Dr. Abdullrahman Alghamdi* who assisted and supported me along the way.

I am grateful for the funding provided for my studies by the Saudi Interior Ministry, represented by the Border Guard, as well as the support from Heriot-Watt University.

Most of all, I thank ALLAH for giving me everything.

Sultan K. AL-otaibi.

ACADEMIC REGISTRY

Research Thesis Submission

Name*:*	**Sultan K. Alotaibi**		
School/PGI:	**School of Engineering and Physical Sciences/Electrical Electronics and Computer Department**		
Version: *(i.e. First, Resubmission, Final)*	**Final**	Degree Sought:	**PhD**

Declaration

In accordance with the appropriate regulations I hereby submit my thesis and I declare that:

1) the thesis embodies the results of my own work and has been composed by myself
2) where appropriate, I have made acknowledgement of the work of others and have made reference to work carried out in collaboration with other persons
3) the thesis is the correct version of the thesis for submission and is the same version as any electronic versions submitted*.
4) my thesis for the award referred to, deposited in the Heriot-Watt University Library, should be made available for loan or photocopying and be available via the Institutional Repository, subject to such conditions as the Librarian may require
5) I understand that as a student of the University I am required to abide by the Regulations of the University and to conform to its discipline.

* *Please note that it is the responsibility of the candidate to ensure that the correct version of the thesis is submitted.*

Signature of Candidate*:*		Date:	

Submission

Submitted By *(name in capitals):*	

Signature of Individual Submitting:	
Date Submitted:	

For Completion in Academic Registry

Received in the Academic Registry by *(name in capitals):*			
1.1 Method of Submission *(Handed in to Academic Registry; posted through internal/external mail):*			
1.2 E-thesis Submitted			
Signature:		Date:	

Table of Contents

Lists of Figures

Lists of Tables

Glossary

dB	Decibel
W	Width of coupling gab wall
G	Coupling gab length
G2	Coupling gab length between the second and third resonators.
G1	Coupling gab length between the first and the second resonators.
A	Area.
f_0	Resonant Frequency
F_1	First cut-off frequency
F_2	Second cut-off frequency
K	Coupling coefficient
K_{12}	Coupling coefficient between resonators 1 and 2
K_{23}	Coupling coefficient between resonators 2 and 3
K_{34}	Coupling coefficient between resonators 3 and 4
λ_γ	Guide wavelength
λ	Wavelength
Q	Quality factor.
Q_e	External quality factor.
σ	Conductivity (Sm^{-1})
DR	Dielectric Resonator
MHz	Mega Hertz (10^6 Hz)
GHz	Gega Hertz (10^9 Hz)
d	distance
C	Cutting from the separation plate corner
C_1	Cutting from left corner of the separation plate

C_2	Cutting from right corner of the separation plate
L_1	Position of the input port
L_2	Position of the output port
g	Conductance
FBW	Fractional band width
R	Resistance
c	Capacitance
L	Inductance
mm	millimetre
I/O ports	Input/Output ports

List of Publications by the Candidate

During the period of study for his PhD, the author received the 2nd year prize (for students who have completed approximately 2 years of study). This prize is awarded to those who have made excellent progress in their research; judging criteria include: quality, originality, quantity, awareness of wider literature, and visibility (e.g. publications, talks). Moreover, he is a reviewer of journal and conferences. In addition, paper no 10 in the following list has been **chosen as an IMS 2008 Student Paper Competition Finalist**. Furthermore, he has written 12 research papers:

1- **Al-otaibi, S**. and J. -S. Hong, "Novel coupled folded waveguide resonator filter", Microwave and Optical Technology Letters, Volume 48, Issue 9 , (2006) pp.1846-1850. **(Journal)**

2- **Al-otaibi, S.** and J. -S. Hong, "Folded-Waveguide Resonator Filter With Asymmetric Frequency Response", in 36th European Microwave Conference Proceedings, Manchester, 2006, pp. 646-648.

3- **S. Alotaibi** and J. -S. Hong, "Electromagnetic design of folded-waveguide resonator filter with single finite-frequency transmission zero," INTERNATIONAL JOURNAL OF RF AND MICROWAVE COMPUTER AIDED ENGINEERING, vol. 18, pp. 1, 2008. **(Journal)**

4- **S. K. Alotaibi** and J. -S. Hong, "Miniature folded waveguide resonators," presented at Microwave Conference, 2007. European, 2007.

5- **S. K. Alotaibi** and J. -S. Hong, "DESIGN METHODOLOGY OF ELECTROMAGNETIC COUPLED FOLDED-WAVEGUIDE RESONATOR FILTER," Published at Saudi Innovation Conference SIC proceeding , 2007. Newcastle, May 2007.

6- **S. K. Alotaibi** and J. -S. Hong, "Novel Folded Waveguide Resonator Filter Using Slot Technique," *Microwave and Wireless Components Letters, IEEE*, vol. 18, pp. 182-184, 2008. **(Journal)**

7- **Sultan K. Alotaibi** and J.-S. Hong, "Novel substrate integrated folded waveguide filter," *Microwave and Optical Technology Letters*, vol. 50, pp. 1111-1114, 2008, **(Journal)**

8- **S. K. Alotaibi** and J. -S. Hong, " Substrate Integrated Folded-Waveguide Filter with Asymmetrical Frequency Response," Accepted to be published at the 38th European Microwave Conference proceeding in 2008, sponsored by IEEE.

9- Z. Hao, J. -S. Hong, and **S. K. Alotaibi**, " A novel Ultra Wideband Bandpass Filter using Broadside Coupled Structures on Multilayer Organic Liquid Crystal Polymer Substrate," Accepted to be published at the 38th European Microwave Conference proceeding in 2008, sponsored by IEEE.

10- **S. K. Alotaibi**, J. -S. Hong and Zhang-Cheng Hao, " Multilayer Folded-Waveguide Dual-Band Filter," Published at The IEEE MTT-S International Microwave Symposium 2008 (IMS2008) in the USA.

11- **S. K. Alotaibi** and J. -S. Hong, "Substrate Integrated Folded-Waveguide Filter with Asymmetrical Frequency Response," Publish at Saudi Innovation Conference proceeding SIIC, 2008. Leeds, June 2008.

12 - Zhang-Cheng Hao, Jia-Sheng Hong, **Sultan K. Alotaibi**, Jonathan P. Parry, and Duncan Hand " Ultra-Wideband Bandpass Filter with Multi Notch-Bands on Multilayer Liquid Crystal Polymer Substrate," Accepted to be published at the IET Microwave & AP journal. **(Journal).**

Chapter 1

Introduction and Thesis Outline

1.1 Motivations

Cavity resonator filters of various types are essential components in wireless communication and radar systems. These filters are used to separate and combine, or select and reject, signals from RF/Microwave systems and applications. Increasing consumer demand for convenience and flexibility, miniaturisation and a small footprint with low cost have had a significant impact on the development of a new cavity resonator filter. For many applications, such as multipole and multilayer filters, it would be desirable to reduce the footprint of this type of resonator because the height of the micromachined cavity is usually quite small.

Thus, the microwave engineering community has recently increased interest in exploring the development of cavity resonators. However, there are several challenges that a filter designer may face. The most challenging is that it is still large in size, particularly its footprint as compared with that of microstrip resonators. For this purpose, several topologies of folded waveguide FWG resonators have been introduced and investigated in this thesis. The development of the so-called folded waveguide (FWG) resonator has been reported in [1], which stems from the concept of folding standing waves of a conventional TE_{101} mode waveguide resonator. The cavity folded waveguide FWG resonator is a metallic enclosure that confines the electromagnetic energy. The stored electrical and magnetic energies inside the cavity determine its equivalent inductance and capacitance. The energy dissipated by the finite conductivity of the cavity walls determines its equivalent resistance. In order to reach the point where investigation is feasible, a fast and accurate simulation tool for the structures under investigation is required. Hence, a major initial objective of this work is to deal with the design, simulation and fabrication of a folded waveguide FWG resonator filter.

1.2 Aims and Objective

The aim is to develop a cavity resonator for the design of RF/microwave filters, which can be found in wide applications in wireless communication, radar and other RF/microwave systems. Furthermore is to design technique for a "cavity folded waveguide FWG resonator filter" in microwave filter applications and assemble the required resonator for the given specifications. In order to reach the aim, a cavity folded waveguide resonator that was introduced by J. S Hong [1, 2] for X-band applications has been used for development. In this thesis, numbers of designs and topologies for a folded waveguide FWG resonator filter with high Q and low losses are characterised for filter application. This thesis is constructed around the following objectives:

- To reduce the footprint of the cavity resonator, since the height of the micromachined cavity is usually quite small, with a quality factor similar to that of the conventional design.

- To propose a topology for cavity and substrate resonator filter.

- To propose improvement configurations by exploring the advantages and developing a compact dual passband filter using folded-waveguide resonators with a multilayer structure.

- A Substrate Integrated folded waveguide SIFW resonator filter using a folded structure has been addressed in this thesis to be designed using the same structure of the FWG.

1.3 Thesis structure guide

This thesis is divided into eight chapters. These chapters give the reader a background to the history of the microwave filter, resonators, resonator types, folded waveguide resonator filters, cavity filters, substrate integrated filters, coupling structure and the design method of the microwave filter.

Chapter 1 is a brief introduction about the motivation of the project, the aims and objectives, and the thesis outline.

Chapter 2 presents an overview of the microwave filter's history. It introduces the basic concepts of resonators, resonator types, and the advantages of cavity resonators, applications, drawbacks, and geometries. The fundamental filter parameters present an overview of what should be taken into consideration when building a folded waveguide FWG resonator filter. The second section of this chapter covers a review of some articles which show the benefits of using a cavity resonator.

Chapter 3 The design methods of a filter are covered in this chapter.

Chapter 4 is where the main contribution of the research and the proposed model is to be found. In this chapter, we will be concerned with the design of the implementation of a folded waveguide FWG resonator. Moreover, in this chapter a novel folded waveguide resonator with about a 75 % reduction of the volume from the conventional size has been described. For comparison, two types of folded waveguide resonators have been studied, i.e. the quarter-wavelength resonator of square shape and the newly proposed triangular shape. In addition, a demonstration of a filter application for miniature triangular folded waveguide resonators has been designed and simulated using an EM simulator.

Chapter 5 will be concerned with the design of coupled folded waveguide resonator FWG filters. This includes a primary investigation into developing a compact and low-loss bandpass filter using novel folded waveguide resonators with a footprint reduction. A slot coupling between adjacent resonators is introduced, which is characterized using full-wave EM simulations and verified experimentally. Two designs of 2-pole folded waveguide resonator filters of this type have been considered, fabricated and tested. Simulation and measurement results are presented in this chapter to validate the design and to show the advantages of this type of filter.

Chapter 6 In this chapter design and develop of a cavity resonator filter using a folded structure has been describes, furthermore, this chapter deals with the simulation and implementation for two designs of coupled folded waveguide (FWG) resonator filters and their frequency responses. The design procedure for both is almost the same; hence, the plan was divided into three stages. In the first stage, the dimensions and the excitation port location were obtained from the 1-pole cavity resonator for the optimum external quality factor (Qe) that is required. In the second stage, the same dimensions

obtained from the 1-pole resonator were used; varying the gap length (G), the wall width (W) and a corner of the separation plate cutting (C) to attain the required coupling coefficients (K_{12}, K_{23} and K_{34}) to get an approximate design for the 2-pole resonators that could be used in the 4-pole resonator. After obtaining these results, the 4-pole resonator was simulated with the dimensions obtained by readjusting the values of G, W and C until the specified resonator requirements were obtained. The implementation of these designs and their experimental results are the core contents of this chapter, with certain specifications.

Chapter 7 outlines numbers of experiments conducted to develop a Substrate Integrated folded-waveguide SIFW resonator filter using a folded structure. This chapter deals with the simulation and implementation for two designs of SIFW resonator filter and their frequency response.

Chapter 8 concludes the work described in the previous chapters and gives an outlook on the proposed future work in this field of research.

Chapter 2

Literature survey

2.1 Introduction:

Microwave and millimetre-wave components for wireless communication systems and radars are traditionally built with waveguide technology that offers low-loss and high quality factors (Q). Realization of these components in planar form is generally avoided, owing to the low quality factor and higher losses of those circuits that are caused by the presence of the substrate material. However, with the recent developments in microwave micromachining, it is now possible to make microstrips or CPW line resonators suspended on a membrane [3], cavity propagating or evanescent mode resonators [4, 5], and dielectric resonators [6]. These offer low-loss and high-Q, which can be monolithically integrated with other passive components and active devices on a single chip. Microwave resonator filters are essential to microwave engineering and constitute one of the most significant group of circuits and therein.

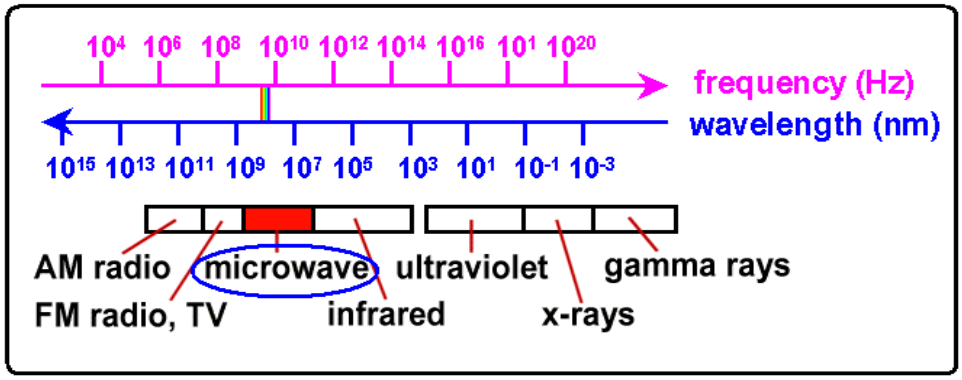

Figure 2-1: Frequency allocations [8]

Microwave filters are two-port networks that are used to separate and combine or select and reject signals at various frequency in a wide range of RF/Microwave system and tools [7] . While filters may differ in physical realiztion, the general structure of the circuit network is common to all filters. Microwave filters are used to control frequencies from 300 MHz to 300 GHz within the electromagnetic spectrum. Most microwave technology

applications nowadays are used for communications systems, radar systems and environmental remote sensing systems. Figure 2-1 shows the frequency allocations [8]. RF and microwave communications systems are pervasive, especially today when wireless connectivity promises to provide voice and data access to "everyone, anywhere, at any time". A microwave communication system normally consists of a transmitter subsystem, including a microwave oscillator, waveguides, and a transmitting antenna, and a receiver subsystem that includes a receiving antenna, transmission line or waveguide, a microwave amplifier, and a receiver. The object of this chapter is to provide an overview of the microwave filter's history and to capture the essence of past research and the present trends in microwave filter applications in modern communication systems. To understand the design ideas and the problems that must be overcome during the filter designs for filter applications, the necessary knowledge is explained for the realization of this thesis.

2.2 Microwave filter's history:

From the early times of telecommunication systems, filters in electrical circuits have played a significant role and have progressed steadily with the advance of communication technology. In 1910, the introduction of the delivery service telephony system a novel transmission system of multiplex communication considerably reformed the technological landscape surrounding telecommunications and introduced a new generation into telecommunications [9]. It became necessary to develop new technology to extract and identify signals contained within a specific frequency band, and this technological advance further accelerated the research and development of filter technology [9]. The development of passive electrical wave filters and the theory behind them in 1915 are attributed to Wagner and Campbell. Since then, the theory and practice of filter design has advanced with a consequent broadening of the term "filter". A filter is defined as a network, which requires having a prescribed response for a given excitation. The response requirement may be either in time or frequency; in the latter case, characteristic selectivity is implied [9].

Prior to the Second World War, a microwave filter had been designed, and W. P. Mason and R. A. Sykes [10] published a significant early paper in 1937. They used A, B, C, and D parameters although not in matrix form to trace the image impedance, image phase and attenuation functions of a large variety of useful filter sections. During the Second World War years of 1941 to 1945, the most important advances and applications, using mainly

image parameters, were made at various laboratories in the United States (e.g. at the M.I.T. Radiation Laboratory, the Harvard Radio Research Laboratory, and Bell Laboratories, NRL). At the Radiation Laboratory, the emphasis was on waveguide cavity filters, while at the Radio Research Laboratory, broad-band low-pass, bandpass work concentrated on high-pass coaxial filters for ECM applications and narrow-band tuneable coaxial resonator filters for search receivers. Much of this work was described in the M.I.T. Radiation Laboratory Series by Fano and Lawson [11]. Network theory was the most advanced theory in engineering in that case; S. Darlington having published his famous cascade synthesis theory in 1939 [12]. He succeeded in writing a clear and concise summary of Arlington's theory by Fano and Lawson [11]. Chapter 10 of [13] on the design of microwave filters contains some surprisingly modern designs, e.g. describing filters with finite frequency attenuation poles and dual mode cavities. Filters are among the most widely used components for radio frequency as well as for microwave communications. Lumped element inductors and capacitors can be used at lower frequencies to design filters, while at microwave frequencies, transmission line sections and waveguide elements are typically used.

Microwave filters are basically frequency selective elements. The filtering performance results in frequency dependent reactance provided by inductors and capacitors. In microwave frequencies, lumped element inductors and capacitors cannot be used and thus transmission line sections that behave as inductors and capacitors are used. Minimizing the losses in the passband of a filter is important, since it not only reduces the overall losses for a transmitter but also improves the noise figure when used with a receiver. Filters can be designed using the periodic structures, the image parameter or the insertion loss methods. In the image parameter, the method design is simple. However, the response in the passband and the stopband cannot be precisely controlled. In the insertion loss method, design starts with a low-pass prototype based on the maximally flat, or Chebyshev, response and the insertion loss in the passband as well as in the stopband can be defined and controlled, based on the number of sections chosen and the components used. The design methods has been describes in the following chapter. Filters play important roles in many RF/microwave applications as they are used to separate or combine different frequencies. The main filter roles reject undesirable signal frequencies outside the filter passband. The electromagnetic spectrum is limited and shared; filters are used to select or confine the RF/ microwave signals within assigned spectral limits. Emerging applications such as wireless communications continue to challenge

RF/microwave signals with ever more stringent needs higher performance, smaller size and lower cost. This requirement causes rapid expansion towards microwave and millimetre wave frequencies. Resonators are a basic part of microwave communication circuits and these microwave resonators are used in a variety of applications including filters, oscillators, frequency meters, tuned amplifiers and other applications. The resonators will be discussed in more detail in section 2.5.

In particular, the revolution in information technology and mobile communication demands more and more channel bandwidth. This requirement causes rapid expansion towards microwave and millimetre wave frequencies [14]. Microwave and millimetre wave components for wireless communication systems and radars are traditionally built with waveguide technology that offers low-loss and high quality factor (Q) circuits. This technology, however, produces circuits that are large in size and weight, high in cost, incompatible with monolithic circuits and have an increased fabrication complexity, especially at higher frequencies [15]. Realization of these components in planar form is generally avoided because of the low quality factor and higher losses of those circuits that are caused by the presence of the substrate material. However, with the recent developments in microwave micromachining it is now possible to make microstrip or CPW line resonators suspended on membranes [3], cavity propagating or evanescent mode resonators[4]-[16], and dielectric resonators [6] that offer low-loss, high-Q and narrow bandwidth; these can be monolithically integrated with other passive components and active devices on a single chip. Microwave resonators, such as bandpass filters with stringent requirements, are finding an increasing range of applications in modern communication systems. The concept of folded waveguide resonators was introduced by J. S Hong [1] for X-band applications. In this report, a cvity folded waveguide FWG resonators are characterized for filter applications. The cavity resonator is a metallic enclosure that confines the electromagnetic energy. The stored electric and magnetic energies inside the cavity determine its equivalent inductance and capacitance. The energy dissipated by the finite conductivity of the cavity walls determines its equivalent resistance.

2.3 Filter Classification:

Filters may be classified, according to frequency response, into four basic types:

I. Low-pass filters (LPFs): transmit all signals between zero frequency and some upper limit ωc and attenuate all frequencies above the cut off value.

II. High-pass filters (HPFs): pass all frequencies above a lower cut off value ωc and reject all frequencies below ωc.

III. Bandpass filters (BPFs): pass all frequencies in a range ω1 to ω2 and reject frequencies outside this range.

IV. Bandstop filters (BSFs): attenuate frequencies in the range of ω1 to ω2.

In most applications, only bandpass filters are desirable. Depending on the requirements and specifications, RF/microwave filters are designed as lumped or distributed element circuits; they may be realized in various transmission line structures such as waveguide, coaxial line, and microstrip.

2.4 Filter parameters:-

There are two main areas of interest for a filter: the passband where it accepts signals and allows them through and the stopband where it rejects them. An ideal filter would have a response something like that shown in Figure 2-2. Here, it can be seen that there is an immediate transition between the passband and the stopband. Moreover, in the passband the filter does not introduce any loss and in the stopband no signal has been allowed through.

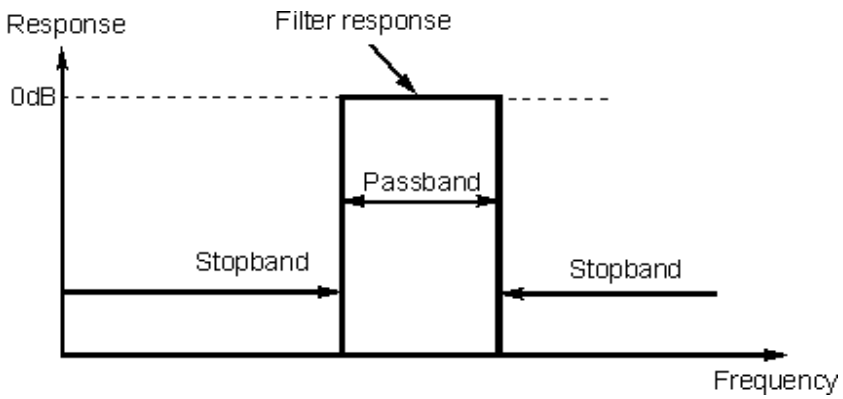

Figure 2-2: The response of an ideal filter[17].

In reality, it is not possible to realize a filter with these characteristics, so a typical response would be more like that shown in Figure 2-2. It is obvious from the diagram that there are several differences. The first is that there is some loss in the passband. Secondly, the response does not fall away infinitely fast. Thirdly, the stopband attenuation is not infinite, even though it is large. Finally, it will be noticed that there is some in-band ripple [17].

2.5 RF and microwave resonators:

Any structure that is able to contain at least one oscillating in electromagnetic (EM) field at RF frequency can be used as an RF resonator. RF and microwave resonators are lumped element networks, or distributed circuit structures, that exhibit minimum or maximum real impedance at a single frequency or at multiple frequencies. The resonant frequency f_0 is the frequency at which the input impedance or admittance is real. The resonant frequency may be further defined in terms of a series, or shunt mode, of resonance; the series mode is associated with small values of input resistance at the resonant frequency, while the shunt mode is associated with large values of resistance at the resonant frequency [18]. Some typical lumped and distributed resonators are shown in Figure 2-3.

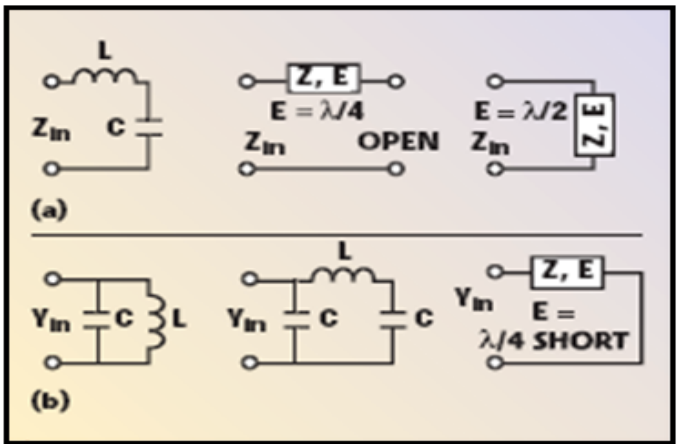

Figure 2-3: Typical resonant circuit; (a) series and (b) shunt resonator[18].

2.5.1 RF Resonator:-

A resonator is the basic building block of a transmitter or receiver subsystem. In this section, an explanation of the resonators, with a special focus on the cavity resonator, is given.

2.5.1.1 Cavity Shapes

Cavity shapes have been studied deeply and in this section the most shapes that are used to design a cavity resonator or a filter are presented.

2.5.1.2 Rectangular cavity:

A rectangular cavity is shown in . In addition, the electric filed distributions for the TE_{101} and TE_{102} resonant mode can clearly be seen. Electric and magnetic energy is stored within the cavity, and power can be dissipated in the metallic walls of the cavity, as well as in the dialectic filling the cavity [19].

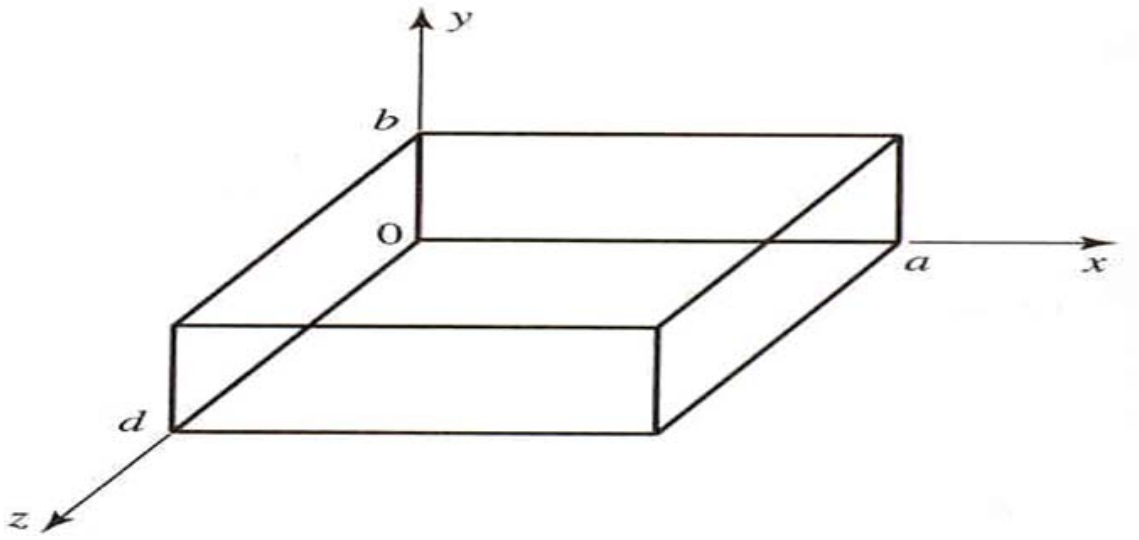

Figure 2-4 Rectangular Cavity Resonator.

The main advantages associated with using a cavity resonator are low-loss characteristics and practical application feasibility up to 100 GHz. However, the greatest drawback of the waveguide resonator is its size, which is significantly larger than other resonators available in the microwave sector. When both ends of a waveguide with conducting plates are closed, the closed structure forms a cavity and is referred to as a cavity resonator. Waveguide resonators have long been used in the high frequency range. Resonators can also be constructed from a closed section of the waveguide, which should not be surprising since waveguides are a type of transmission line. Because of radiation loss from open-ended waveguides, waveguide resonators are usually short circuited at both ends, thus forming a closed box or cavity. It may be thought of as a section of a rectangular waveguide closed at both ends by conducting plates, as shown in Figure 2-5. The rectangular cavity is only one of many cavity

devices that are useful as high-frequency resonators. The author has been concentrating on this type of the resonator filter and more details will be presented later in this chapter.

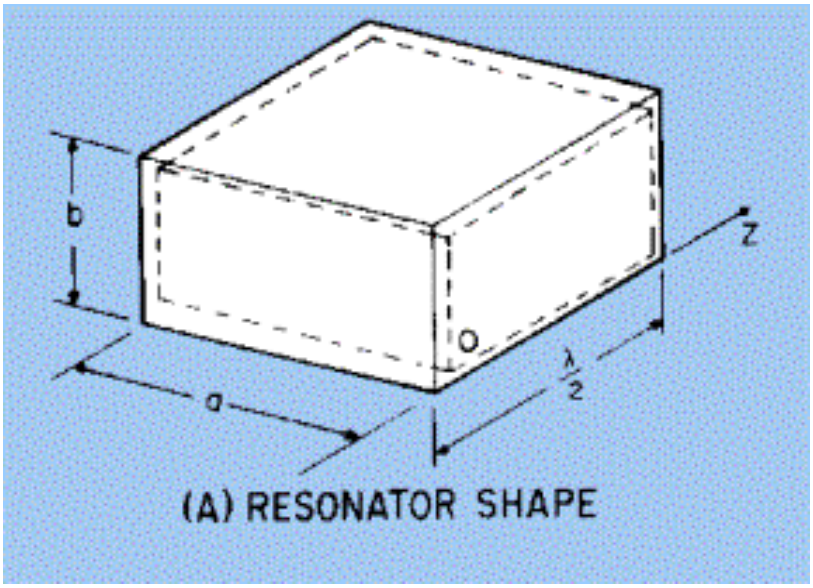

Figure 2-5: Rectangular waveguide cavity resonator [20].

2.5.1.3 A cylindrical cavity:

A cylindrical cavity may be a hollow, metallic pipe enclosed at both ends by conducting plates, as shown in Figure 2-6.

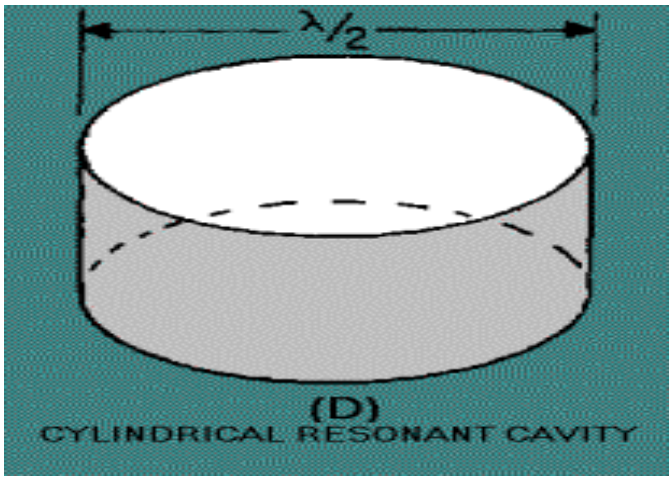

Figure 2-6: Development of a cylindrical resonant cavity [20].

2.5.1.4 Other cavity shapes:

Figure 2-7 illustrates several cavity shapes that are commonly used. It should be remembered from the previously stated definition of a resonant cavity that perhaps any completely enclosed conductive surface, regardless of its shape, can act as a cavity resonator [20].

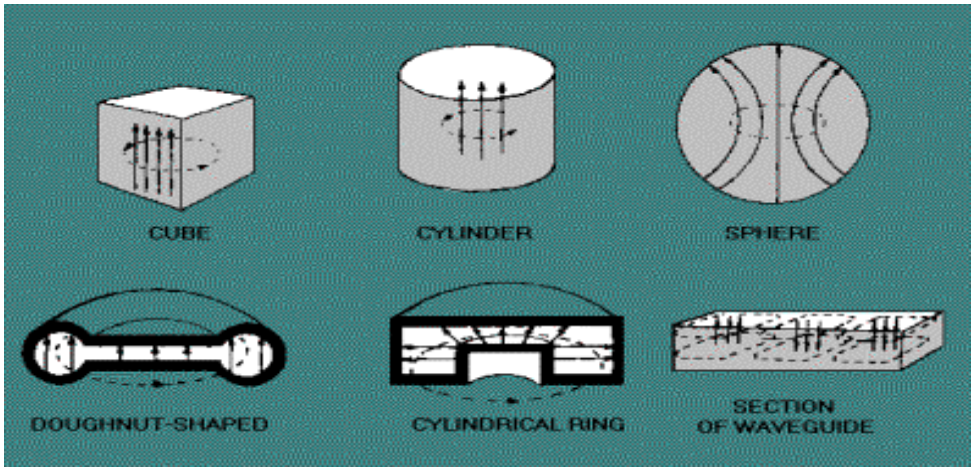

Figure 2-7: Several types of cavities [20].

2.5.1.5 Microstrip resonator:-

A microstrip resonator is any structure that is able to contain at least one oscillating electromagnetic field, and they come in numerous forms. In general, microstrip resonators for filter design may be classified as [21]:

1.) Lumped-element or quasi lumped-element resonators
2.) Distributed or patch resonators

A microstrip resonator is a general loss transmission line, using a microstrip at odd multiple lengths of half a wavelength of the guided wave at various terminations to control an oscillator output of nominal frequency with frequency stability. It can open or shorten sections of line that provide the right impedance for instability, rectangular $\lambda/2$ resonating line sections, circular disks, circular rings, and triangular microstrip etc. [21].

2.5.1.6 Dielectric resonators:

A small cube or disc of low loss, high dielectric constant material can be used as a microwave resonator. Such a resonator is generally smaller in cost, size and weight than

the equivalent metallic cavity, and can be very easily incorporated into microwave integrated circuits and coupled to planar transmission lines. Materials with dielectric constants between 10 and 100 are commonly used, with barium tetratitanate and titanium dioxide being typical examples. Conductor losses are absent but dielectric losses usually increase with dielectric constant. Qs up to several thousand can be achieved, however. By using an adjustable metal plate above the resonator, the resonant frequency can be mechanically tuned. Dielectric resonators are integrable and provide all the advantages of an integrated circuit in terms of space, weight, etc., and offer higher Qs as well as better temperature stability over conventional waveguide resonators. Cohn in [22] reported compact bandpass filters using dielectric resonators made of TiO2 and since then, the ease of using high Q temperature compensated dielectric resonators has been advancing tremendously. The dielectric filter technology based on high-Q ceramic materials has been contributing to the great reduction in size of mobile telecommunication equipment, particularly cellular handsets and base stations. Moreover, it has a low cost and extensive mass productivity. Since the end of the 1960s, significant development efforts have been made and great progress achieved in DR filter technology, in [23-25].

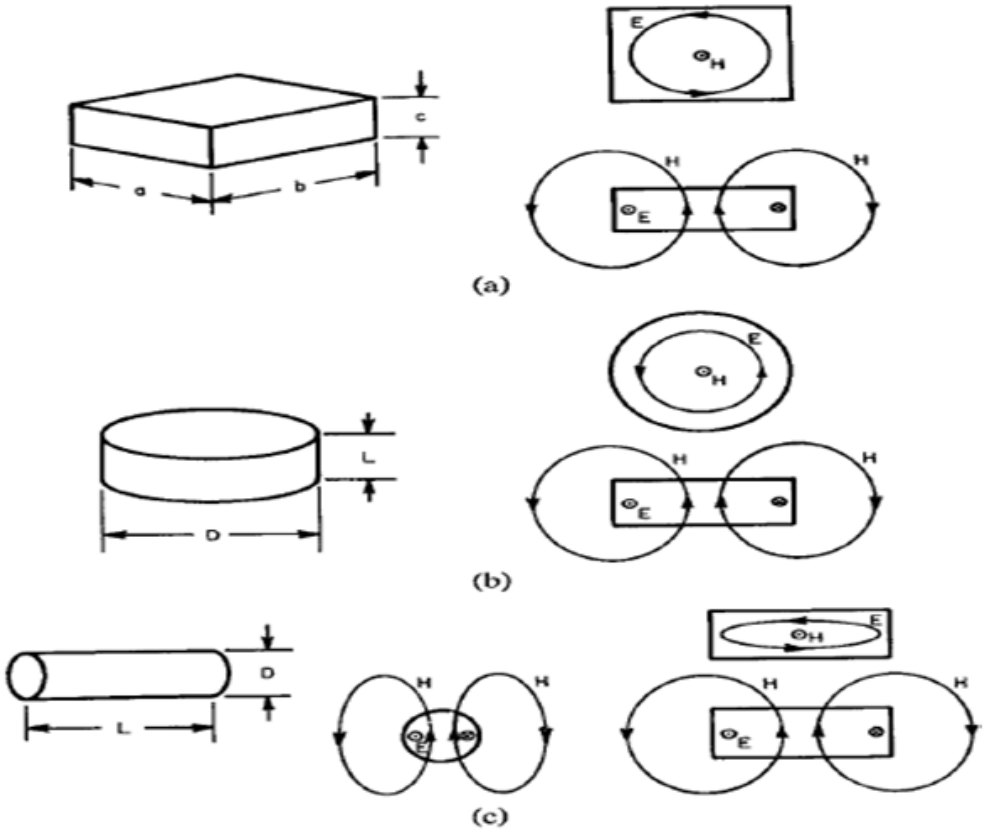

Figure 2-8: Fundamental mode fields for three dielectric-resonator configurations.

(a) Rectangular resonator, a and b > c. (b) Cylindrical resonator, L < D. This case is preferable for most filter applications. (c) Cylindrical resonator, L > D.

There are various possible operating modes for dielectric resonator filters. The list includes single transverse magnetic TM modes, single transverse electric TE modes, dual hybrid electromagnetic (HEM) modes, triple (TM) modes and triple TE modes. These modes have an impact on the filter size, unloaded Q and spurious performance. DR filters are the most commonly used; a single mode filter operating in the TE01 mode, provides low loss and good spurious-free performance. Furthermore, an elliptic function response can be realized by this type of filter to reduce further the loss and volume. Three convenient shapes for a dielectric resonator are shown in Figure 2-8. The most practical is usually a cylindrical disk whose length L is less than its diameter D. With this shape, the lowest-frequency resonant mode has a circular electric-field distribution, as shown in Figure 2-8(b). The magnetic field is strongest on the axis of the disk and at a sufficient distance outside the disk the field resembles that of an axial magnetic dipole. For the L greater than D Figure 2-8 (c), the fundamental mode has an equivalent magnetic dipole moment transverse to the axis [26].

2.6 Cavity Resonators

By definition, a resonant cavity is any space completely enclosed by conducting walls that contain oscillating electromagnetic fields and possess resonant properties. The stored electric and magnetic energies inside the cavity determine its equivalent inductance and capacitance, and the energy dissipated by the finite conductivity of the cavity walls determines its equivalent resistance. In theory, a given resonator has an infinite number of resonant modes, and each mode corresponds to a definite resonant frequency. When the frequency of an impressed signal is equal to a resonant frequency, maximum amplitude of the standing wave occurs, and the peak energies stored in the electric and magnetic fields are equal. The mode having the lowest resonant frequency is known as the dominant mode [14]. When both ends of a waveguide with conducting plates are closed, the closed structure forms a cavity and is referred to as a cavity resonator. In a resonator, it is expected that the wave will yield a standing wave because of its reflection at the closed ends. Simply put, those standing wave patterns (modes) that satisfy the boundary conditions at each of the six walls will exist. When a

mode is able to exist at a certain frequency called the resonant frequency it traps energy at that frequency. In this case, one wall, say at z = 0, is fixed, whereas the opposite wall is moved back and forth. The movable wall changes the length of the cavity in the z direction which, in turn, changes its resonant frequency [14].

The cavity has many advantages and uses at microwave frequencies. Resonant cavities have a very high Q and can be built to handle relatively large amounts of power. Cavities with a Q value in excess of 30,000 are not uncommon. The high Q gives these devices a narrow bandpass and allows very accurate tuning. Simple, rugged construction is an additional advantage. Although cavity resonators built for different frequency ranges and applications have a variety of shapes, the basic principle of operation is the same for all. In practice, the rectangular-cavity resonator, circular-cavity resonator, and re-entrant cavity resonator are commonly used in many microwave applications [20]. Some advantages of the cavity resonator include the following.

2.6.1 Advantages of the cavity resonator:-

- Combination of compact size and high quality factor
- Reliability and ruggedness
- Potential for manufacture in large volumes at low cost
- Power handling capacity
- Lower losses (resistive and dielectric)
- Frequency and bandpass response stability
- No dielectric, so non-linearities in high fields are less
- Allows very accurate tuning
- Dimensional stability against vibration, changes in temperature, and pressure.

2.6.2 Resonant frequency of the cavity

Two variables determine the primary frequency of any resonant cavity. The first variable is PHYSICAL SIZE: in general, the smaller the cavity, the higher its resonant

frequency. The second controlling factor is the SHAPE of the cavity. Cavity resonators are energized in basically the same manner as waveguides and have a similar field distribution [20]. If the cavity shown in Figure 2-9 were energized in the TE mode, the electromagnetic wave would reflect back and forth along the Z axis and form standing waves, as shown in Figure 2-10. These standing waves would form a field configuration within the cavity that would have to satisfy the same boundary conditions as those in a waveguide.

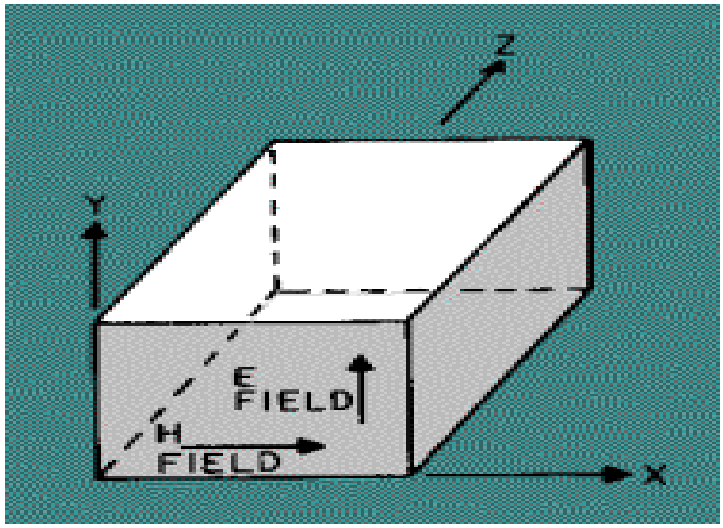

Figure 2-9: Rectangular cavity resonator [20].

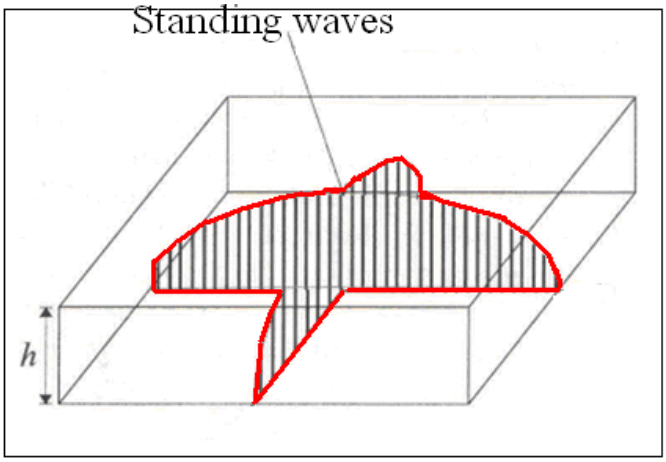

Figure 2-10: Conventional TE101 waveguide resonator with standing waves. [5]

2.6.3 Quality Factor of the cavity resonator:

A definition of Q is, "Energy stored in the cavity divided by energy dissipated per radian of oscillation". The energy Ed dissipated per radian is related to the dissipated power Pd by the relationship Ed times angular frequency = Pd. Clearly, if there are

more radians per second (the frequency is higher) there are more dissipated Joules per second (Watts). The energy stored rises with the volume, but the power dissipated rises with the surface area of the cavity's inside-walls. The energy dissipated per radian rises proportional to volume, since frequency is inversely proportional to the cavity's linear dimensions. Given constant skin depth, then all cavities would have the same intrinsic Q factor. Because the skin depth falls with frequency to the half power, the Q factors achievable falls as the square root of the frequency [1]. The effective use of a loss estimation tool requires knowledge of resonator unloaded Q. In general, resonator Qu is a function of resonator geometry, material resistivity, surface finish, dielectric loss tangent, and method of construction. The effect of dielectric losses in the resonator is that the conductor surfaces. If losses in the conductors give a Qc and dielectric losses give a $Q_d = \frac{1}{\tan\delta}$, then the unloaded quality factor resonator Qu obeys the relationship:

$$\frac{1}{Q_u} = \frac{1}{Q_c} + \frac{1}{Q_d} \qquad (2\text{-}1)$$

The quality factor Q of the resonator cavity is defined by:

$$Q = \frac{\omega(\text{time average of energy stored in the system})}{\text{energy loss per second in the system}} \qquad (2\text{-}2)$$

Now $$Q = \frac{\omega_o}{2\,\delta\omega} \qquad (2\text{-}3)$$

$$Q = \frac{f_0}{f_{2_{3db}} - f_{1_{3db}}} \qquad (2\text{-}4)$$

Finally the unloaded quality facot is given by

$$Q_u = \frac{Q}{1 - |S_{21}|} \qquad (2\text{-}5)$$

It is now possible to make miniature silicon micromachined high-Q waveguide resonators [4, 16, 27-29] as building blocks for the development of high performance microwave filters. The quality factor and the power handling that can be achieved with

this type of resonator is much higher than that attainable with traditional microstrip resonators, either printed on a dielectric substrate or suspended in air with the support of a thin dielectric membrane. However, as compared with the membrane-supported microstrip resonator, the micromachined cavity resonator is large in size, particularly its footprint. For many applications, such as for the development of multi-pole filters, it would be desirable to reduce the footprint of this type of resonator since the height of the micromachined cavity is usually quite small [5].

The analytical method of designing the folded waveguide seems to be difficult for complex structures, so the Sonnet 'em' [30] and Ansoft's High Frequency Structure Simulator (HFSS) package software programs have been adopted for the 'em' design of the waveguide. The output values from the Sonnet 'em' modelling have been compared with those of the analytical equations that were presented. The folded waveguide resonator is designed using the Sonnet and HFSS tools to obtain the optimum dimensions for the device. In order to achieve this, the S-parameters and more specifically, the transmission coefficient parameters have been investigated. The important parameters that are to be varied in order to obtain the optimum desired frequency as well as for the optimum Q-factor are given as follows [32]:

- The dimensions of the device specify the resonating frequency. It should be noted that the resonator should resonate at around $\lambda/4$
- The height of each cavity of the resonator determines the energy losses in the resonator, thus affecting the Q-factor of the resonator as well as the transmission coefficients.

It is also of prime interest that the S_{21} parameters should lie around 0 dB and should be at least below -35 dB in order to test them using the network analyser.

2.6.4 Tuning of the cavity resonator:

Energy can be inserted into, or taken from, a cavity by the same methods that are used to couple energy into and out of waveguides. The operating principles of probes, loops and slots are the same, whether used in a cavity or in a waveguide. Therefore, any of the following three methods can be used with cavities to inject or remove energy. The resonant frequency of a cavity can be varied by changing any one of three parameters:

1. Cavity volume
2. Cavity capacitance
3. Cavity inductance.

Changing the frequencies of a cavity is known as TUNING. The mechanical methods of tuning a cavity may vary with the application, but all methods use the same electrical principles. A mechanical method of tuning a cavity by changing the volume (VOLUME TUNING) is illustrated in Figure 2-11. Varying the distance 'd' will result in a new resonant frequency because the inductance and the capacitance of the cavity are changed by different amounts. If the volume is decreased, the resonant frequency will be increased. The resonant frequency will be lower if the volume of the cavity is made larger [20].

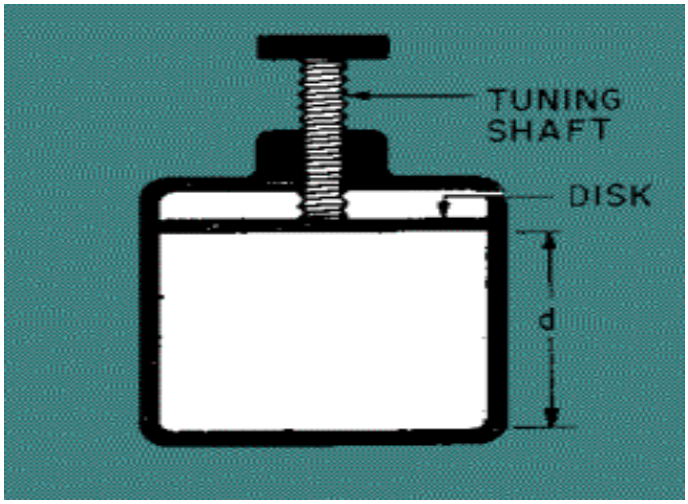

Figure 2-11: Cavity tuning by volume [20].

CAPACITIVE TUNING of a cavity is shown in Figure 2-12. An adjustable slug or screw is placed in the area of maximum E lines. The distance 'd' represents the distance between two capacitor plates. As the slug is moved in, the distance between the two plates becomes smaller and the capacitance increases. The increase in capacitance causes a decrease in the resonant frequency. As the slug is moved out, the resonant frequency of the cavity increases [20].

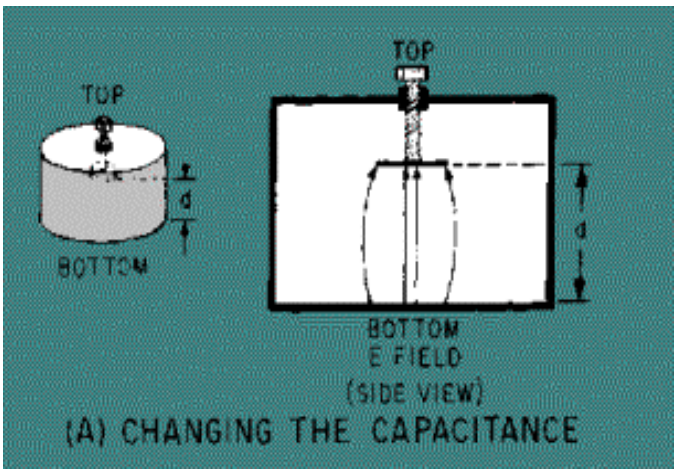

Figure 2-12: Methods of changing the resonant frequency of a cavity. CHANGING THE CAPACITANCE [20].

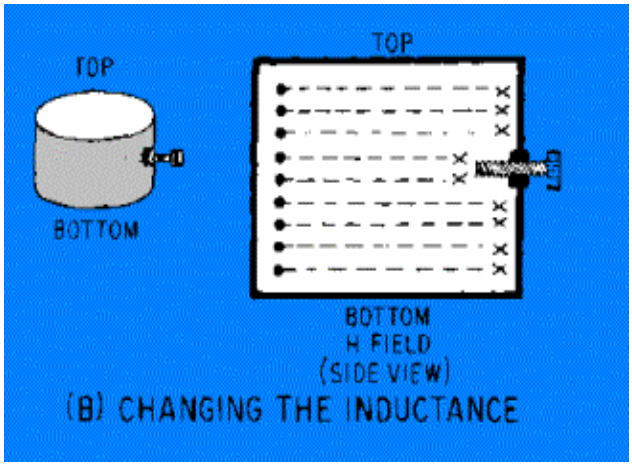

Figure 2-13: Methods of changing the resonant frequency of a cavity. CHANGING THE INDUCTANCE [20].

Inductive tuning is accomplished by placing a non-magnetic slug in the area of maximum H lines, as shown in Figure 2-13. The changing H lines induce a current in the slug that sets up an opposing H field. The opposing field reduces the total H field in the cavity, and therefore reduces the total inductance. Reducing the inductance by moving the slug in raises the resonant frequency. Increasing the inductance by moving the slug out lowers the resonant frequency [20]. This is applicable in the wavelength rang $2a \rangle \lambda \rangle a,$ and for the centred cylinder ($x = a/2$) in the wider range $2a \rangle \lambda \rangle 2a/3$ [74].

2.7 Rectangular cavity & Modelling of the folded waveguide FWG resonator:

The rectangular cavity and the electric field distribution for the TE_{101} and TE_{102} resonant modes are shown in Figure 2-14. It consists of a length *d* of rectangular

waveguide shorted at both ends (z =0,d). To solve for the electric and magnetic fields that satisfy the boundary conditions of the cavity, we might begin with the wave equations and use the method of separation of variables. It is easier to start with TE and TM waveguide fields, that already satisfy the necessary boundary conditions on side walls (x = 0,a and y = 0,b) of the cavity. Then it is only necessary to enforce the boundary conditions that $E_x = E_y = 0$ on the end walls at z = 0, d [19]. The transverse electric fields (Ex, Ey) of the TE_{mn} or TE_{mn} rectangular waveguide mode can be written as [19] :

$$\bar{E}_t(x,y,z) = \bar{e}(x,y)[A^+ e^{-j\beta_{mn}z} + A^- e^{-j\beta_{mn}z}] \qquad (2\text{-}6)$$

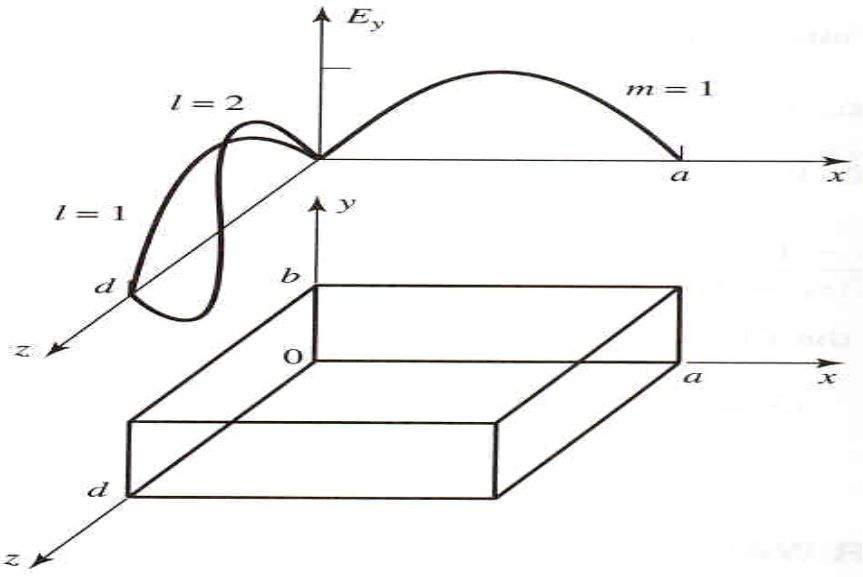

Figure 2-14: Rectangular Waveguide Resonator.[19].

The rectangular cavity is a waveguide version of the short-circuit $\lambda/2$ transmission line resonator. A resonant wave number for the rectangular cavity can be defined as [19]:

$$k_{mnl} = \left[\left(\frac{m\pi}{a}\right)^2 + \left(\frac{n\pi}{b}\right)^2 + \left(\frac{l\pi}{d}\right)^2\right]^{\frac{1}{2}} \qquad (2\text{-}7)$$

Referring to the $TE_{mn}l$ or TM_{mnl} resonant mode of the cavity, where *m,n,l* represent variation in the standing wave in *x,y,z* directions. Then the resonant frequency of the $TE_{mn}l$ or TM_{mnl} mode is given as [19] :

$$f_{mnl} = \frac{k_{mnl}}{2\pi\sqrt{\mu_r\varepsilon_r}} = \frac{c}{2\pi\sqrt{\mu_r\varepsilon_r}}\left[\left(\frac{m\pi}{a}\right)^2 + \left(\frac{n\pi}{b}\right)^2 + \left(\frac{l\pi}{d}\right)^2\right]^{\frac{1}{2}} \qquad (2\text{-}8)$$

A schematic view of the folded waveguide resonator is shown in Figure 2-15.

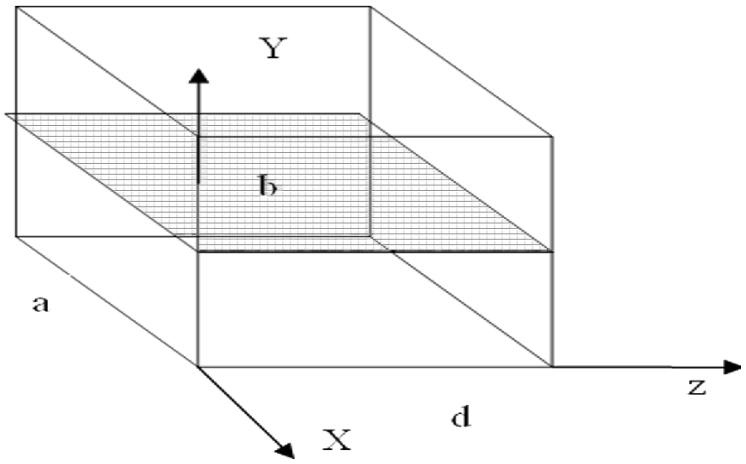

Figure 2-15: A Schematic view of the folded waveguide resonator.

In general, the solutions for the fields in a normal waveguide resonator can be expressed as follows [33]:

$$E_y = \frac{-2A^+ k_{nml} Z_0 a}{\pi} \sin\frac{\pi x}{a} \sin\frac{\pi z}{d} \qquad (2\text{-}9)$$

$$H_x = \frac{2jA^+a}{d}\sin\frac{\pi x}{a}\cos\frac{\pi z}{d} \quad (2\text{-}10)$$

$$H_z = -2jA^+\cos\frac{\pi x}{a}\sin\frac{\pi z}{d} \quad (2\text{-}11)$$

The approximated solutions for the electro magnetic fields in the folded waveguide resonator can be expressed as

$$E_y = \frac{-2A^+k_{nml}Z_0a}{\pi}\sin\frac{\pi x}{2a}\sin\frac{\pi z}{2d} \quad (2\text{-}12)$$

$$H_x = \frac{2jA^+a}{d}\sin\frac{\pi x}{2a}\cos\frac{\pi z}{2d} \quad (2\text{-}13)$$

$$H_z = -2jA^+\cos\frac{\pi x}{2a}\sin\frac{\pi z}{2d} \quad (2\text{-}14)$$

n,m,l represents the number of half sinovariations in the x, y,z directions.
and A^+ represents the amplitude constants for the modes propagating

The frequency of the folded cavity can be estimated by the following general equation:

$$f_{101} = \frac{ck_{nml}}{4\pi} = \frac{c}{4}\left[\left(\frac{l}{a}\right)^2 + \left(\frac{m}{b}\right)^2 + \left(\frac{n}{d}\right)^2\right]^{\frac{1}{2}} \quad (2\text{-}15)$$

where c = Velocity of light (3×10^8 m/s).
a = Dimension of the cavity in x direction.
b = Dimension of the cavity in y direction .
d = Dimension of the cavity in z direction .
and $l,m.n$ represents the modes.

2.7.1 Folded waveguide resonator concept

The concept of folded standing waves of a TE101 mode was introduced by Jason Hong [1]. The novel realizations of half-wavelength and quarter-wavelength resonators of this type are described in [1]. Full-wave EM simulations were carried out to verify the operation mode, and the test structure of a folded waveguide quarter-wavelength

resonator was designed, fabricated and tested in [1]. Experimental results are presented to validate the simulation and to show some interesting and useful characteristics. With the advent of micromachining techniques in fabricating microwave circuits, it is now possible to make miniature silicon micromachined high-Q waveguide resonators as building blocks for the development of high performance microwave filters. The quality factor and the power handling that can he achieved with this type of resonator is much higher than that attainable with traditional microstrip resonators, either printed on a dielectric substrate or suspended in air with the support of a thin dielectric membrane. However, compared with the membrane-supported microstrip resonator, the micromachined cavity resonator is large in size, particularly its footprint. For many applications, such as for the development of multi-pole filters, it would be desirable to reduce the footprint of this type of resonator since the height of a micromachined cavity is usually quite small. Almost all the reported micromachined cavity resonators are constructed based on the conventional TE_{101}-mode waveguide resonator of Figure 2-16. However, if we fold this conventional TE_{101} waveguide resonator along its x-axis while maintaining its standing waves, a so-called folded waveguide half-wavelength resonator can be obtained, as illustrated in Figure 2-17, which occupies only a half of the footprint of the conventional TE_{101} waveguide resonator. If we can now further remove the half of the fold-waveguide half-wavelength resonator while maintaining the standing waves on the other half, we have the so-called folded waveguide quarter-wavelength resonator of Figure 2-18, which has only a quarter of the footprint of the conventional TE_{101} waveguide resonator.

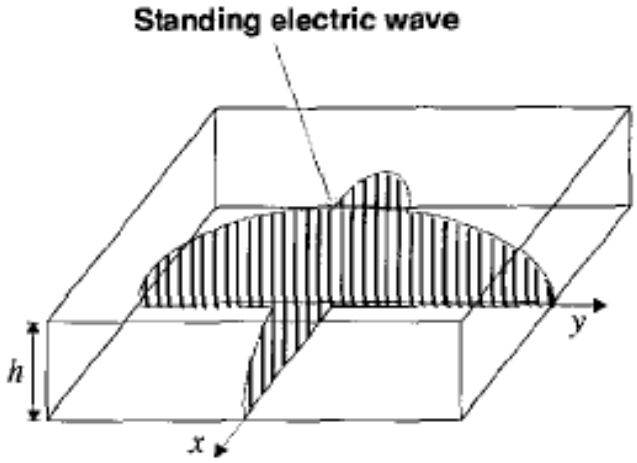

Figure 2-16: Conventional TE 101 waveguide resonator [5]

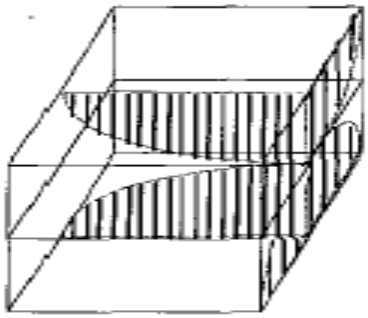

Figure 2-17: Folded waveguide half-wavelength resonator [5].

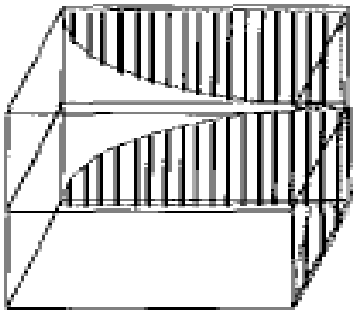

Figure 2-18: Folded waveguide quarter-wavelength resonator with standing waves resonator [5].

2.7.2 Novel Realizations of FWG resonator.

The proposed folded waveguide resonator concept is attractive for constructing compact cavity resonators with small footprints. The full-wave EM simulations were performed out using commercially available software [40]. Figure 2-19 illustrates a conceptual folded waveguide quarter-wavelength resonator that has two orthogonal slots on the common metal plate, on which the EM simulated electric standing wave pattern is shown in Figure 2-19 (a). It can be observed from Figure 2-19 (b) that this standing wave pattern is a quarter of that of the conventional TE_{101} waveguide resonator. Since the proposed folded waveguide resonators can maintain the resonant modes resembling to the TE101 mode in a conventional cavity resonator, they will have a similar high-Q property. Figure 2-20 shows field distributions for (a) the fundamental mode and (b) the second mode for the FWG cavity resonator.

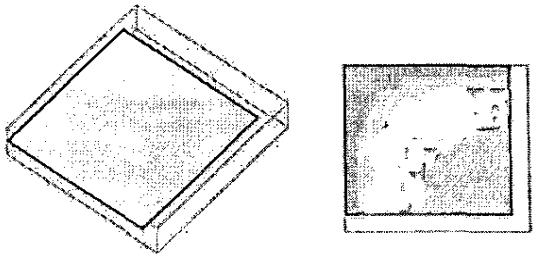

Figure 2-19: (a) Realization of the folded waveguide quarter-wavelength resonator. (b) Standing wave pattern of the folded waveguide quarter- wavelength resonator [5].

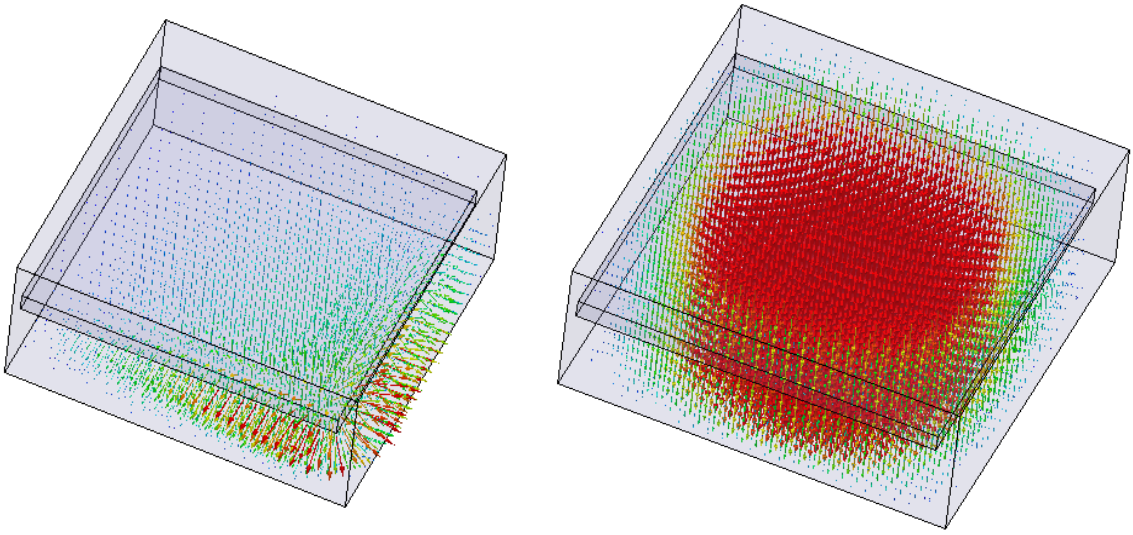

Figure 2-20: The distribution of field for the FWG cavity. (a) mode 1 and (b) mode 2

2.7.3 Experimental Demonstration of FWG resonator.

It is obvious that the proposed folded waveguide resonators would be suitable not only for the micromachined devices, but also for the waveguide devices fabricated using conventional techniques. For the demonstration, a folded waveguide quarter-wavelength resonator is presented, shown in Figure 2-16, Figure 2-17 and Figure 2-18. This designed resonator is comprised of two halves of a cavity with a metal plate inserted between them. The cavity has a size of 21 x 21 x 7 mm. The metal plate has a thickness of 1 mm and the two orthogonal slots are 1 mm wide. A novel excitation scheme is also implemented, and for the two-excitation port measurement the input/output (I/O)

excitation ports are located in an orthogonal manner. The demonstrator is fabricated on an industrial brass material.

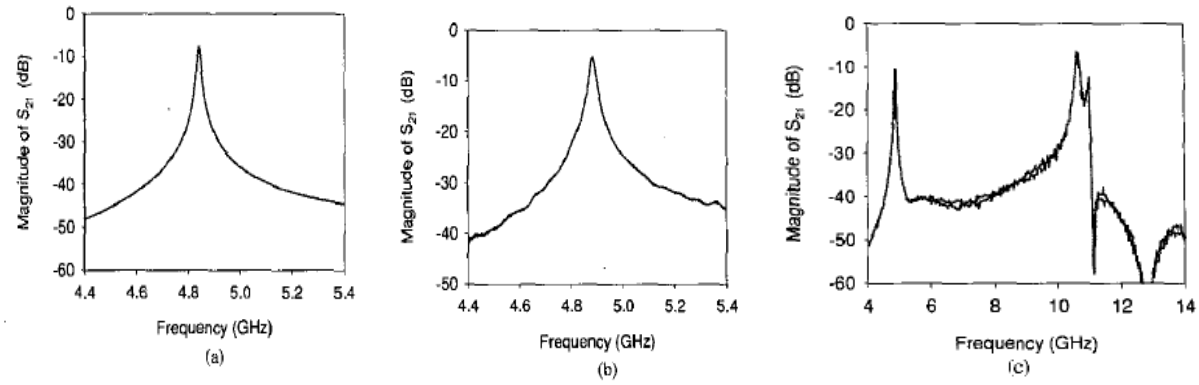

Figure 2-21: (a) Simulated resonant frequency response. (b) Measured resonant frequency response. (c) Measured wideband frequency response of the fabricated folded waveguide quarter-wavelength resonator [5].

The full-wave EM simulation shows that the designed demonstrator has a fundamental resonant frequency of 4.841 GHz and an unloaded Q of 736 where the conductivity of brass is taken as 1.57×10^7 S/m. The simulated resonant frequency response is plotted in Figure 2-21. The fabricated demonstrator was measured using an HP network analyzer and the measured performance is given in Figure 2-21. The measured resonant frequency was 4.881 GHz, which is in good agreement with the simulated one and the slightly higher frequency is due to the rounded corners of the fabricated cavity. The measured unloaded Q is 539, which is lower than the simulated result and can be attributed to the surface roughness of the fabricated cavity. Nevertheless, the experimental results have verified the operation of this new type of compact waveguide resonator. The experiment was also carried out to measure the wideband frequency response of the demonstrator, and the measured results are plotted in Figure 2-21 (c). It is interesting to observe that the spurious resonant modes appear only above 10 GHz and there is a wide stop band between the fundamental and the first spurious resonant mode. This is a desired characteristic for designing bandpass filters based on the fundamental mode. Another interesting characteristic is that there are two spurious resonant modes that are much closer to each other at around 10.5 GHz, and that need to be more investigated in the future.

2.7.4 Folded waveguide FWG resonator filter:

In, a primary investigation was conducted into developing compact waveguide filters using novel folded waveguide (FWG) quarter-wavelength resonators. The coupling between two folded waveguide quarter-wavelength resonators is described in [2]. For the demonstration of filter applications, a 2-pole folded waveguide resonator filter was designed. This designed filter is comprised of two coupled folded waveguide resonators, as described in the previous section and shown in Figure 2-22.

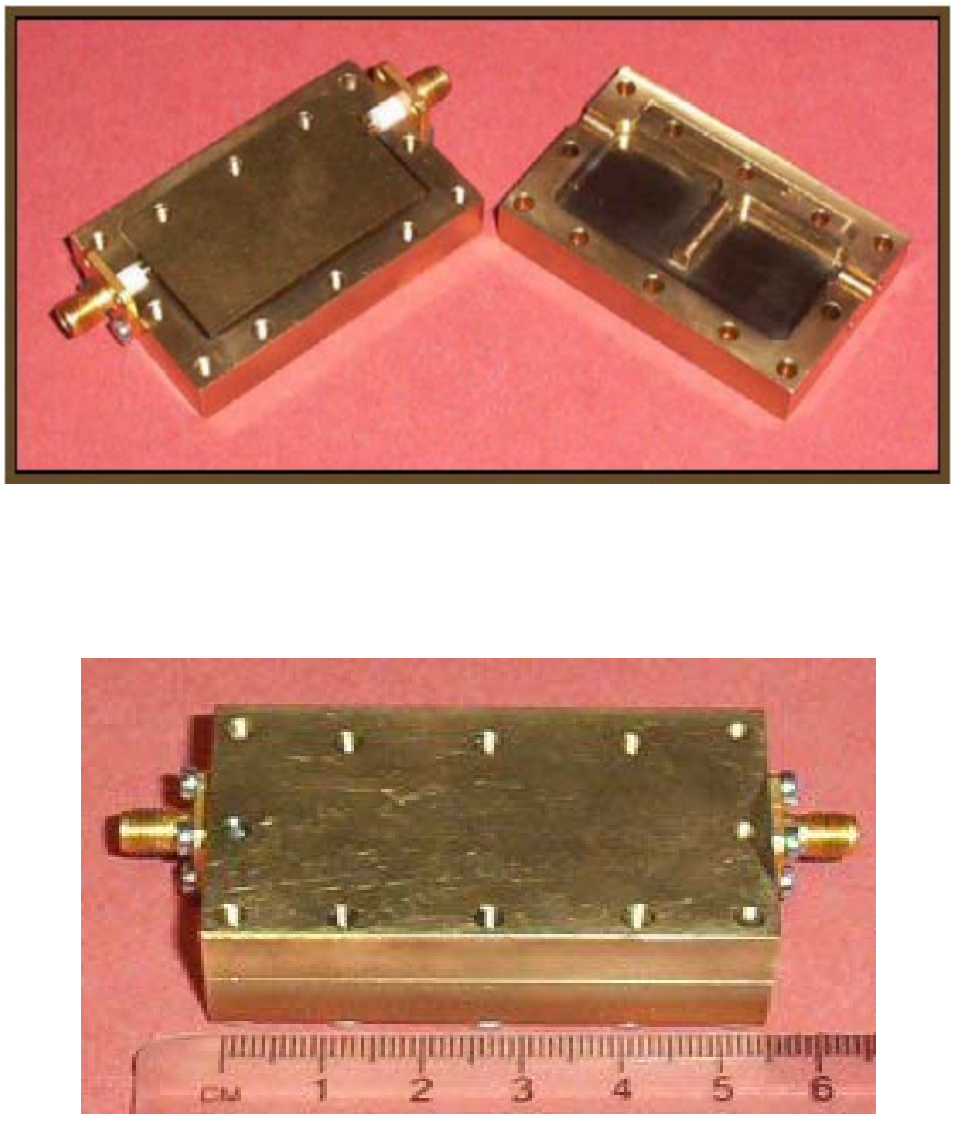

Figure 2-22: Fabricated filter before and after assembly [2].

The tapped-line input and output have been investigated in [2] and employed for realization of this type of filter, as indicated in Figure 2-23.

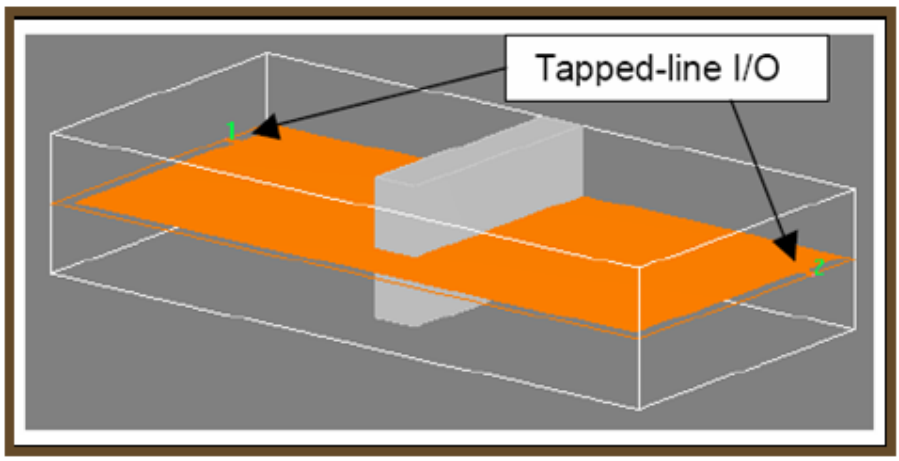

Figure 2-23: 3-D model of 2-pole coupled folded waveguide resonator filter [2].

The fabricated filter was measured using an HP microwave network analyzer, and the measured results are plotted in Figure 2-24. The filter responses shown in that Figure were measured without any tuning. In general, the measured responses are in good agreement with the simulated ones. Very low insertion loss across the passband has been obtained, with a midband insertion loss of 0.25 dB. This is due to the high Q of this type of resonator. The measured Q is about 650, which is slightly lower than the simulated result which is 736 and can be attributed to the surface roughness of the fabricated folded waveguide resonators.

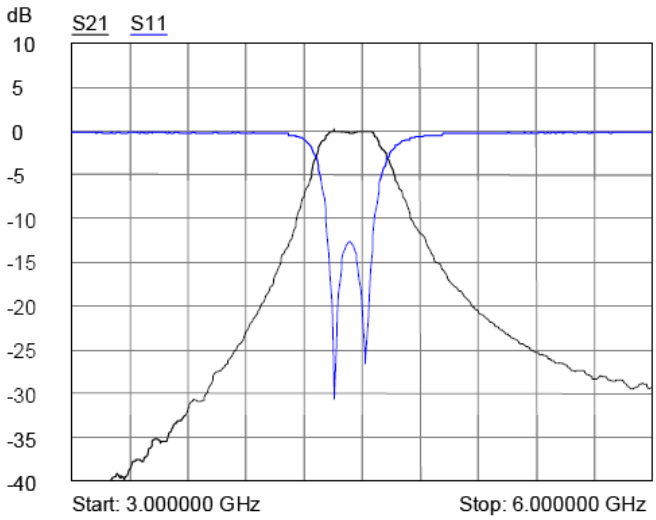

Figure 2-24: Measured performance of the fabricated 2-pole folded waveguide [2].

2.7.5 Folded waveguide FWG and coupling method:

Coupled resonator circuits are of significant importance in the design of RF microwave filters, in particular the narrow bandpass filters that feature in many applications. There

is a general technique for designing coupled resonator filters in the sense that it can be applied to any type of resonator regardless of its physical structure. It has been applied to the design of the waveguide filters [34, 35] , dielectric resonator filters [36], ceramic combine filters [37], microstrip filters superconducting filters and micromachined filters [3]. This design method is based on coupling coefficients of inter-coupled resonators and the external quality factors of the input and output resonators.

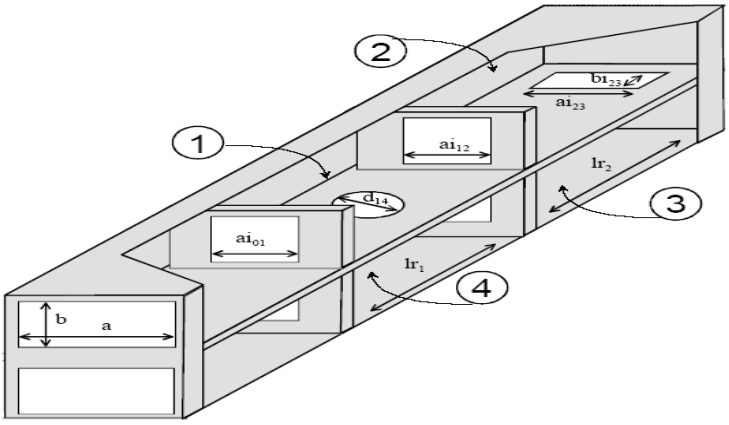

Figure 2-25: A 4th order folded waveguide filter with a cross-coupling between cavity 1 and cavity 4. The filter is symmetric around the mid-plane [38].

2.8 Substrate Integrated Waveguide SIFW Filter

The substrate integrated waveguide synthesized on a planar substrate with linear periodic arrays of metallic vias or metallic slots by standard printed circuit board (PCB) or other planar circuit processes has provided a very attractive platform on which to design low-cost and highly integrated waveguide filters [39, 40]. Rectangular waveguides (RWG) are a common method of low loss propagation of electromagnetic waves. The research into compact and efficient waveguides has been considerable in the last few decades, allowing a large number of devices to come into use in the mm-wave spectrum. The most fundamental of these the rectangular waveguide (RWG) is today present in a wide range of applications from wireless local area networks to airborne radar and intelligent transportation systems. Unfortunately, rectangular waveguides and many other commonly used devices are by nature three-dimensional, and can be difficult to integrate with planar circuitry. Moreover, at the lower part of the mm-wave sector, RWGs have large dimensions and a considerable weight. To overcome these problems, several novel techniques relying on existing circuit fabrication have been proposed for the fabrication of waveguides. These have included low temperature co-

fired ceramics (LTCC) [40, 41], microwave laminates [42] and photoimageable thick films [43]. However, their 3-D nature can cause difficulties in manufacturing accuracy and planar circuitry integration.

There is an increasing need for microwave systems which use smaller sizes devices and enhance performance. Both resonator filter topology and dielectric substrate are important determiners of microwave volume and some of these filters' topologies require tight coupling. Recently, several techniques have been used to form substrate integrated waveguides (SIW) [44, 45]. These guides are dielectric filled and are formed from the substrate material. This has the benefit of simple integration with planar devices and a size reduction of $1/\sqrt{\varepsilon_r}$. These structures can be easily integrated with planar circuits and devices, and, furthermore, because they form dielectric filled waveguide, both the width and guided wavelength are reduced by a factor of $1/\sqrt{\varepsilon_r}$, where ε_r is the relative dielectric constant of the substrate material. Since these guides are formed from the substrate material, they are referred to as substrate integrated waveguides (SIW). Substrate integrated waveguides have clear advantages over RWGs including low cost, simple integration with planar devices, and a size reduction of a factor. However, even with this size reduction SIW are large at RF frequencies. In [46, 47] the authors demonstrated a substrate integrated folded waveguide (SIFW) that resulted in a further reduction in the size of SIWs.

In this thesis, we propose a substrate integrated folded waveguide (SIFW) based on the concept of the folded waveguide [1, 2].

2.8.1 Microstrip Filters with Cross-Couplings:

In this section, microwave filters realized with cross coupling structures are described briefly. New, cross-coupled planar filter structures have been proposed recently, including the microstrip dual mode [48] filter, the dual-plane multi-coupled line filters [49] and the microstrip square open-loop resonator filters [1], as shown in Figure 2-26.

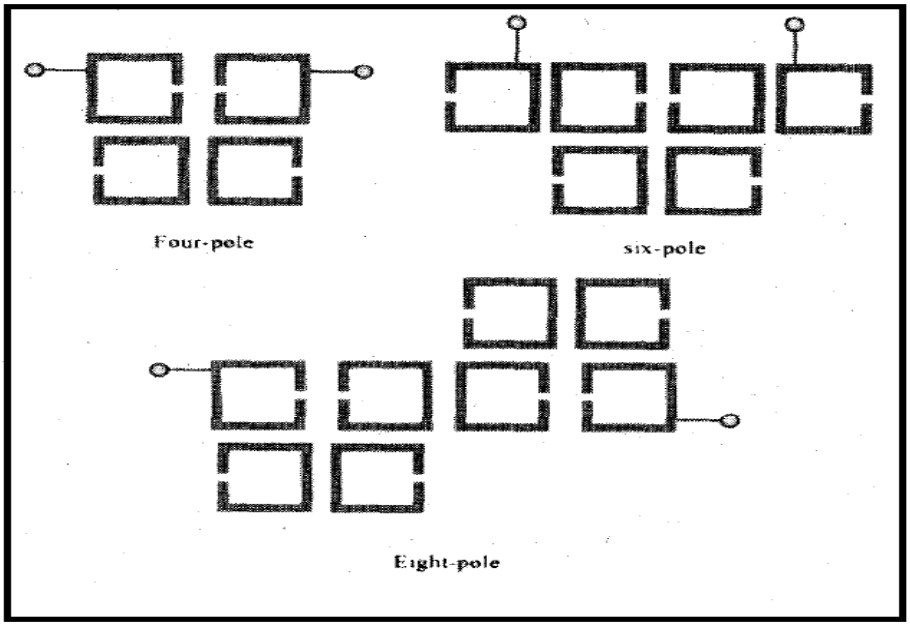

Figure 2-26: Some cross-coupled planar microwave bandpass filters comprised of coupled microstrip square open-loop resonators [32].

For the coupling structure of Figure 2-27, the electric and magnetic field distributions on the coupled arms of two resonators are comparative so that neither the electric coupling nor the magnetic coupling can be ignored. Hence, in this case the coupling may be referred to as the mixed coupling.

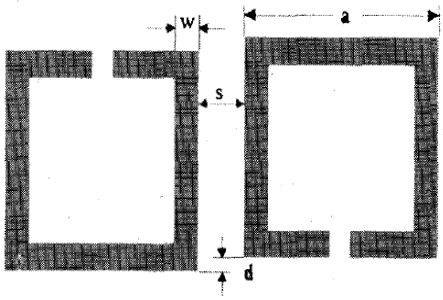

Figure 2-27: Mixed coupling structure .

Shown in Figure 2-28 are the typical resonant frequency responses of the mixed-coupled open-loop resonators. It can be seen that as the coupling spacing ‘s’ decreases, the two resonant peaks move outwards and the trough in the middle deepens, which implies an increase in the coupling [32].

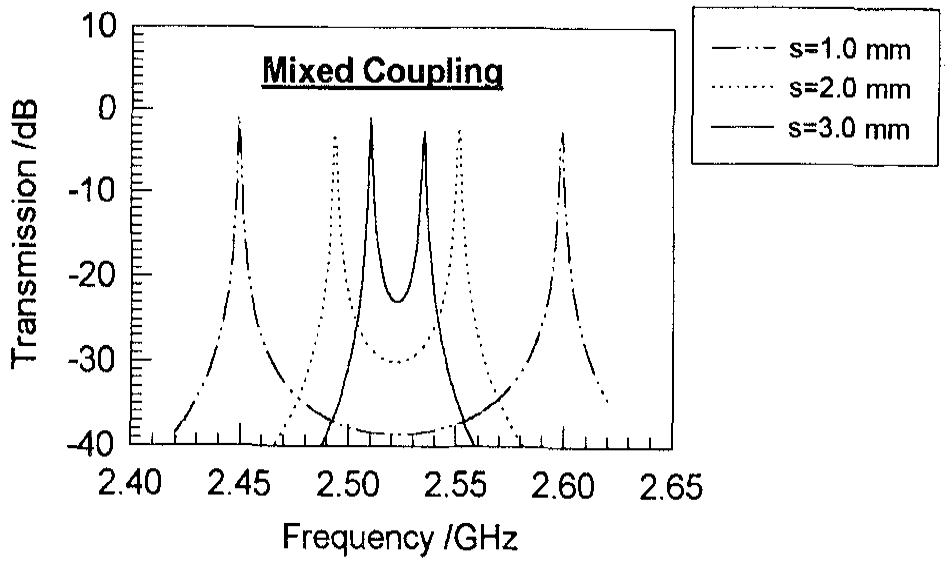

Figure 2-28: Typical resonant mode splitting phenomena of a mixed-coupled microstrip square open-loop resonator [32].

2.9 Dual-Band Filter

Recent developments in wireless communication and radar systems have presented new challenges to design and produce high quality miniature components with a dual-band operation. Advances in wireless systems have created a need for dual-band operation for microwave filters. Bandpass filters are important components of wireless systems as they enable band selection in RF transceivers; separating the different receiver functions of interest and isolating a specific band from interferers in dense wireless traffic. As wireless systems converge into common devices, it will be increasingly important to have miniaturized filters that can select more than one band at a time. One fabrication technology that has been demonstrated to be suitable for extremely compact filtering is low-temperature, co-fired ceramic (LTCC) [50, 51]. The synthesis method of a self-equalized dual-passband filter has also been presented [31, 52-54]. The coupling between two modified open-loop resonators is used to create a dual-band filter in microstrip technology [55]. Polynomial approaches and coupling matrices are applied to the design of dual-band bandpass [36, 56, 57] and bandstop filters [58] in waveguide technology. Other forms of dual-band bandpass filters have also been reported in [59-61].

2.10 Summary

From this background literature, the author learned about microwave resonators and their applications as filters in modern communications systems. In particular, he gained knowledge about cavity resonators and coupled waveguide resonators for filter applications. The developments, design trends and their aspects were surveyed during the background reading. In this chapter a review of some articles which show the benefits of using a cavity resonator were presented. The smaller size is being almost exclusively the improving factor in this stage that will be covered in further chapters. Once the background reading was completed, a thorough investigation of several configurations or improving the FWG resonator was made. It was deduced that the FWG performance improves with a smaller quality factor or similar of 736 with a smaller footprint. As a next step, the design method was very important stage of the author's that needed to be understood. In the next chapter the major design methods are discussed briefly and the conversion of a lowpass prototype filter to a bandpass filter is explained.

Chapter 3

Filter Design Methodologies

3.1 Introduction:

Once the background reading was completed, a thorough investigation of several configurations or improving the FWG resonator was made. The design method is very important stage to the author's to achieve his aim in the right and quickest way. In this chapter, the major design methods are discussed briefly.

3.2 Design method

Microwave filter design usually starts with a lowpass prototype filter with normalized impedance and frequency values. Based on a given specifaction, the filter approximation, i.e., Butterworth (maximally flat), Chebyshev (equal ripple), elliptic and generalised Chebyshev (pseudo-elliptic), are applied to approximate the ideal response and satisfy the design requirements. The lowpass prototype filter network can be transformed to practical microwave filter with one of the filter classifications that explained in section 2.3 in the previous chapter which are designed by system requirement. In order to derive these frequency characteristics, frequency and impedance transformations are used to convert the lowpass prototype design to the desired impedance level and frequency range. After the frequency transformations and the impedance scaling, the resultant networks are called lumped element filters. That method will be discussed in more details in section 3.2.3. Moreover the major design methods are discussed briefly.

3.2.1 Periodic Structures:

An infinite transmission line, or waveguide periodically loaded with reactive elements, is referred to as a periodic structure. As shown in Figure 3-1, periodic structures can take various forms, depending on the transmission line media being used. Often, the loading elements are formed as discontinuities in the line, but in any case they can be modelled as lumped reactance across a transmission line. Periodic structures support slow-wave propagation (slower than the phase velocity of the unloaded line), and have passband and

stopband characteristics similar to those of filters; their application may be found in travelling-wave tubes, masers, phase shifters, and antennas [7].

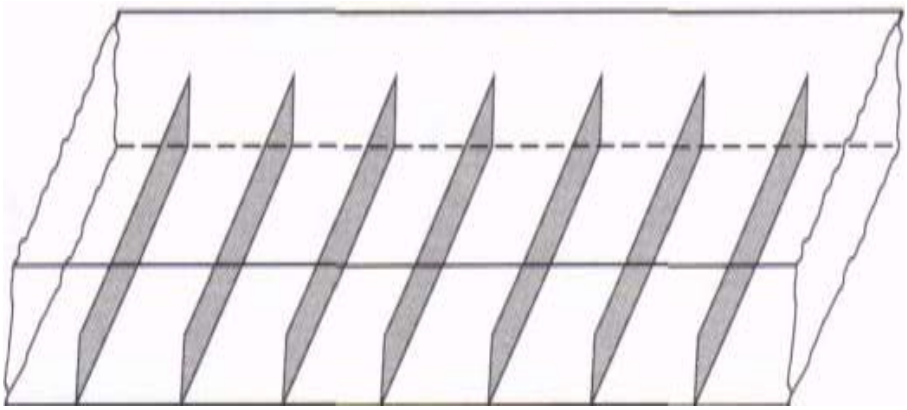

Figure 3-1: Periodic diaphragms in a waveguide [7].

3.2.2 Image Parameter Method:

The image parameter method of filter design involves the specification of passband and stopband characteristics for a cascade of two-port networks, and so is similar to the periodic structures that were studied in the previous section 3.2.1. The method is relatively simple but has the disadvantage that an arbitrary frequency response cannot be incorporated into the design. This is in contrast to the insertion loss method, which is the subject of the following section 3.2.3. Nevertheless, the image parameter method is useful for simple filters and provides a link between infinite periodic structures and practical filter design. The image parameter method also finds an application in solid-state travelling-wave amplifier design [7].

3.2.3 Insertion Loss Method

The perfect filter would have zero insertion loss in the passband, infinite attenuation in the stopband, and a linear phase response (to avoid signal distortion) in the passband. Of course, such filters do not exist in practice, so compromises must be made; herein lies the art of filter design. The image parameter method of the previous section 3.2.2 may yield a usable filter response, but not if there is no clear-cut way to improve the design. The insertion loss method, however, allows a high degree of control over the passband and stopband amplitude and phase characteristics, with a systematic way to synthesize a

desired response. The necessary design trade-offs can be evaluated to best meet the application requirements. If, for example, a minimum insertion loss is most important, a binomial response could be used; a Chebyshev response would satisfy a requirement for the sharpest cut off. If it is possible to sacrifice the attenuation rate, a better phase response can be obtained by using a 1inear phase filter design. And in all cases, the insertion loss method allows filter performance to be improved in a straightforward manner, at the expense of a higher order filter. The design process is illustrated in Figure 3-2. For the prototypes discussed in 3.2.3.2, the order of the filter is equal to the number of reactive elements [7].

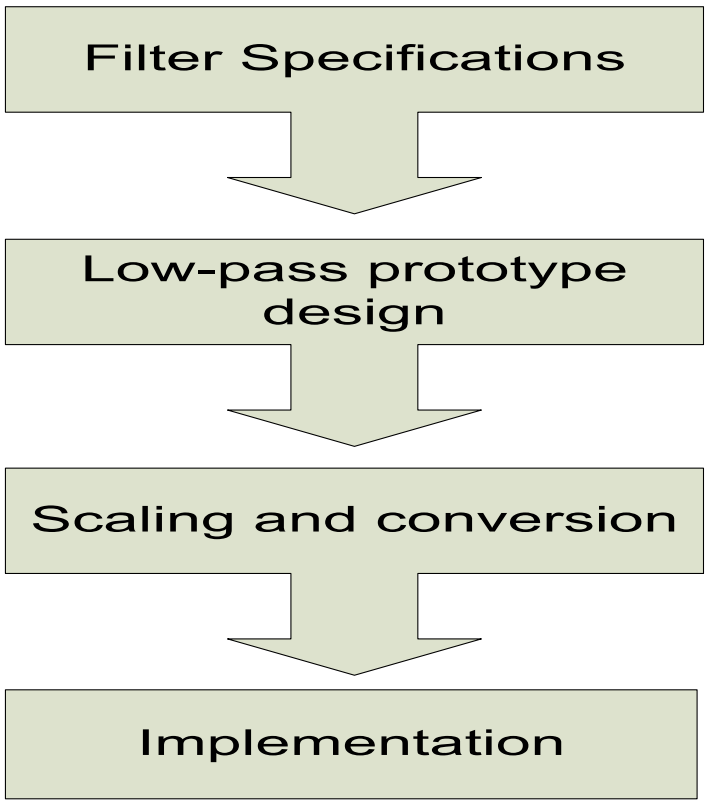

Figure 3-2: A block diagram showing the steps of filter design (insertion loss method) [7].

3.2.3.1 Low-pass Prototype Filters:

Bandpass filters serve a variety of functions in communication, radar and instrumentation subsystems. Of the techniques available for the design of bandpass filters, those techniques based upon the low-pass elements of a prototype filter have yielded successful results in a wide range of applications. Low-pass prototype elements are the normalized values of the circuit components of a filter that have been synthesized for a unique passband response and, in some cases, a unique out-of-band response [62]. Low-pass prototype filters are lumped element networks that have been synthesized to provide a

desired filter transfer function. The element values have been normalized with respect to one or more filter design parameters to offer the greatest flexibility, ease of use and tabulation. The elements of the low-pass prototype filter are the capacitors and inductors of the ladder networks of the synthesized filter networks, as shown in Figure 3-3.

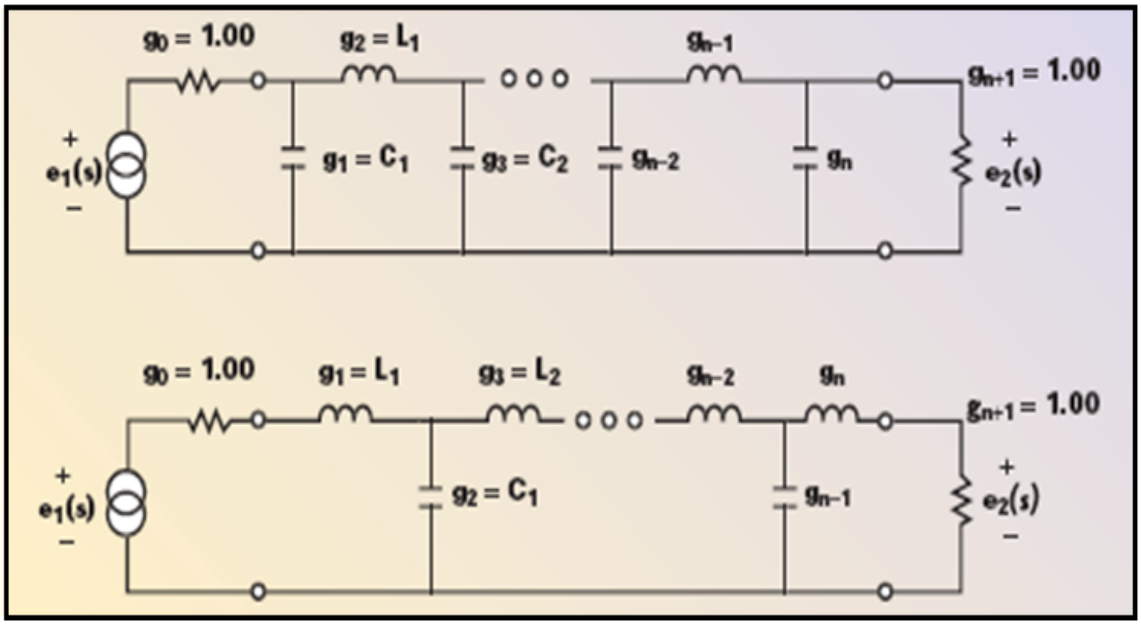

Figure 3-3: Elements of the low-pass prototype filter [62].

Usually, microwave filter design starts with a low-pass prototype filter. This is because:-

- The synthesis of a low-pass filter is easier
- Tabulated elements for low-pass prototype filters are available
- A low-pass prototype filter can easily be transformed to a practical filter, such as low-pass, high-pass, bandpass and bandstop filters [62].

3.2.3.2 Low-pass Converted to a Bandpass:-

A low-pass filter may be converted to a bandpass filter by employing a suitable mapping function. A mapping function is simply a mathematical change of variables such that a transfer function may be shifted in frequency [62]. The mapping function may be intuitively or mathematically derived. A known low-pass to bandpass mapping function may be illustrated mathematically, where:

$$f' = \frac{f_0}{\Delta f}\left(\frac{f}{f_0} - \frac{f_0}{f}\right) \quad (3\text{-}1)$$

$$\Delta f = f_2 - f_1 \quad 3\text{-}2)$$

where:

$f_0 = \sqrt{f_1 f_2}$, $\Delta f = f_2 - f_1$ and f_0, f_1 and f_2 represent the centre, lower cut off and higher cut off frequencies of the corresponding bandpass filter, respectively.

3.3 Summary

This chapter summarizes the three designed methods. The first design method is image parameter method that involves the specification of passband and stopband characteristics for a cascade of two-port networks, and so is similar to the second design method which is the periodic structures that relatively simple but have the disadvantage that an arbitrary frequency response cannot be incorporated into the design. The third design method is the insertion loss method that could let the engineers to has zero insertion, infinite attenuation in the stopband, and a linear phase response in the passband. Thus, the insertion loss method is the convenient method to design a filter that will be used in this thesis. Filter specifications were then set to design and fabricate a filter, in order to validate the maximum improvement. Designed and discussed of folded cavity resonator FWG can be found in more details in the following chapter.

Chapter 4

Folded Waveguide (FWG) Resonator

4.1 Introduction

Once the analysis of the convenient design method has been chosen from the previous chapter in section 3.2. In this chapter, we will be concerned with improvement and implementation of folded waveguide FWG resonator, as presented in [1] in different manner. Moreover, we will evaluate different structures for the realization of microwave cavities with high-Q, the result of which will be a high spurious free range and a reduced footprint. The most important, in this chapter a novel folded waveguide resonator with about a 75 % reduction of the volume from conventional size will be described. For comparison, two types of folded waveguide resonators have been studied, i.e. the square-shaped quarter-wavelength resonator and the newly proposed triangular shape. In addition, demonstrators of a filter application of miniature triangular folded waveguide resonators have been designed and simulated using an EM simulator.

4.2 Miniature Folded Waveguide FWG Resonators Realization

In this section, we propose a new miniature triangular folded waveguide resonator, which has only a half of the footprint of the square folded waveguide resonator [1]. A comparison study is carried out for these two different shapes of FWG resonators, and they are evaluated by full-wave EM simulation and experiments. For filter applications, a preliminary investigation is also presented with a compact 2-pole bandpass filter consisting of two triangular folded waveguide resonators. For our description, Figure 4-1 duplicates a folded waveguide quarter-wavelength resonator for both designs; Figure 4-1 (a) shows a square folded waveguide quarter-wavelength resonator, and the proposed triangular version is shown in Figure 4-1 (b), where two orthogonal slots on the common metal plate allow the standing waves to be folded and continued over the bottom and top halves of the cavity.

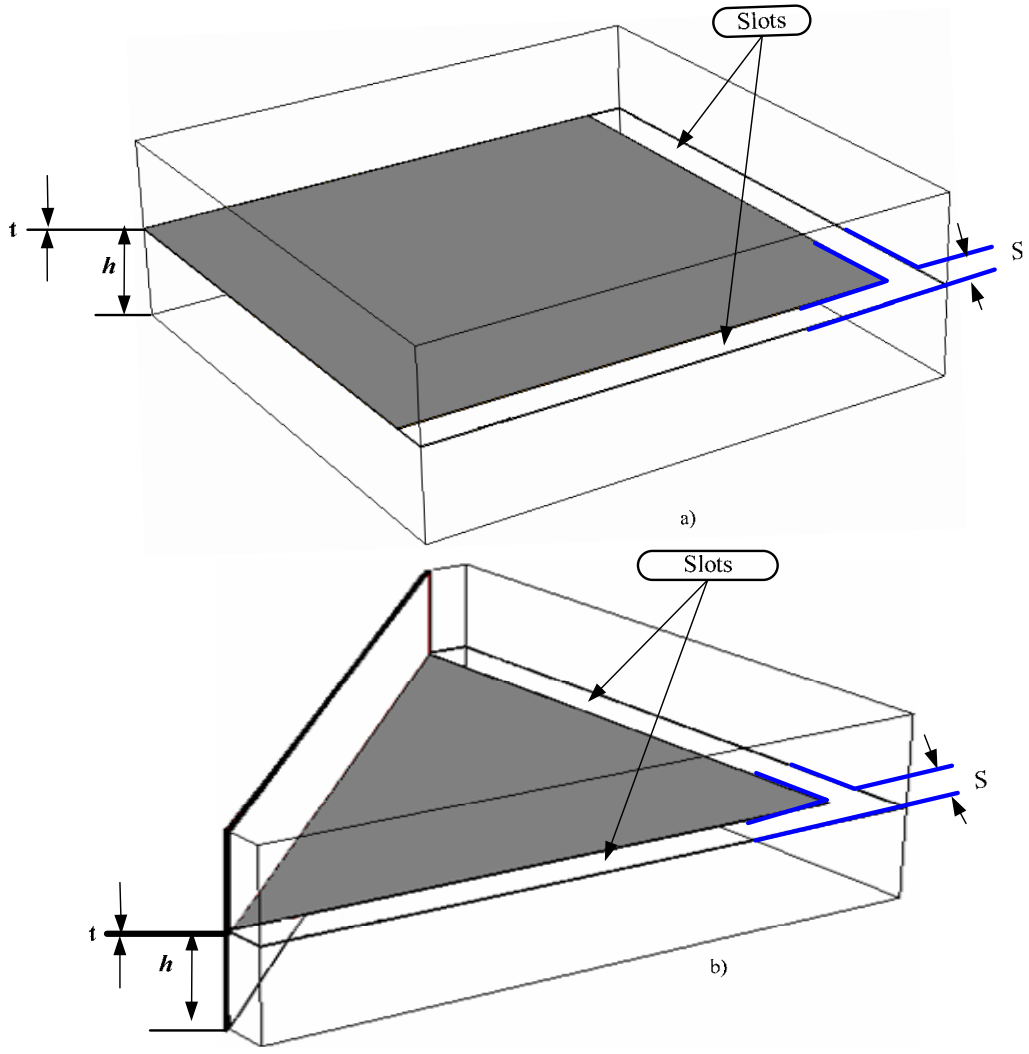

Figure 4-1: - (a) Square folded waveguide quarter-wavelength resonator. (b) Triangular folded waveguide quarter-wavelength resonator.

The investigation involved experimenting with the variance of the common metal plate thickness (t), the fixed height and distance between the wall, and the common plate of h = 3.5mm and S = 1.5mm, respectively. Thinner metal plate can be easier shaped, resulting in a metal-loaded cavity with smaller volume and mass. It is found that there is not much difference in the quality factor for different values of (t) as long as the metal plate thickness is much larger than the skin depth. For our investigation, the skin depth of the conductor (brass) is about 1.8 um at resonant frequency. Further investigation was carried out to reduce the size of the square folded waveguide quarter-wavelength resonator while obtaining a better or similar Q. To this end, a triangular folded waveguide resonator was designed with a size of a reduction of 75 % from the conventional waveguide resonator and near 50% from the square folded cavity

resonator while the measured unloaded Q is 658 of the square FWG resonator, taht is lower than the triangular FWG resonator which has 535. The miniature folded waveguide resonator has been investigated in the light of a commercially available electromagnetic (EM) simulator [63]. The comparison of the original EM fields for the two FWG resonator designs is illustrated in Figure 4-2, where Figure 4-2 (a) is the current distribution and Figure 4-2 (b) is the charge distribution. It is apparent that both the triangular and square FWG resonators have stronger currents along the two orthogonal edges of the metal plate and a maximum charge at the same corner. The similarity in the field distribution suggests a similar quality factor, which has been shown by EM simulation as well. Thus, the triangular FWG resonator has a smaller size whilst not degrading the quality factor.

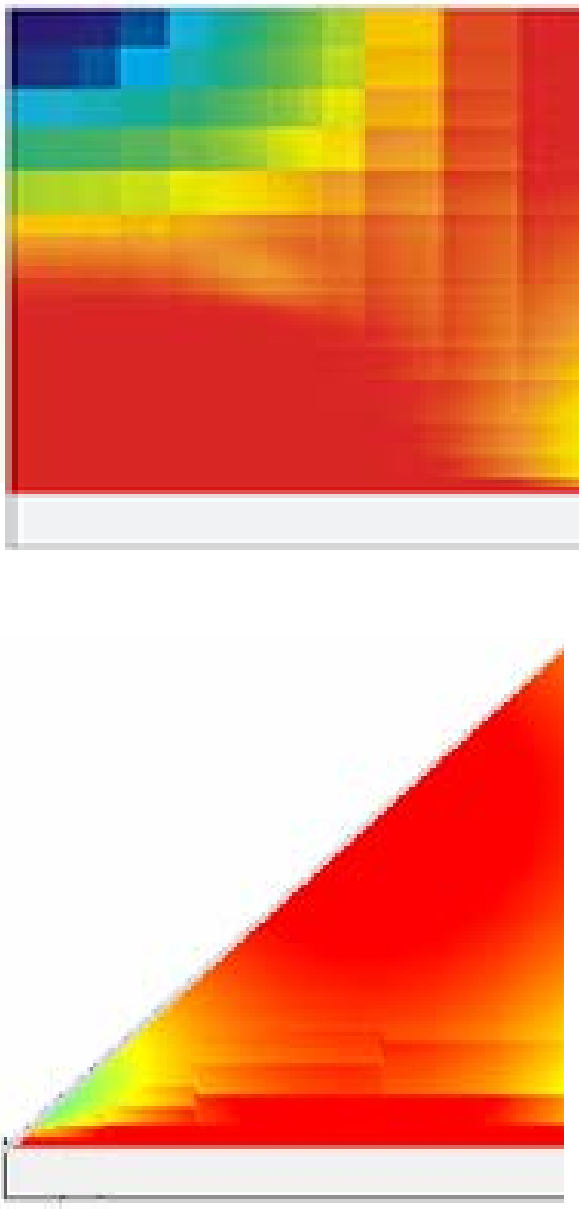

(a) Current

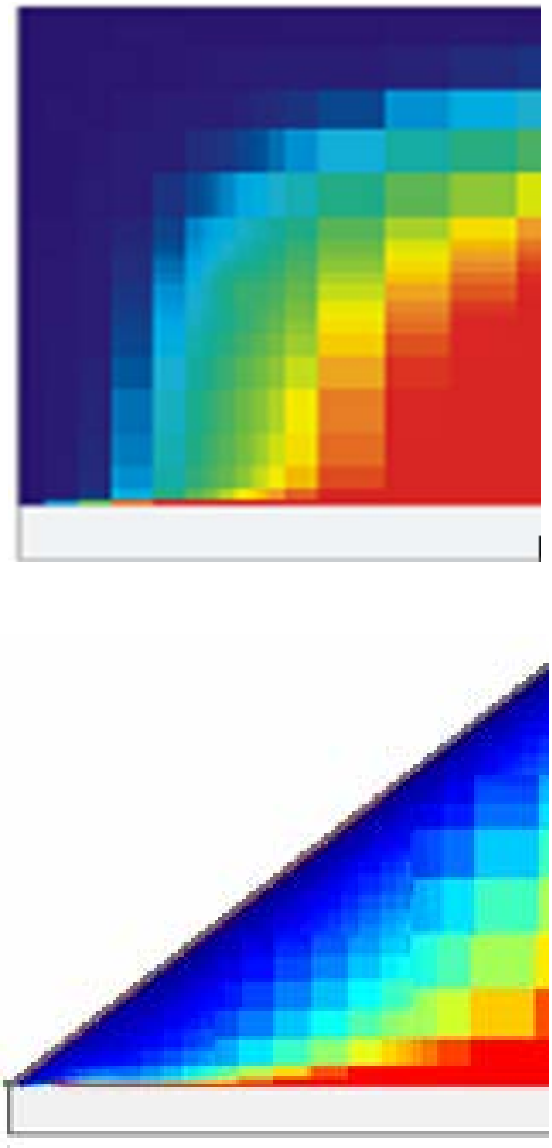

(b) Charge

Figure 4-2 Field distribution of the square and triangular folded waveguide quarter-wavelength

4.3 Fabrication and Experimental Results of Miniature FWG Resonators

For the demonstration, the square and triangular FWG resonators were fabricated from an industrial brass material. Figure 4-3 and Figure 4-4 show the components of the fabricated square and triangular FWG resonators, respectively. The square and triangular designs are comprised of two identical halves, and these are shown in Figure 4-3 (a) and Figure 4-4 (a), respectively. The two halves with a recess of 3.5 mm are separated by a common brass plate, shown in Figure 4-3 (b) and Figure 4-4 (b). The common separated plate is inserted as shown in Figure 4-3 (c) and Figure 4-4 (c). Finally, the completely assembled resonators, as illustrated in Figure 4-3 (d) and Figure 4-4 (d), have a size of 26mm×26mm including 6mm-thick walls along all sides.

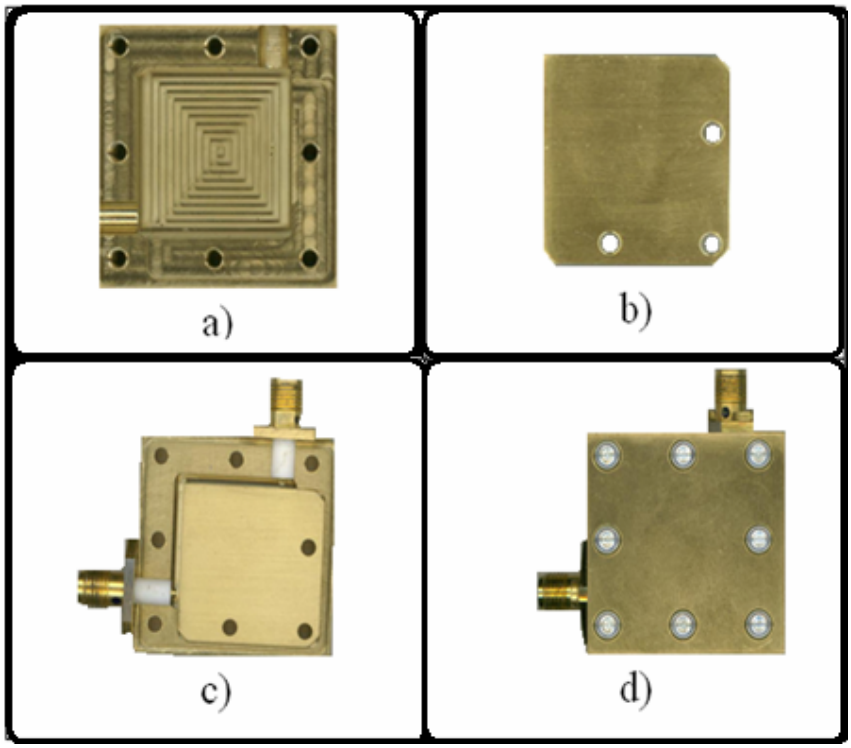

Figure 4-3 A fabricated single square FWG resonator before assembly (a, b and c) and after assembly (d).

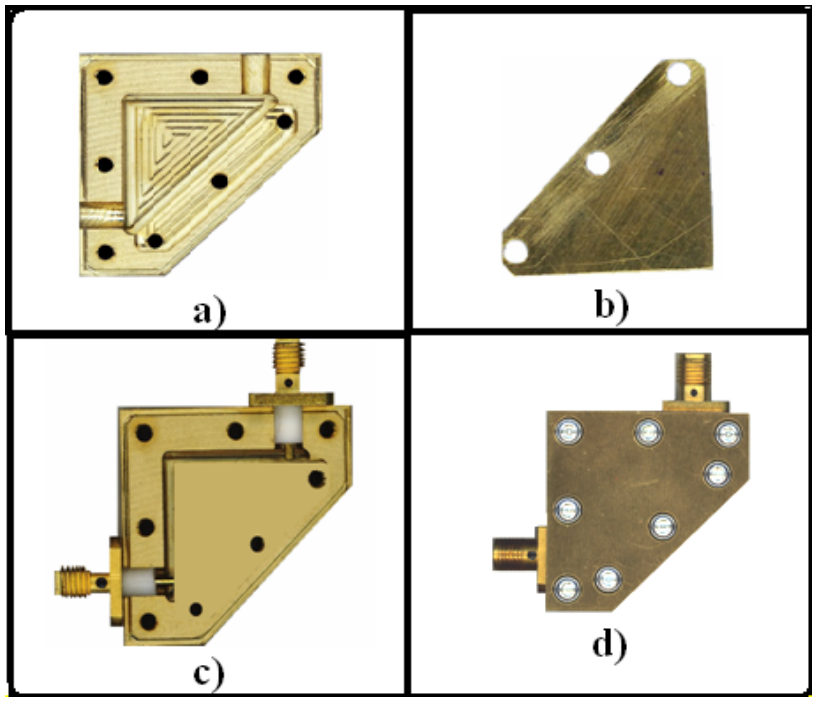

Figure 4-4 A fabricated single triangular FWG resonator before assembly (a, b and c) and after assembly (d).

Table 4-1 shows the simulation and experimental results comparison of the resonant frequency and unloaded Q of the folded waveguide resonators, as a function of the cavity type.

Table 4-1: The experiment with a difference in cavity.

Cavity type	Simulation		Experimental	
	f_0	Q_u	f_0	Q_u
Square	4.8	735	4.746	658
Triangular	4.8	695	6.09	535

There is an experimental unloaded quality factor similarity between the square and triangular cavity resonators in Table 4-1. The measured unloaded quality factors are, as expected, similar, with a size of reduction of about 75 % from the conventional waveguide resonator and near 50% from the square folded cavity resonator. Furthermore, in this experimentation the thickness of a common metal plate of square cavity resonator has been varied. Table 4-2 shows the comparison of the resonant frequency and unloaded Q of the folded waveguide resonators, as a function of the thickness of the common metal plate (t). For all the cavity resonators, the conductor is brass.

Table 4-2: The experiment with different thicknesses of common plate.

Common plate thickness (t) mm	Experimental	
	f_0	Q_u
1	4.75	658
0.05	4.889	678

It is clear from Table 4-2 that there is a similarity in the experimental unloaded quality factor between (1 mm and 0.05mm) thicknesses of the common plate. The measured unloaded quality factors are similar, as expected. This is because in both cases the metal plate thickness is much larger than the skin depth. With the higher thicknesses, there is a core region of the plate that does not contribute to the actual current flow because of the skin depth. So, when the thickness is reduced from 1 mm to 0.05 mm, the cross section area available for the current flow is still same. Hence, the losses are almost same. However, if the thickness of the plate is reduced to an extent less than the skin depth, then that will dramatically increase the losses and affect quality factor.

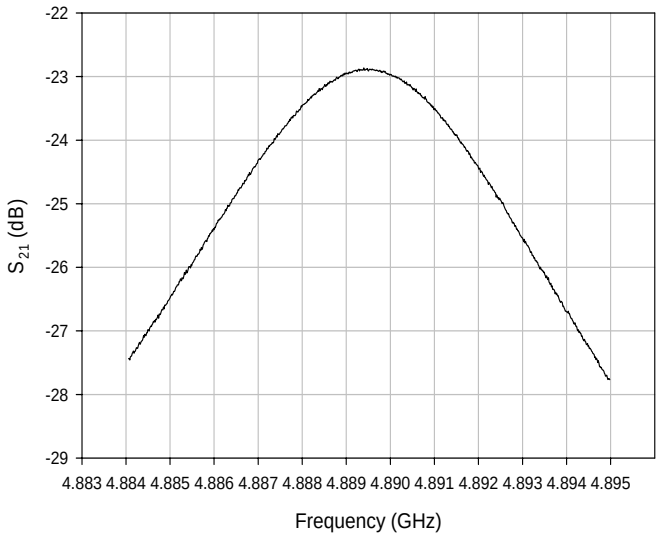

Figure 4-5 Measured resonant frequency response of the FWG resonator.

The S-parameters of the fabricated FWG resonators were measured using a calibrated HP network analyzer. Figure 4-5 plots the measured resonant frequency when the common plate thickness is 0.05 mm. The experiment was also carried out to measure the wideband frequency response of the demonstrator, and the measured result is plotted in Figure 4-6.

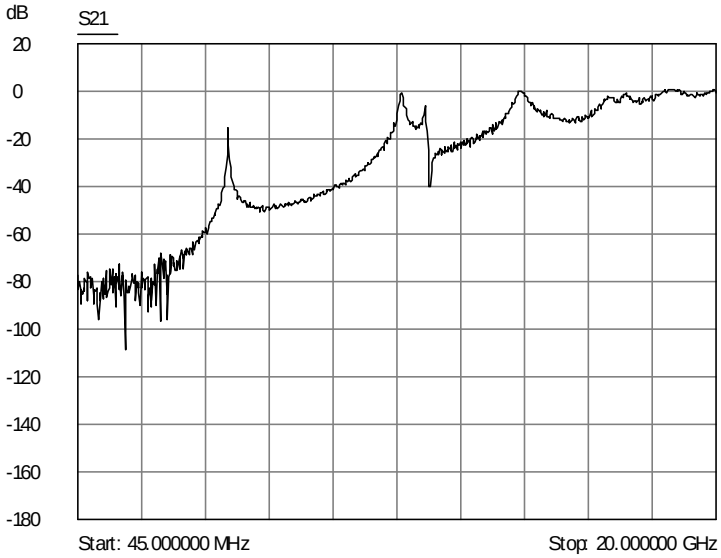

Figure 4-6: Measured wideband frequency response of the fabricated FWG quarter-wavelength resonator.

4.4 Filter Realization and Simulation of Miniature FWG Resonator

Figure 4-7 shows 3D model of a 2-pole filter with coupled triangular FWG resonators. A typical simulated frequency response of coupled folded waveguide resonators is plotted in Figure 4-8. In this case, the coupling aperture is 3.6 mm wide; each of the coupled cavities has a size of 21 x 21 x 6 mm and two 1 mm wide orthogonal slots

inserted in the metal plate. As can be seen from that Figure, two split mode frequencies (resonant peaks) are observable. Denote these two split frequencies as f_1 for the first peak and f_2 for the second peak. The coupling coefficient can then be evaluated by:

$$k = \frac{f_2^2 - f_1^2}{f_2^2 + f_1^2} \tag{4-1}$$

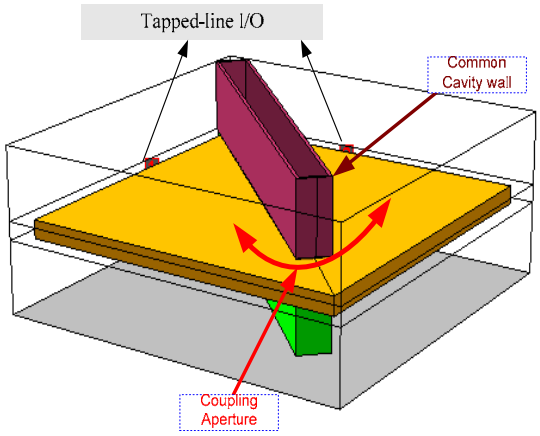

Figure 4-7 3D model of a 2-pole filter with coupled triangular FWG resonators.

It can be shown that the coupling can easily be controlled by the size of the aperture, and the coefficient k is larger when the coupling aperture becomes wider. The first split mode was measured at f_1 = 5.66 GHz while the second one was at f_2 = 5.95 GHz. This results in a coupling coefficient k = 0.05. The filter was designed to have a bandwidth of 470 MHz at 6035 MHz, representing a fractional bandwidth of about 7.78%. The full-wave simulations were carried out to confirm the design, and the results plotted in Figure 4-9. Full wave EM simulations were performed to characterize the coupling.

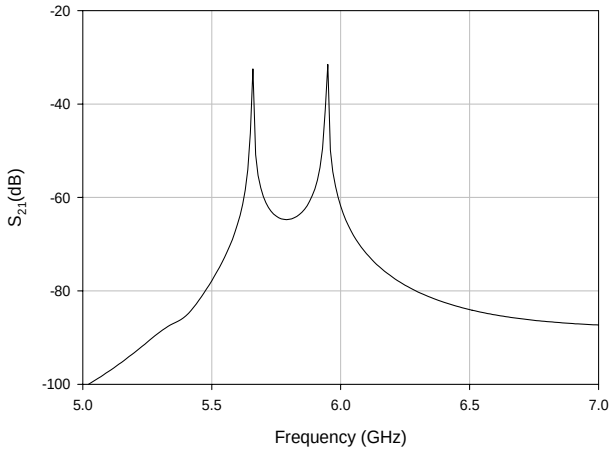

Figure 4-8. Simulated frequency response of the coupled triangular FWG resonators.

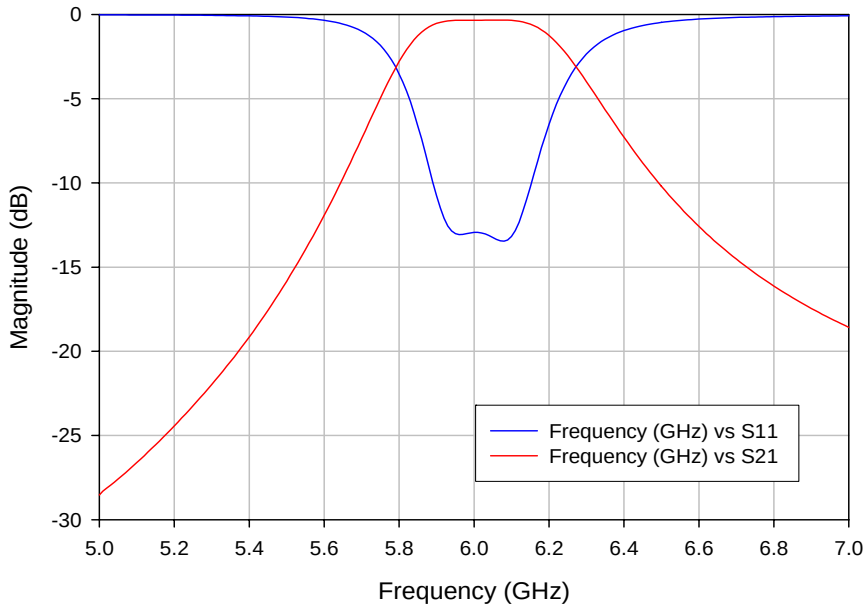

Figure 4-9 Performance of the compact and low-loss filter using miniature FWG resonators.

4.5 Summary

This chapter aims to describe of the development of FWG resonator. A new proposed triangular folded waveguide resonator with about a 75 % reduction of the volume from conventional size about a half of the footprint of the square folded waveguide resonator has been describe. A Comparison study has been carried out to demonstrate the small size and high Q of this type of resonator. The full-wave EM simulations have been verified the mode operation. In this chapter, a preliminary investigation into a filter application for miniature triangular folded waveguide resonators has also been presented. It is expected that this type of resonator will be very attractive for developing compact waveguide filters that will be discussed in the next chapter.

Chapter 5

Coupled Folded waveguide (FWG) Filter using Slot technique

5.1 Introduction

The next aim of the work was to show the benefits of the achieved improvement in FWG resonator's structure. A fully FWG resonator was designed as an illuminating example of the benefits of that resonator's structures in chapter 4. In this chapter, we will be concerned with the design of coupled folded waveguide resonator FWG filters. This includes a primary investigation into developing a compact and low-loss bandpass filter, using novel folded-waveguide resonators with a footprint reduction. A slot coupling between adjacent resonators is introduced, which is characterized by using full-wave EM simulations and verified experimentally. Two designs of 2-pole folded waveguide resonator filters of this type have been considered, fabricated and tested. Simulation and measurement results are presented to validate the design and to show the advantages of this type of filter. Moreover, in this chapter, an even more compact FWG resonator filter using a novel slot technique is reported. The attainable size reduction is about 50%, and the filter design is based on theoretical and full-wave electromagnetic (EM) simulations. It shows that a transmission zero (TZ) on either high or low side of the passband can be implemented in a simple manner, which leads to a pair of asymmetrical frequency responses. Two filter designs of this type are demonstrated with theoretical, EM-simulated and measured results.

Furthermore, this chapter presents a primary investigation into developing a compact dual passband filter using novel folded-waveguide resonators with a multilayer structure. A new coupling scheme for dual-band operation is realized, with both slot and aperture couplings used for the implementation. For the demonstration, a 4-pole dual-band filter of this type has been designed, fabricated and tested. Simulation and experimental results are presented to validate the design and to show the advantages of this type of filter. Moreover, the investigation of a multilayer of dual passband filter using a slot technique with substrate integrated folded waveguide (SIFW) material has been tested.

5.2 FWG filter using a Slot technique

The proposed filter configuration is shown in Figure 5-1 , where a slot with the length *SL* is introduced onto an inserted metal plate of an otherwise quarter-wavelength FWG resonator. The metal plate has a thickness of *t* and the upper and lower air-filled half cavities have a depth of *h*/2. Owing to the new slot introduced, a pair of resonant modes, which have the same resonant frequency, can be excited. Thus, a 2-pole filter can be developed based on this compact structure, whose size is only about half of a same order filter using the two quarter-wavelength FWG resonators reported previously in chapter 4, resulting in a significant size reduction. Moreover, the new filter configuration of Figure 5-1 (a) can easily realize an advanced coupling structure (as seen in Figure 5-1 (b), bringing about some interesting filtering characteristics.

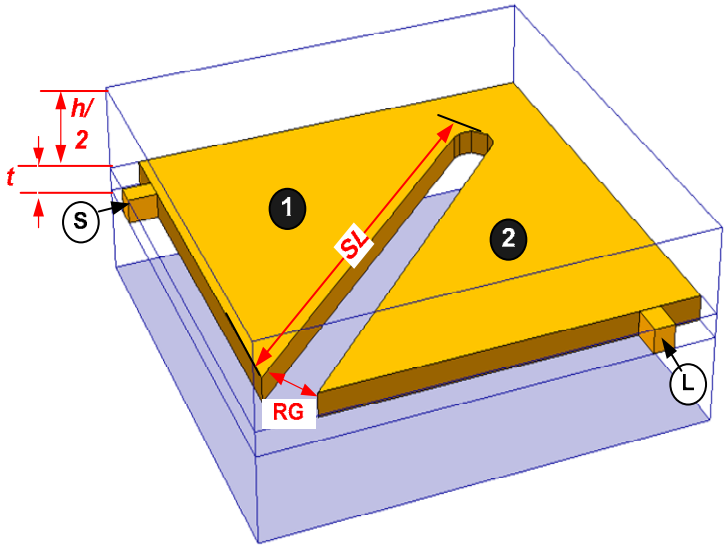

(a)

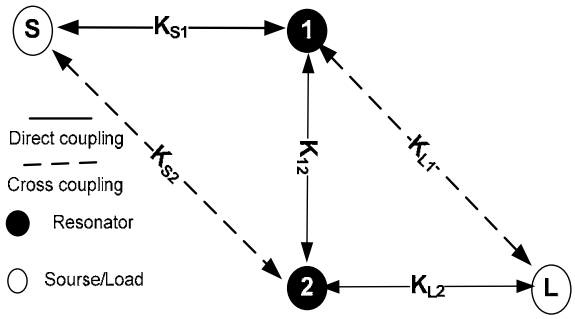

(b)

Figure 5-1 : a) Configuration of a 2-pole folded-waveguide resonator filter using a slot technique; where *t* is the thickness of the separation plate, and *h/2* is the depth of the upper and lower cavities. b) Coupling structure for the filter.

In the coupling structure of Figure 5-1 (b), the input (S) and output (L) are coupled to both resonators and there is one direct coupling between adjacent resonators, denoted by K_{12}. This coupling is realised through the opening slot between the adjacent FWG resonators 1 and 2, and can be easily controlled by a slot, denoted by G in Figure 5-1 (a). In order to design a 2-pole cavity resonator filter with TZ from either side with the aim of reducing its footprint, the following sections deals with theory, simulation and implementation of two designs of coupled folded waveguide (FWG) resonator filter with TZ for either high or low side band, respectively. Moreover their frequency response will be discussed in more details in this chapter.

5.2.1 Theoretical analysis

To design any filter with good accuracy, we must start with theoretical analysis. In this section the proposed designs are a two-order asymmetric response filter with one transmission zero located in either sides to the passband filter. A synthesis method of coupled resonator filters with the source/load-multi-resonator coupling proposed in [64] may be used. Based on the coupling structure of Figure 5-1 (b) and taking advantage of the changeable sign of K_{12} against the slot length, the proposed filter configuration of Figure 5-1 (a) can be designed to have a finite-frequency transmission zero (TZ) on either side of the passband; resulting in an asymmetrical frequency selectivity. For our demonstration, two generalized coupling matrices, with TZ on the high side of the passband and TZ on the low side of the passband, are given by M1 and M2, respectively:

$$M1 = \begin{bmatrix} 0 & 1.02 & 0.065 & 0 \\ 1.02 & 0 & 1.25 & 0.065 \\ 0.065 & 1.25 & 0 & 1.02 \\ 0 & 0.065 & 1.02 & 0 \end{bmatrix} \tag{5-1}$$

$$M2 = \begin{bmatrix} 0 & 1.02 & 0.065 & 0 \\ 1.02 & 0 & -1.125 & 0.065 \\ 0.065 & -1.125 & 0 & 1.02 \\ 0 & 0.065 & 1.02 & 0 \end{bmatrix} \tag{5-2}$$

M1 and *M2* are the so-called *n*+2 coupling matrices [65], which involve the nodes for the source (S) and load (L), with *n* the degree of filter. In our case, *n* = 2. Comparing *M1* with *M2*, one can note that the only difference lies in the elements that are related to K_{12}. It will be shown later that this difference can be implemented with two filters that

are similar in size except for the slot length. As a consequence, they exhibit opposite frequency selectivity. Both filters are designed with a commercially available electromagnetic (EM) simulator[31, 63]. The theoretical responses using these two coupling matrices will be demonstrated, along with the EM simulation and experiment results in sections 5.2.2 and 5.2.3 respectively.

5.2.1.1 TZ from the High side:

Initially, the design was started with a coupled folded resonator filter with TZ in the high side band. For the symmetrical design, the TZ located in the high side band was caused by either a cross coupling between the (source and Resonator 2) or (Load and Resonator 1) S2 and L1, respectively. Figure 5-2 shows the theoretical response of TZ in the high side band.

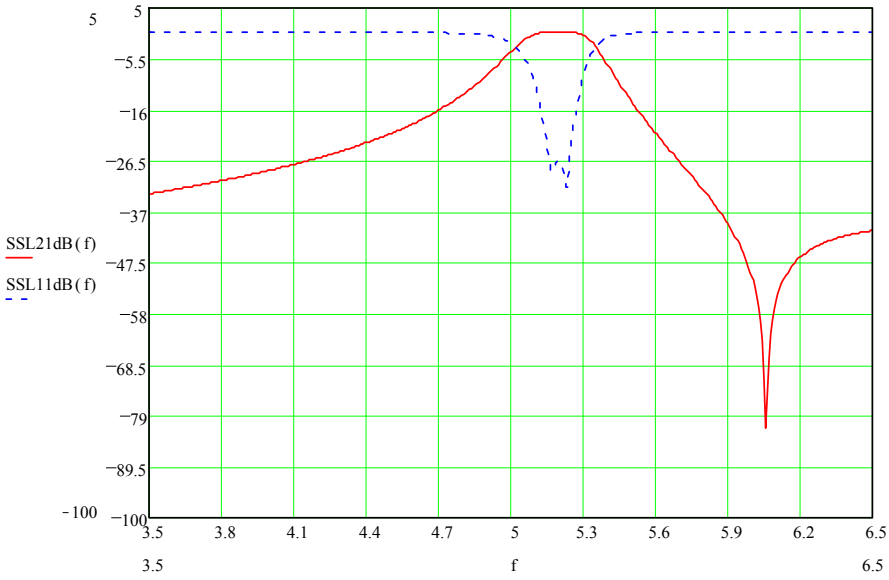

Figure 5-2: Theoretical Responses of the filter with TZ in the High side band.

The requirement of this filter design is f_0 = 5.2 GHz and a fractional band width FBW of 7.5% will be designed. Using the design parameters obtained from the matrix [M1], the implementation of the filter is carried out in several steps, that will be described in section 5.2.3. The phase response of this filter that was also carried out is shown in Figure 5-3.

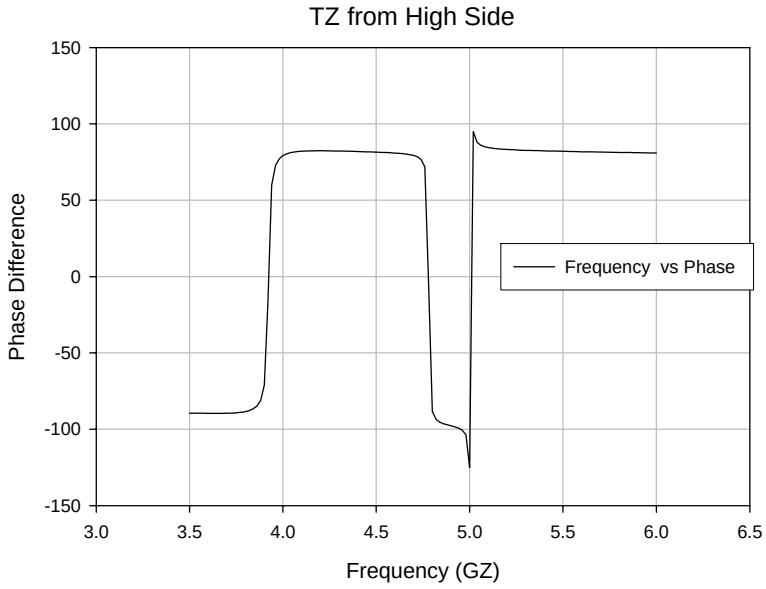

Figure 5-3: Phase Response of the filter with TZ in the High side band.

5.2.1.2 TZ from the Low side:

The second design is a bandpass filter with TZ located in the low side band. In order to achieve that the negative coupling between the adjacent resonators 1 and 2 is introduced in the coupling matrix 5-2. The resulting shifted in the TZ from the high side to the low side band is shown in Figure 5-4. The specification of this filter is f_0 = 4.9 GHz with a fractional band width FBW of 7.0%.

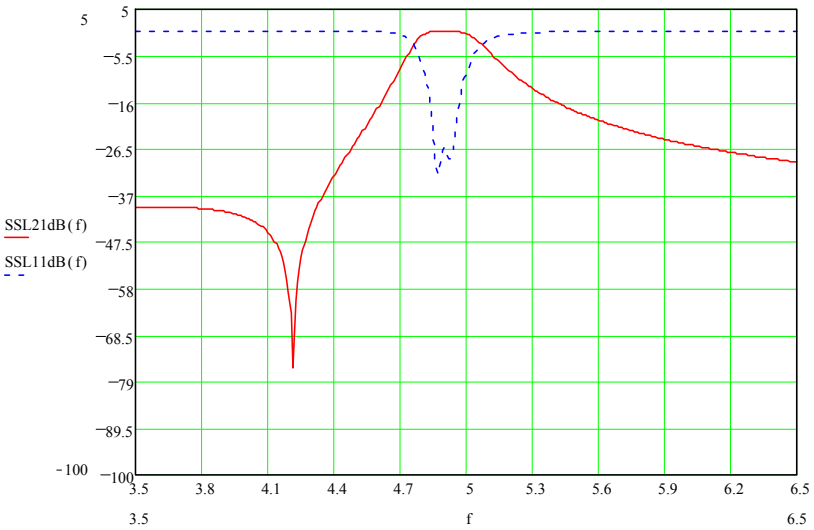

Figure 5-4: Theoretical Responses of the filter with TZ in the Low side band.

Moreover, the phase response for this filter has been shifted by 180, as shown in Figure 5-5. The implementation of the filter is carried out in several steps, that will be described in section 5.2.3.

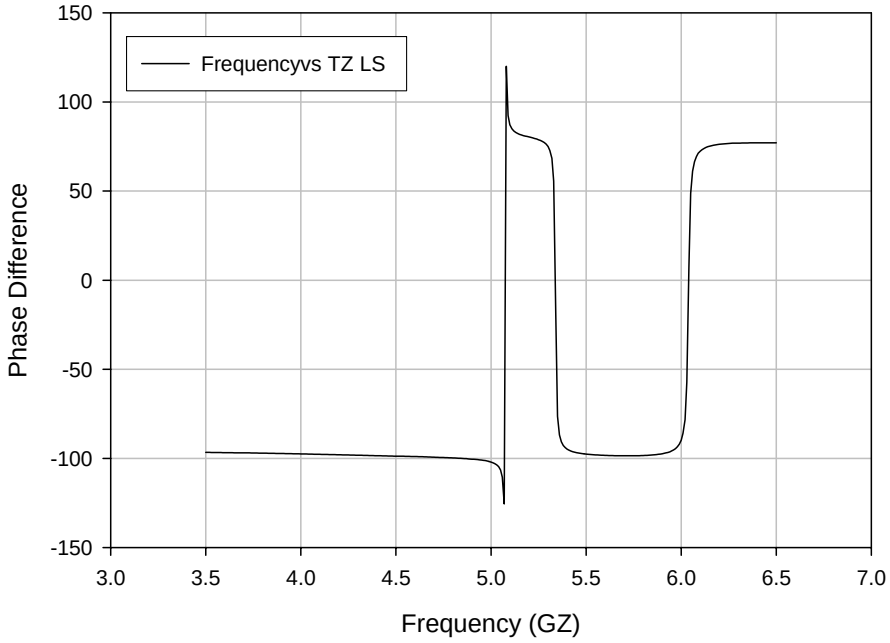

Figure 5-5: Phase Response of the filter with TZ in the Low side band.

5.2.2 Modelling of the FWG filter using a slot technique

Based on requirements, the plan was divided into many stages. In the first stage, the slot in the separation plate was introduced, then the length of the slot was increased until met the required result. Followed by, the length of the coupling gap between the resonators was varied in order to control the BW of the filter and attain the required coupling coefficients K_{12} to get an approximate design for the 2-pole resonator filter with a slot in the separation plate that could be used in the further stage. The proposed bandpass filter configuration and its coupling structure are shown in Figure 5-6. The filter was designed and implemented using 2-pole folded-waveguide resonators. In Figure 5-6, RG is the coupling gap between adjacent resonators, *t* is the thickness of the separation plate, *h/2* is the depth of the upper and lower cavities, and *SL* is the length of the slot.

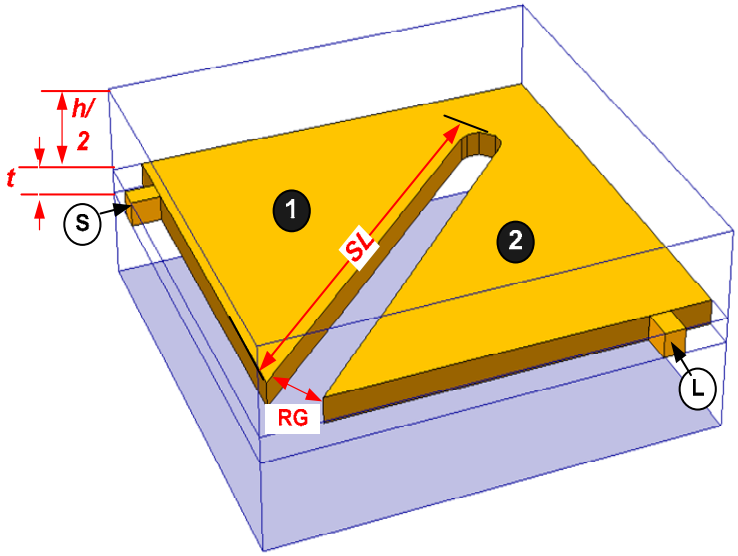

(a)

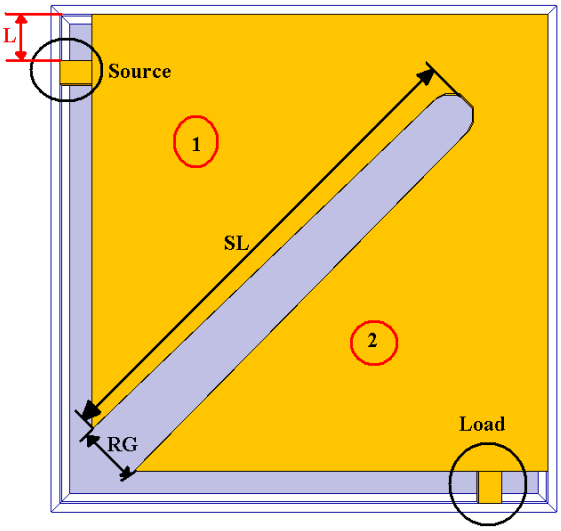

(b)

Figure 5-6: Layout for bandpass filter design (a) Side View, (b) top View.

5.2.2.1 Design and modelling of the FWG filter using a slot technique:

The initial idea came from the square folded waveguide quarter-wavelength resonator design that discussed in chapter 4 section 4.2 which is carried out to in this chapter to be a reference model This involved experimenting with varied cavity dimensions, e.g. Slot Length (SL) and Resonator Gap RG, and the Length excitation port location (L), as shown in Figure 5-6 and that will be explained in more details later in this chapter. In this section, the simulation results were carried out for 1-pole and 2-pole resonator filters which were based on the design shown in Figure 5-7 until the required design is achieved.

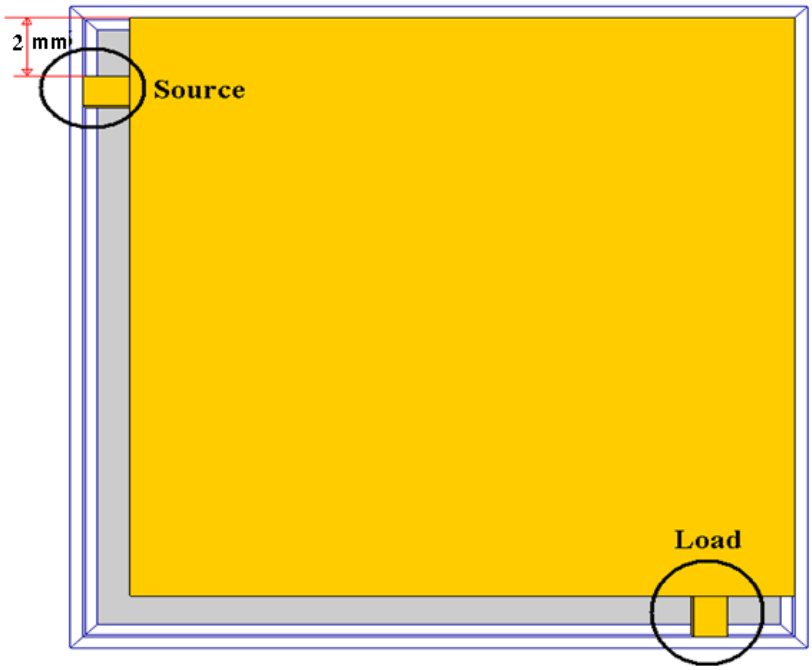

Figure 5-7 1-pole resonator filter.

The following Figure 5-8 shows the results that were obtained when the length of excitation port L = 2 mm, and before any slot introduced in the separation plate which means there is no resonator gap *RG* between resonators.

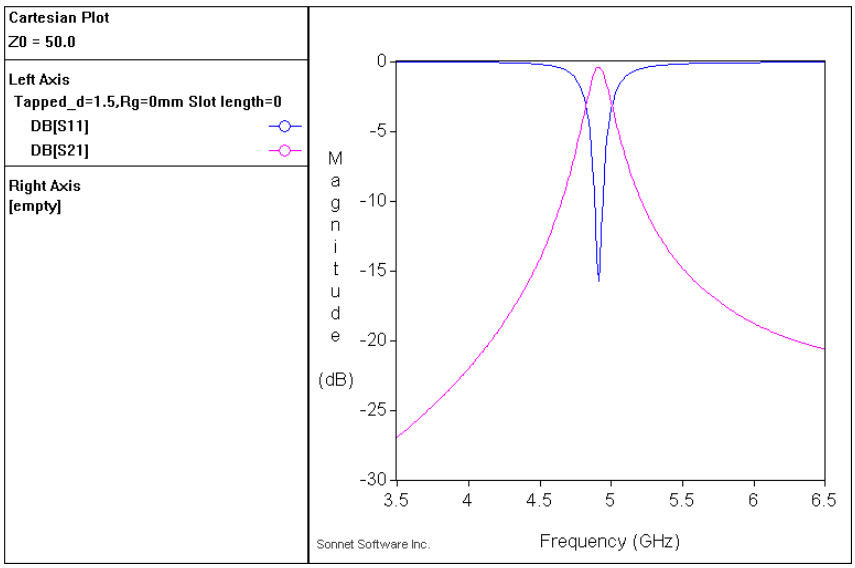

Figure 5-8: Frequency response for a 1-pole resonator.

5.2.2.2 Design (1) TZ in the high side band

The best simulation design of the bandpass filter with TZ in the high side band (which was submitted to the mechanical workshop for fabrication) was chosen when *L* = 2mm, *SL* = 11.8 mm and *RG* = 1.8 mm that is shown in Figure 5-9 and its response is shown in Figure 5-10.

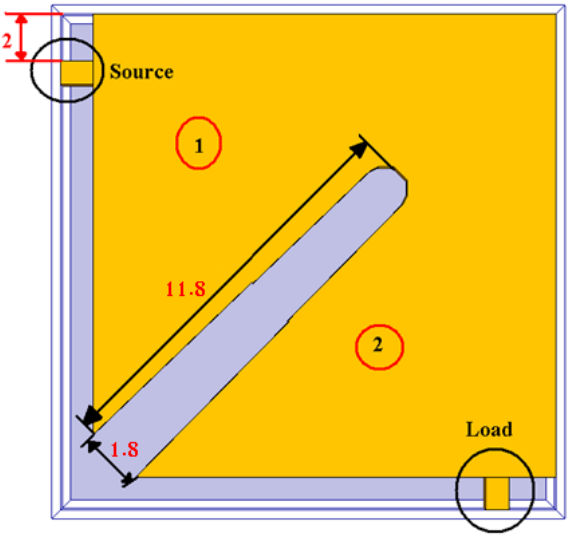

Figure 5-9: Layout of the best design of a 2-pole resonator filter with TZ in the high side band and its dimensions.

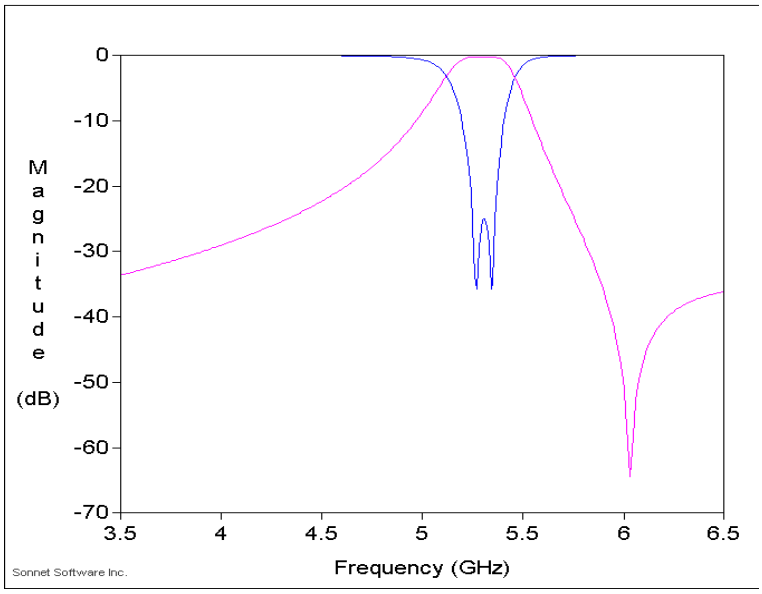

Figure 5-10 : The response of the best design of a 2-pole resonator filter.

5.2.2.3 Design (2) TZ from low side band

The best simulation design for the bandpass filter with TZ in the low side band (which was submitted to the mechanical workshop for fabrication) was chosen when L = 2mm, SL = 15.8 mm and RG = 1.8 mm and that is shown in Figure 5-11 and its response is shown in Figure 5-12.

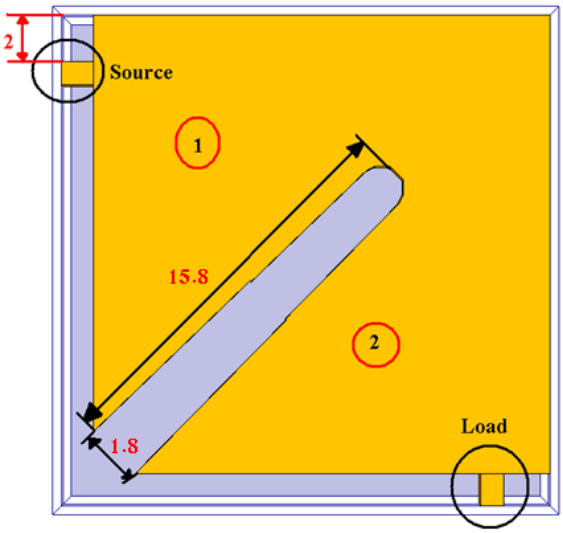

Figure 5-11: Layout of the best design of a 2-pole resonator filter with TZ in the low side band and its dimensions.

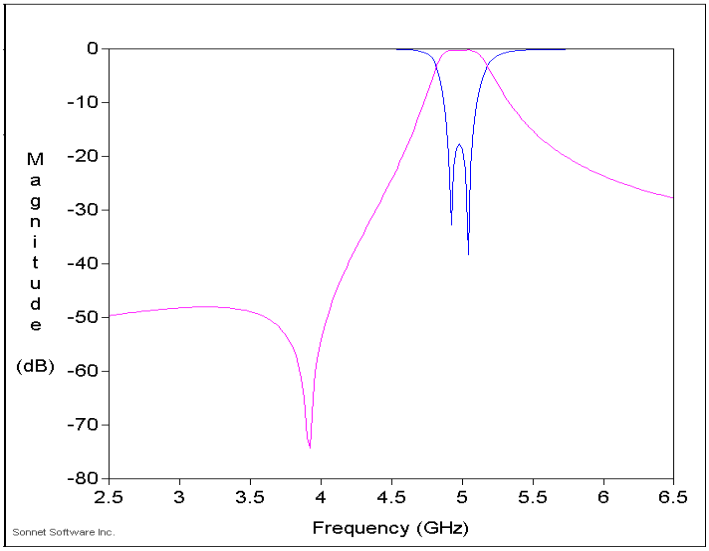

Figure 5-12: The responses of the best design of a 2-pole resonator filter with TZ in the low side.

5.2.3 Fabrication of the filter

In order to fabricate a 2-pole cavity resonator filter with TZ with a reduction on the footprint of the design, this section deals with the implementation for two designs of coupled folded waveguide (FWG) resonator filters and its frequency response. The first design deals with TZ zero in the high side band and the second TZ on the low side band. The implementation of the design and the experimental results are the core contents of this section, with certain specifications. The slot technique can be implemented to design a 2-pole resonator filter in order to reduce the size of the quarter-wavelength resonator. This section will evaluate the structures for the realization of microwave cavities with a high spurious free range and a reduced footprint. Moreover, a miniaturized resonator/filter

with a slot is introduced. The slot perturbs the fundamental resonance and lowers the resonant frequency, which makes the patch resonator compact. However, the round corner only slightly perturbs the second resonance and keeps the second resonant frequency unchanged, which takes the fundamental and second resonance frequencies further apart [66].

5.2.3.1 Implementation of a 2-pole cavity resonator filter:

The folded waveguide 2-pole resonator, shown in Figure 5-13**,** was fabricated and represented by two designs. The differences between them are the slot length (*SL*) to attain the requirement for each. When we consider designing a 2-pole resonator filter that has a TZ on the high side, the dimensions are *SL* =11.8 mm and its *RG* =1.8mm and *L* = 2mm. For the second design of the 2-pole resonator filter that has TZ on the low side band, the diminutions are *SL* = 15.8 mm, *RG* =1.8mm and L = 2mm.

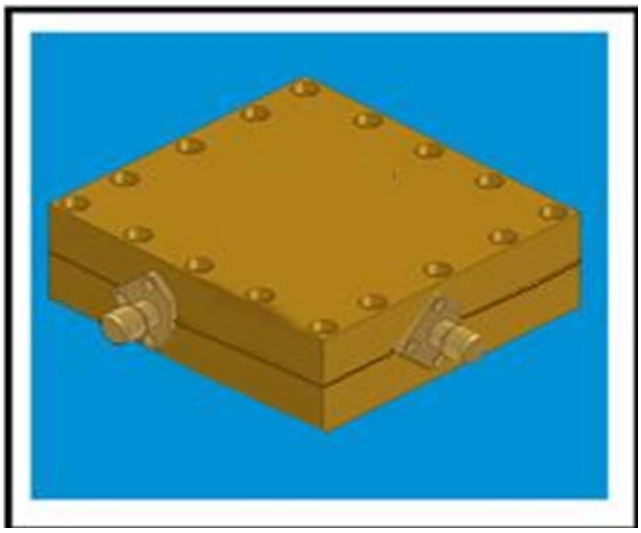

Figure 5-13: 2-pole cavity resonator filter.

To measure the coupling, the coupled resonators are weakly excited by the two ports. This can be done by using EM simulation [63]. Figure 5-14 plots the typical simulated results for two interesting cases. The physical dimensions of these two cases are identical; except for the slot length SL. Case 1 has a slot length of 11.8 mm, while case 2 has a slot length of 15.8 mm. It can be seen that the two cases have the similar magnitude response of S_{21}, where a pair of resonant peaks indicate the mode split which can be used to extract the coupling magnitude of K_{12}. However, the most notable characteristic as seen in

Figure 5-14 is the phase response of S_{21}. The two cases exhibit opposite phase responses implying that the signs of K_{12} for these two cases can be different. Therefore, we can vary the slot length to obtain the opposite sign of coupling, which is very useful in realizing some interesting filtering characteristics.

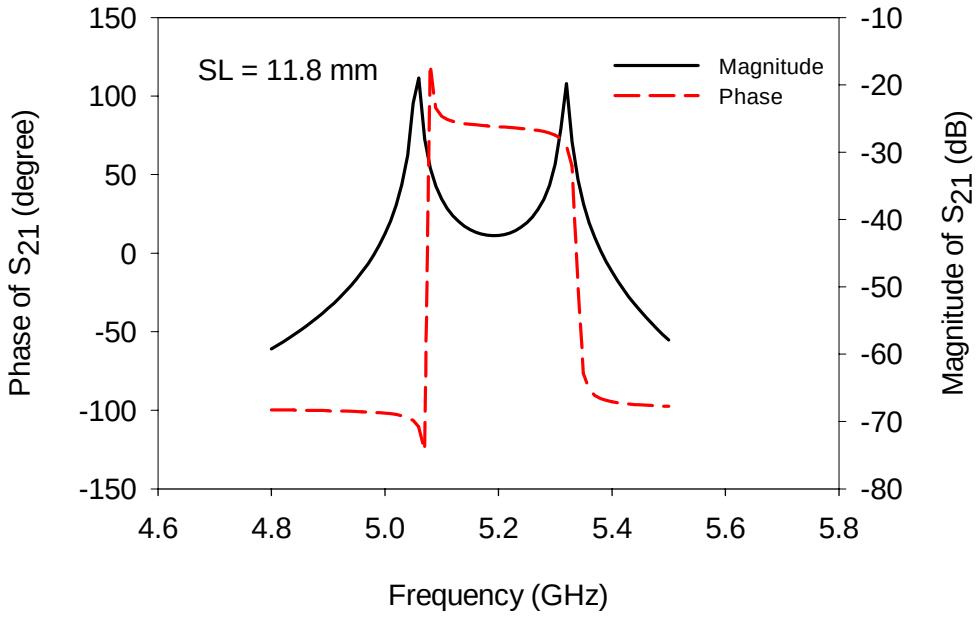

(a)

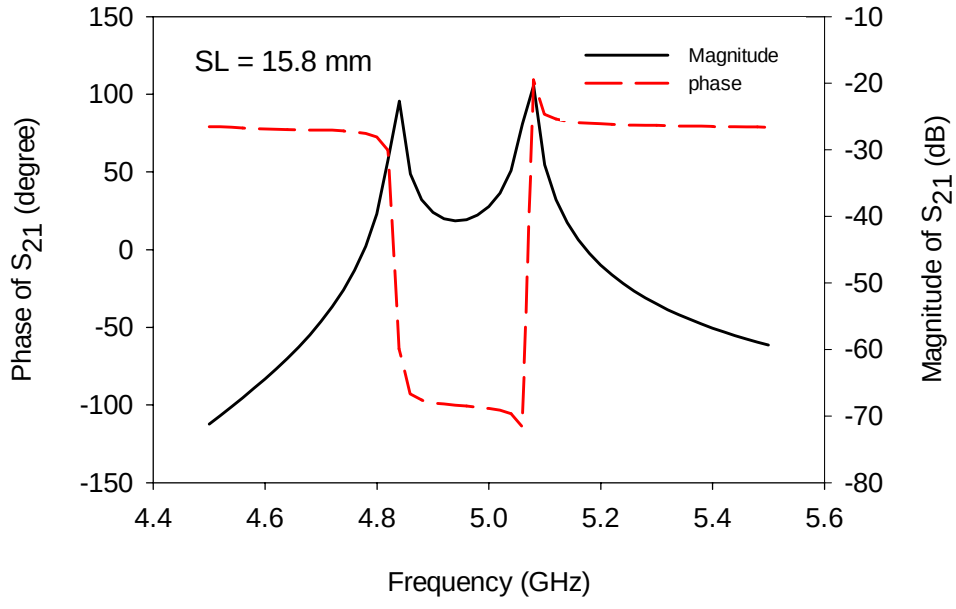

(b)

Figure 5-14: Coupling characteristics against the slot length SL. (a) SL = 11.8 mm. (b) SL = 15.8 mm.

5.2.3.2 Experiment Results

The two designed filters were fabricated using an industrial brass material with a conductivity of 1.57×10^7 S/m. Figure 5-15 illustrates the physical realization for one of the filters.

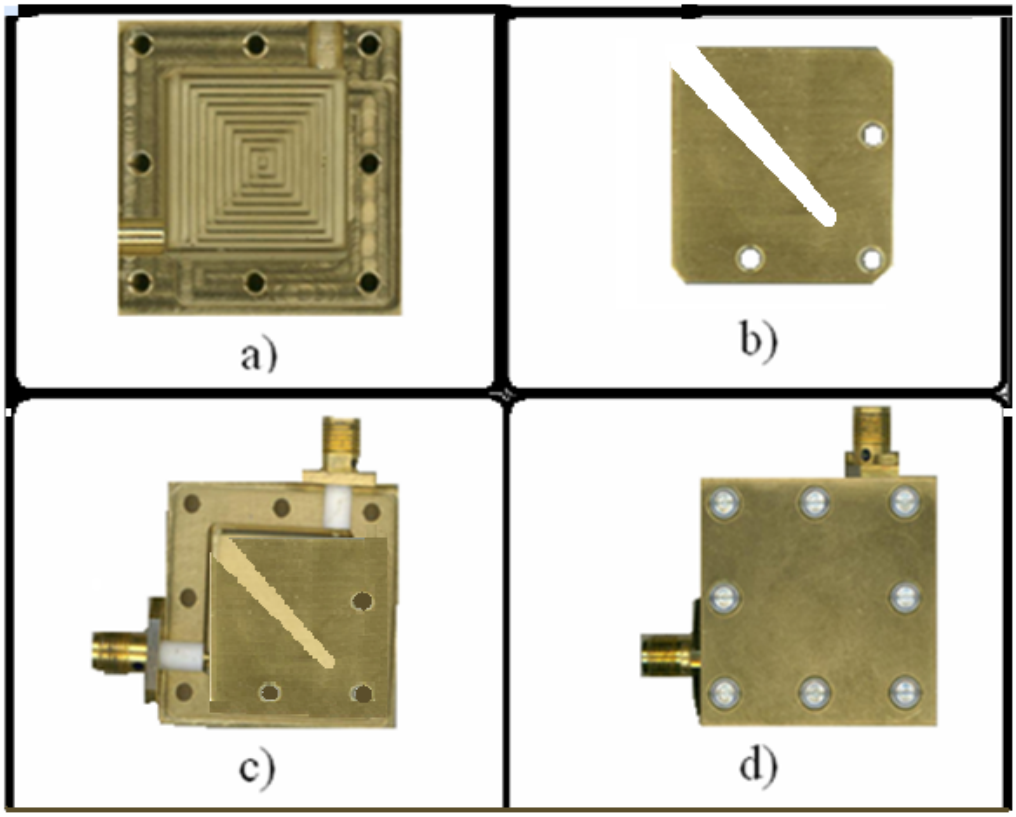

Figure 5-15: Fabricated 2-pole slotted FWG resonator filter before assembly (a, b and c) and after assembly (d).

It is comprised of two identical halves of a cavity (one of them is shown in Figure 5-15 (a). Each of the halves has a size of 21mm × 21mm with a recess depth of 3.5mm, and are separated by a brass plate with a slot, as shown in Figure 5-15 (b). The metal plate has a thickness of 1mm. Two SMA connectors from input/output (I/O) excitation ports are tapped onto the slotted plate, as shown in Figure 5-15 (c). Note that the physical realization and dimensions for the two filters are exactly the same, except for the slot length. The filter shown in Figure 5-15 is the one with a longer slot, which aims to produce a TZ on the low side of the passband. The other filter has a shorter slot for a TZ on the high side of the passband. The S-parameters of the fabricated filters were measured using a calibrated network analyzer. The experimental results, together with

the EM-simulated and theoretical results for each of the filters, are shown in Figure 5-16 and Figure 5-17, respectively.

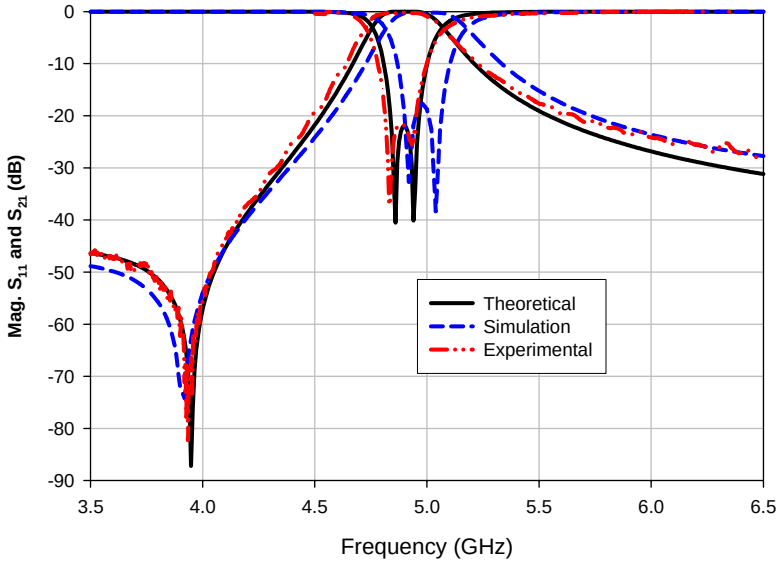

Figure 5-16: Frequency response of the proposed 2-pole FWG resonator filter with a TZ on the low side of passband.

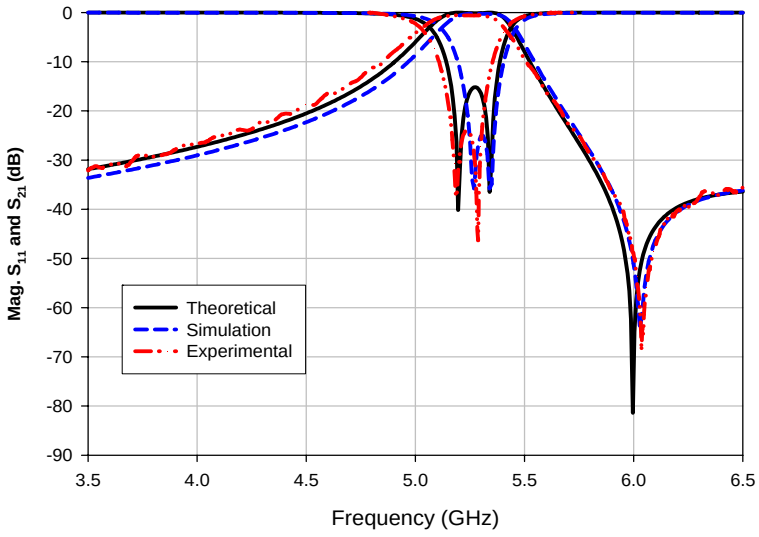

Figure 5-17: Frequency response of the proposed 2-pole FWG resonator filter with a TZ on the high side of passband.

In general, there is good agreement between the measurement and simulation/theory. Both filters have a similar fractional bandwidth of about 4%. The centre frequencies are slightly different because of the different slot lengths. In Figure 5-16, the filter with the longer slot exhibits a desired asymmetric frequency response with the TZ on the low side of the passband as expected. The measured insertion loss at the mid-band is about 0.5 dB, including the losses from the two SMA connectors. The filter with the shorter slot also shows a desired asymmetric frequency response with the TZ allocated on the

upper stopband, as depicted in Figure 5-17. The similar insertion loss of 0.5 dB at the midband was measured for this filter, and both filters show good return loss responses in the passband. The experiments were also carried out to measure the wideband frequency responses of both filters and the measured results are plotted in Figure 5-18 and Figure 5-19.

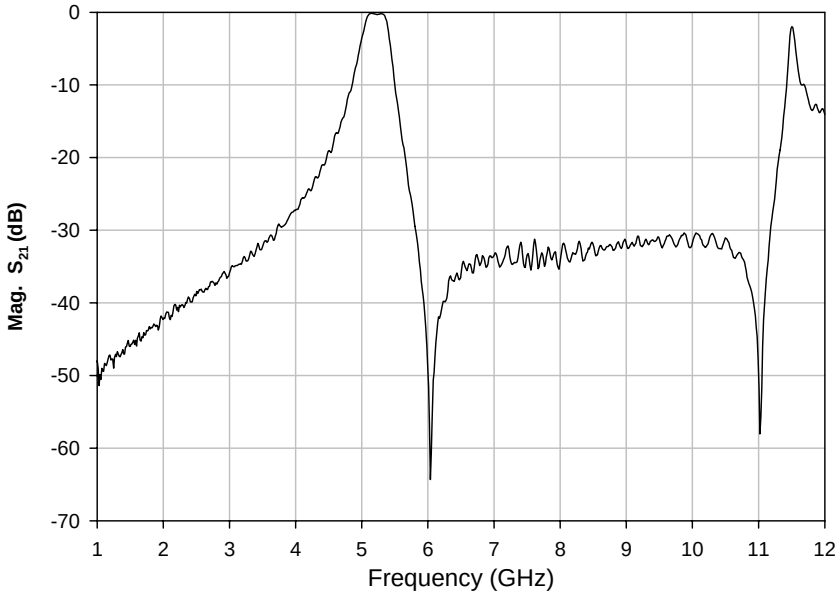

Figure 5-18: Measured wideband frequency response of the fabricated 2-pole FWG resonator filter with TZ on the high side of passband.

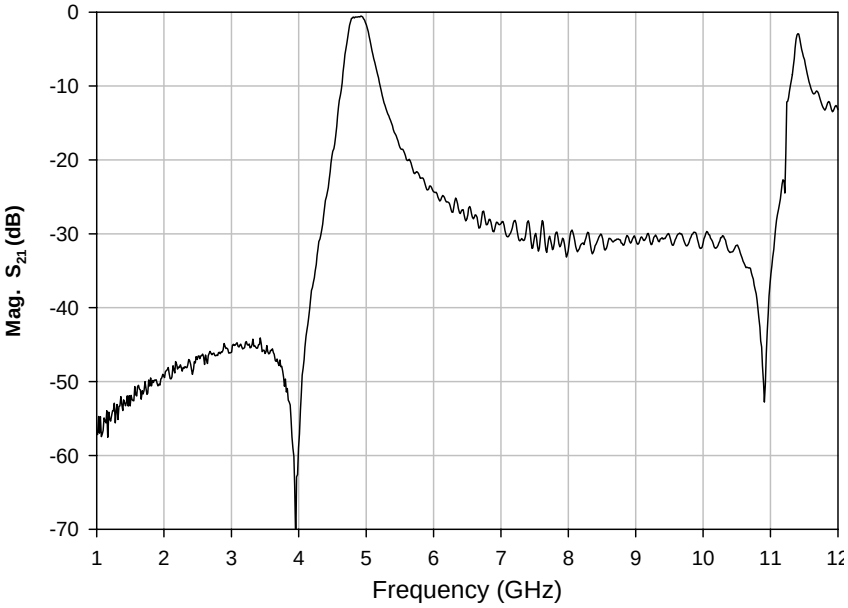

Figure 5-19: Measured wideband frequency response of the fabricated 2-pole FWG resonator filter with TZ on the low side of passband.

5.3 FWG Dual-band filter

Using the same structure of FWG that discussed in section 5.2 FWG dual-band filter has been proposed. The proposed FWG dual-band filter is illustrated in Figure 5-20. It is notable that there are two inserted metal plates that have a slot with the length SL. Each of the metal plates has a thickness of (*t*) and the upper and the lower air-filled half cavities have a depth of *h/2* to form a so-called slotted FWG cavity. Owing to the new slot introduced, a pair of resonant modes, which have the same resonant frequency, can be excited within each slotted FWG cavity. Thus, a single slotted FWG cavity, which has the same size as that of a quarter-wavelength FWG resonator [1], can be used as a double-tuned resonator circuit; resulting in a significant size reduction for the development of new compact filters. The proposed filter has a multilayer structure, which allows the couplings between adjacent slotted FWG cavities to be introduced through the aperture on the common cavity wall, as indicated.

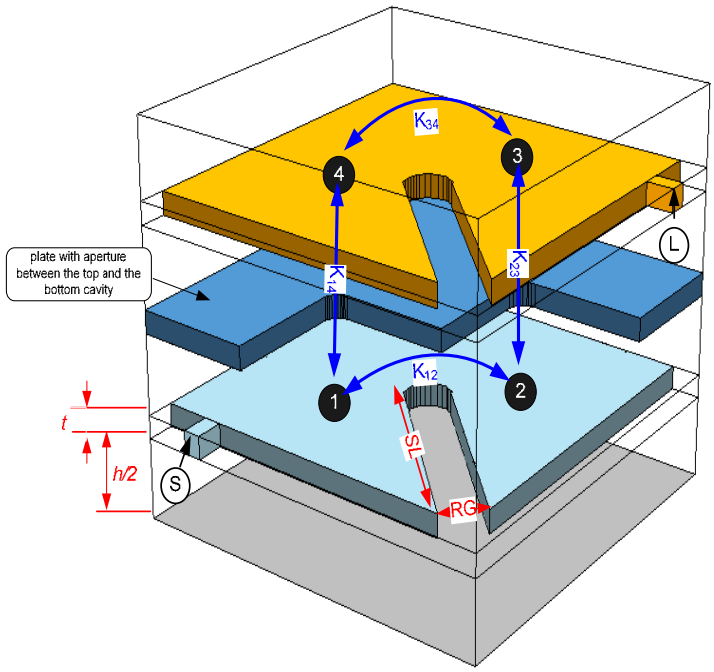

Figure 5-20: Proposed FWG dual-band filter structure where t is the thickness of the metal plate, and *h/2* is the depth of each half cavity.

The proposed dual-band filter exhibits a coupling scheme, as shown in Figure 5-21. In this coupling scheme, the input (S) is directly coupled to resonator 1 while the output (L) is directly coupled to resonator 3. These couplings are realized by tapping the I/O excitation ports onto resonators 1 and 3 respectively, as can be seen from Figure 5-20. The coupling between resonators 1 and 2 is facilitated by the slot of length *SL* and gap

RG as shown in Figure 5-20. This is the same for the realization of the coupling between resonators 3 and 4. In the coupling scheme of Figure 5-21, there are other two important couplings, namely the coupling between resonators 2 and 3 and the coupling between resonators 1 and 4. These two couplings are realized by opening apertures on the common cavity wall between the two FWG cavities, as shown in Figure 5-20. For the proposed filter structure of this design, a small cross coupling can exist between the input and resonator 2, as well as the output and resonator 4. These cross couplings are indicated in the coupling scheme of Figure 5-21, though it can be shown that they are not important for realizing the dual-band operation.

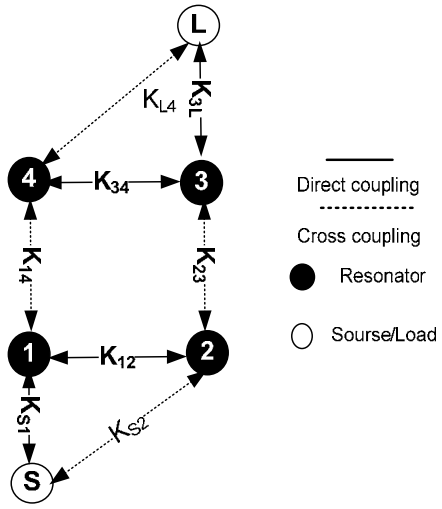

Figure 5-21: Coupling scheme for the proposed dual-band filter.

5.3.1 External and unloaded quality factor and coupling coefficients

In this section, we have investigated a number of different arrangements to obtain an external and unloaded quality factor and coupling coefficients.

5.3.1.1 External Quality factor (Qe)

Figure 5-22 (a) shows the structure of the proposed new technique of a quarter-wavelength folded waveguide resonator, where a grounded post in the middle of resonator 2 is presented to attain the external quality factor (Q_e) from its response, where two orthogonal slots are etched along the edge of a common metal plate while resonators 3 and 4 have been short-circuited from the sides in order to be neglected.

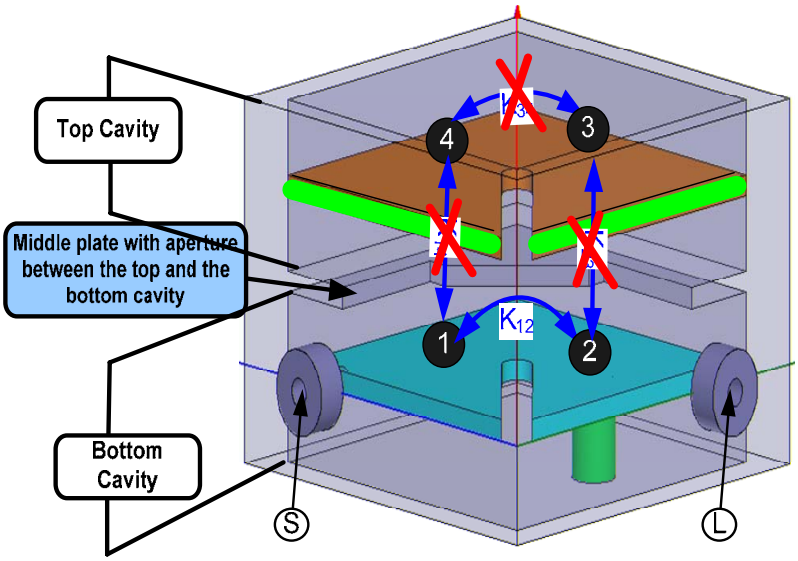

a)

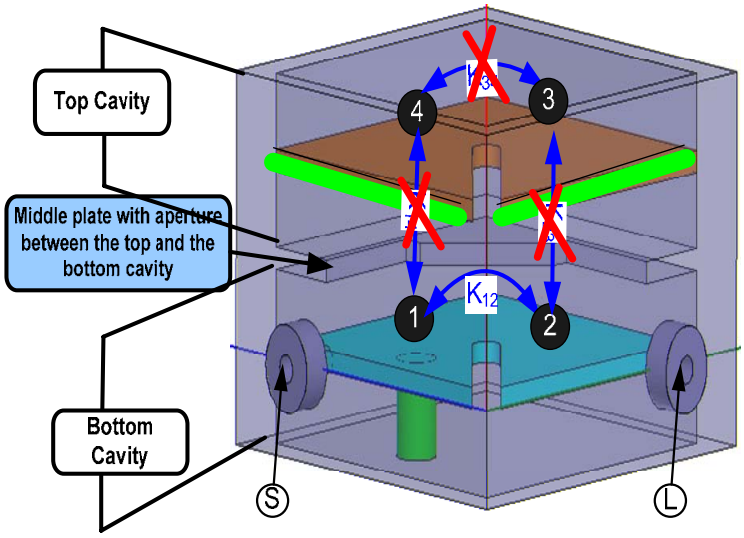

b)

Figure 5-22: The proposed technique to extract; (a) External quality factor (b) Unloaded quality factor.

As shown in Figure 5-22, a single tapped input arrangement is used to extract the quality factor. By adjusting the locations of source (S) and load (L) with a variety of positions, a designed external quality factor can be obtained. The external quality factor can be characterized using the full-wave simulation [63] of the excited input or output resonators. Figure 5-23 depicts the extracted external quality factor (Q_e) and a central frequency f_c against a different excitation port length location (L) from the edge. It was noticed that the quality factor (Q_e) is directly proportional to the length of the excitation port location (L), whereas the central frequency f_c is inversely proportional to the excitation port length location (L). From this design curve, we can obtain the initial dimensions for the designed external quality factor practically the position of excitation

port length location from the edge which is gave the required external quality factor (Q_e). Figure 5-24 shows the resonant frequency characteristics of the scattering parameters. Note that due to the increasing of the excited ports (S and L) locations from the edge effect the external quality factor (Q_e) increases as shown from the responses. More investigation was given to the new technique to show how can we get one resonant frequency and try to move the second resonant frequency away in order to get a single resonant frequency to calculate the quality factor. The external quality factor was extracted from the simulated frequency response with well known formula [32]:

$$Q_e = \frac{f_c}{\delta f_{3\,dB}} \tag{5-3}$$

Where f_c and $\delta f_{3\,dB}$ are the resonant frequency and the 3-dB bandwidth of the single resonator, respectively.

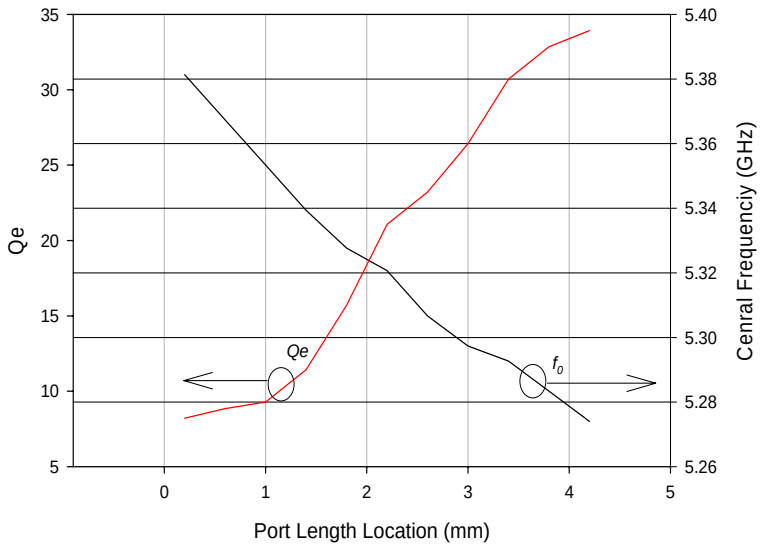

Figure 5-23: Design curves to extract the external quality factor Qe against the excitation port length location (L).

5.3.1.2 Unloaded Quality factor (Qu)

Figure 5-22 (b) shows a grounded post in the middle of resonator 1 to calculate the unloaded quality factor (Q_u) from its response (where two orthogonal slots are etched along the edge of common metal plate), while resonators 3 and 4 have been short-circuited from the sides to be both neglected. The unloaded Q can be found from [32]:

$$Q_u = \frac{Q_L}{1 - S_{12}(f_0)} \tag{5-4}$$

The full-wave EM simulation shows that the designed demonstrator has a fundamental resonant frequency of 5.27 GHz and an unloaded quality factor Q_u of 714.

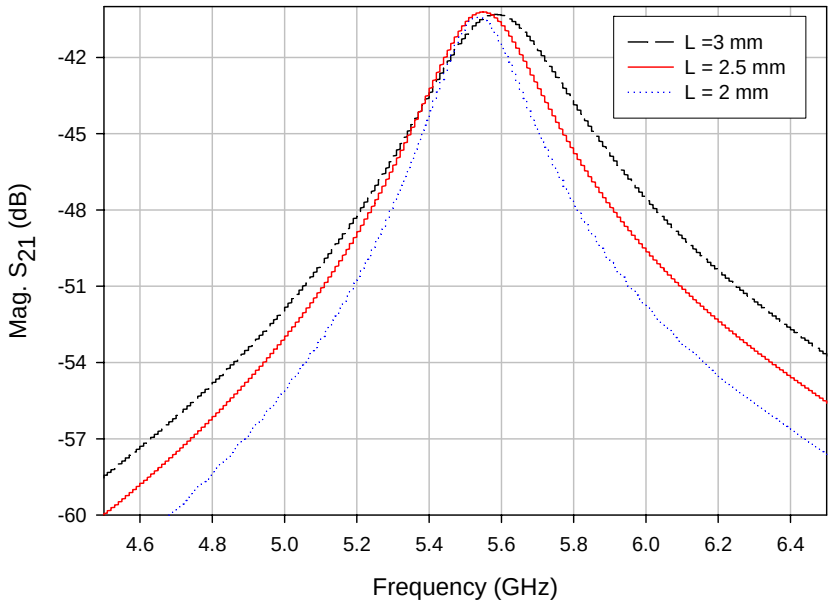

Figure 5-24: Resonant frequency characteristics of the scattering parameters when L is varying.

5.3.1.3 Coupling coefficient

Direct coupling and cross coupling are very important to realize a designed dual-band bandpass filter. The direct coupling K_{12} = K_{34} was extracted by employing a 2-pole filter model, as shown in Figure 5-25 with two input (S) /output (L) probes. A slot with the length of *SL* is introduced onto the inserted metal plate. The metal plate has a thickness of *t* and the upper and lower air-filled half cavities have a depth of *h/2*. For the other parameters fixed, the larger K_{12} and K_{34} result in a larger separation of the dual-bands, while the bandwidth of each passband is almost unchanged. The passband bandwidth is controlled mainly by the other parameters, namely K_{23} and K_{14}, K_{S1} and K_{3L}. The larger of these couplings leads to a larger bandwidth for each passband, which is illustrated in Figure 5-26. In this figure, K_{12} and K_{34} are fixed so does the separation of the two passband bands regardless of their bandwidths. The generalized coupling matrix for the design is given by M1:

$$M1 = \begin{bmatrix} 0 & 0.95 & 0 & 0 & 0 & 0 \\ 0.95 & 0 & 0.5 & 0 & 1.8 & 0 \\ 0 & 0.5 & 0 & 1.8 & 0 & 0 \\ 0 & 0 & 1.8 & 0 & 0.5 & 0.95 \\ 0 & 1.8 & 0 & 0.5 & 0 & 0 \\ 0 & 0 & 0 & 0.95 & 0 & 0 \end{bmatrix} \tag{5-5}$$

The elements of the coupling matrix [m] give the normalized coupling coefficients and the scaled external quality factor.

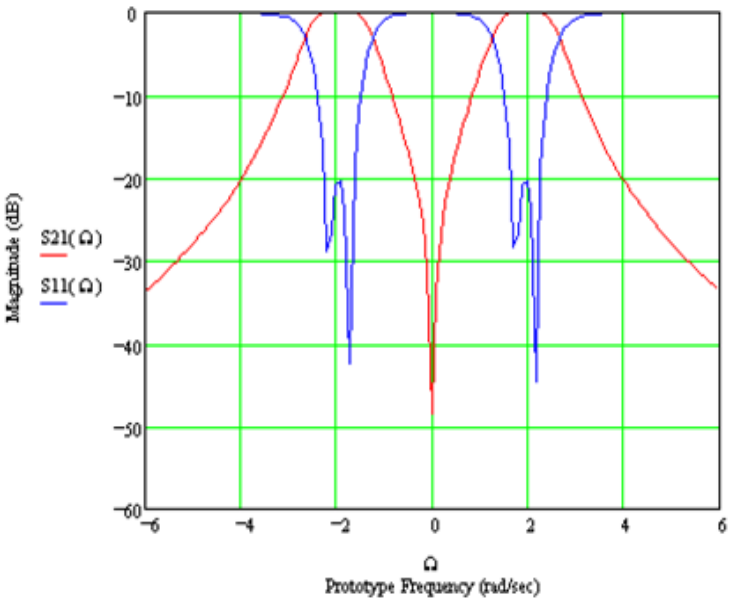

(a)

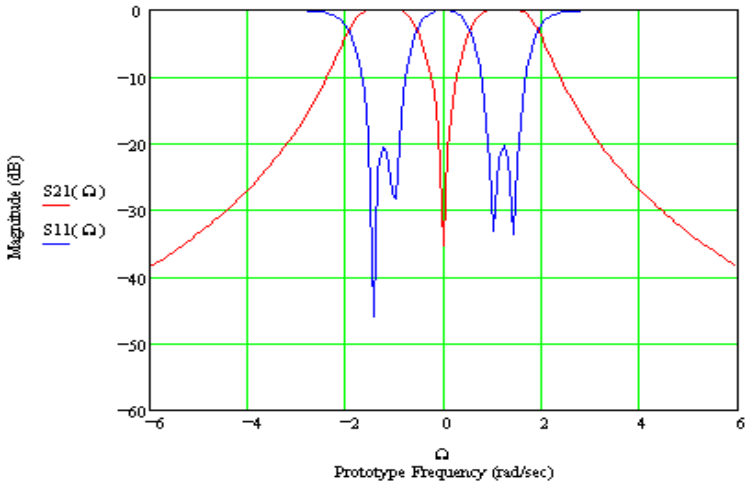

(b)

Figure 5-25: Dual-band frequency characteristic against the couplings K_{12} and K_{34} for the other parameters fixed. (a) $K_{12} = K_{34} = 2.0$. (b) $K_{12} = K_{34} = 1.3$.

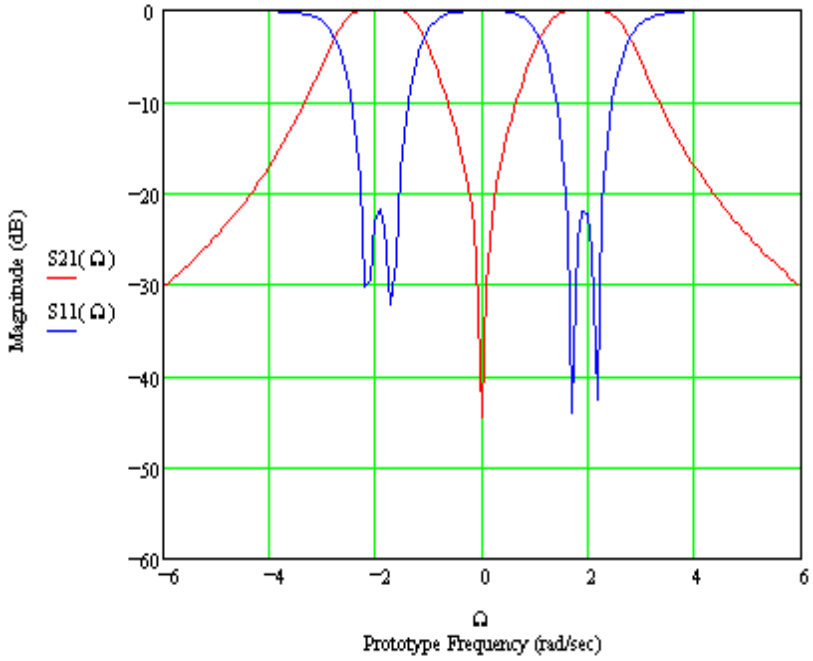

(a)

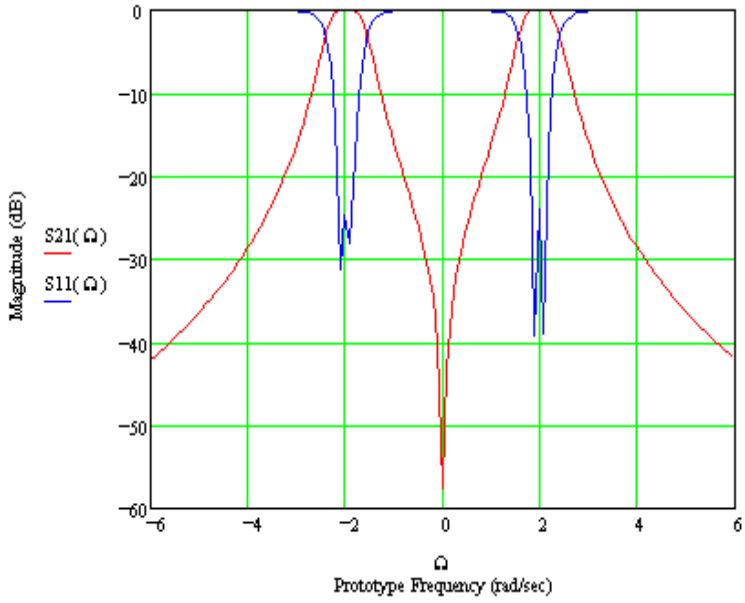

(b)

Figure 5-26: Dual-band frequency characteristic against the couplings for K_{12} and K_{34} fixed. (a) K_{s1} = K_{3L} = 1.05 and K_{23} = K_{14}= 0.6. (b) K_{s1} = K_{3L} = 0.75 and K_{23} = K_{14}= 0.3.

To extract the direct coupling, the coupled resonators were weakly excited by the two ports. This can be done by using full-wave electromagnetic (EM) simulation [63]. As can be seen from Figure 5-28 (a typical response for extracting direct coupling), two split mode frequencies (resonant peaks) are observed to extract the direct coupling. Denote these two split frequencies as f_1 for the first resonant peak and f_2 for the second

resonant peak. By varying the slot length (SL), different resonating frequencies can be found. The coupling coefficient can be evaluated [65] by.

$$K_{ij} = \frac{(f_{p2})^2 - (f_{p1})^2}{(f_{p2})^2 + (f_{p1})^2} \tag{5-6}$$

Where f_{p1} and f_{p2} are the lower and higher split resonant frequencies of a pair of coupled resonators.

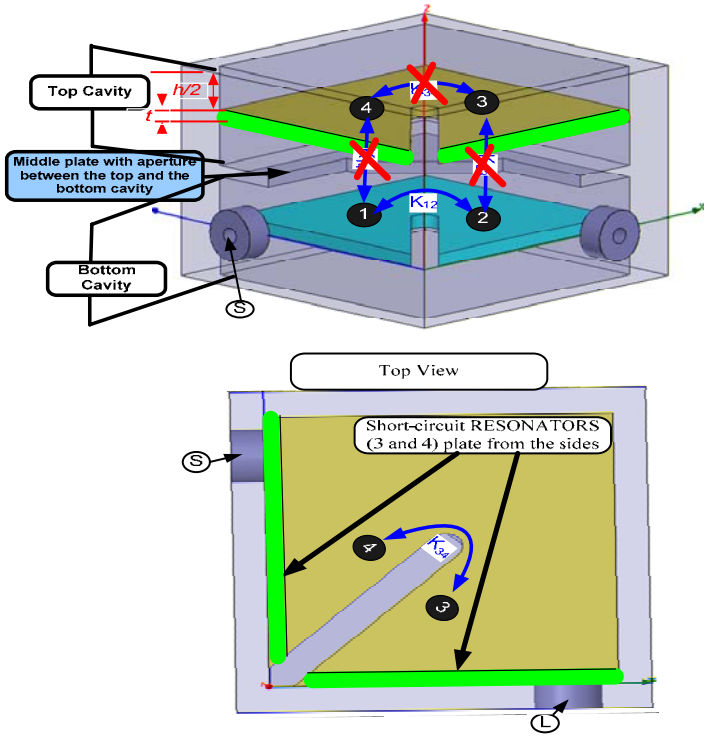

Figure 5-27: Configuration of the proposed dual passband filter to extract the direct coupling between K_{12}= K_{34}; where t is the thickness of the separation plate, and h/2 is the depth of the upper and lower in each cavities.

Figure 5-29 plots an extracted direct coupling coefficient with a different *SL*. It can be seen from that Figure that when *SL* increases, the direct coupling between adjacent resonators is decreased. Referring to the coupling matrix (5-5), the direct coupling between resonators 1 and 2 which is the same coupling between resonators 3 and 4 is about 0.13. From this, we can get the initial diminution of the slot length (*SL*) on the common separation plate of K_{12} = $K_{34,}$ which is about 14.6mm.

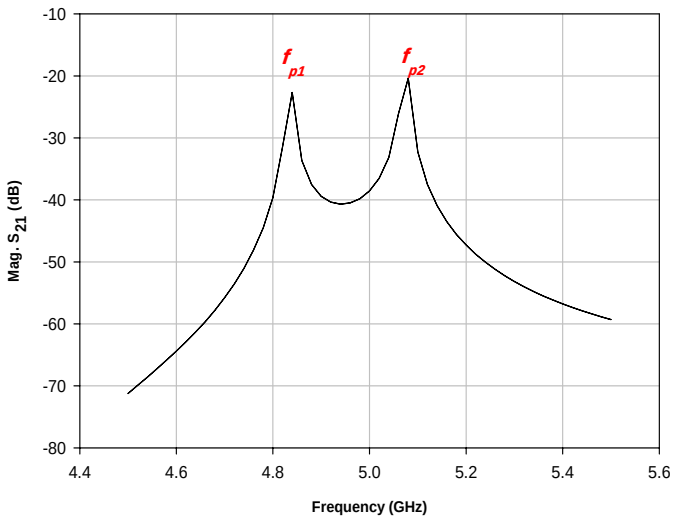

Figure 5-28: Typical frequency response simulated for extracting the coupling coefficient.

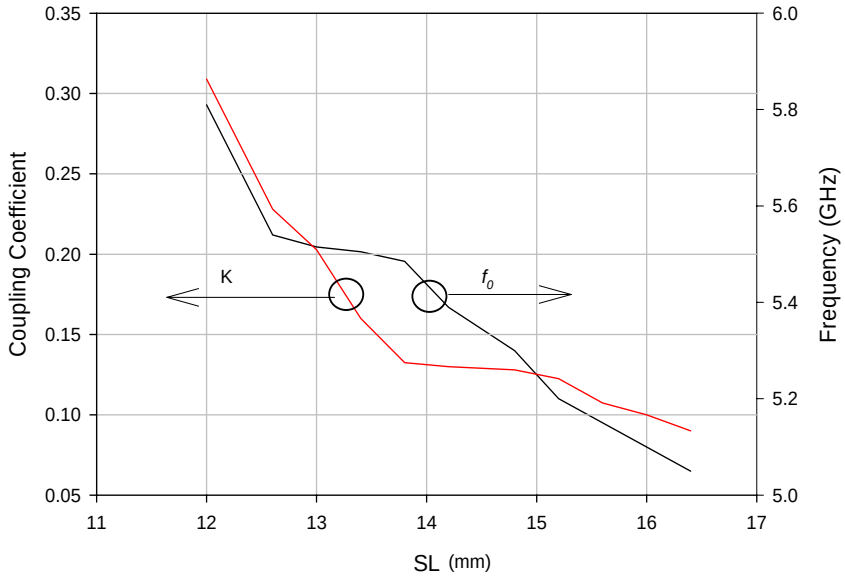

Figure 5-29: Design curves for the proposed slot length (SL) on the common separation plate K_{12} = K_{34}.

To investigate the cross coupling between two non-adjacent resonators (resonators 1 and 4 which are the same as 2 and 3) and (1 and 3 which is the same of 2 and 4) located in the top and bottom layer, many structures have been manipulated. One of these is shown in Figure 5-30. It is shown in Figure 5-30 and Figure 5-31 that the structure of the cross coupling between resonators 1 and 4 is the same as the coupling between resonators 2 and 3, and the second cross coupling between resonators 1 and 3 is the same as the coupling between resonators 2 and 4, respectively. These two couplings are realized by opening apertures on the common cavity wall between the two FWG cavities.

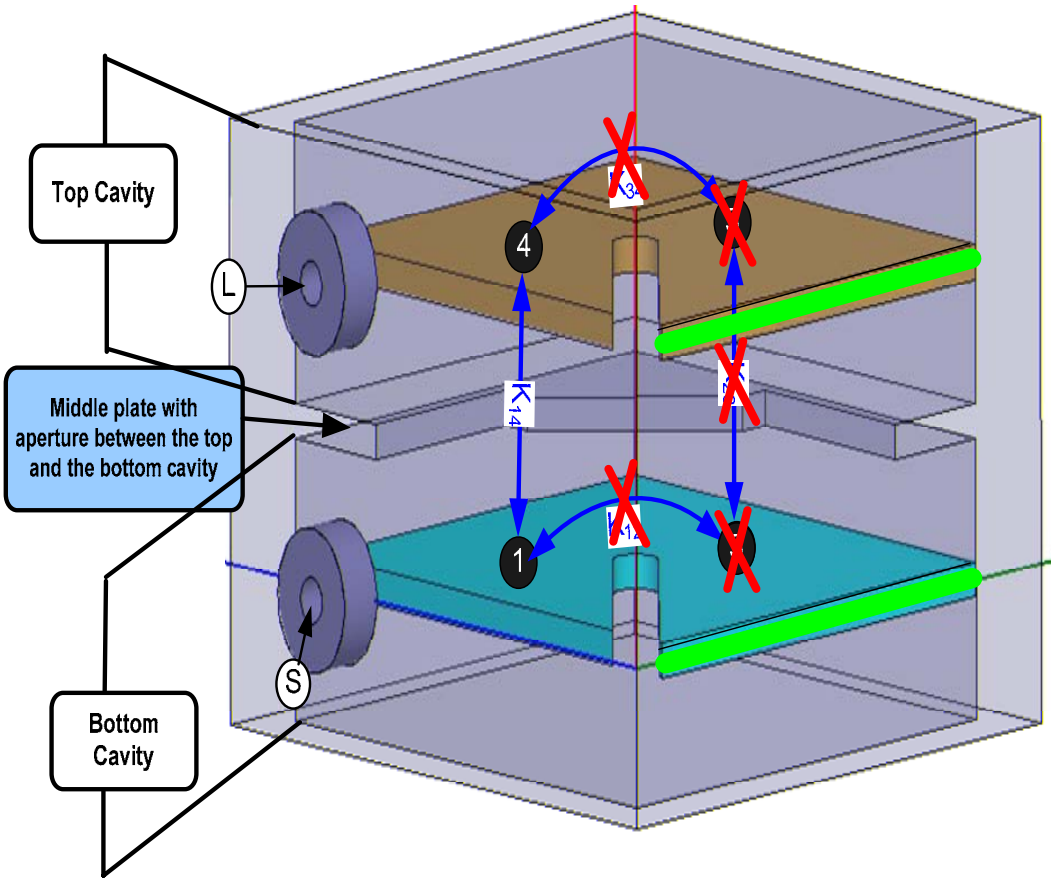

Figure 5-30: Configuration of the proposed dual passband filter to extract the direct coupling between K_{14}= K_{23}.

As shown in Figure 5-32, the coupling aperture where the coupling is realized through an aperture on the common cavity middle plate between the two FWG cavities can be adjusted by its geometrical parameters L1, L2 and ML to realize a designed cross coupling coefficient. Cavities can be adjusted by the geometrical parameters L1, L2 and ML. The coupling matrix, in terms of the cross coupling between resonators 1 and 4 (which is the same as the coupling between resonators 2 and 3) is about 0.023, while the weakest cross coupling between resonators 1 and 3 (which is the same as the coupling between resonators 2 and 4) is about 0.0047. As shown in Figure 5-32, we can get the initial diminutions of L1 = 5mm, L2 = 8.5mm and ML = 14.6mm, which the gives the required values of the coupling coefficients.

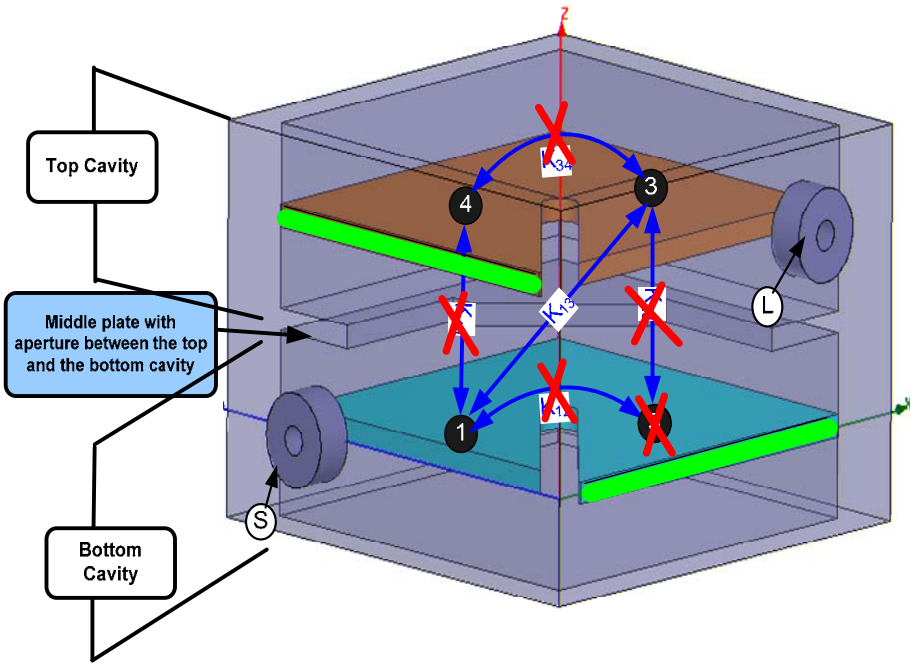

Figure 5-31: Configuration of the proposed dual passband filter to extract the direct coupling between K_{13}= K_{24}.

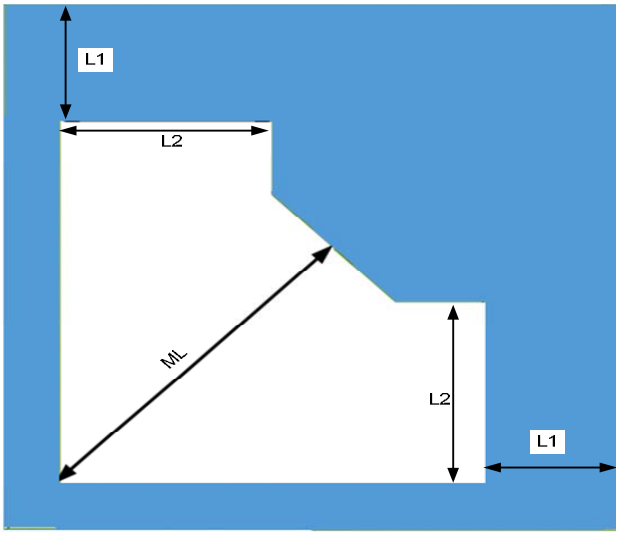

Figure 5-32: Top view of the common cavity middle plate between two FWGs.

A design curve for normalized cross coupling is plotted in Figure 5-33, and the initial dimensions of the coupling aperture can be obtained. It can be seen that *L1* is more critical for tuning a cross coupling coefficient than other geometrical parameters such as *L2* and *ML*. As *L1* increases, the cross coupling coefficient is decreased. On the other hand, *L2* and *ML* have little impact on the cross coupling coefficient.

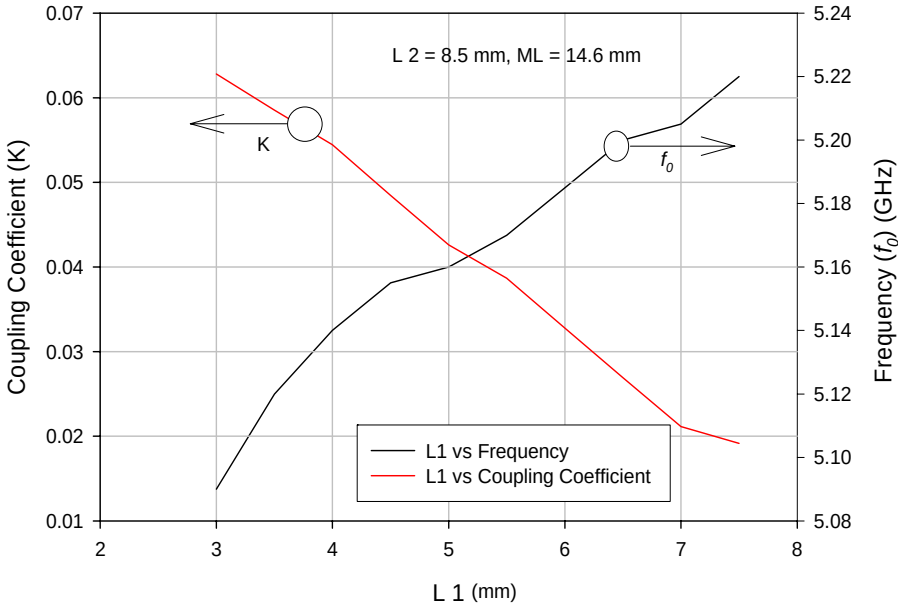

Figure 5-33: Design curves for the proposed aperture on the common cavity plate K14 = K23, varying L1.

Electric and magnetic fields are plotted in Figure 5-34 to show their contribution for realizing the coupling coefficient. From Figure 5-34 (a), it can be clearly seen that the cross coupling is mainly realized by magnetic field coupling, which occurs at the edge of the coupling aperture. This also indicates that the cross coupling coefficient is very sensitive to *L1*. From Figure 5-34 (b), it can be seen that the direct coupling between adjacent resonators is controlled by magnetic field coupling.

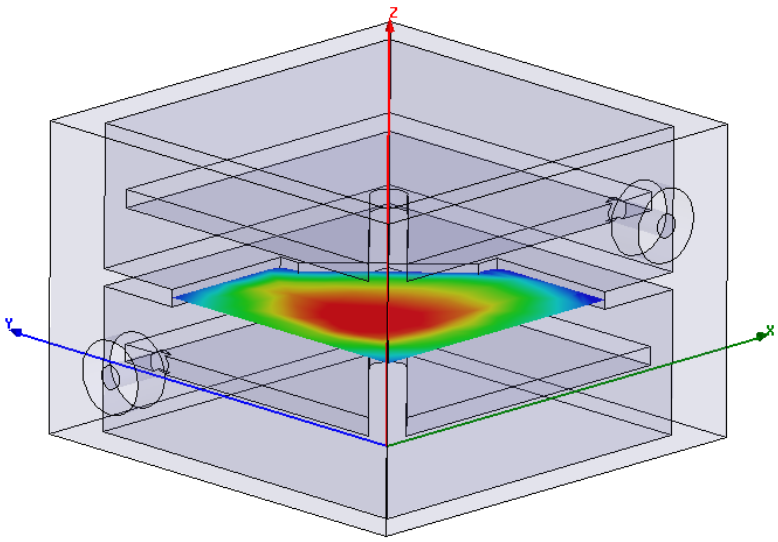

(a)

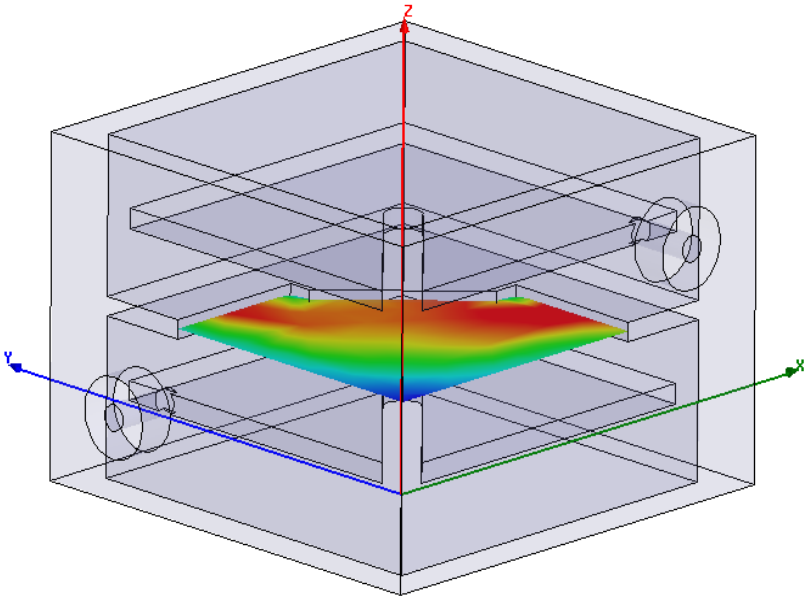

(b)

Figure 5-34: a) E-field distributions of the proposed dual band bandpass filter at 4.9 GHz, (b) H-field distributions of the proposed dual band bandpass filter at 4.9 GHz,

As predicted the direct coupling is sensitive to the slot length *SL*. With the help of a full-wave simulator [63], the final geometric dimensions of the coupling aperture can be shown in Figure 5-35. The simulated coupled cavities have a size of 21mm x 21mm x 8 mm and two 1mm wide orthogonal slots are etched onto the middle metal plate.

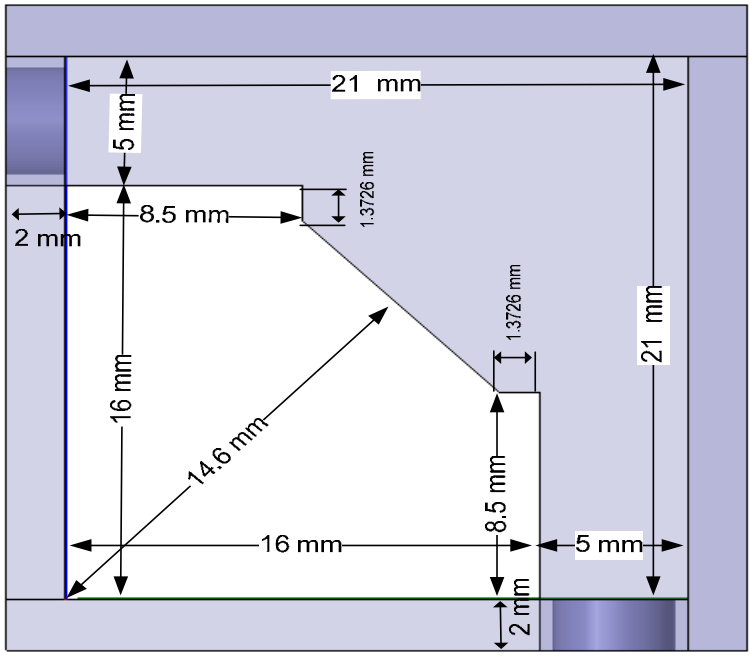

Figure 5-35: Final dimensions of the coupling aperture.

For the coupling scheme in Figure 5-21, the most significant couplings for the dual-band operation are K_{12} and K_{34}. Figure 5-36 (a) shows the typical modal split characteristic due to the coupling between resonators 1 and 2 for a specific slot. In the coupling scheme of Figure 5-21, there are other two important couplings the coupling between resonators 2 and 3 and the coupling between resonators 1 and 4. These two couplings are realized by opening apertures on the common cavity wall between two FWG cavities, as shown in Figure 5-20. The typical aperture coupling characteristic is shown in Figure 5-36 (b). These two couplings control the separation of the two passbands, i.e. from the centre frequency of the first passband to the centre frequency of the second passband. This interesting characteristic is shown in Figure 5-25.

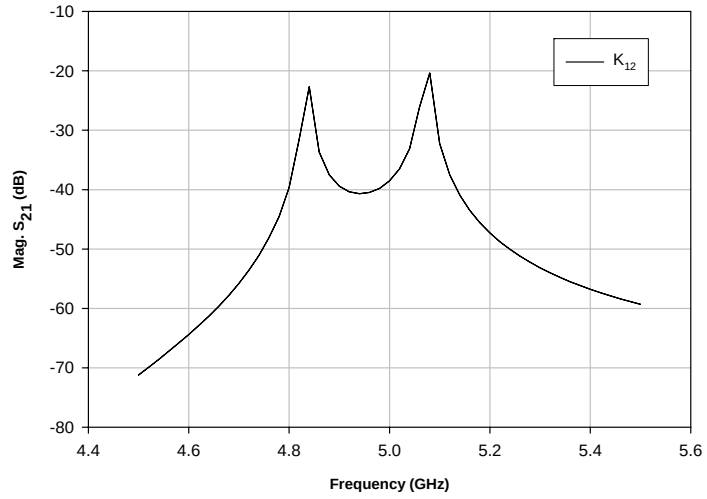

(a)

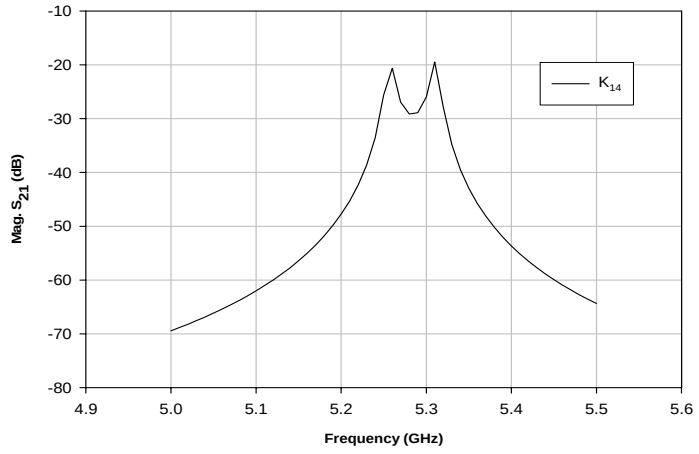

(b)

Figure 5-36: Typical coupling characteristics. (a) Slot coupling. (b) Aperture coupling.

5.3.2 Dual-band operation Demonstration

For our demonstration, a 4-pole dual-band filter of this type has been successfully designed using a commercially available electromagnetic (EM) simulator [63]. The

realization of the dual bandpass filter is presented in Figure 5-37, where the components of the 4-pole dual passband filter are shown. It is comprised of two identical halves (one of them is shown in Figure 5-37 (a). Each identical half has a brass plate with a slot (as shown in Figure 6-29 (b), which is inserted to form a dual-mode FWG, as illustrated in Figure 5-37 (c). A common cavity wall with an aperture (in Figure 6-29 (d) is used in order to facilitate the couplings between the two identical halves of the dual-mode FWG cavities, as shown in Figure 5-37 (e). The cavity size is 21mm × 21mm × 6mm for each half, with a recess depth of 3.5mm. The metal plate has a thickness of 1mm and the two ports (circular cross section) are 0.4mm wide. The input/output (I/O) excitation ports are located orthogonally to each other in the top and bottom plate respectively, as shown in Figure 5-37 (f). The cavity was fabricated in the Heriot-Watt University mechanical workshop from an industrial brass material, where the conductivity of brass is taken as $1.57xl0^7$ S/m. The testing was carried out to measure the performance of the fabricated filter, using the HP network analyzer in the microwave lab in the Electrical and Electronic Department at Heriot-Watt University. Referring to the measured results in Figure 5-38, one finite transmission zero located between the two separated passbands can be clearly observed with the attenuation of around 50 dB at around 5.3 GHz, which realizes a high out-of-band rejection. It would seem that the transmission zero results from a cancellation of the two signal paths, i.e. S-1-2-3-L and S-1-4-3-L, as indicated in Figure 5-21. At the lower band, the minimum measured insertion loss is about 1 dB at 4.855 GHz with a 3 dB bandwidth of 4.5%. At the upper band, the minimum measured insertion loss is 0.5 dB at 5.55 GHz and the 3 dB bandwidth is 4.1%. In general, the simulated and measured results are in good agreement. The higher measured insertion loss at the lower band is due to some mismatch in the middle of the passband. The slightly different passband bandwidths and asymmetrical frequency responses appear to be the effects of some minor cross couplings.

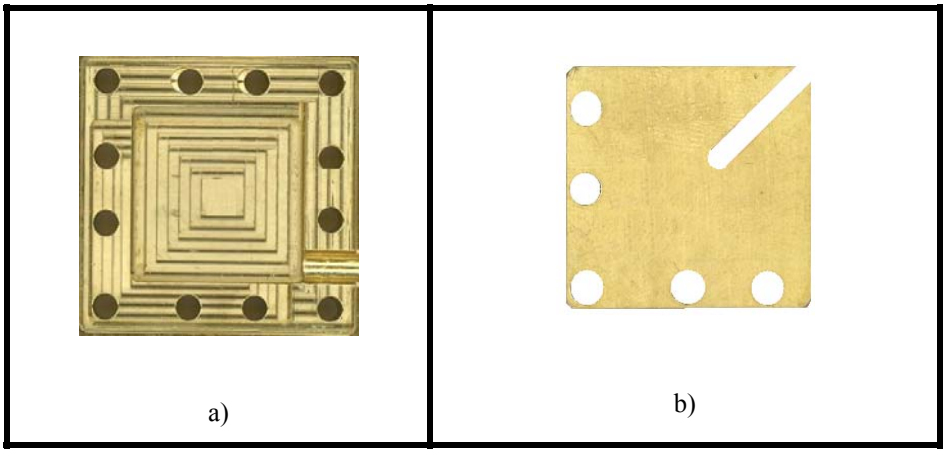

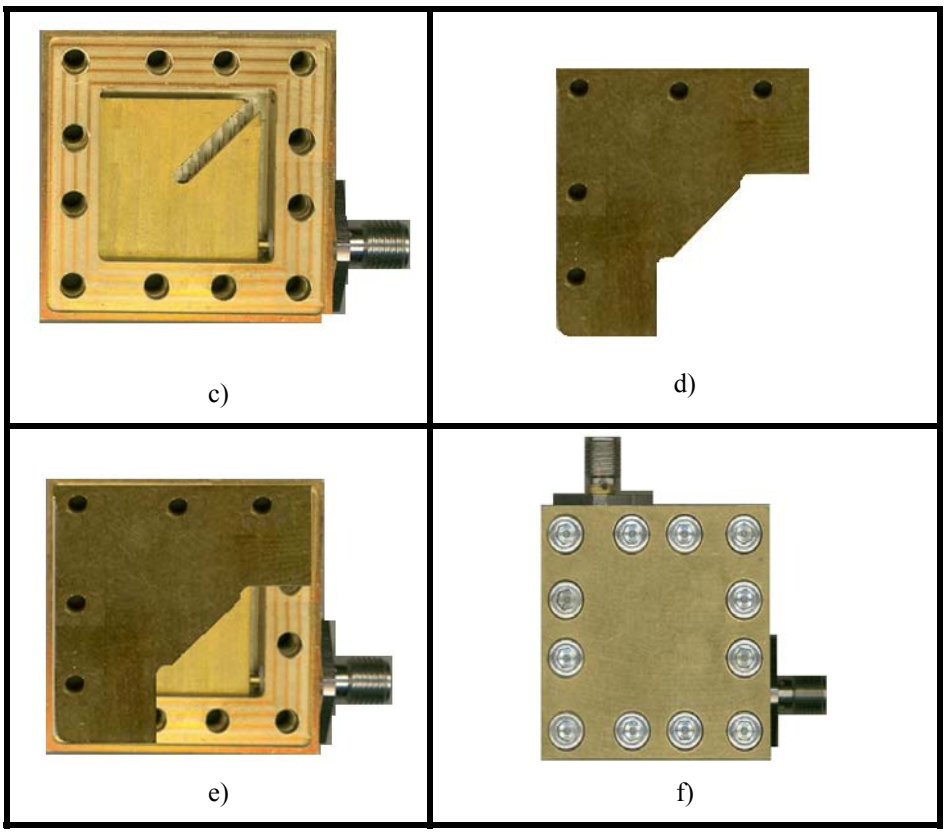

Figure 5-37: Fabricated dual-band FWG filter before assembly (a, b, c, d, and e) and after assembly (f).

The experiment was also carried out to measure the wideband frequency response of the filter demonstrator, and the measured and simulation results are plotted in Figure 5-39 for a comparison. There is a wide stopband between the fundamental and the first spurious passband, which appeared at about 9.8 GHz. Figure 5-40 is shown the simulation wideband frequency response of 4-pole folded waveguide resonator filter.

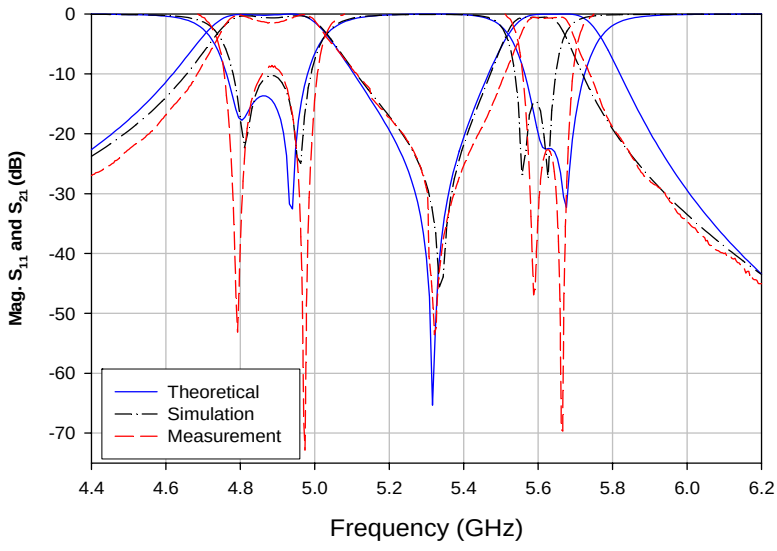

Figure 5-38: Simulated, theoretical and measured frequency response of S11 and S21 for a dual passband 4-pole FWG resonator filter.

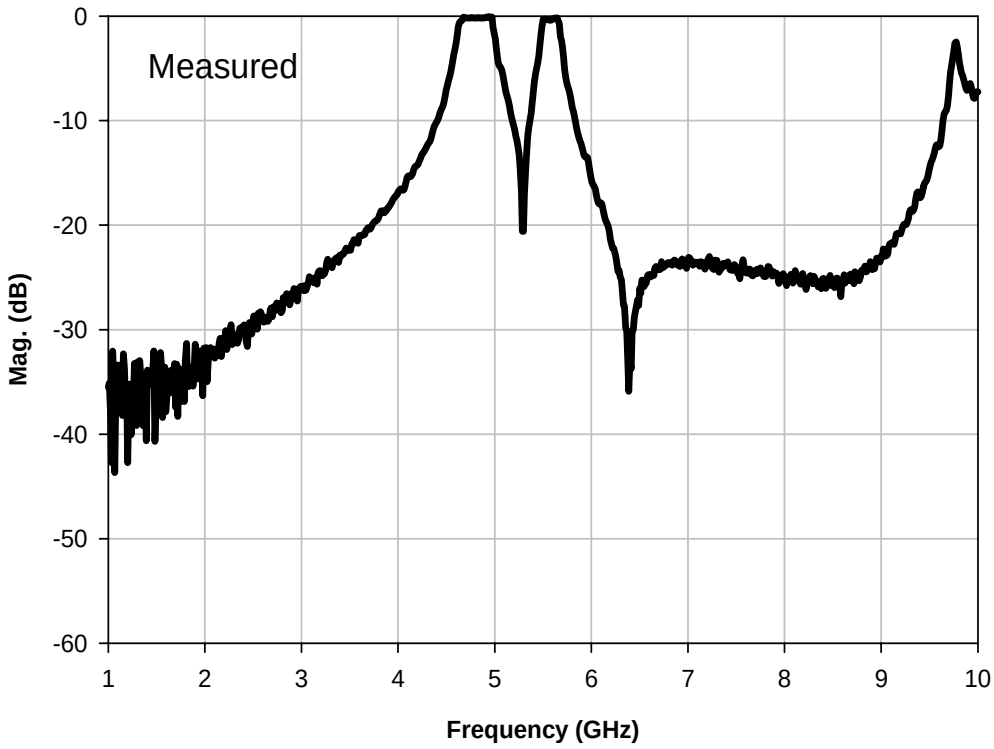

Figure 5-39: Measured wideband frequency response of the fabricated 4-pole folded waveguide resonator filter.

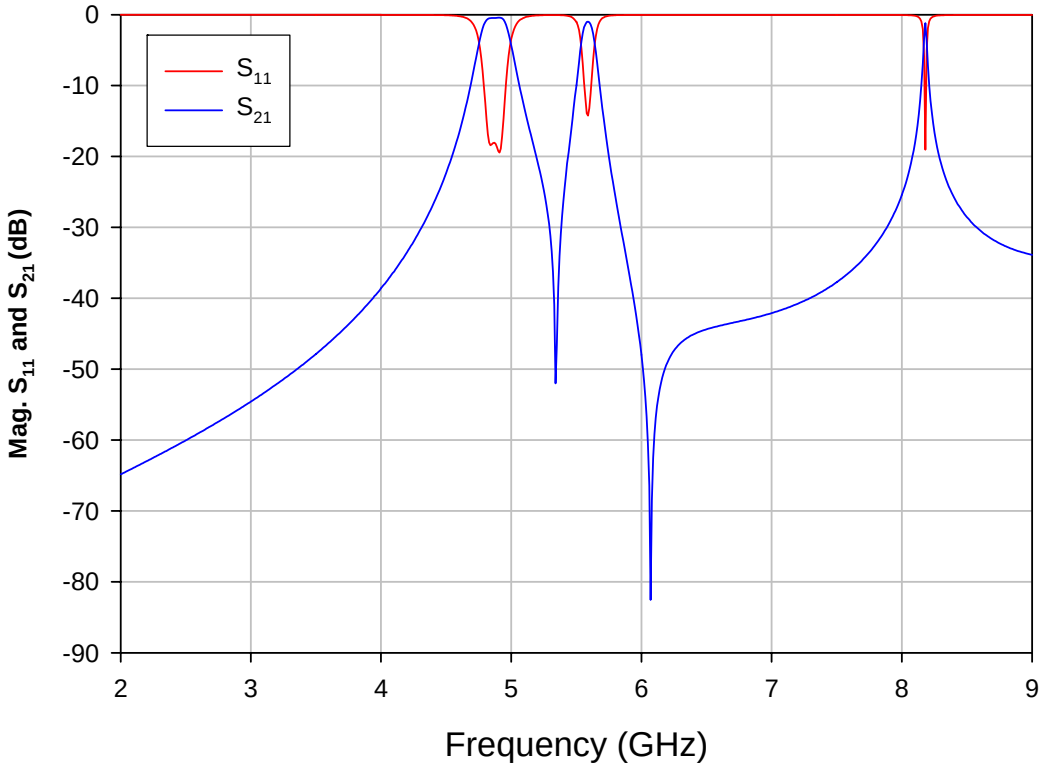

Figure 5-40 : Simulation wideband frequency response of 4-pole folded waveguide resonator filter.

5.3.3 4-pole multilayer substrate integrated folded waveguide SIFW dual-band filter

In this section, 4-pole SIFW dual passband filter, using a double layer of slotted folded waveguide resonators, is presented in Figure 5-41 and Figure 5-42. For our demonstration, a 4-pole dual-band filter of this type was successfully designed using a commercially available electromagnetic (EM) simulator [63]. The 4-pole dual passband filter design is based on a new coupling scheme and simulated with a compact multilayer structure. The design has been verified with the EM simulation.

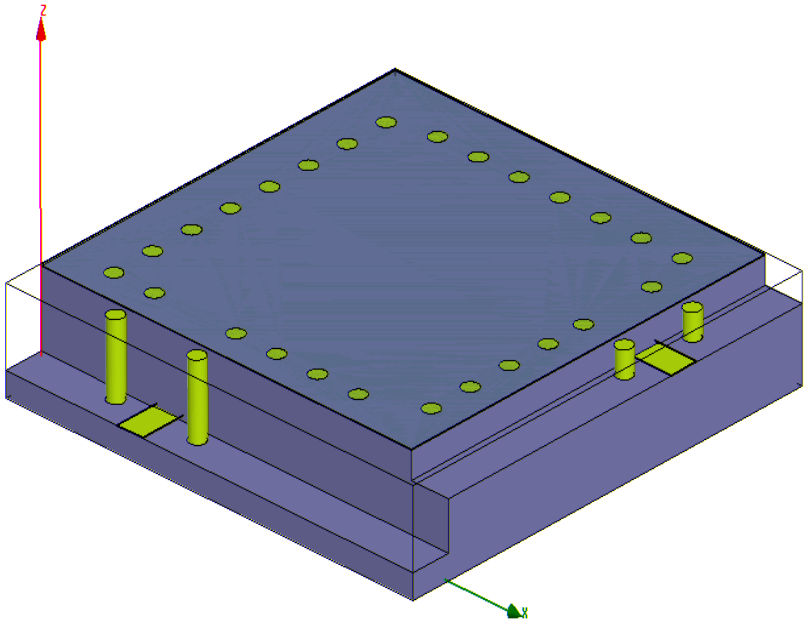

Figure 5-41: Proposed SIFW dual-band filter.

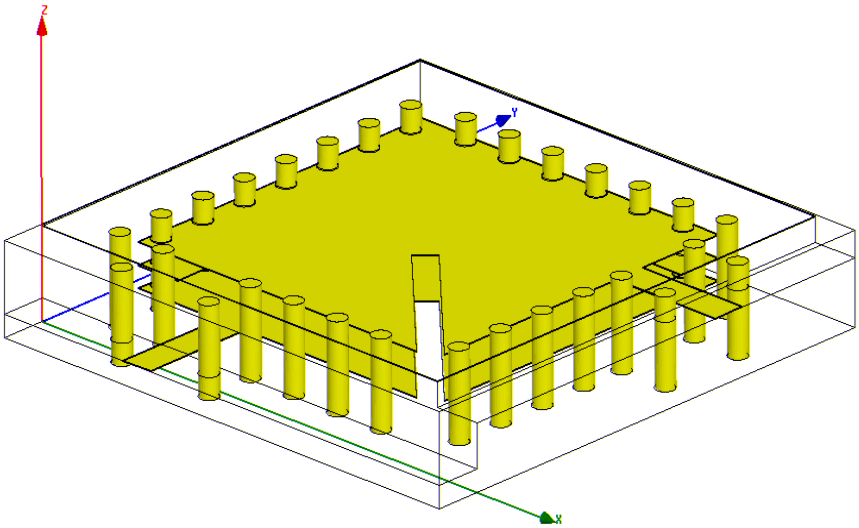

Figure 5-42: The side view of the proposed SIFW dual-band filter.

The simulation was also carried out to measure the frequency responses of the proposed filter, and the result is plotted in Figure 5-43.

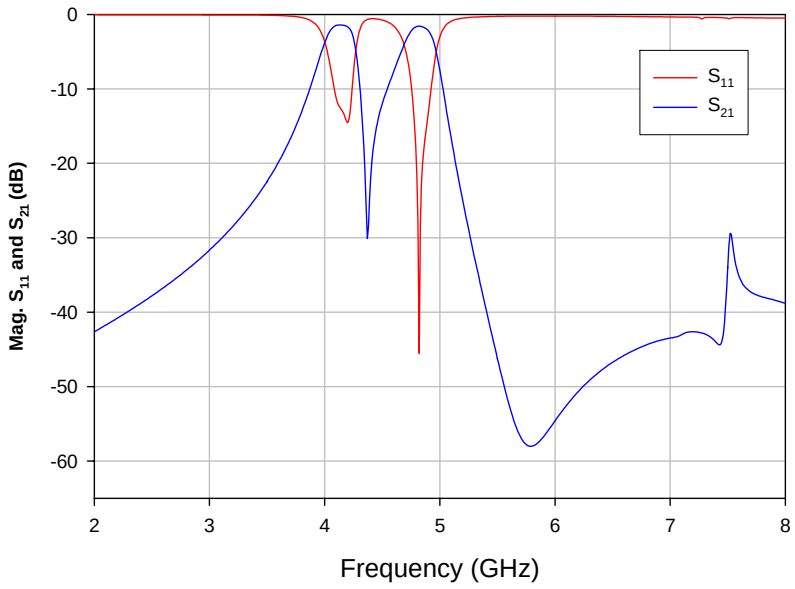

Figure 5-43: Simulated frequency response of S_{11} and S_{21} for a dual passband 4-pole SIFW resonator filter.

5.4 Summary

A new type of compact folded waveguide resonator filter using a novel slot technique was proposed. From the above results, it may be concluded that when the excitation port Length (*L*) varied, the return loss (S_{11}) was most dominant for this parameter. When the resonator gap (*RG*) in the corner varied, the most dominant parameter was the band width (BW). When the slot length in the separation plate varied, the TZ was the foremost affected. The best design for the bandpass filter with TZ for the high side band was when *SL* = 11.8 mm, *RG* =1.8mm and *L* = 2mm, and with TZ from the low side band when *SL* = 15.8 mm, *RG* =1.8mm and *L* = 2mm. Two designs of this type of filter with a finite-frequency transmission zero on either side of the passband have been demonstrated theoretically and experimentally. The ability to produce an asymmetric frequency response by simply changing the slot length is of interest. This chapter presents a primary investigation into developing a compact dual passband filter using novel folded waveguide resonators with a multilayer structure. A new coupling scheme for dual-band operation is realized, with both slot and aperture couplings being used for the implementation. For the demonstration, a 4-pole dual-band filter of this type was designed, fabricated and tested. Simulation and experimental results were presented to validate the design and to show the advantages of this type of filter. In addition, this new type of filter with a compact multi-layer structure and low loss is attractive for implementation with advanced device technologies, such as micromachining, LTCC and LCP technologies.

Chapter 6

Coupled Folded Waveguide (FWG) Filter

6.1 Introduction

The aim of this thesis is to design and develop a cavity resonator filter using a folded structure, and this chapter deals with the simulation and implementation for two designs of coupled folded waveguide (FWG) resonator filters and their frequency response, as shown in Figure 6-1 and Figure 6-2.

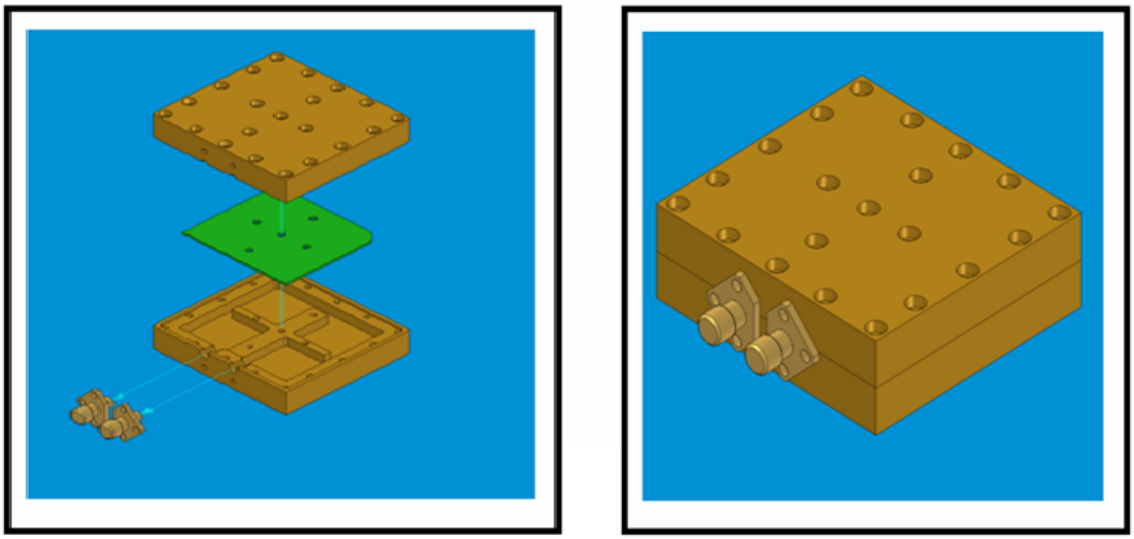

Figure 6-1: 4-pole cavity resonator filter (design 1).

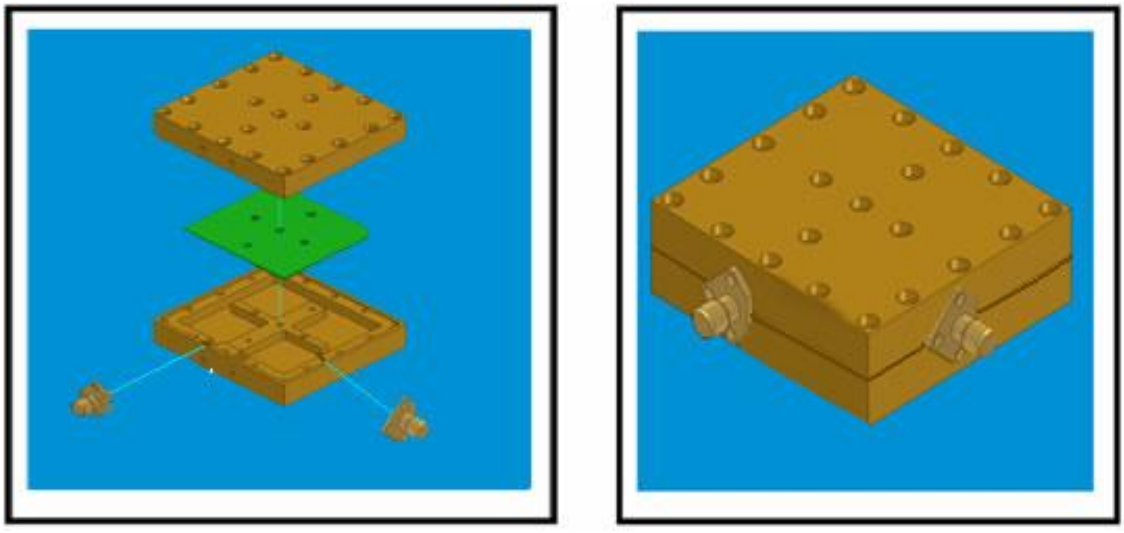

Figure 6-2: 4-pole cavity resonator filter (design 2).

The design procedure for both is almost the same; hence, the plan was divided into three stages. In the first stage the dimensions and the excitation port location were obtained from the 1-pole cavity resonator for the optimum external quality factor (Q_e) that is required. In the second stage, the same dimensions obtained from the 1-pole resonator were used, varying the gap length (G), the wall width (W) and a corner of the separation plate cutting (C) to attain the required coupling coefficients (K_{12}, K_{23} and K_{34}) to get an approximate design for the 2-pole resonators that could be used in the 4-pole resonator. After obtaining these results, the 4-pole resonator was simulated with the dimensions obtained by readjusting the values of G, W and C until the specified resonator requirements were obtained. The implementation of these designs and the experimental results are the core contents of this chapter, with certain specifications.

6.2 Novel coupled folded waveguide (FWG) resonator filter

In Figure 6-3 the first design of bandpass filter configuration and its coupling structure are shown. The filter is designed and implemented using four FWG resonators. Each of the FWG resonators [1] can maintain a fundamental resonant mode resembling TE_{101} mode with a smaller footprint amounting to only a quarter of that of the conventional TE_{101}mode cavity. Thus, the proposed 4-pole filter has size of approximately of a half of conventional TE_{101}mode cavity that operating at the same frequency. The filter is developed to realise the coupling structure of Figure 6-3b. In this structure, there are three significant coupling coefficients between adjacent resonators, namely K_{12}, K_{23} and $K_{34,}$ which are realised through opening the gaps between adjacent FWG resonators, as can be seen from the 3D view in Figure 6-3 (a). The coupling coefficient k_{ij} specifies the coupling between resonators i and j of the filter. When k_{ij} is evaluated, only resonators i and j are considered in the structure. For the symmetry, the couplings between resonators 1 and 2 and between resonators 3 and 4 are identical. Thus, there are two basic coupling structures to be investigated. The bandpass filter may be represented by an equivalent circuit, as shown in Figure 6-4 (a), where Q_{ei} and Q_{eo} are the external quality factors denoting the input and output couplings. The coupling coefficients and the external quality factors may be synthesized from a low-pass prototype filter, as shown in Figure 6-4 (b) where the rectangular boxes represent frequency invariant immittance inverters defined through a transmission matrix [32].

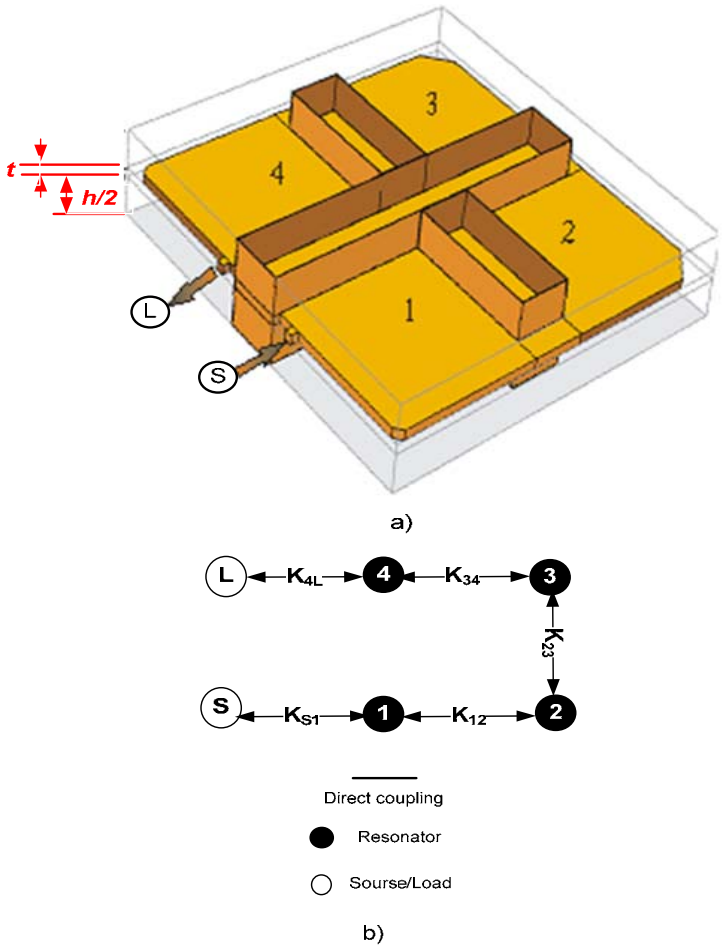

Figure 6-3: (a) Configuration of a 4-pole FWG resonator filter, (b) Coupling structure for the filter.

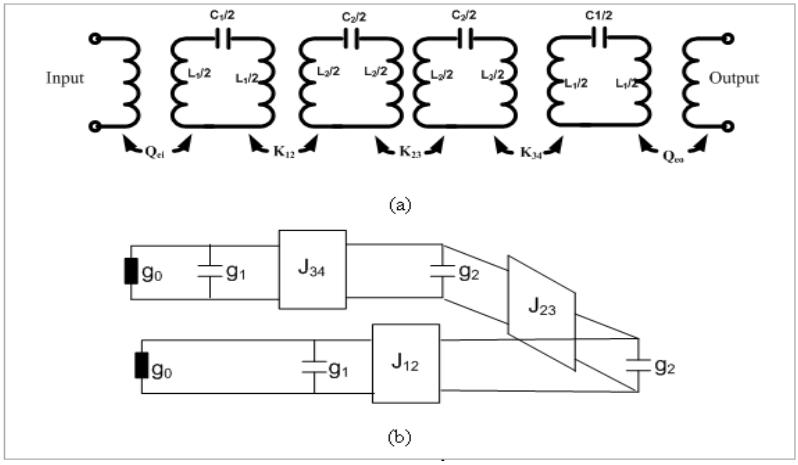

Figure 6-4: (a) An equivalent circuit of the 4-pole resonator filter. (b) An associated low-pass prototype filter.

In this work, a coupled FWG resonator bandpass filter was designed to have a fractional bandwidth (FBW) of 2.8 % at a centre frequency f_0 = 4.485 GHz. A 4-pole (n = 4) Tchebychev lowpass prototype with a passband ripple of 0.04321 dB was chosen. Also available were the values of g_o = 1.0, g_1 = 0.9314, g_2 = 1.2920. $J_{12} = J_{34} = 1$ and J_{23} = 0.90499. The external quality factors and coupling coefficients of the bandpass filter can be calculated by [32]:

$$Q_{ei} = Q_{eo} = \frac{g_0 g_1}{FBW} \tag{6-1}$$

$$K_{12} = K_{34} = \frac{FBW}{\sqrt{g_1 \times g_2}} \tag{6-2}$$

$$K_{23} = \frac{FBW.J_{23}}{g_2} \tag{6-3}$$

Thus, the coupling coefficients for the adjacent resonators in the theory are $K_{12} = K_{34} = 0.0255$ and $K_{23} = 0.0196$. The external quality factors $Q_{ei} = Q_{eo} = Q_e = 33.26$. The implementation of the filter was carried out in several steps, as described below.

6.2.1 1-pole resonator:

To realise the calculated external quality factor Q_e=33.26, a single resonator with a tapped input arrangement (see Figure 6-5) was simulated using a commercially available electromagnetic (EM) simulator [63]. This involved experimenting with the varied excitation port position (L) to achieve the desired external quality factor. The external quality factor was extracted from the simulated frequency response, as shown in Figure 6-6.

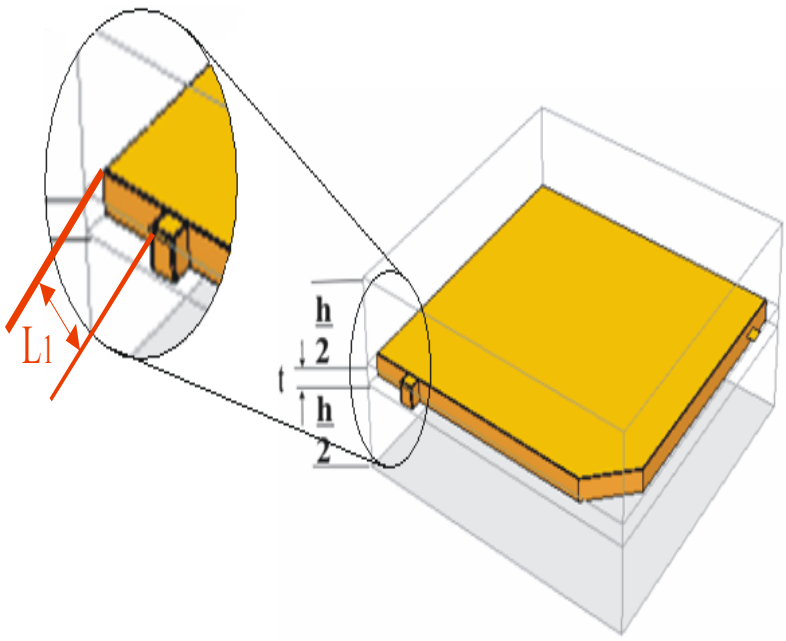

Figure 6-5: 3D Layout of 1-pole design.

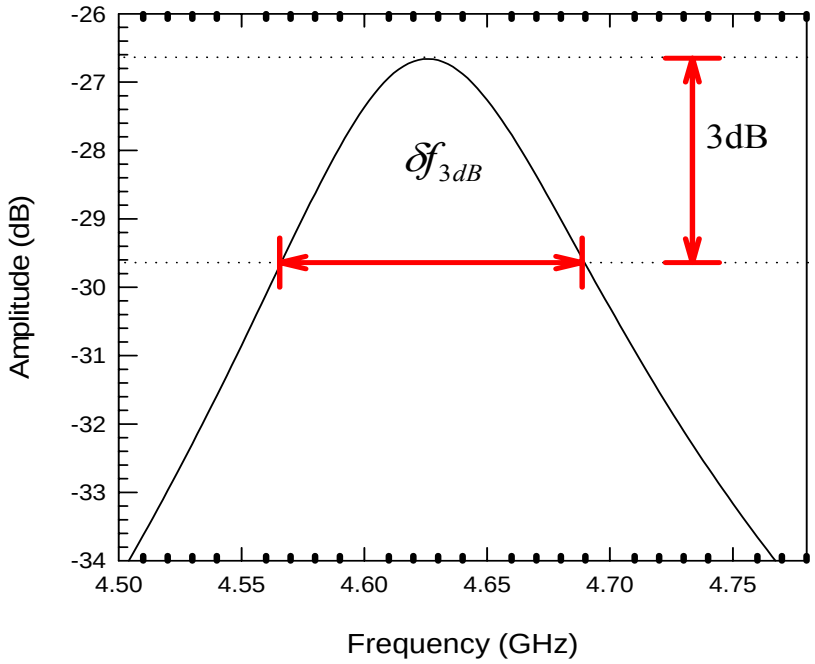

Figure 6-6: Typical frequency response simulated for extracting the external quality factor Qe.

6.2.1.1.1 Summary from the simulation results for 1-pole

From the results in the Appendix A, it may be concluded that when the excitation port Length (L) increases, the resonant frequency also increases, which causes a shift in the resonant frequency (f_0) to the right and then decreases the external quality factor (Q_e). When cutting (C) in the corner increases the resonant frequency, (f_0) increases also, while the external quality factor decreases and the resonant frequency is shifted to the right. When the excitation port length (L) and cutting (C) of the separation plate were varied, the desired and best external quality factors (Q_e), which will be used in further stages of the project, were obtained. The desired results to attain the requisite external quality factor (33.26) and excitation port L = 2.4mm.

6.2.2 2-pole and 4-pole resonator filters:

The next step of the filter design was to characterize the desired couplings between adjacent FWG resonators for each pair of resonators (K_{12} = K_{34} = 0.0255 and K_{23} = 0.0196). This was done by employing a 2-pole filter model in Figure 6-7 (a) with two input/output probes. Then, the combination of the coupling gap (G) between the resonators and corner cuttings (C) was varied to find the desired coupling coefficient from the simulated frequency response, as shown in Figure 6-7 (b). The corner cuttings

were introduced to compensate for the centre frequency shifting caused by the coupling gap G. The coupling K_{ij} of any pair of adjacent resonators was obtained by [32].

$$K_{ij} = \frac{(f_{p2})^2 - (f_{p1})^2}{(f_{p2})^2 + (f_{p1})^2} \tag{6-4}$$

where f_{p1} and f_{p2} are the lower and higher split resonant frequencies of a pair of coupled resonators.

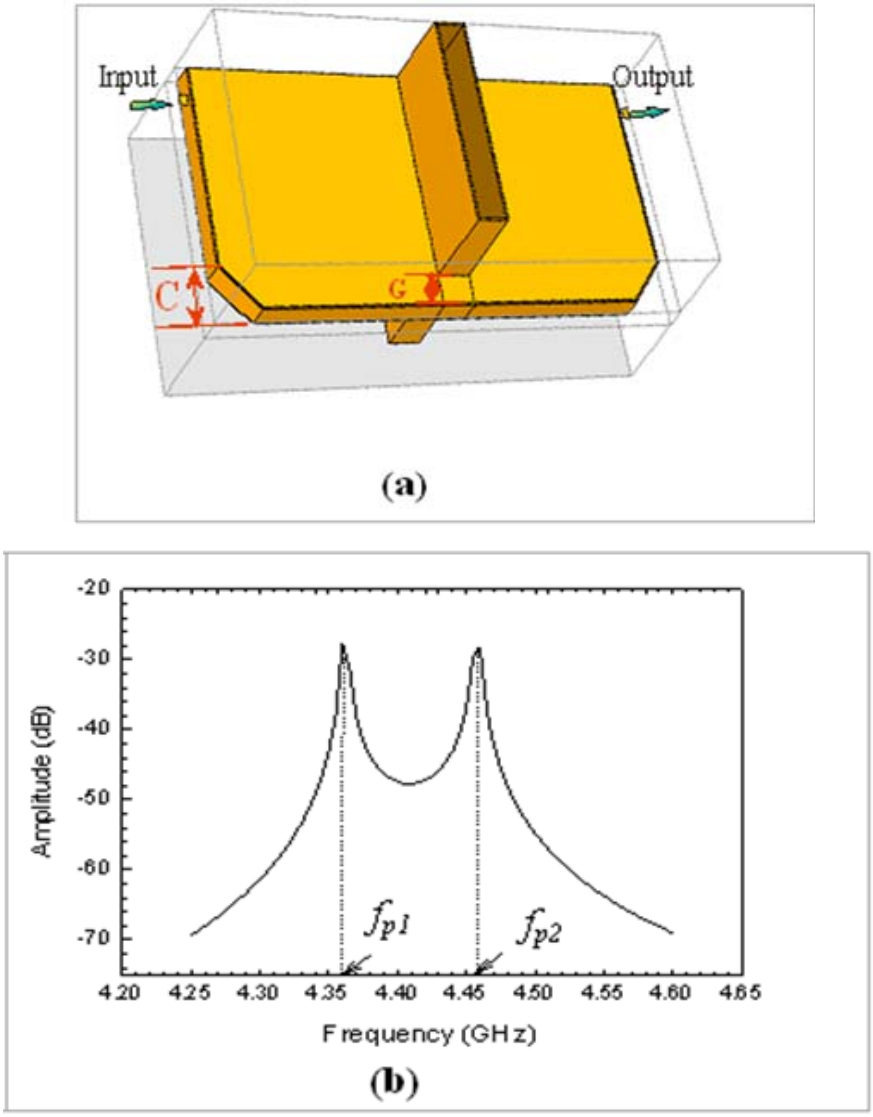

Figure 6-7: (a) 3D Layout of a 2 -pole design. (b) Typical frequency response simulated for extracting the coupling coefficient

6.2.2.1 Approach of extracting the coupling coefficient (K)

The same dimensions of the cavity obtained from the 1-pole resonator were used to give the desired result of Qe is 33.26, and the different coupling gap (G) between the resonators and its wall width (W) were varied to achieve the required coupling

coefficient of K_{12} = K_{34} = 0.0255 and K_{23} = 0.0196 using a sonnet S/W [63]. The parameters to be varied were coupling gap length (G), coupling wall width (W) and cuttings (C) of the separation plate corners.

6.2.2.1.1 Coupling gap length (G) and coupling wall width (W)

In these parameters, the coupling gap length (G) and the coupling wall width (W) between the two resonators in the 2-pole design, shown in Figure 6-8, were varied to obtain the desired specifications.

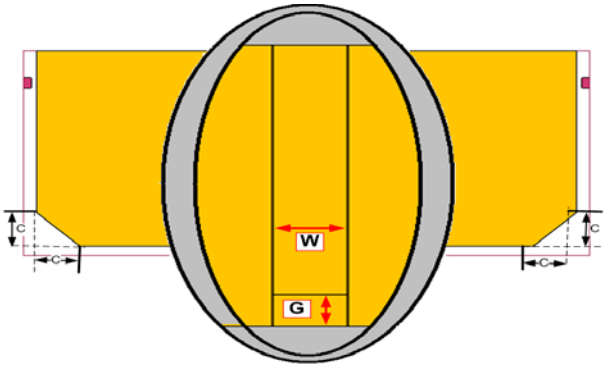

Figure 6-8: Top View of the coupling gap length (G) and coupling wall width (W)

6.2.2.1.2 Cuttings (C) of the separation plate corners

This was achieved by cutting (C) a different length from the two corners (C_1 and C_2) of the separation plate between the top and the bottom halves of the cavity (shown in Figure 6-9) until the required specifications were achieved.

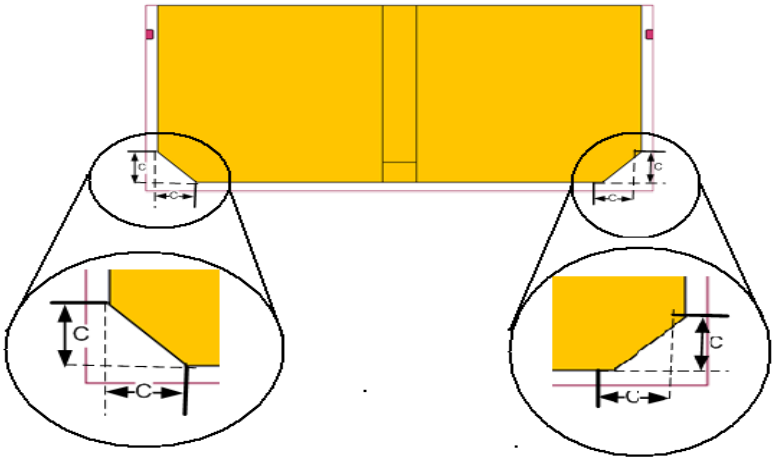

Figure 6-9: Top View of corner cutting (C).

6.2.2.2 Extracting the coupling coefficient (K)

The filter was developed to realize the coupling structure of Figure 6-10 (b). In this structure, there were three significant coupling coefficients between the adjacent resonators, namely K_{12}, K_{23} and K_{34}, which were realized through opening gaps between the adjacent FWG resonators, as can be seen from the 3D view in Figure 6-10 (a). The coupling coefficient k_{ij} specifies the coupling between resonators i and j of the filter. When k_{ij} were evaluated, only resonators i and j were considered in the structure.

For the symmetry, the couplings between resonators 1 and 2 and between resonators 3 and 4 were identical. Thus, there were two basic coupling structures to be investigated.

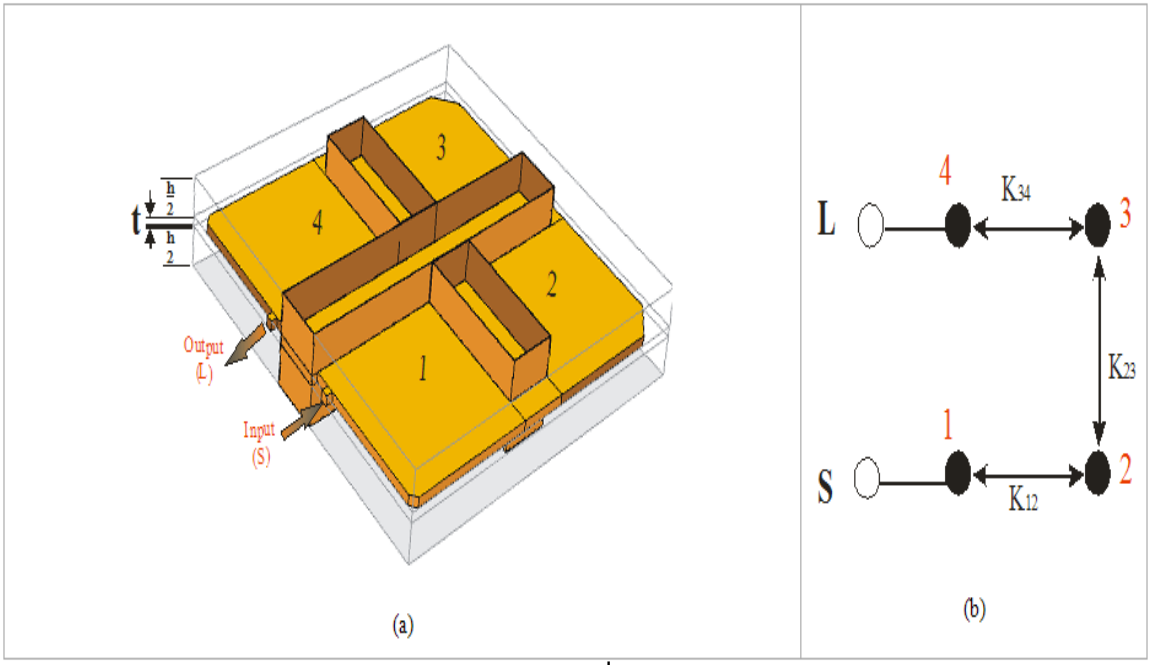

Figure 6-10: (a) Configuration of a 4-pole FWG resonator filter (b) Coupling structure for the filter.

They could be calculated using the conductance of the element values for the Chebyshev pass-band filter of the 4-pole resonator (g_0, g_1, g_2 and g_3) [32].

Where

$$g_0 = 1$$
$$g_1 = 0.9314$$
$$g_2 = 1.2920$$

$$K_{12} = K_{34} = \frac{FBW}{\sqrt{g_1 \times g_2}} \qquad (6\text{-}5)$$

From this formula, the coupling coefficient between the first and second resonators K_{12} which is symmetrically equal to that between the third and fourth resonators K_{34} is:

$$K_{12} = K_{34} = 0.0255$$

In addition, the coupling coefficient between the second and third resonators is given by the equation:

$$K_{23} = \frac{FBW.J_{23}}{g_2} \qquad (6\text{-}6)$$

where $J_{23} = 0.90499$

Hence $K_{23} = 0.0196$.

During simulations, the coupling coefficient (K) was calculated using the cut-off frequencies (F_1 and F_2) of the frequency response shown in Figure 6-11Figure 6-11. The coupling coefficient K_{ij} was calculated by the equation (6-7).

$$K_{ij} = \frac{(f_2)^2 - (f_1)^2}{(f_2)^2 + (f_1)^2} \qquad (6\text{-}7)$$

where f_{p1} and f_{p2} are the lower and higher split resonant frequencies of a pair of coupled resonators.

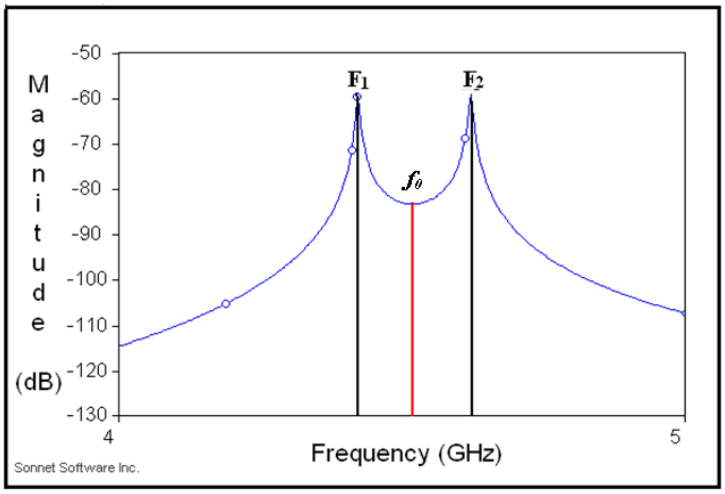

Figure 6-11: Frequency response of the 2-pole resonator to calculate the coupling coefficient K and the resonant frequency f_0

The central frequency (f_0) is calculated by the following equation (6-8).

$$Central\ frequency \quad f_0 = \frac{F_1 + F_2}{2} \tag{6-8}$$

6.2.3 Simulation results for coupling coefficients (K)

In this section, the frequency simulated responses for the coupling coefficients are presented.

6.2.3.1.1 Extracting coefficients K_{12}, K_{23} and K_{34}

In this section, results for the coupling coefficients K_{12}, K_{23} and K_{34} calculated from the simulated frequency responses are presented. Here, the coupling wall width 'W' was varied at 3, 7 and 8 mm; moreover the coupling gap 'G' was also varied as well. Furthermore, for each coupling gap length, the cutting (C) area of the separation plate corners was varied. The appropriate results are presented as follows.

6.2.3.1.1.1 Coupling Gap is 3mm when the coupling wall width (W) = 8mm

Table 6-1 presents the results obtained when the length of the coupling gap length (G) is 3mm with varied cutting (C) from both corners of the separation plate.

Table 6-1: Resonant frequency and coupling coefficient simulation results at a coupling gap length G =3mm

Cutting(C)	F_1 GHz	F_2 GHz	f_0 GHz	K
0	4.355	4.525	4.44	0.03872
1	4.375	4.55	4.4625	0.0392
2	4.44	4.62	4.53	0.0397
3	4.525	4.72	4.6225	0.0421
3.4	4.525	4.75	4.637	0.0484

6.2.3.1.1.2 Coupling Gap is 3.5mm

Table 6-2 below presents the results obtained when the length of the coupling gap length (G) is 3mm with varied cutting (C) from both corners of the separation plate.

Table 6-2: Resonant frequency and coupling coefficient simulation results at a coupling gap length G =3.5mm

Cutting(C)	F_1 GHz	F_2 GHz	f_0 GHz	K
0	4.27	4.51	4.39	0.0546
1	4.29	4.54	4.415	0.0565
2	4.35	4.61	4.48	0.0579

6.2.3.1.1.3 Coupling Gap is 2.6mm when the coupling wall width (W) = 7mm

Table 6-3 below presents the results obtained when the length of the coupling gap length (G) is 2.6mm with varied cutting (C) from both corners of the separation plate.

Table 6-3: Resonant frequency and coupling coefficient simulation results at a coupling gap length G=2.6mm

Cutting(C)	F_1 GHz	F_2 GHz	f_0 GHz	K
0	4.388	4.466	4.427	0.0176
1	4.42	4.5	4.46	0.0179
2	4.488	4.572	4.53	0.0185
3	4.578	4.666	4.622	0.0190
3.2	4.6	4.69	4.645	0.0193
3.4	4.62	4.712	4.666	0.0197
4	4.684	4.78	4.732	0.0202

By cutting (C) off 3.4mm from the corners of the separation plate, the coupling coefficient has the nearest value required for K_{23}.

6.2.3.1.1.4 Coupling Gap is 3mm when the coupling wall width (W) = 7mm

Table 6-4 below presents the results obtained when the length of the coupling gap length (G) is 2.6mm with varied cutting (C) from both corners of the separation plate.

Table 6-4: Resonant frequency and coupling coefficient simulation results at a coupling gap length G= 3mm

Cutting(C)	F_1 GHz	F_2 GHz	f_0 GHz	K
0	4.36	4.58	4.409	0.0222
1	4.394	4.492	4.443	0.0224

2	4.46	4.564	4.512	0.0230
3	4.55	4.658	4.604	0.0234
3.2	4.568	4.68	4.624	0.0242
3.4	4.588	4.702	4.645	0.0246
4	4.65	4.77	4.71	0.0254

By cutting (C) off 3.4mm from the corners of the separation plate, the coupling coefficient has the nearest value required for K_{12} and K_{34}.

6.2.3.1.1.5 Coupling Gap is 2.6 mm the coupling wall width (W) = 3mm:

Table 6-5 below presents the results obtained when the length of the coupling gap length (G) is 3mm with varied cutting (C) from both corners of the separation plate.

Table 6-5: Resonant frequency and coupling coefficient simulation results at a coupling gap length G= 2.6mm

Cutting(C)	F_1 GHz	F_2 GHz	f_0 GHz	K
1	4.428	4.494	4.461	0.0148
2	4.496	4.566	4.531	0.0154
3	4.586	4.658	4.622	0.0158
3.2	4.606	4.68	4.643	0.0159
3.4	4.626	4.702	4.664	0.0163
4	4.692	4.772	4.732	0.0169

6.2.3.1.1.6 Coupling Gap is 3mm when the coupling wall width (W) = 3mm

Table 6-6 below presents the results obtained when the length of the coupling gap length (G) is 3mm with varied cutting (C) from both corners of the separation plate.

Table 6-6: Resonant frequency and coupling coefficient simulation results at a coupling gap length G =3mm

Cutting(C)	F_1 GHz	F_2 GHz	f_0 GHz	K
0	4.37	4.45	4.41	0.0181
1	4.402	4.484	4.443	0.0184
3	4.556	4.648	4.602	0.0198

3.2	4.576	4.668	4.622	0.0199
3.4	4.596	4.69	4.643	0.0202
4	4.662	4.76	4.711	0.0208

6.2.3.2 Conclusions from the simulation results K_{12}, K_{34} and K_{23}

The 4-pole coupled folded waveguide filter containing four resonators with couplings between them was designed. This 4-pole resonator filter is composed of three 2-pole resonators. The design of these three 2-pole resonators was accomplished from the simulations carried out in section 6.2.2. The 4-pole coupled folded waveguide resonator filter was designed as a bandpass filter. In section 6.2.3.1.1.4, the coupling wall width (W) = 7 mm and coupling gap length (G) = 3 mm at the cutting (C) of the separation plate of 3.4mm from both corners is the desired value for (K_{12} and K_{34}). Also from section 6.2.3.1.1.3, the coupling wall width (W) = 7mm and the coupling gap length (G) = 2.6 mm cutting (C) from both corners of the separation plate of 3.4mm is the reasonable coupling coefficient value for K_{23}, as calculated and obtained at the same cutting (C) of K_{12} with wall width (W) = 7mm and coupling gap length (G) = 3 mm. Figure 6-12 (a) depicts the extracted coupling coefficient K and central frequency f_0 against different cutting (C) from both corners of the inserted plate for a fixed coupling gap G = 2.6mm. One can see that the coupling coefficient K and central frequency f_0 almost increase linearly with the increase of cutting length (C). A similar observation can be obtained for any other given G. Figure 6-12 (b) depicts the extracted coupling coefficient K and central frequency f_0 against the different coupling gap G between adjacent resonators for a fixed corner cutting (C) of 3.4mm. It was noticed that the coupling coefficient (K) is directly proportional to the coupling gap length (G), whereas the central frequency f_0 is inversely proportional to the G.

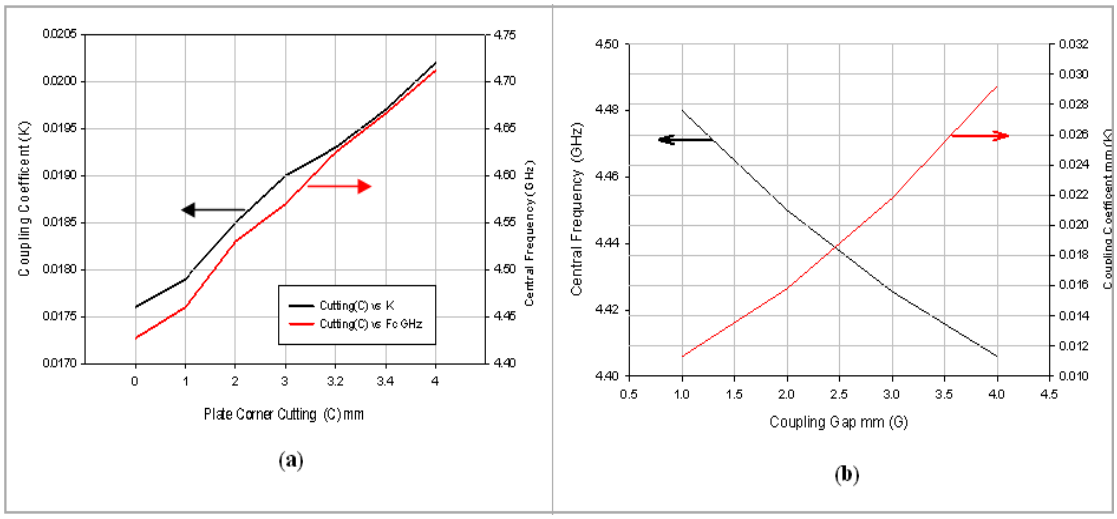

Figure 6-12: (a) The coupling coefficient at various cuttings from both corners for fixed gap G (2.6mm) (b) The coupling coefficient K_{23} at various gaps (G) for fixed corner cutting C (3.4mm).

6.3 Implementation of a 4-pole cavity resonator (Design 1):

The folded waveguide FWG 4-pole cavity resonator, shown in Figure 6-13, was fabricated. Figure 6-14 shows the components of the 4-pole cavity folded waveguide resonator filter.

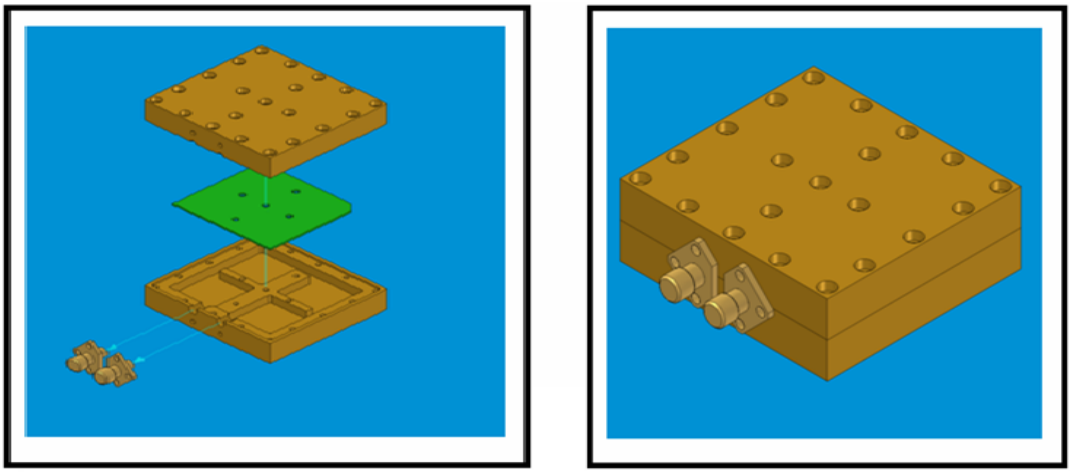

Figure 6-13: Layout of the 4-pole resonator filter (Design 1).

It is comprised of two identical halves (one of them is shown in Figure 6-14 (a). The two halves are separated by a brass plate, as shown in Figure 6-14 (b) and consist of two identical halves of a cavity separated by a brass plate between them, as shown in Figure 6-14 (c). The cavity size is 57mm × 61mm × 6mm with a 4.00mm recess depth. The metal has a thickness of 0.9 mm and the two excitation ports (circular cross section) are 0.4mm wide. The input/output (I/O) excitation ports are located next to each other on the same side wall of the resonator cavity, as shown in Figure 6-14 (d). The cavity

resonator was fabricated from an industrial brass material, where the conductivity of brass was taken as 1.57×10^7 S/m.

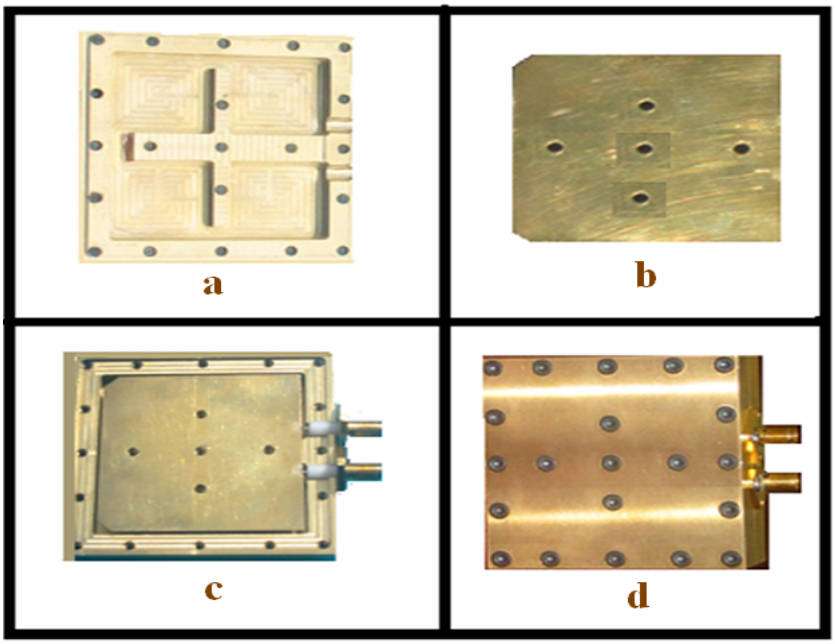

Figure 6-14: Fabricated 4-pole cavity resonator before assembly (a, b and c) and after assembly (d).

The excitation port length L is 2.4 mm (obtained from section 6.2.1) which gave the desired external quality factor of 33.26. The cavity dimensions are shown in Figure 6-15. The fabrication tolerances were +/- 0.05 mm and the bottom face was polished to 6 µm, with a polished internal face.

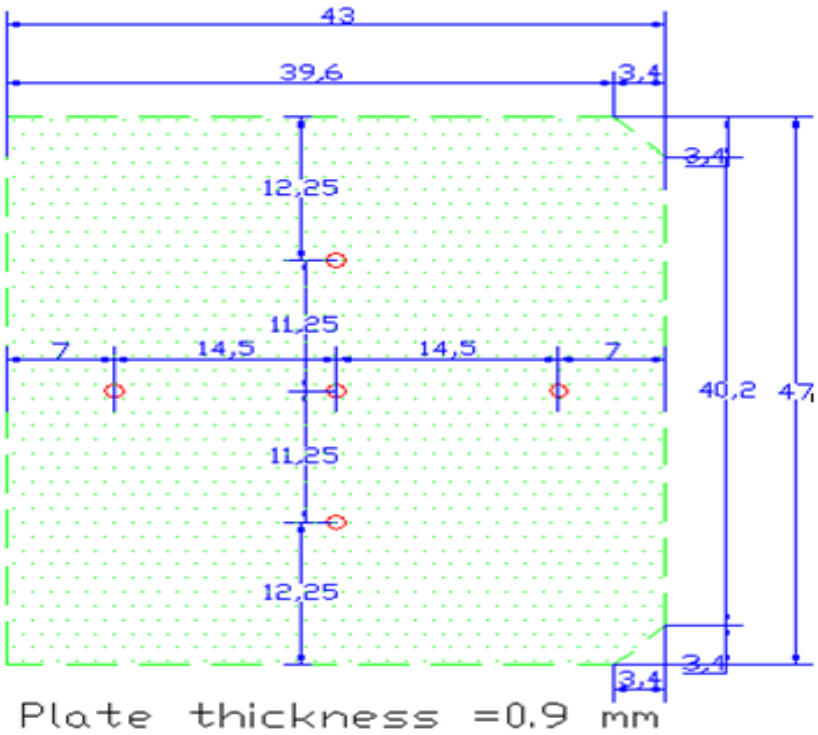

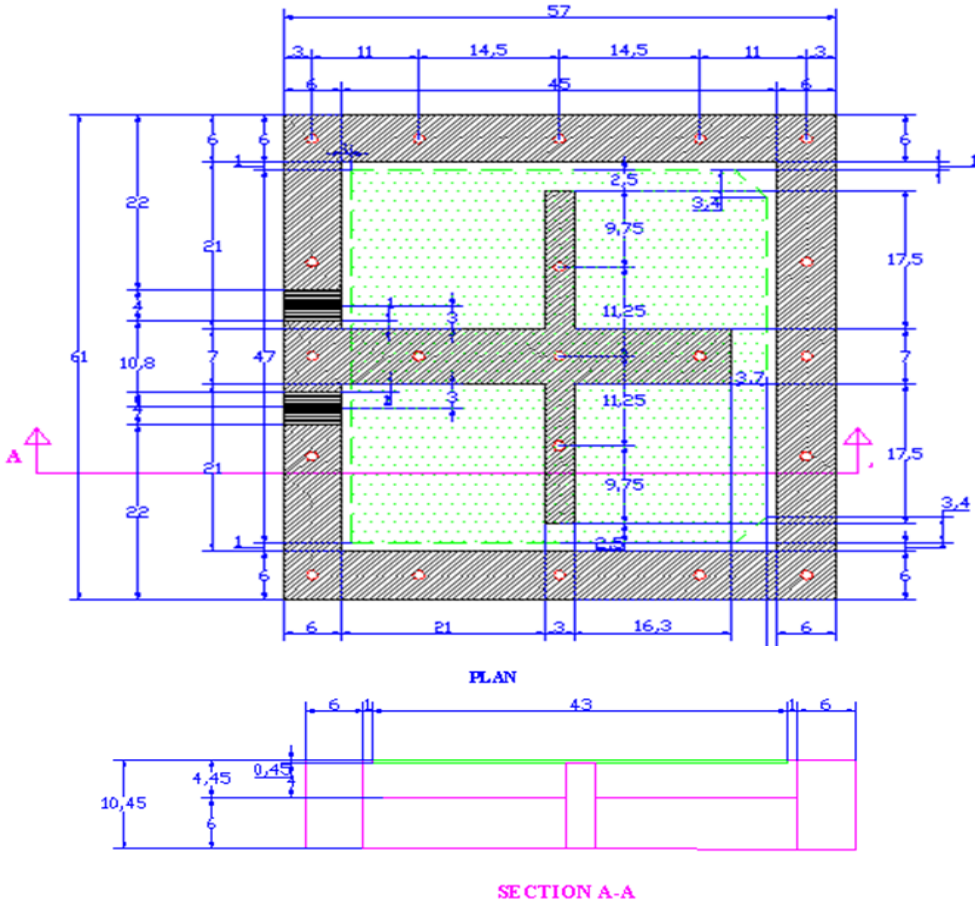

Figure 6-15: Dimensions (mm) of the 4-pole cavity resonator

6.3.1 Verification approach

An HP 8720 Network analyzer was used to measure the performance of the intended 4-pole coupled folded waveguide resonator filter. The approach was used to measure the 4-Pole cavity response, as shown in Figure 6-16.

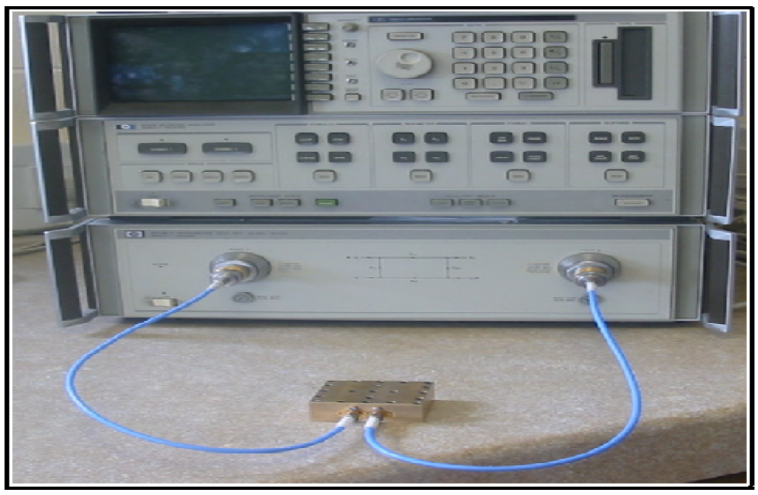

Figure 6-16: Cavity is connected to the HP network analyzer

6.3.2 Results:

The S-parameters of the fabricated FWG filter were measured using a calibrated HP network analyzer. Figure 6-17 plots the measured and EM simulated results, along with the theoretical ones for comparison; where a good agreement between the measurement and simulation can be observed. The filter showed a desired symmetric frequency response with a low insertion loss in the passband. The measured insertion loss at the midband was about 1 dB, including the losses from the two SMA connectors. In Figure 6-17 (a) and (b), normalized frequencies were used in the plots for the theoretical centre frequency 4.485 GHz, the measured centre frequency of 4.39 GHz and the simulated centre frequency of 4.49 GHz. The experiment was also carried out to measure the wide-band frequency response of the demonstrator, and the measured result is plotted in Figure 6-18 .

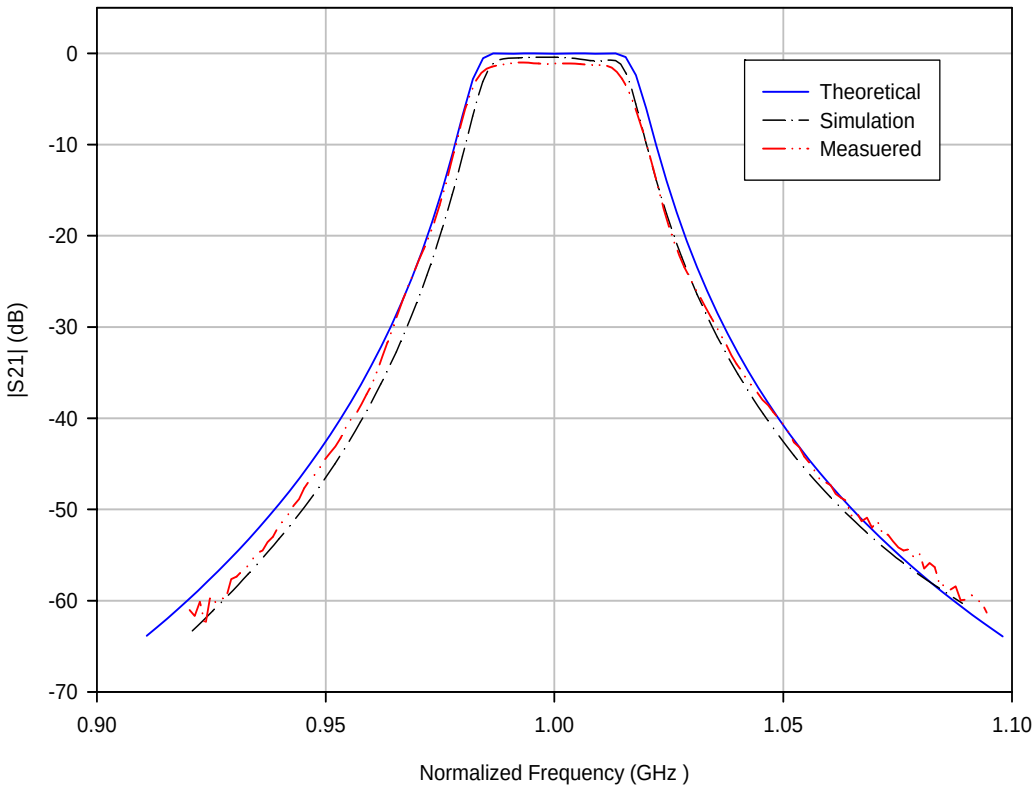

(a)

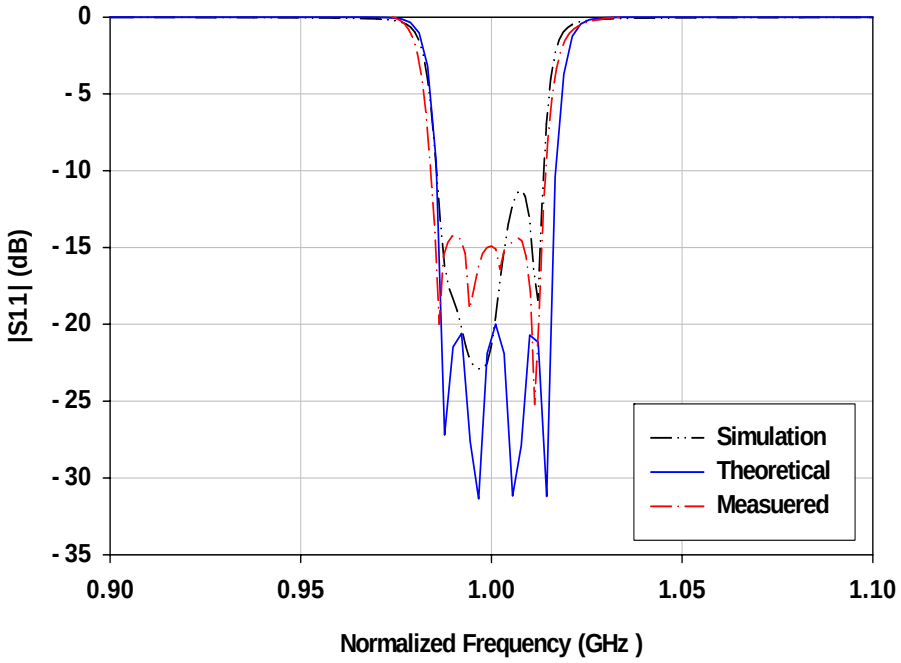

(b)

Figure 6-17: Simulated, theoretical and measured frequency response (a) is insertion losses and (S_{21}) where (b) is return losses (S_{11}).

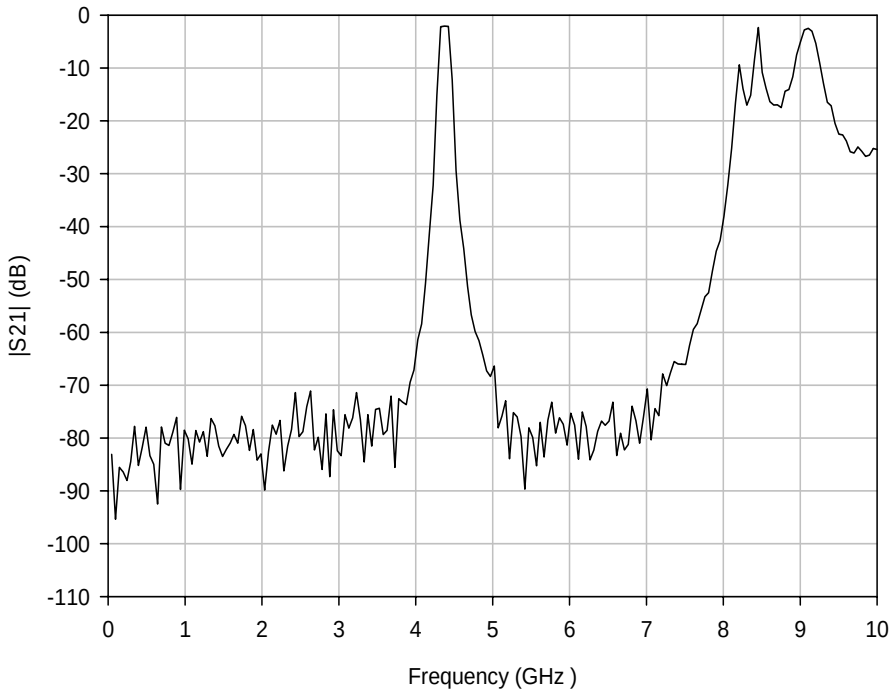

Figure 6-18: Measured wide-band frequency response of the fabricated 4-Pole cavity.

The following Table 6-7 compares the frequency responses of the theoretical, simulated and fabricated 4-Pole FWG resonator filter. The slight discrepancies are caused by the tolerances in both fabrication and simulation.

Table 6-7: Comparison of theoretical, simulated and measured results.

	Theory	Simulation	Measurement
f_0 (GHz)	4.485	4.49	4.39
FBW	0.028	0.027	0.027

6.4 Implementation of a 4-Pole cavity resonator (Design 2):

The second design, mentioned earlier in this chapter, is a new 4-Pole bandpass filter design based on FWG resonators. The filter exhibits an asymmetric frequency response and combines a compact size with high quality factors. It is obvious that the FWG resonator filter will be suitable not only for micromachined devices, but also for waveguide devices that are fabricated by using conventional techniques. A demonstrator was fabricated and tested. Theoretical, simulated and measured results are presented. The fabricated of folded waveguide (FWG) resonator filter with asymmetric frequency response design is shown in Figure 6-19.

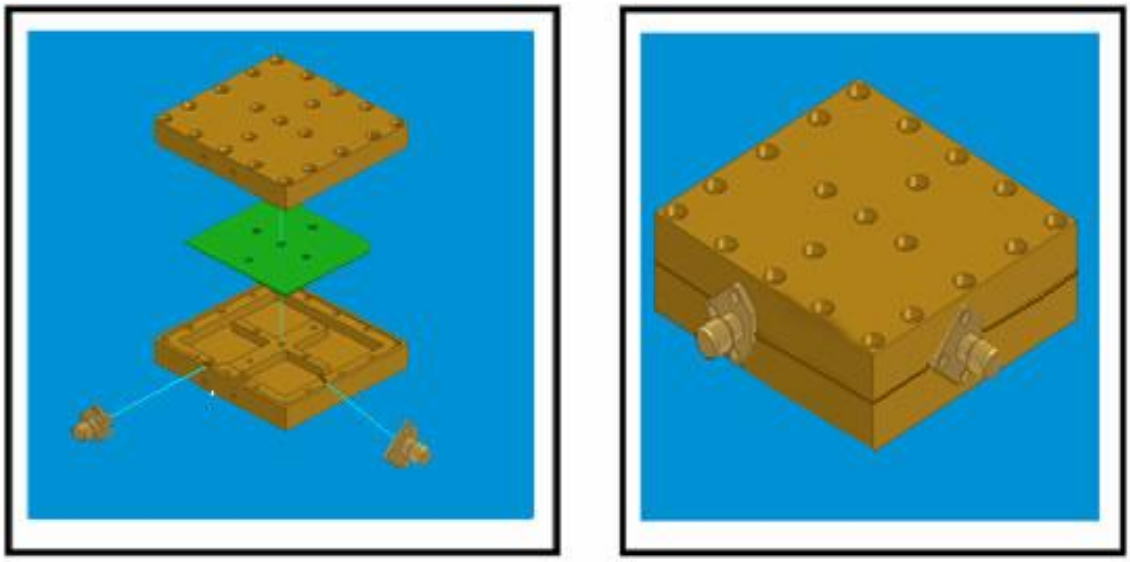

Figure 6-19: 4-Pole cavity resonator filter (design 2).

6.4.1 Filter Design

The proposed bandpass filter configuration and its coupling structure are shown in Figure 6-19. The filter was designed and implemented using 4-Pole folded waveguide resonators. The 3D schematic of the filter is shown in Figure 6-20 (a). In that figure, G is the coupling gap between the adjacent resonators, *t* is the thickness of the separation plate, *h/2* is the depth of the upper and lower cavities, and C is the corner cutting. The

coupling structure to realize the filter is shown in Figure 6-20 (b), where S is the source, L is the load, and coupling coefficient K_{ij} specifies the coupling between resonators i and j of the filter. The proposed design is a four-order asymmetric response filter with one transmission zero located in the high side band of the filter. A synthesis method of coupled resonator filters with the source/load-multi-resonator coupling proposed in [64] may be used. The generalized coupling matrix [m] for our filter design is given by:

$$[m] = \begin{bmatrix} 0 & 1.86 & \underline{0.75} & 0 & 0 & 0 \\ 1.86 & -0.495 & 1.304 & 0 & 0 & 0 \\ \underline{0.75} & 1.304 & 1.05 & 0.628 & 0 & 0 \\ 0 & 0 & 0.628 & 0.06 & 0.766 & 0 \\ 0 & 0 & 0 & 0.766 & 0 & 1.021 \\ 0 & 0 & 0 & 0 & 1.021 & 0 \end{bmatrix} \tag{6-9}$$

The elements of the coupling matrix [m] give the normalized coupling coefficients and scaled external quality factors. In this case, the coupling matrix will have a non-zero entry of m_{S2} (coupling between S and resonator 2, underlined elements in the matrix [m]) for the desired cross coupling; it will also have non-zero diagonal elements.

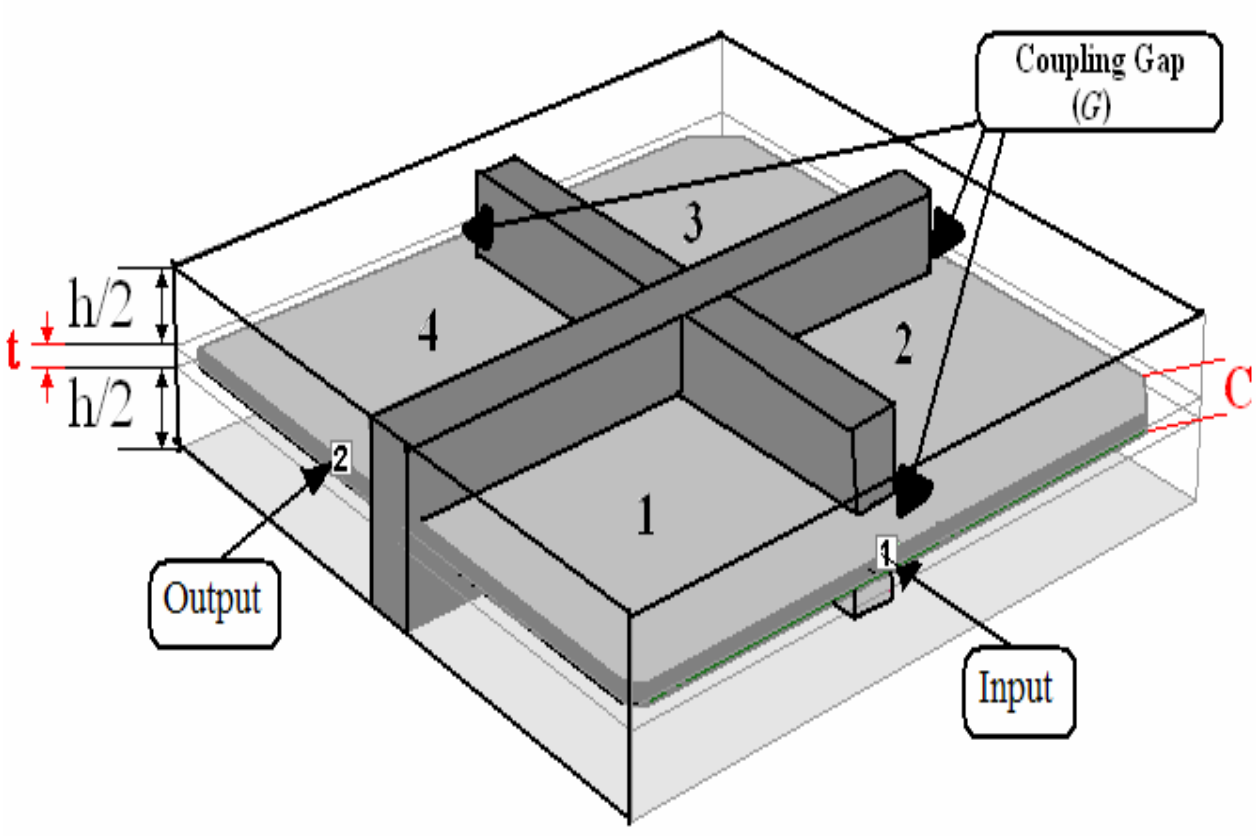

(a)

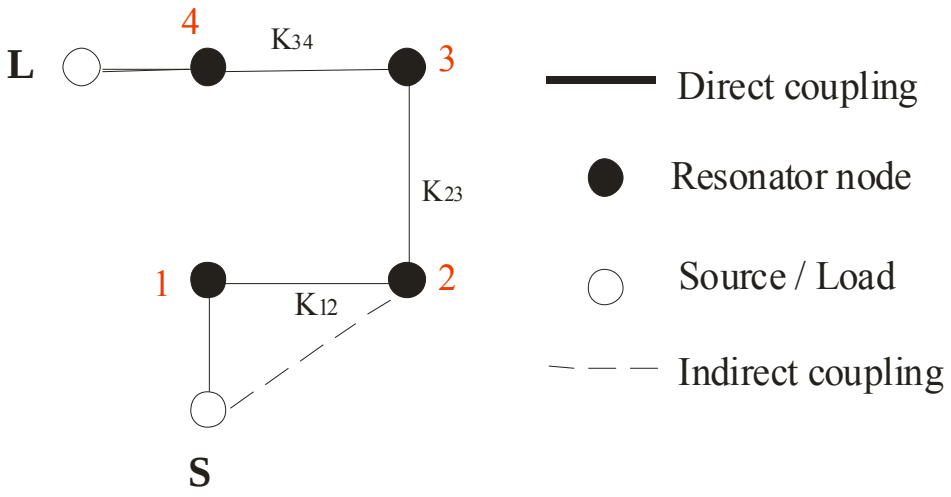

(b)

Figure 6-20: a) Configuration of a 4-Pole folded waveguide resonator filter, b) Coupling structure for the filter.

6.4.1.1 Extracting external quality factor (Qe)

For our filter design, f_0 = 4.45 GHz and fractional bandwidth FBW = 0.05. Using the design parameters obtained from the matrix [m], the implementation of the filter was carried out in several steps, as described below. The external quality factor associated with input/output (I/O) coupling for the filter design can be found from the generalized coupling matrix [m]. For example, the external quality factor Q_{e4} (external quality factor of the output resonator) is calculated by [65]:

$$Q_{e4} = \frac{1}{FBW \cdot m_{L4}} \tag{6-10}$$

To realize the calculated external quality factor, a single resonator with a single tapped input arrangement was simulated using a commercially available electromagnetic (EM) simulator [63]. This involved experimenting with the varied excitation port position L1 and cutting from the separation plate corner C to achieve the desired external quality factor, which was extracted from the EM simulated resonant frequency response (as shown in Figure 6-22), as described in section 6.2.1.

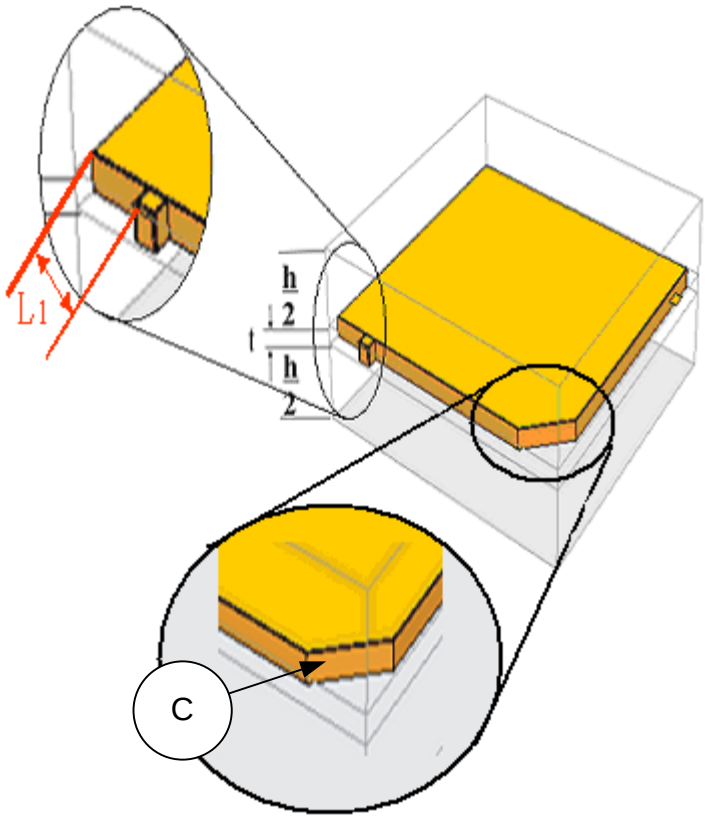

Figure 6-21: 3D Layout of a single-pole design while C and L1 are clear.

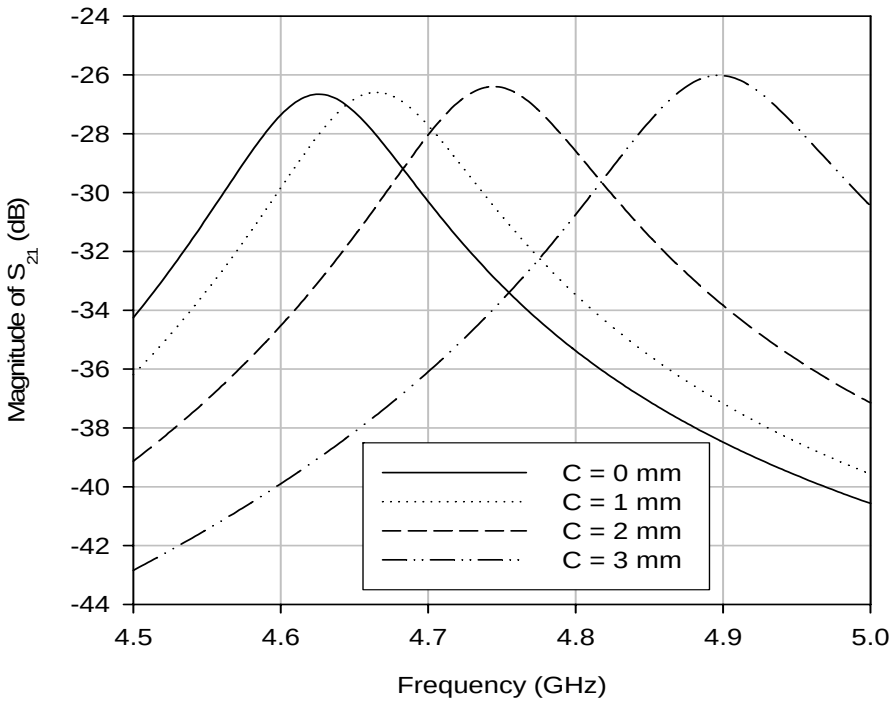

Figure 6-22: Simulation responses to obtain Qe and C.

From Figure 6-22, it is clear that the central frequency has shifted to the right and the reason for that is the variation in corner cutting *C* (from 0 to 3 mm) while the excitation

port position L1 = 2.2 mm. In Figure 6-23, it may be seen that when cutting (C) in the corner increases the central frequency, (f_0) increases as well, while the external quality factor decreases.

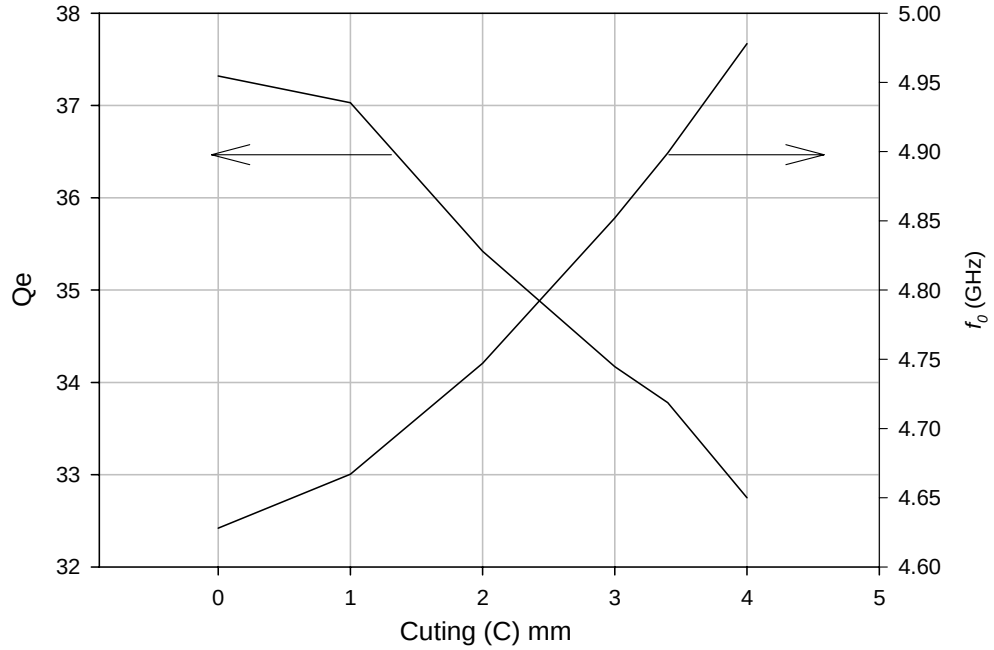

Figure 6-23: The values of f_0 and Qe for different C

6.4.1.2 Extracting coupling coefficients

The next step of the filter design was to characterize the desired couplings between the adjacent resonators for each pair of resonators, i.e. K_{12}, K_{23} and K_{34}. For example, the coupling coefficient K_{34} between resonators 3 and 4 was calculated at 0.0383. To realize these coupling coefficients, 2-Pole coupled resonator structures one for each coupling coefficient were simulated. These 2-Pole resonator designs were achieved by employing the two input/output (I/O) probes that were very weakly coupled and were used to excite the coupled resonators in order to simulate mode splitting characteristics. Then, the coupling gap *G* was varied between the coupled folded waveguide resonators, as shown in Figure 6-24

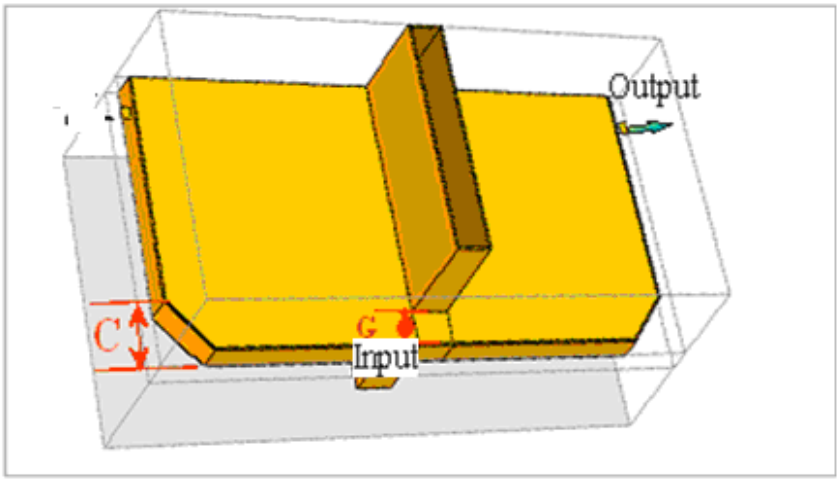

Figure 6-24: 3D Layout of the two -pole design while G is clear.

For the simulated resonant frequency, the coupling K_{ij} was obtained by the method used in [32]; using Sonnet EM, a commercially available electromagnetic simulator [63]. Strictly speaking, for our design the coupled resonators needed to be tuned individually, which was achieved by introducing corner cuts *C* of the separation plate as indicated in Figure 6-21. It was found that these corner cuts had little impact on the couplings. The two coupled resonators were kept at the same frequency around the centre frequency of the filter. This was particularly valid for the designed narrow-band filters. Typical simulated frequency responses of 2-Pole coupled folded waveguide resonators are shown in Figure 6-25, for different values of the coupling gap *G* with a fixed length of the excitation port location L_1 = 2.2mm. In this case, the locations of the I/O excitation ports were not critical as long as the two split resonant modes could be observed in the EM simulation.

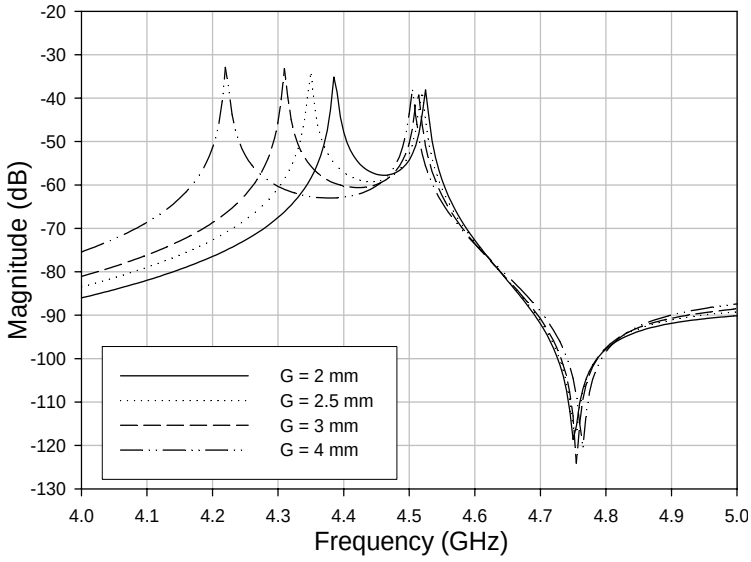

Figure 6-25: Typical frequency response simulated for extracting the coupling coefficient for fixed L1 = 2mm

It can be seen clearly in Figure 6-25 that two dominant resonant frequencies split away from the resonance condition as a result of the electromagnetic couplings. The coupling can easily be controlled by the size of the coupling gap G, and the coupling was stronger when the coupling gap became wider. This, however, also shifted down the central frequency between the two split modes. The understanding of these coupling natures would be helpful in realizing the filter. Figure 6-26 depicts the extracted coupling coefficient K and central frequency f_0 against the different coupling gap G between the adjacent resonators for a fixed excitation port length location (L_1 = 2.2 mm) from the coupling wall. Table 6-8 lists the extracted design parameters for all the direct couplings.

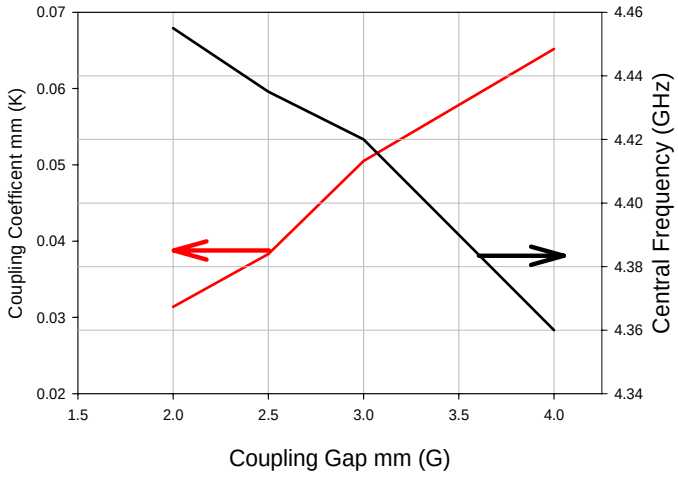

Figure 6-26: The coupling coefficient varying when increasing G for fixed C from both corners.

Table 6-8: The extracted parameters for the filter design.

The Coupling	Coupling gap (G) mm	f_0 GHz	K
K_{12}	4	4.36	0.0652
K_{23}	2	4.455	0.0314
K_{34}	2.5	4.435	0.0383

It was found that the location of excitation port 1, i.e. L_1, affects the allocation of transmission zero, but not the inter-resonator coupling. This observation is shown for a fixed coupling gap of 2.5 mm in Figure 6-27. L_1 affects the cross-coupling between the source and resonator 2 as well. For the 4-pole filter, the general effects of excitation port length location L_1 can be seen from Figure 6-28. It shows that the return loss in the passband depends on the excitation port location. This suggests that to have a good passband response, the allocation of the transmission zero may not be controlled independently.

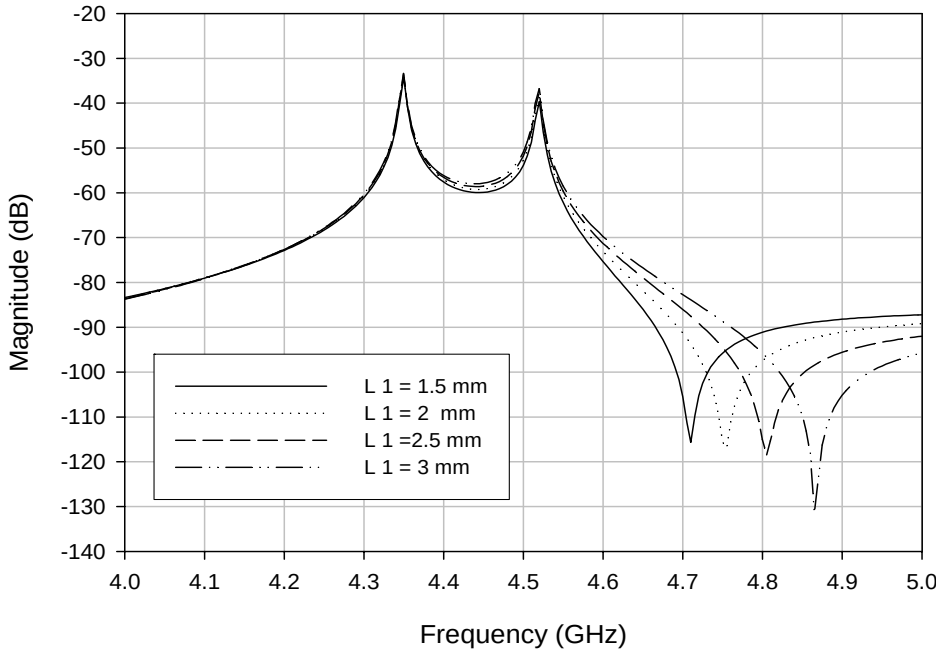

Figure 6-27: Typical frequency response of coupled resonators simulated for a different length of excitation port L1 for fixed G = 2.5mm

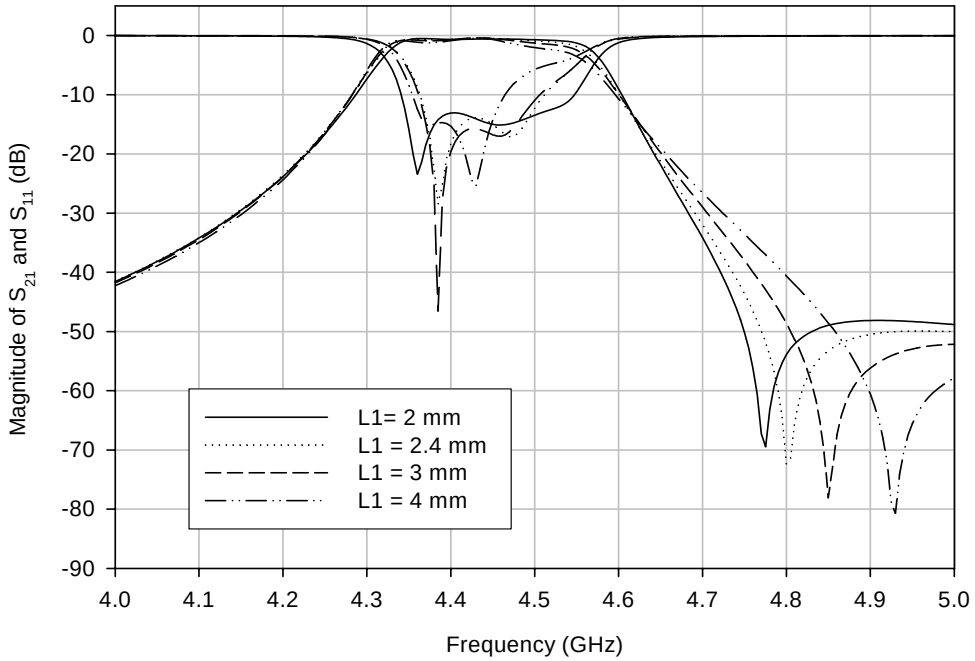

Figure 6-28: Typical frequency response of a 4-pole filter simulated for a different value of excitation port L1.

6.4.1.3 Filter demonstration

The proposed folded waveguide resonator filter will be suitable not only for micromachined devices, but also for conventional fabrication techniques. The designed folded waveguide resonator filter was fabricated from an industrial brass material.

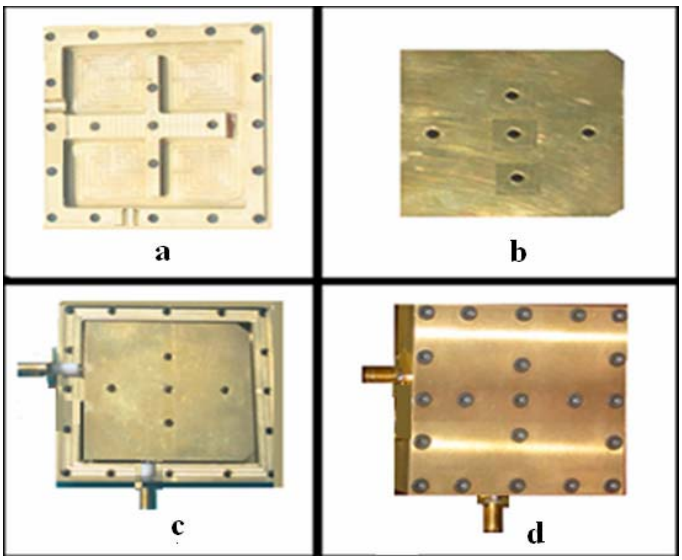

Figure 6-29: Fabricated 4-pole folded waveguide resonator filter before assembly (a, b and c) and after assembly (d).

Figure 6-29 shows the fabricated demonstrator before and after assembly, where the two I/O probes, which were tapped into the plate between the two half, can clearly be seen. The fabrication tolerances were +/- 0.05mm and the bottom face was polished to 6μm, with a polished internal face. The fabricated 4-pole folded waveguide resonator filter is comprised of two identical halves (one of these is shown in Figure 6-29 (a). The two halves with a recess of 4 mm, which will form the required cavity, were inserted with a 1mm-thick brass plate, as in Figure 6-29 (b). Two SMA connectors as I/O excitation ports were tapped to the plate, shown in Figure 6-29 (c). The completely assembled filter, as illustrated in Figure 6-29 (d), has a size of 57mm × 57mm, including 6mm-thick walls along all sides. The following Table 6-9 compares the frequency responses of the theoretical, simulated and fabricated 4-Pole folded waveguide resonator filter. The slight discrepancy is caused by the tolerances in both fabrication and simulation.

Table 6-9: Comparison of theoretical, simulated and measured results.

	Theory	Simulation	Measurement
f_0 (GHz)	4.45	4.48	4.41
FBW	0.05	0.057	0.058

Figure 6-30 gives the details of the dimensions of the demonstrator. Figure 6-30 (a) shows the dimensions of the plate which was inserted between the two halves, and the cutting from the corners was done to compensate for resonant frequencies. Figure 6-30 (b) shows the dimensions of one half of the cavity filter and the plan section A-A. The S-parameters of the fabricated filter were measured using a calibrated HP network

analyzer. Figure 6-31 plots the theoretical results, along with the EM simulated and measured results for comparison, where a good agreement between them can be observed. As can be seen, an attenuation pole of finite frequency on the upper side of the pass-band led to a higher selectivity on this side of the passband. The filter shows a desired asymmetric frequency response with a low insertion loss in the passband. The measured insertion loss at the midband was about 1 dB, as shown in Figure 6-31a, including the losses from the two SMA connectors. The measured return loss was about 14 dB, as shown in Figure 6-31b. The unloaded quality factor of the similar resonator was tested to be about 500[1].

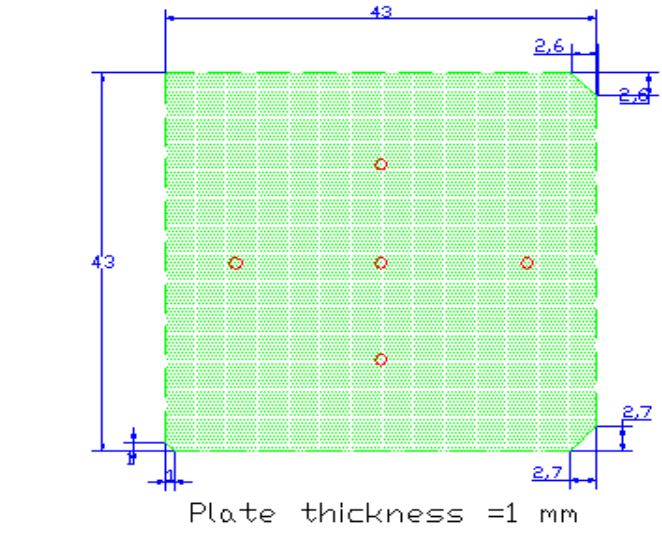

(a)

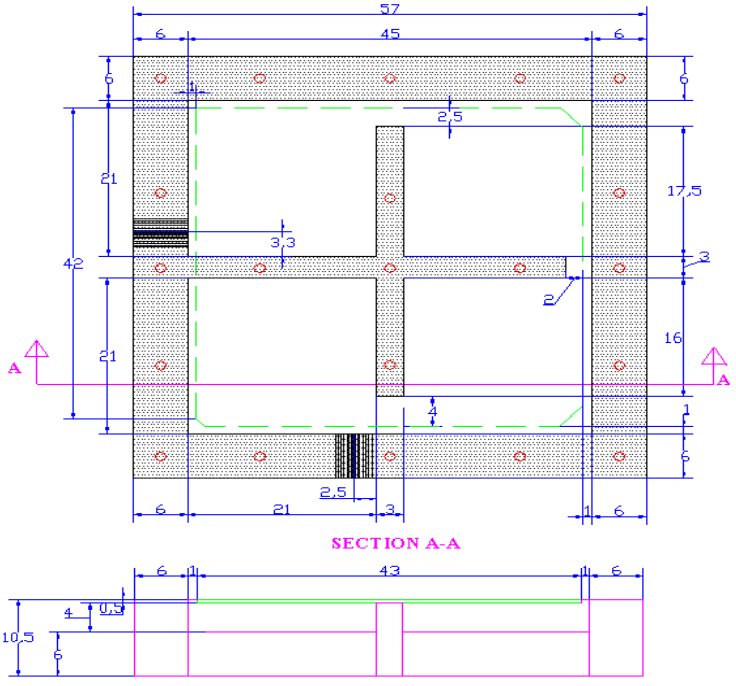

(b)

Figure 6-30: (a) Dimensions (mm) of a separation plate between the two halves (b) Dimensions (mm) of one half of the 4-Pole cavity resonator filter.

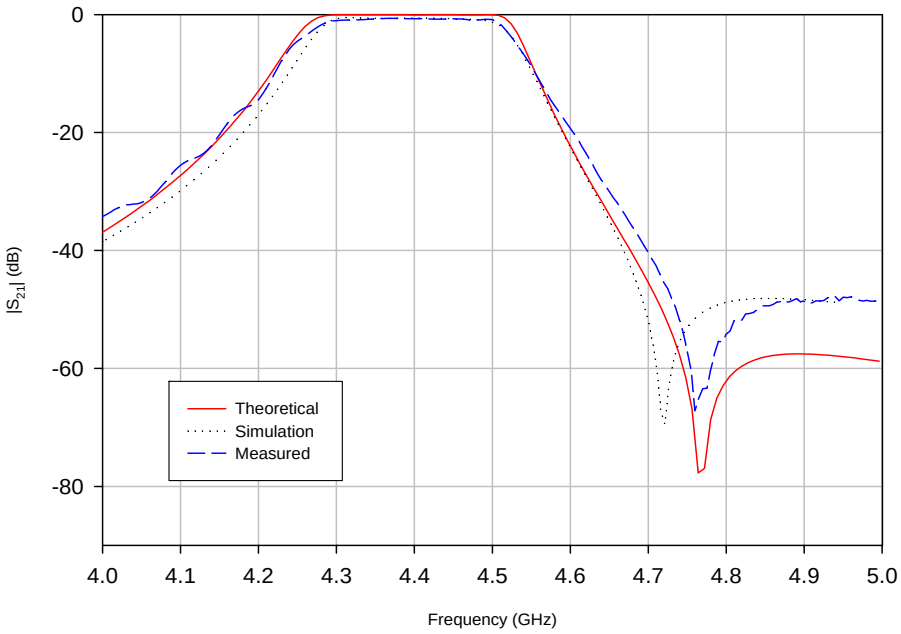

a)

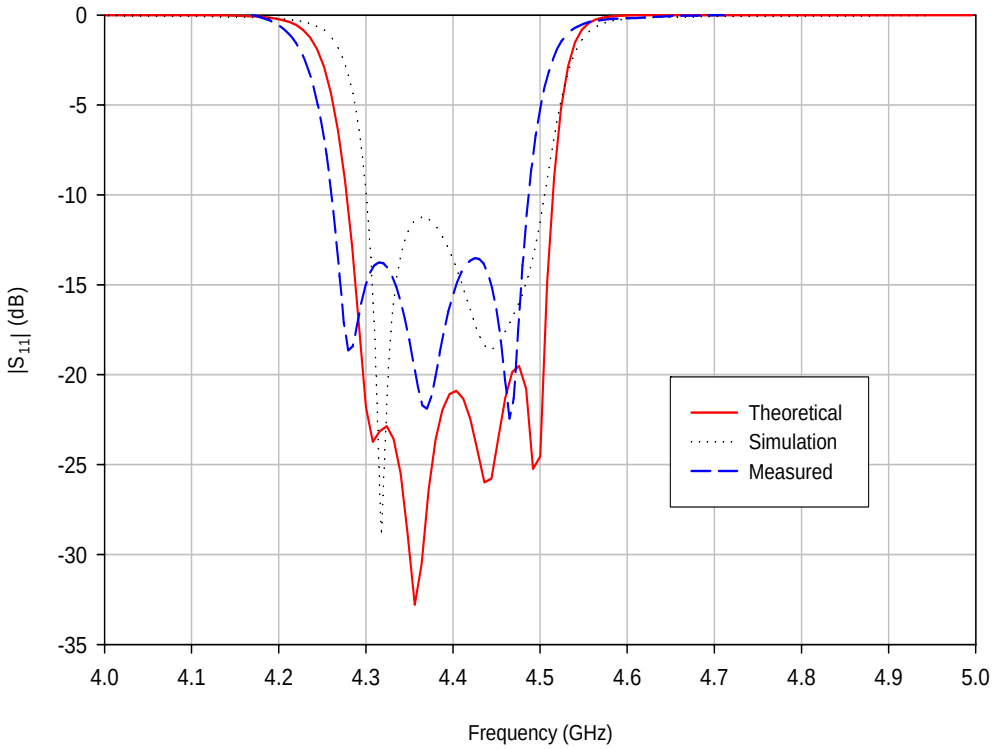

b)

Figure 6-31: Measured and simulated responses of the 4-pole folded waveguide resonator filter (a) S21, (b) S11.

The experiment was also carried out to measure the wide-band frequency response of the demonstrator, and the measured results are plotted in Figure 6-32. It is interesting to observe that the spurious resonant modes appeared only above 8.5 GHz and there was a wide stopband between the fundamental and the first spurious resonant mode. This is

because the TE_{102} mode in a conventional waveguide resonator cannot be excited in the folded waveguide resonator due to different boundary conditions. This is a desired characteristic for designing bandpass filters based on the fundamental mode.

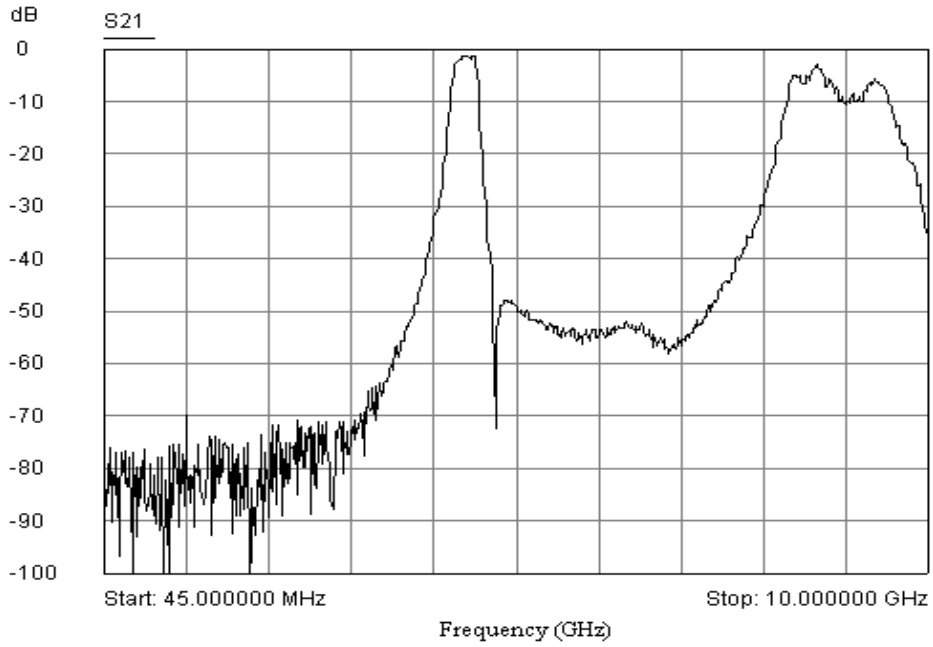

Figure 6-32: Measured wide-band frequency response of the fabricated 4-pole folded waveguide resonator filter.

6.5 Summary:

The two designs of the 4-Pole coupled FWG resonator filter were designed, fabricated and tested. Their designs and implementations were based on the full-wave electromagnetic simulation, and validated by the experiment. The measured and simulated results were in very good agreement. Owing to the high Q of the FWG resonators, the new filters were shown to have a low insertion loss in the passband with a very compact size. This was achieved with the knowledge of the 1-pole compact folded waveguide resonator. Initially, a 2-Pole resonator was designed and the result was the 4-Pole design. It was achieved using Auto CAD software in the dimension part, and was fabricated in the Heriot-Watt University Mechanical and Physical workshops. Next, testing was carried out to analyze the performance of the fabricated resonators, using the HP network analyzer in the microwave lab in the Electrical and Electronic Department at Heriot-Watt University. These new types of low loss and compact size filters are expected to be attractive for implementations with advanced device technologies, such as micromachining and LTCC. With this chapter, the first two, rather precisely predetermined aims were completed. The final aim of this thesis is to investigate configurations for further improvement of SIFW resonator filters that will be addressed in the next chapter.

Chapter 7

Substare Integrated Folded Wavguide (SIFW) Filter

7.1 Introduction

The design procedure of designing FWG resonator filters that used in the previous chapter is almost the same of this chapter. In this chapter numbers of experiments have been conducted to develop a Substrate Integrated folded waveguide SIFW resonator filter using a folded structure. Hence, this chapter deals with simulation and implementation for two designs of SIFW resonator filter and their frequency response, as shown in Figure 7-1 and Figure 7-2. The first design is a novel Substrate Integrated folded waveguide SIFW resonator filter, and an aperture coupling between the adjacent resonators is introduced, which is characterized using full-wave EM simulations and verified experimentally will be described in 7.2. The second design is a Substrate Integrated Folded waveguide SIFW filter with an asymmetrical frequency response which is described in 7.3. In this design, a filter uses an advanced coupling scheme to achieve a desired asymmetric frequency response with an attenuation pole of finite frequency on the high side of the passband filter.

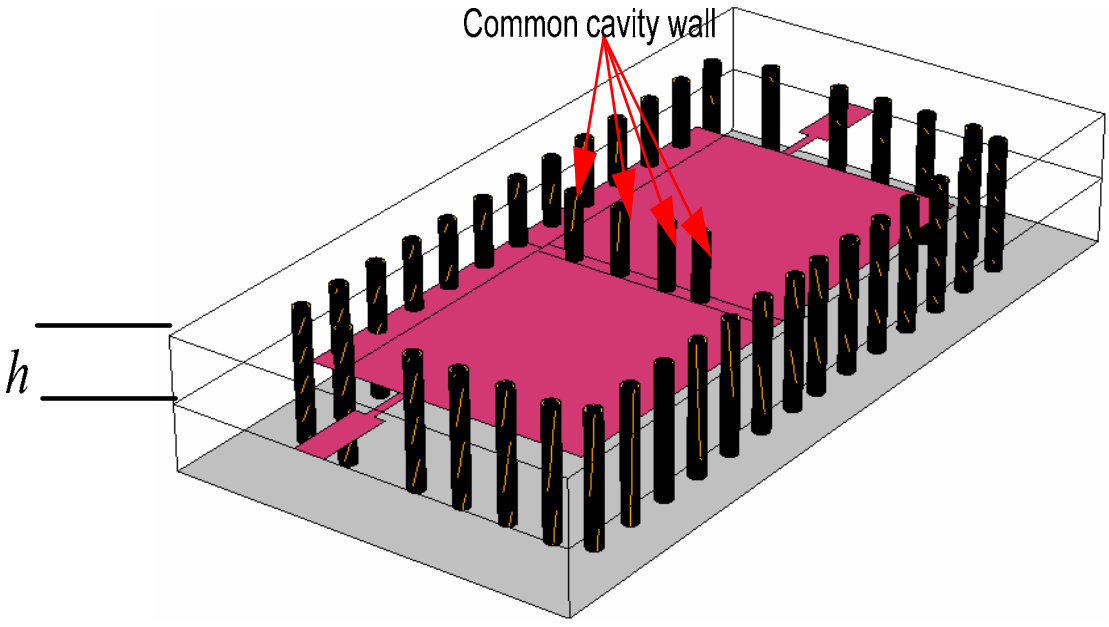

Figure 7-1: 3D image of the proposed SIFW filter Design (1).

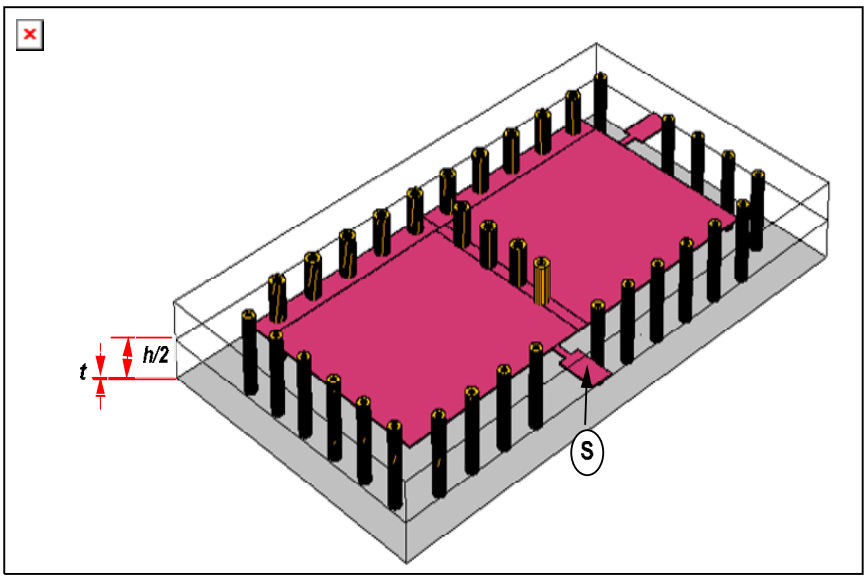

Figure 7-2: 3D image of the proposed SIFW filter Design (2).

The demonstrators of both designs have been discussed in 7.2.5 and 7.3.1 respectively, and an aperture coupling between adjacent resonators is introduced. Both designs are 2-Pole substrate integrated folded waveguide SIFW resonator filter type. For compression, a 2-Pole BPF centred at 4.675 GHz with a fractional bandwidth of 7.4% was designed, fabricated, and measured. Simulations and experimental results are presented to validate the design and to show the advantages of these types of filters. For both structures, a full-wave simulator was employed for designing the filter, and the proposed filter circuit design was implemented. It was found that the experimental result of the constructed filter is in close agreement with the simulation result. This filter also provides an improved selectivity characteristic with a compact size compared with conventional resonator filters. The simulation result is presented to show the advantages of this type of filter, and the proposed SIFW filter structures are promising for LTCC and LCP technologies.

7.2 A substrate Integrated folded waveguide (SIFW) resonators filter (Design 1):

The proposed substrate integrated folded waveguide (SIFW) is based on the concept of the folded waveguide [1]. It was recently presented that a novel type of compact waveguide resonator has been developed, stemming from the concept of folding standing waves of a conventional TE_{101}-mode waveguide resonator. It has been shown that a so-called folded waveguide quarter-wavelength resonator has only a quarter of the footprint of the conventional TE_{101} waveguide resonator, but still preserves a similar

high-Q property. In section 7.2.2. a single resonator of the substrate integrated waveguide (SIFW) has been design. Furthermore, a proposed 2-pole substrate integrated folded waveguide resonator filter, as shown in Figure 7-1 has been designed based on a single resonator structure. The coupling between two folded waveguide quarter-wavelength resonators will be described in 7.2.4, and will include full-wave electromagnetic (EM) simulation and experimental validation. Moreover, the realization of a 2-Pole filter demonstrator is presented, which is verified both by simulation and experimentation.

7.2.1 Cavity Size

The initial size of the SIFW cavity can be determined by corresponding the resonance frequency for the TE_{101} dominant mode, using the following formula [44]:

$$f_{101} = \frac{c}{4\pi\sqrt{u_r \varepsilon_r}} \sqrt{\left(\frac{\pi}{w_{eff}}\right)^2 + \left(\frac{\pi}{l_{eff}}\right)^2} \tag{7-1}$$

Where w_{eff} and l_{eff} are the effective width and length of the resonant SIFW cavity, respectively given by:

$$\text{Leff} := l - \frac{d^2}{0.95 \cdot p} \tag{7-2}$$

$$\text{Weff} := W - \frac{D^2}{0.95 \cdot p} \tag{7-3}$$

where w and l are the width and length of the SIFW cavity, respectively. Note that d and p are the diameter of the metallic via and the space between adjacent vias, respectively, while c is the velocity of light in the vacuum, and μ_r and ε_r are the relative permeability and the relative permittivity of the substrate [67].

7.2.2 1- pole SIFW resonator

To realize `and attain a good unloaded quality factor Qu, a single resonator of the substrate integrated waveguide (SIFW) with two striplines connected to two excitation ports as denoted by the S and L arrangement and vias wall (see Figure 7-3) was

simulated using a commercially available electromagnetic (EM) simulator [63]. The 1-pole resonator was designed using a folded substrate integrated waveguide SIFW structured. This was done by manipulating many design structures and varying many parameters, e.g. box size, excitation port locations L, via hole (d) and the distance between the via (p) based on equations (7-12) and (7-13). The dielectric constant of 3.2, a substrate thickness of h = 0.762 mm with loss tan δ = 0.003 for each layer has been considered.

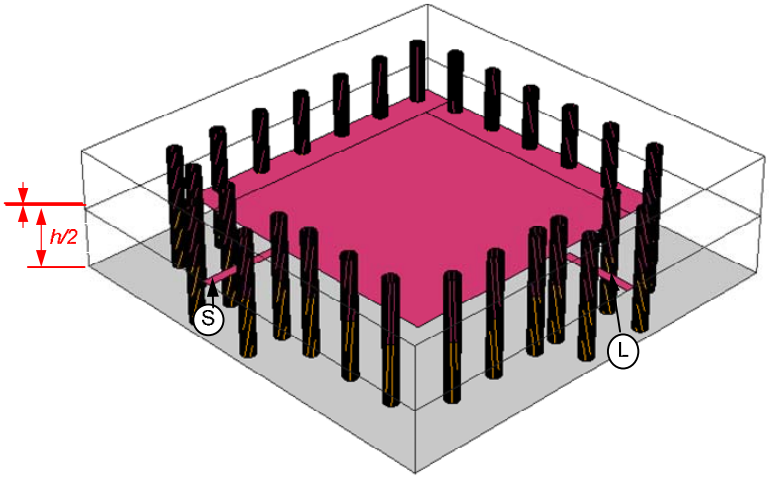

Figure 7-3: Top view of a 1-pole resonator layout

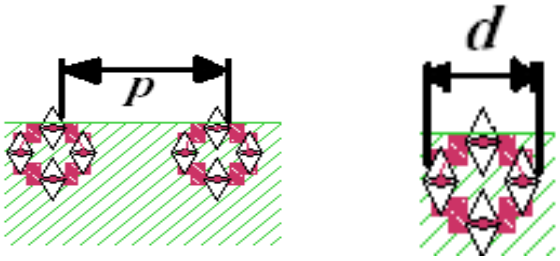

(a) (b)

Figure 7-4: (a) Distance between the via holes. (b) Via hole Diameter

7.2.3 Simulation results of the single SIFW resonator:

The following sections contain the simulation results for 1-pole resonator design using the folded substrate integrated waveguide SIFW structure in order to reach the required result.

7.2.3.1 Diameter of via d at 0.2 mm and varying the distance between the vias p

The following Table 7-1 shows the results that were obtained when the diameter of via d at 0.2 mm and varying the distance between the vias p:

Table 7-1: Simulation results for d=0.2 mm.

P mm	f_0 GHz	Q_u
0.4	6.65	224
1	6	216
1.5	5.2	203
2.5	4.5	189

The following Figure 7-5 shows the relation between f_0 and Q_u when the diameter of the via *d* was fixed at 0.2 mm and the distance between the via *p* was varied.

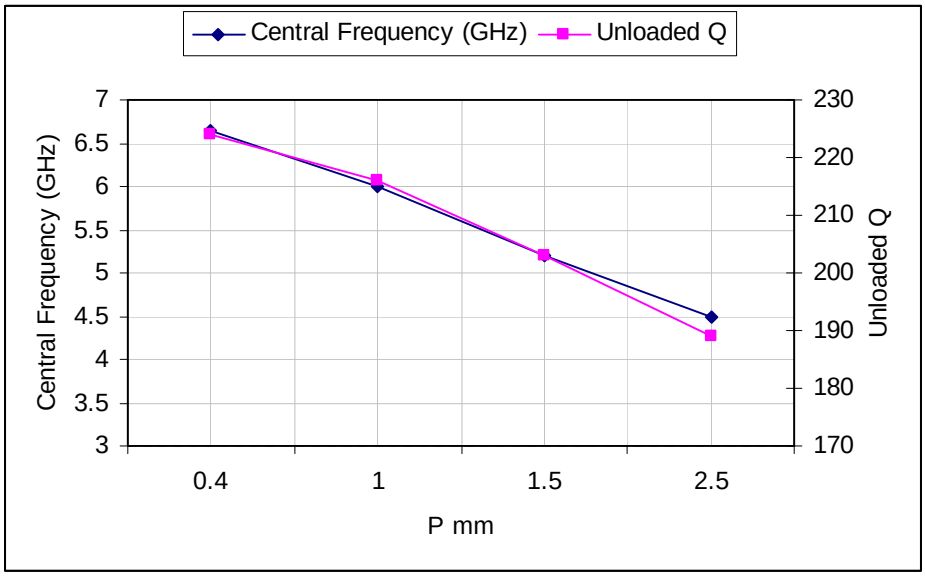

Figure 7-5: Relation between f_0 and Qu when d =0.2mm and p is varied

7.2.3.2 *Diameter of via d at 0.5 mm and the distance between the vias p is varied*

The following Table 7-2 shows the results that were obtained when the diameter of via *d* at 0.5 mm and by varying the distance between the vias *p*:

Table 7-2: Simulation results for d=0.5mm.

P mm	f_0 GHz	Q_u
0.4	6.1	214
1	5.5	205
1.5	4.8	195
2.5	4	154

The following Figure 7-6 shows the relation between f_0 and Q_u when the diameter of the via d was fixed at 0.5 mm and the distance between the via p was varied.

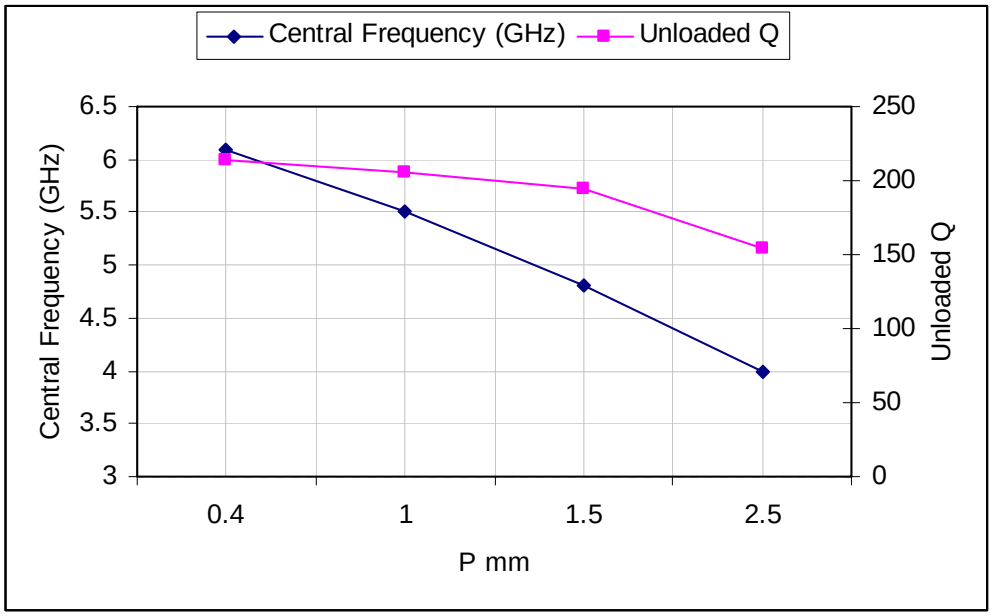

Figure 7-6: Relation between f_0 and Qu when d =0.5mm and p is varied

7.2.3.3 Diameter of via d *at 0.8 mm and the distance between the vias* p is varied

The following Table 7-3 shows the results that were obtained when the diameter of via d was at 0.8 mm and the distance between the vias p varied.

Table 7-3: Simulation results for d=0.8 mm.

***P* mm**	**f_0 GHz**	**Q_u**
0.4	6.9	226
1	6.4	197
1.5	5.8	185
2.5	5	155

The following Figure 7-7 shows the relation between f_0 and Qu when the diameter of the via d was fixed at 0.8 mm and the distance between the via p was varied.

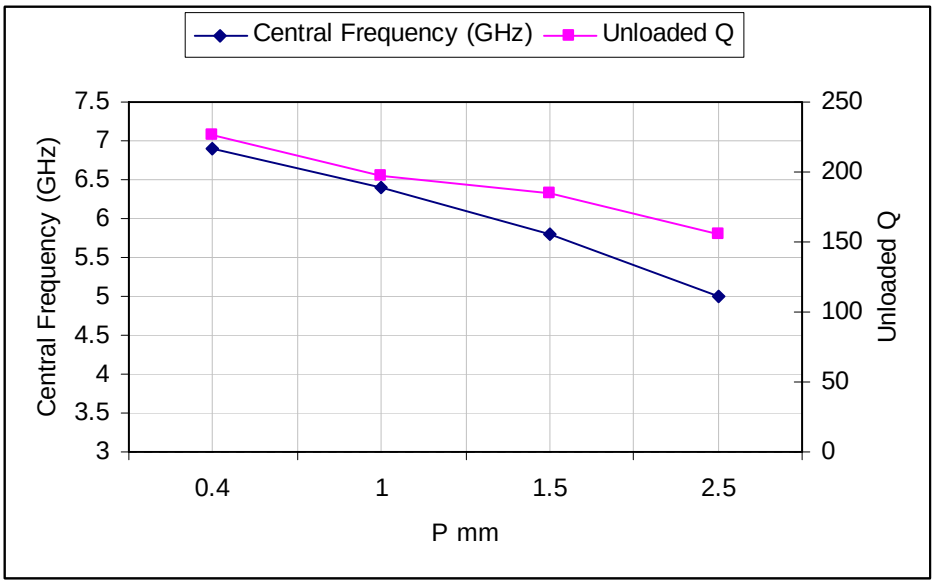

Figure 7-7: Relation between f_0 and Qu when d =0.8mm and p is varied

From the above experiments results the convenient and required design when the metallic vias diameter *d* was 0.5 mm to synthesize the SIW cavities and the spaces between these metallic vias were *p* 1.5 mm. This design will be used for further stages in this chapter to design 2-pole SIFW resonator filter.

7.2.4 2-Pole of SIFW resonator

The next step to design SIFW filter is to characterize and introduce the desired couplings between the adjacent SIFW resonators for each pair of resonators. This was done by employing a 2-Pole filter model in Figure 7-9 with two input/output probes. Next, the coupling gap (G) between the resonators was varied to find the desired coupling coefficient from the simulated frequency response.

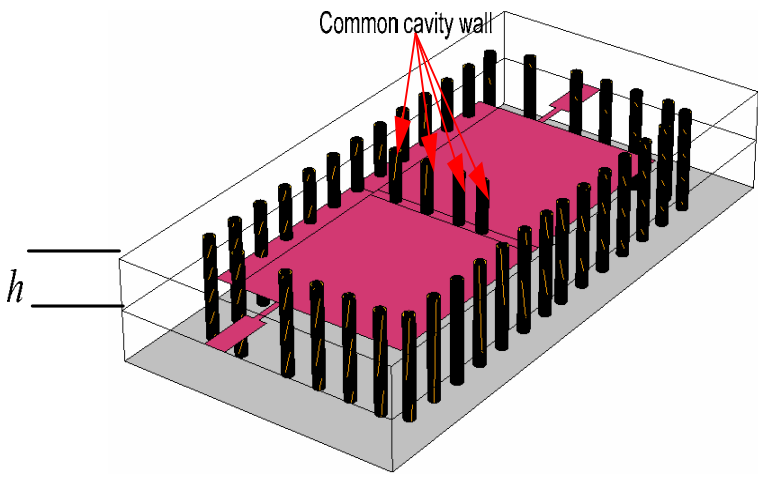

Figure 7-8: 3D view of the proposed SIFW filter Design (1).

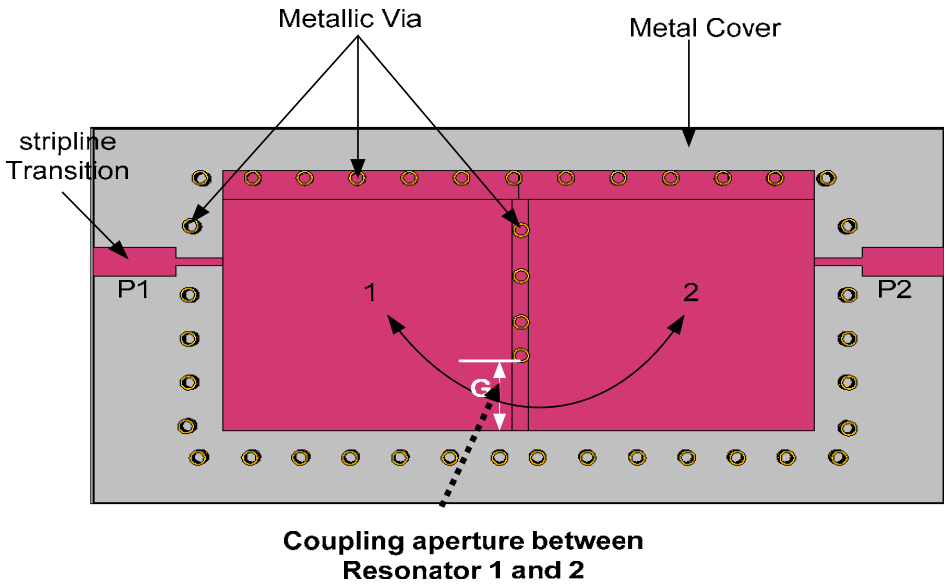

Figure 7-9: Configuration of the proposed SIFW filter.

7.2.4.1 Simulated loss effects in SIFW

EM simulations were also carried out to investigate the loss effects on the SIFW filter due to conductor, dielectric, and vias, respectively. In this section, the difference comparisons of losses are studied. To consider the dielectric loss in the simulation, two cases of a dielectric loss tangent in Table 7-4 are studied; the first case when the loss tan δ is 0.003 and the second case when the loss tan δ is 0. From that, it can be seen the dielectric loss is still dominant in this miniature filter. The loss from the conductor is also significant, whereas the vias, or radiation, loss is negligible.

Table 7-4: A difference comparison of losses.

	Conductor (Plate)	Via	loss tan δ	Qu
Case 1	LossLess	Copper	0	5887
	Copper	LossLess		742
	Copper	Copper		657
Case 2	LossLess	Copper	0.003	464
	Copper	LossLess		330
	Copper	Copper		306

It has been shown in Figure 7-10: Simulated loss effects when conductor losses are considered. In this simulated results only one loss mechanism was considered which is

conductor losses. To simulate the conductor loss, 0.03556 mm thick copper (as fabricated) with a conductivity of 5.8 x 10^7 S/m was assumed.

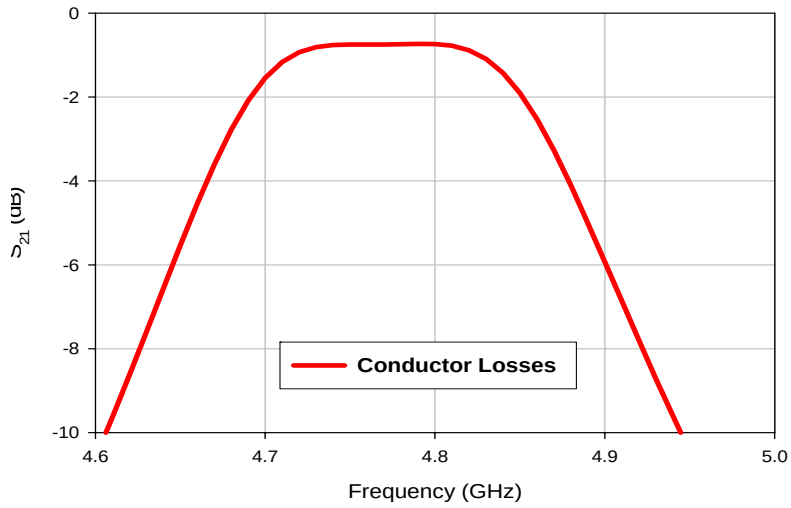

Figure 7-10: Simulated loss effects when conductor losses are considered.

It is shown in Figure 7-11 simulated results that only one loss mechanism was considered, which is dielectric loss. To consider the dielectric loss in the simulation, a dielectric loss tan δ 0.003 was chosen.

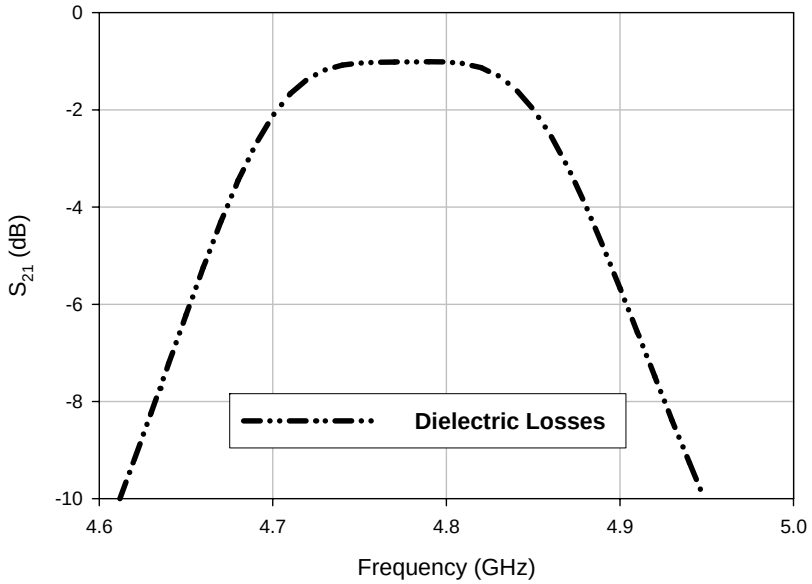

Figure 7-11: Simulated loss effects when dielectric losses are considered.

It is shown in Figure 7-12 simulated results that only one loss mechanism was considered, which is the radiation loss.

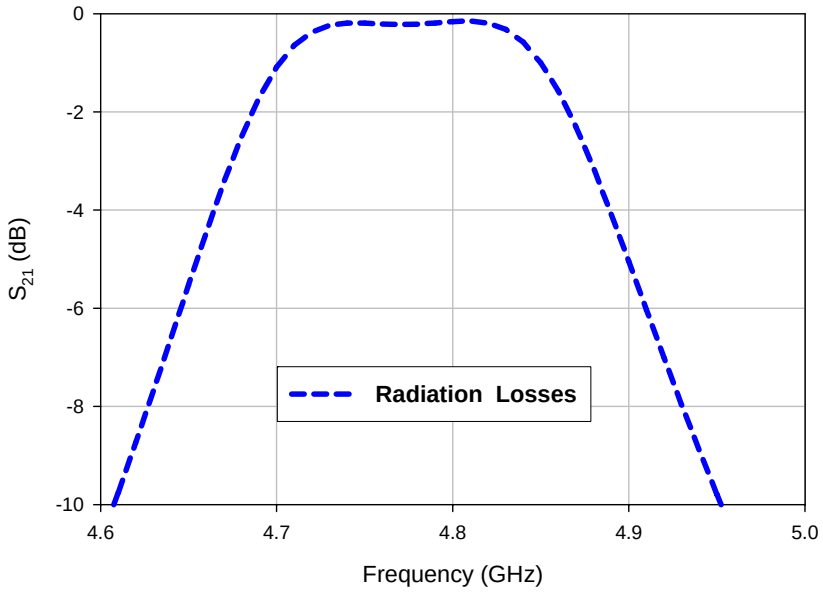

Figure 7-12: Simulated loss effects when radiation losses are considered.

For comparison, Figure 7-13 shows the simulated results using HFSS where each curve shows the passband response when only one loss mechanism was considered. From that figure, one can see that the dielectric loss is still dominant in this miniature filter. The loss from the conductor is also significant, whereas the vias loss is negligible. Each pair of the coupled resonators in the design is modelled in EM software [63].

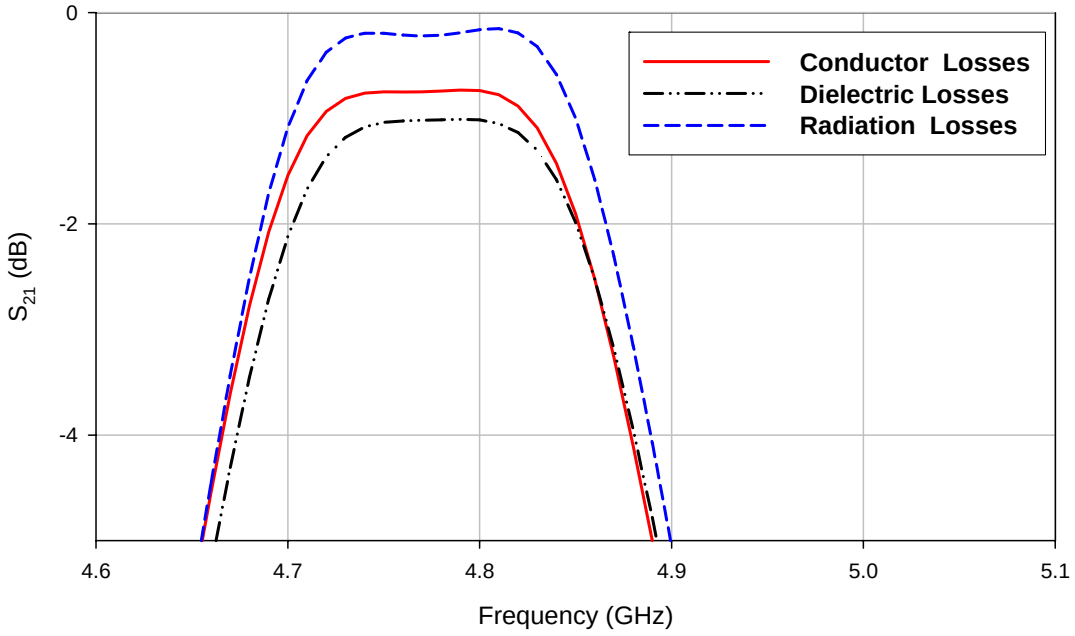

Figure 7-13: Simulated loss effects of different losses

The two striplines connected to two excitation ports as denoted by P1 and P2 in Figure 7-9 were used to excite the coupled resonators and simulate the mode splitting characteristics. In this case, the coupling aperture was 3.2-mm wide; each of the coupled cavities had a size of 12.5mm x 12.2mm x 1.524 mm and two 1-mm wide orthogonal slots inserted in the metal plate. It can be shown that the coupling can easily be controlled by the size of the aperture, and the coefficient k is larger when the coupling aperture becomes wider. The typical coupling response of S_{21} is shown in Figure 7-14. As can be seen from that Figure, two split mode frequencies (resonant peaks) are observable. Denote these two split frequencies as f_1 for the first peak and f_2 for the second peak.

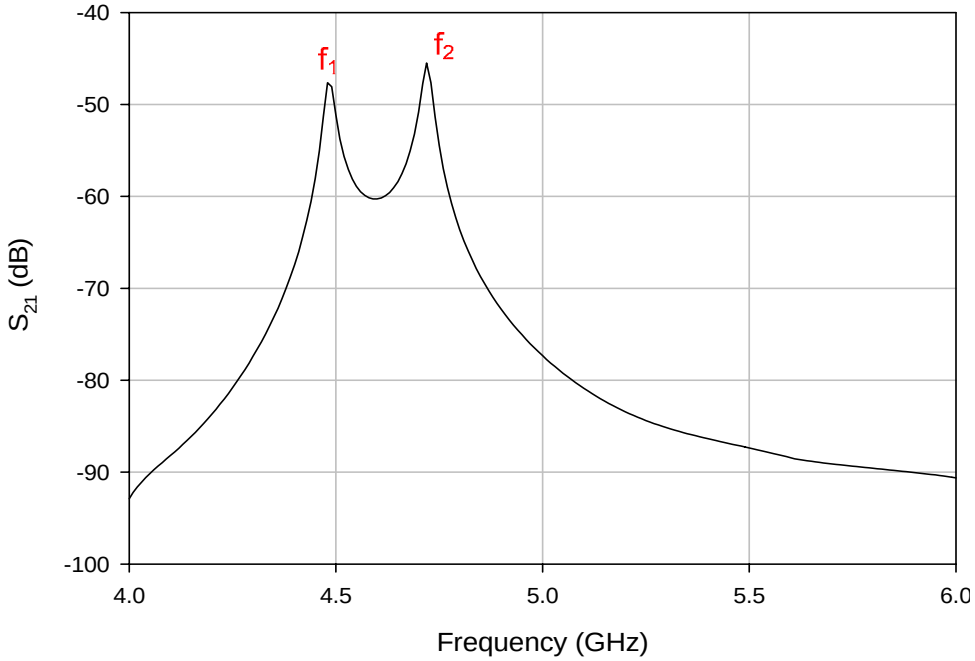

Figure 7-14: Typical coupling response between two resonators.

7.2.5 Demonstration of the (SIFW) resonator filter (Design 1):

The configuration for the double layered folded SIFW filter is shown in Figure 7-15. This filter includes two SIWstripline transitions for the source input and the load output and the two SIW resonators, respectively. In this filter, the two SIW cavity resonators 1 and 2 were coupled to each other by coupling aperture (G), as indicated in Figure 7-9. To introduce a coupling between two adjacent resonators of this type, we investigated a number of different arrangements. Figure 7-9shows a particular proposal to be discussed, where the coupling is realized through an aperture or gap in the common

cavity metal wall, as indicated. To ensure the proposed filter could be conveniently integrated with other microwave circuits, an SIW stripline transition was necessary. The stripline for input/output had a length of 5.5 mm. Moreover, the tapered stripline in the SIW-stripline transition was used to excite the waveguide mode and the SIW stripline transition was designed by matching the impedances of the SIW and the 50 Ω stripline [40]. The SIFW filter was designed to be fabricated using substrate material, GML1000, with a dielectric constant of 3.2 and a substrate thickness of h = 0.762 mm for each layer. In this design, metallic vias were used which had a diameter d of 0.5 mm to synthesize the SIW cavities. The spaces between these metallic vias were p 1.5 mm. The design specification for the given filter as required an FBW of 7.5 % at a centre frequency of 4.675 GHz. The simulated design of the filter matched the requirements given for the filter, and the simulation was done using commercially available electromagnetic (EM) simulation software (Sonnet Software Inc., Release 10.52, Liverpool, NY) [63]. The material (conductor and dielectric) losses were also taken into account. Implementation of the 2-Pole SIFW resonator filter (Design 1) is demonstrated in Figure 7-15. Standard PCB techniques were applied to fabricate the SIFW filter and the vias required by our design. For the demonstration, the designed SIFW filter was first fabricated from PCB material. Figure 7-15 shows the components of the fabricated SIFW filter. It is comprised of two identical halves (the top outside view for one of them is shown in Figure 7-15a). The two halves with a dielectric constant of 3.2 and a substrate thickness of h = 0.762 mm were separated by common 0.03556 mm thick copper (as fabricated) shown in Figure 7-15 b. The inside view of the second half is shown in Figure 7-15c. The completely assembled filter had a size of 25mm × 12.5mm including 5.5mm along the two sides for the stripline transitions. To verify the performance of the proposed SIFW filter, a C-Band filter with two folded SIW cavities was designed and fabricated using a two-layer substrate and multilayer PCB process. The centre frequency and bandwidth of the designed filter were 4.675 GHz and 355 MHz, respectively. The diameter of the via hole d was 0.5 mm and the space between the metallic vias p was 1.5 mm. In order to easily control the coupling between the cavities, we adopted an aperture between the resonators. The passband return loss exhibited a little degradation in the filter because of the fabrication tolerance of the PCB process. The primary reason for that is the tolerance in the substrate parameters and the design. For example, the diameter of the drilled hole was not as expected. The designed diameter was 0.5 mm, whereas the measured diameter was about 0.9 mm. The process

used to realize the filter discussed in this study is the most popular process by which PCB circuits are mass-produced.

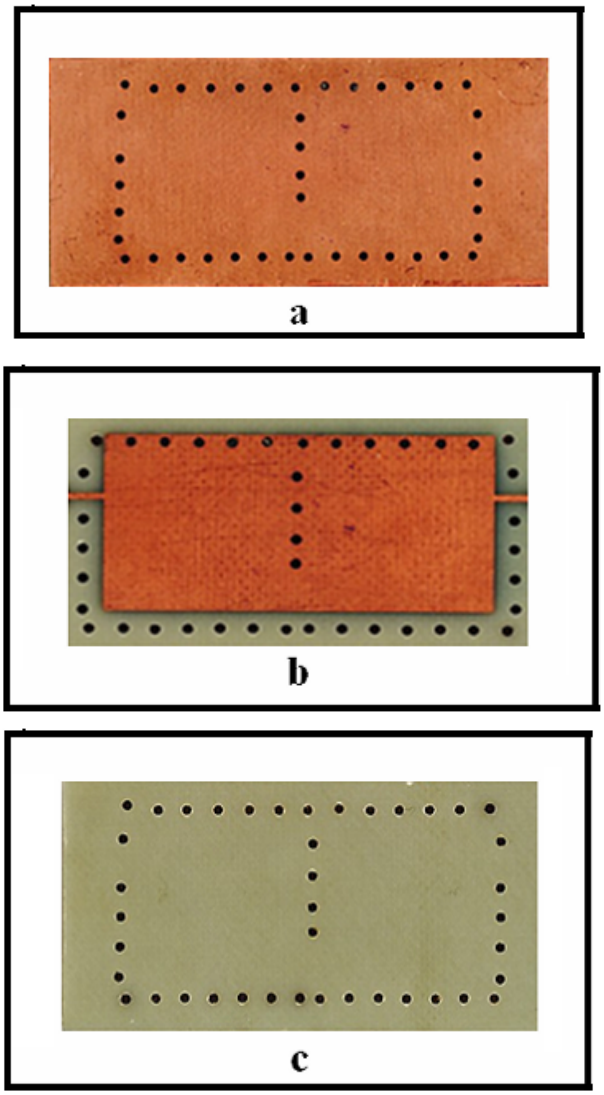

Figure 7-15: Fabricated 2-pole SIFW resonator filter before assembly. (a) Top ground layer on substrate. (b) Middle metal layer on substrate. (c) Bottom substrate with ground layer on the other side.

The filters were tested using a HP microwave network analyzer. The measured and simulation results are given in Figure 7-16 for the SIFW filter. When compared with the simulated results from the EM modelling software, a good agreement can be observed. The FBW of the measured filters was recorded as 7.4 %. The design requirement was for 7.5 % FBW, so the filters demonstrated that they match with the given specifications. The PCB process may be specifically tuned for our filter at a higher cost to yield better performance. SMA connectors, stripline feeds and tapered transition were not deemed bedded from the measurement and therefore contributed to the insertion and

return loss. The measured response was shifted to a slightly higher frequency than the design value and this was due to the fact that perfect sidewall conductors were designed and simulated to allow efficient computation. However, in the fabrication process, vias were used. The experiment was also carried out to measure the wideband frequency response of the filter demonstrator, and the measured and simulation results are plotted in Figure 7-17 for a comparison. There is a wide stopband between the fundamental and the first spurious passband, which appeared at about 9.65 GHz.

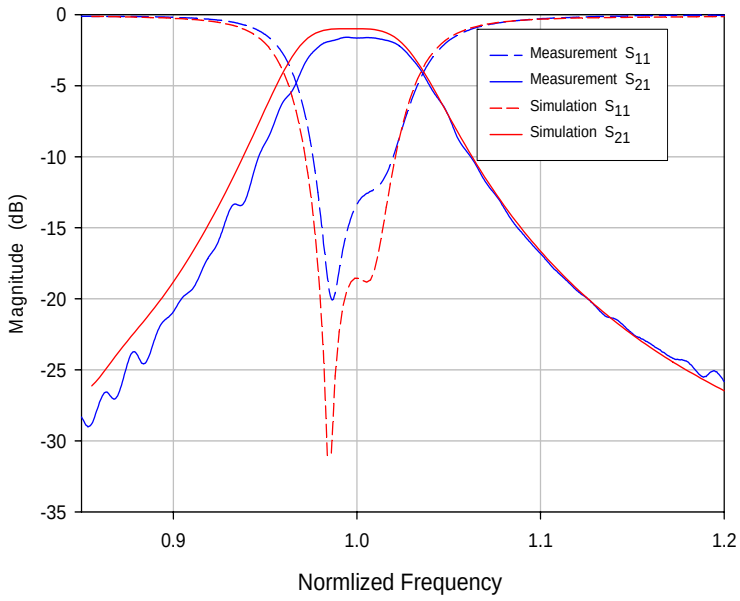

Figure 7-16: Comparison of the simulation and measurement of the proposed SIFW filter.

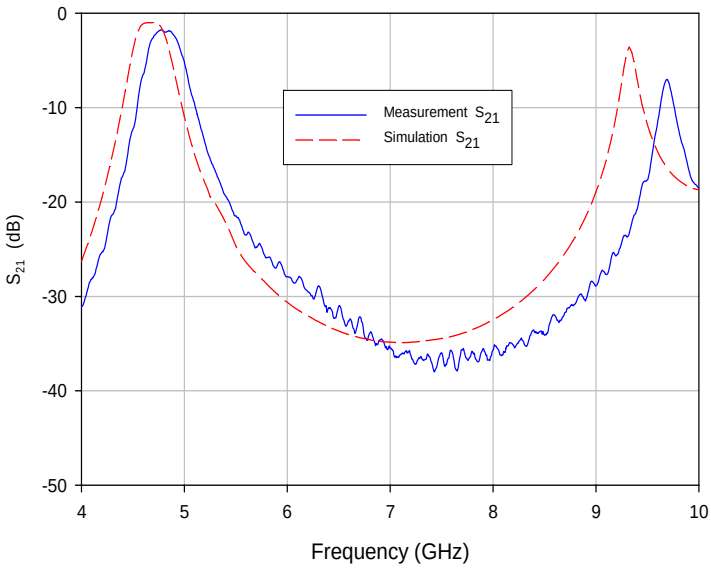

Figure 7-17: Measured wideband frequency response of the fabricated 2-Pole folded waveguide resonator filter.

7.3 A substrate integrated folded waveguide (SIFW) resonator filter (Design 2):

In this part, the second proposed SIFW resonator filter is shown in Figure 7-18. The coupling between two folded waveguide quarter-wavelength resonators is described in section 7.3.1, including full-wave electromagnetic (EM) simulation and experimental validation. In the same section, the realization of a 2-Pole filter demonstrator with TZ from the high side band is presented, and is verified both by simulation and experimentation.

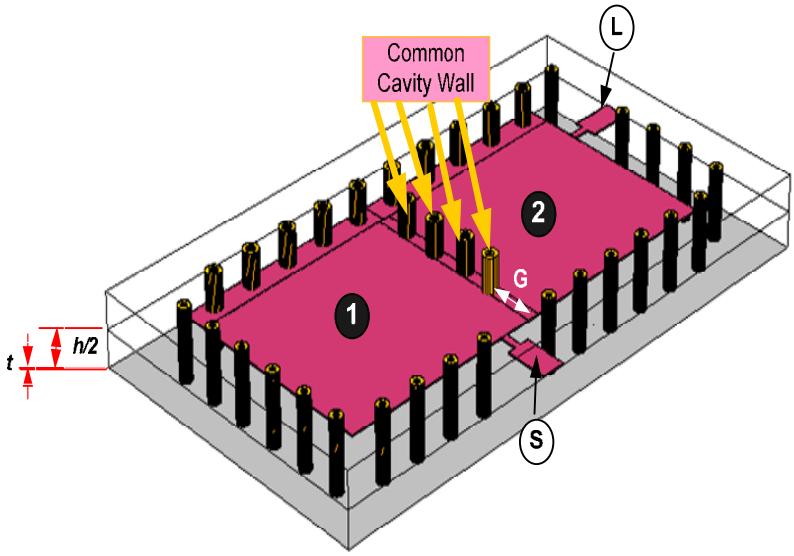

Figure 7-18: 3D view of the second proposed SIFW (design 2)

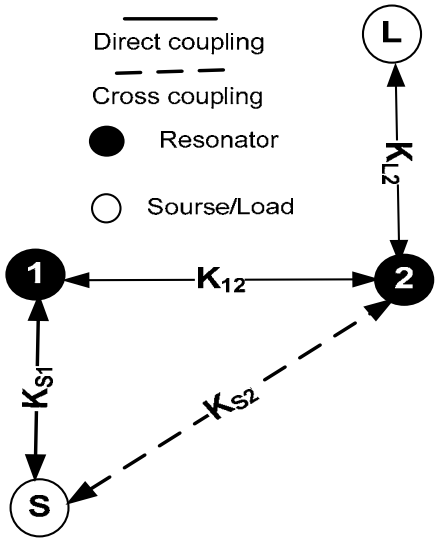

Figure 7-19: The coupling structure of a 2-pole SIFW resonator filter configuration.

7.3.1 Demonstration of the (SIFW) resonator filter (Design 2):

The configuration for the double layered folded SIFW filter with TZ from the high side band is shown in Figure 7-18. This filter includes two SIW stripline transitions for the source input and load output, and two SIFW resonators, respectively. In this filter, there was one significant coupling coefficient between the adjacent resonators, namely K_{12}, which was realized through opening the gaps between the adjacent resonators, as can be seen from that figure. The filter was intended for an attenuation pole of finite frequency on the high side of the passband, leading to a higher selectivity on this side of the passband. To achieve this, the input excitation port (S) was coupled to both resonators 1 and 2, as shown in the coupling structure in Figure 7-19. The two SIW cavity resonators 1 and 2 were coupled to each other by the coupling aperture (G), as indicated in that figure. To introduce a coupling between two adjacent resonators of this type numbers of different arrangements have been investigated. Figure 7-18 shows one particular proposal that is discussed in this chapter, where the coupling is realized through an aperture or a gap in the common cavity metal wall, as indicated. To ensure the proposed filter could be conveniently integrated with other microwave circuits, an SIW stripline transition was necessary. The stripline for input/output had a length of 5.5 mm. Moreover, the tapped stripline in the SIW stripline transition was used to excite the waveguide mode and the SIW stripline transition was designed by matching the impedances of the SIW and 50 Ω. The SIFW filter was designed to be fabricated using substrate material GML1000 with a dielectric constant of 3.2 and a substrate thickness of h = 0.762 mm for each layer. In this design, metallic vias with a diameter *d* of 0.5 mm were used to synthesize the SIW cavities. The spaces between these metallic vias *p* was 1.5 mm. A filter of this type with a fraction bandwidth of about 4.4% at a centre frequency of 4.705 GHz was successfully designed using commercially available electromagnetic (EM) simulation software (Sonnet Software Inc., Release 11.52, Liverpool, NY) [63]. The material (conductor and dielectric) losses, as described in 7.2.4.1, were taken into account. EM simulations was also carried out to investigate the loss effects on the SIFW filter due to conductor, dielectric, and vias, respectively. To simulate the conductor loss, 0.03556 mm thick copper (as fabricated) with a conductivity of 5.8×10^7 S/m was assumed. To consider the dielectric loss in the simulation, a dielectric loss tangent of 0.003 was chosen. From these losses, we can conclude that the dielectric loss was still dominant in this miniature filter. The loss from the conductor was also significant, whereas the vias loss was negligible. Each pair of coupled SIFW resonators in the design was modelled in EM software. The two

striplines connected to two excitation ports as denoted by S and L in Figure 7-18 were used to excite the coupled resonators and simulate the mode splitting characteristics. A typical simulated frequency response of coupled folded waveguide resonators is plotted in Figure 7-20. In this case, the coupling aperture was 2.7 mm wide; each of the coupled cavities had a size of 12.5mm x 12.2mm x 1.524mm and two 1-mm wide orthogonal slots inserted in the metal plate. As can be seen from that figure, two split mode frequencies (resonant peaks) are observable. Denote these two split frequencies as f_1 for the first peak and f_2 for the second peak. It can be shown that the coupling can easily be controlled by the size of the aperture, and the coefficient k is larger when the coupling aperture becomes wider. It was found that the location of the source (S) affects the allocation of transmission zero, but not the inter-resonator coupling. Standard PCB techniques were applied to fabricate the SIFW filter with TZ from the high side band and vias required by our design.

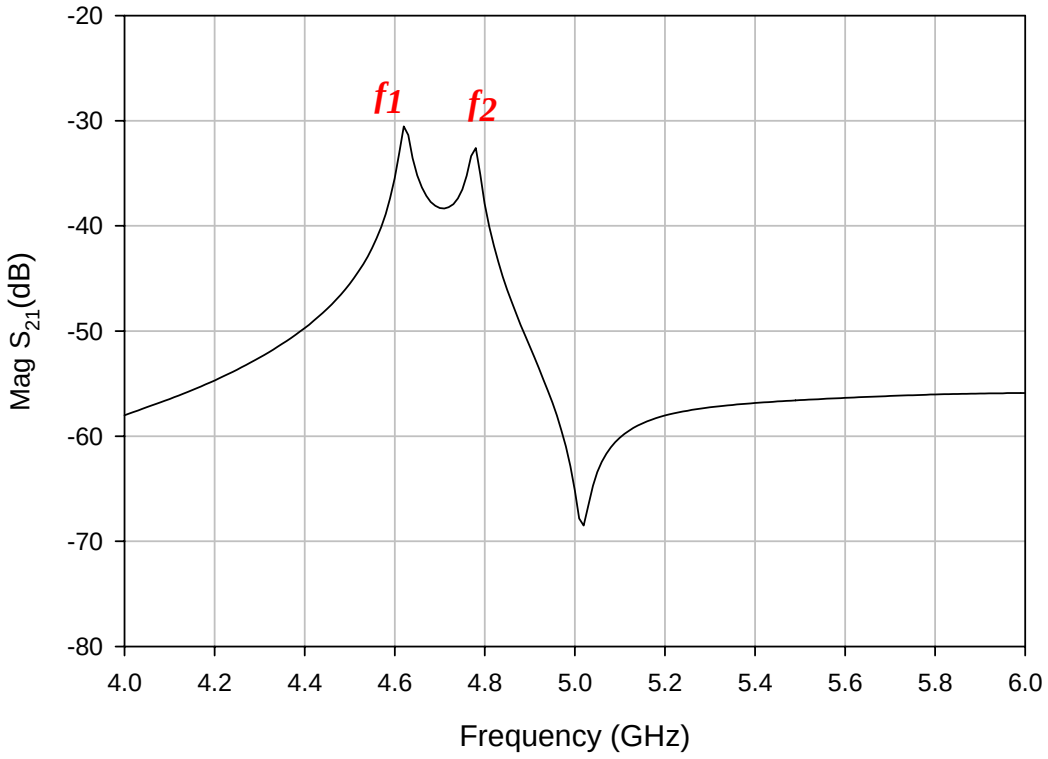

Figure 7-20: Typical coupling response between two resonators.

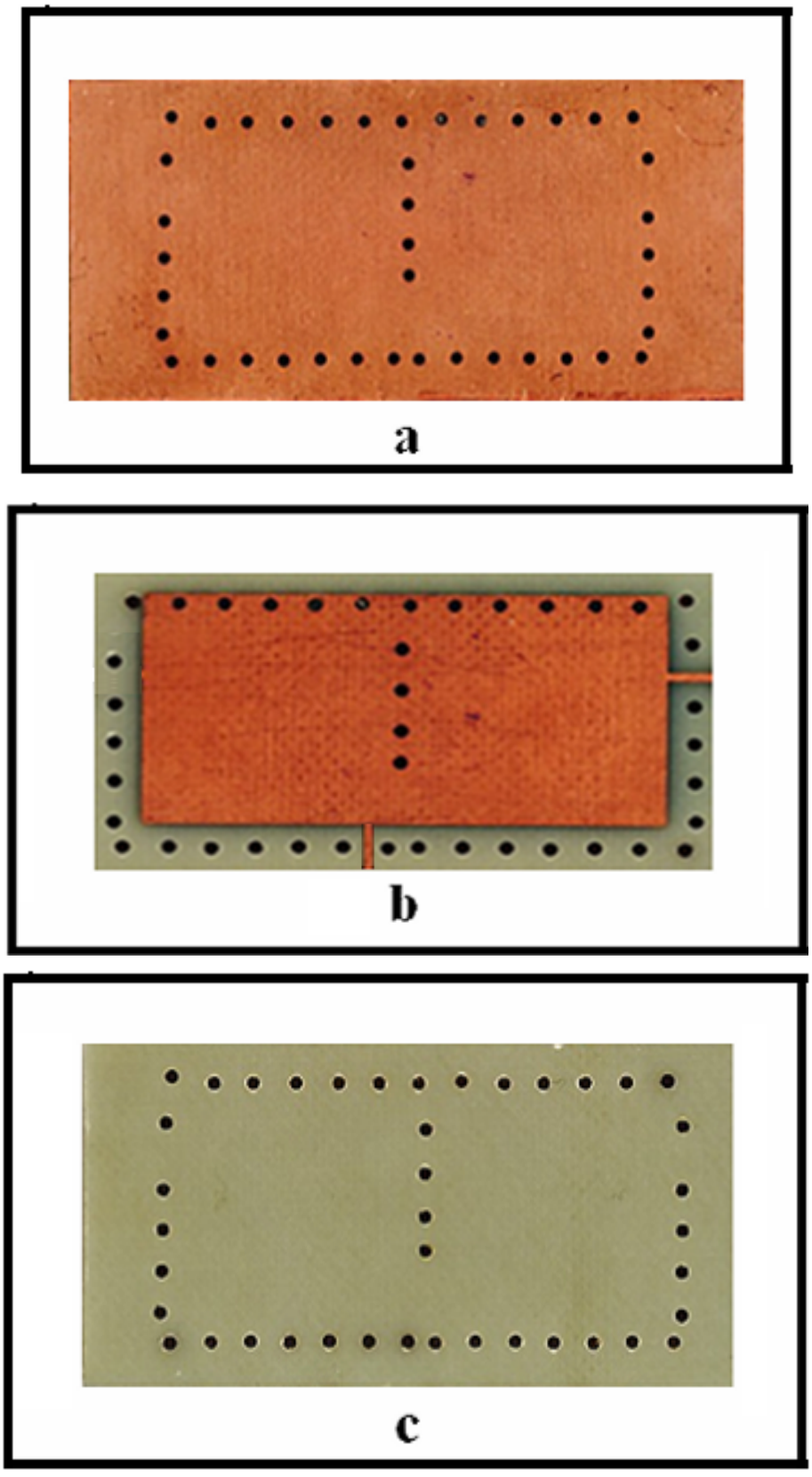

Figure 7-21: Fabricated 2-pole SIFW resonator filter with TZ from high side band before assembly. (a) Top ground layer on substrate. (b) Middle metal layer on substrate. (c) Bottom substrate with ground layer on the other side.

For the demonstration, the designed SIFW filter was fabricated from PCB material. Figure 7-21 shows the components of the fabricated SIFW filter. It was comprised of two identical halves (the top outside view for one of them is shown in Figure 7-21 (a). The two halves with a dielectric constant of 3.2 and a substrate thickness of h = 0.762 mm were separated by a common 0.03556 mm thick copper (as fabricated) shown in Figure 7-21 (b). The inside view of the second half is shown in Figure 7-21 (c). The completely assembled filter had a size of 25mm × 12.5mm including 5.5mm along the two sides for the stripline transitions. To verify the performance of the proposed SIFW filter, a C-Band filter with two folded SIW cavities was designed and fabricated using a two-layer substrate and multilayer PCB process. The centre frequency and bandwidth of the designed filter were 4.7 GHz and 210 MHz, respectively. The diameter of the via hole d was 0.5 mm; the space between the metallic vias p was 1.5 mm. In order to easily control the coupling between cavities, we adopted an aperture between the resonators. The passband return loss exhibited a little degradation in the filter because of the fabrication tolerance of the PCB process. The primary reason for that is the tolerance in the substrate parameters and the design. For example, the diameter of the drilled hole was not as expected. The designed diameter was 0.5 mm, whereas the measured diameter was about 0.85 mm. The process used to realize the filter discussed in this study is the most popular process by which PCB circuits are mass-produced. The filters were tested using a HP microwave network analyzer. The measured and simulation results are given in Figure 7-22 for the SIFW filter with TZ from the high side band. When compared with the simulated results from the EM modelling software, a good agreement can be observed. The FBW of the measured filters was recorded as 4.5%. The design requirement was 4.4% FBW, so the filters demonstrated that they matched with the given specifications. The PCB process may be specifically tuned for our filter at a higher cost to yield better performance. SMA connectors, stripline feeds and tapped transition were not considered from the measurement and therefore contributed to the insertion and return losses. The measured response was shifted to a slightly higher frequency than the design value and this was due to the fact that perfect sidewall conductors were used in the design and simulation to allow efficient computation. However, fabrication vias were used. The experiment was also carried out to measure the wideband frequency response of the filter demonstrator, and the measured and simulation results are plotted in Figure 7-23 for comparison. There was a wide stopband between the fundamental and the first spurious passband, which appeared at about 9.4 GHz.

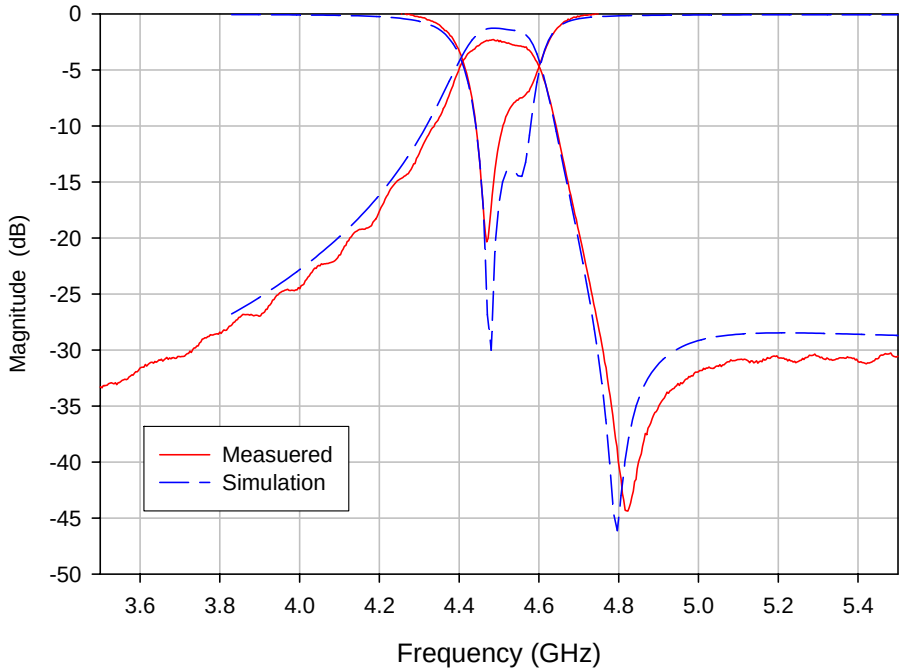

Figure 7-22: Comparison of the simulation and measurement of the proposed SIFW filter.

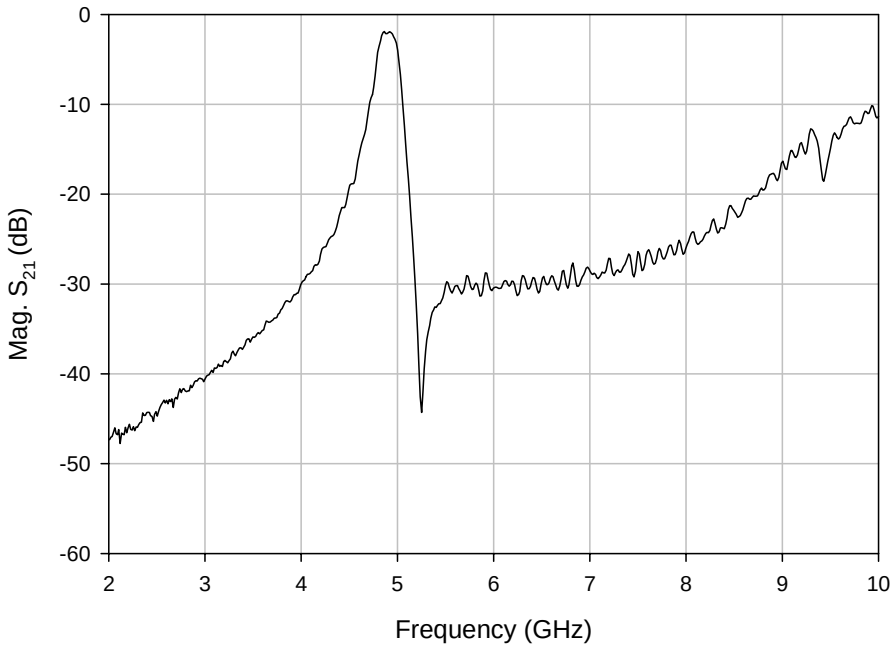

Figure 7-23: Measured wideband frequency response of the fabricated 2-Pole folded waveguide resonator filter.

7.4 Summary

3-D structures can cause difficulties in the manufacturing an accuracy and planar circuitry integration. There is an increasing need for microwave systems which use smaller sizes devices and enhanced performance. Both resonator filter topology and dielectric substrate are important determiners of microwave volume and some of these filters topologies require tight coupling. Recently several techniques have been used to

form substrate integrated waveguides (SIW) e.g LTCC. These guides are dielectric filled and are formed from the substrate material. This has the benefit of simple integration with planar devices and a size reduction of $1/\sqrt{\varepsilon_r}$. These structures can be easily integrated with planar circuits and devices. Furthermore, because they form dielectric filled waveguide, both the width and guided wavelength is reduced by a factor of $1/\sqrt{\varepsilon_r}$, where εr is the relative dielectric constant of the substrate material. Since these guides are formed from the substrate material they are referred to as substrate integrated waveguides (SIW). Substrate integrated waveguides have clear advantages over RWGs including low cost, simple integration with planar devices, and a size reduction of a factor. However, even with this size reduction SIW are large at RF frequencies. We discussed in this chapter a substrate integrated folded waveguide (SIFW) that results in a further reduction in the size of SIWs.

Two novel substrate integrated folded waveguide (SIFW) resonator filters were proposed. The first proposed SIFW bandpass filter is based on multilayer direct-coupled folded quarter-wavelength resonators, and a 2-Pole filter of this type was demonstrated. Transitions to stripline were implemented, allowing the SIFW to be easily integrated with planar transmission lines. Furthermore, the second substrate integrated folded waveguide (SIFW) resonator filter with TZ from the high side band was proposed. This filter is based on multilayer direct and cross coupled folded quarter-wavelength resonators, and a 2-Pole filter of this type was demonstrated. Transitions to stripline were implemented, allowing the SIFW to be easily integrated with planar transmission lines. The proposed SIFW filters structures are promising for LTCC and LCP technologies.

With end of this chapter, the designs and implementations of cavity FWG and SIFW resonator filter were completed based on the full-wave electromagnetic simulation, and validated by the experiment. The next chapter will be the last chapter that conclude this thesis and a number of potential enhancements to the FWG cavity filter will be suggested. There are also opportunities to develop further the background research in that chapter.

Chapter 8

Conclusions and Future Work

8.1 Introduction:

This section critically reviews the previous chapters and discusses possible future work evolved from the research project. Moreover, a comprehensive study of cavity filters, including design, simulation, testing and characterization, was presented. There are areas in which cavity filters will benefit from further work that will provide additional functionality to these filters. Several parameters were taken into account in analyzing the filters' characteristics, such as group delay, phase responses, and transmission zero including high selectivity and bandwidth and their profiles. In this final chapter, a number of potential enhancements to the FWG cavity filter will be suggested. There are also opportunities to develop further the background research. Finally, the chapter concludes with an overall summary of the work that has been presented and studied through the author's PhD.

8.2 Progress of the work

As it was pointed out in the introduction, the main aim was to develop the design techniques for coupled folded waveguide FWG resonator filters in microwave filter applications and to design and assemble the required resonator for the given specifications. This involved achieving a high selectivity passband for specific resonant modes, starting with a 1-pole resonator design and optimising with a 4-pole resonator filter design. In order to achieve this, the first objective was to decide a fast and accurate simulation tool for a folded waveguide resonator. Following some literature review on FWG resonator structure, an overview of the microwave filter's history was presented. It introduced the basic concepts of resonators, resonator types, and the advantages, applications, drawbacks, and geometries of cavity resonator. The fundamental filter parameters presented an overview of what should be taken into consideration when building a folded waveguide FWG resonator filter. Moreover, reviews of some articles which show the benefits of using a cavity resonator were read and analyzed.

As a next step, the design method was a very important stage of the author that needed to be understood. The major design methods in this thesis were discussed briefly, and the conversion of a lowpass prototype filter to a bandpass filter was explained (see Chapter 3). Filter specifications were then set to design and fabricate a filter, in order to validate the maximum improvement. Experimental results were presented to validate the simulation and to show some useful characteristics.

Once the analysis and simulation tool were completed and the design method has been chosen, a thorough investigation of several configurations or improving the FWG resonator was made. It was deduced that the FWG performance improves better or similar quality factor with a smaller footprint. Furthermore, after many simulations it was presumed that the asymmetrical and symmetrical configurations improved the FWG resonator performance; the smaller size being almost exclusively the improving factor in this stage.

The next aim of the work was to show the benefits of the achieved improvement. The first idea was to design a FWG resonator. A fully FWG resonator was designed as an illuminating example of the benefits of that resonator's structures (Chapter 4). At the same time, a survey of possible new techniques that were conveniently integrated within the structure of that filter was made. While slot techniques were considered, this included a primary investigation into developing a compact and low-loss bandpass filter using novel folded-waveguide resonators with a footprint reduction. A slot coupling between adjacent resonators was introduced, which was characterized using full-wave EM simulations and verified experimentally. Two designs of 2-pole folded waveguide resonator filters of this type were considered, fabricated and tested (presented in Chapter 5), and their reflection measured.

The design procedure and method of designing FWG resonator filters was almost the same in chapter's 6 and 7; hence the plan was divided into three stages (presented in Chapter 6). In the first stage, the dimensions and the excitation port location were obtained from the 1-pole cavity resonator for the required optimum external quality factor (Qe). In the second stage, the same dimensions obtained from the 1-pole resonator were used, varying the gap length (G) between adjacent resonators, the wall width (W) and a corner of the separation plate cutting (C) to attain the required coupling coefficients (K_{12}, K_{23} and K_{34}) to get an approximate design for the 2-pole resonators

that could be used in the 4-pole resonator. After obtaining these results, the 4-pole resonator was simulated with the dimensions obtained by readjusting the values of G, W and C until the specified resonator requirements were obtained. The implementation of these designs and the experimental results are the core contents of this thesis with certain specifications.

With this work, the first two, rather precisely predetermined aims were completed. The final aim of the work was to investigate configurations using the same structures of FWG for further improvement of SIFW resonator filters. During this stage of the work, it was suggested that SIFWs have clear advantages over RWGs, including low cost, simple integration with planar devices, and a size reduction. Thus, SIFW was fabricated and validated (presented in Chapter 7). Having designed a validated SIFW filter, stopband improvement of bandpass filter also provided an improved selectivity characteristic with compact size compared with the conventional resonator. Filters could then be achieved by the integration of the two structures in a single structure with a bandpass filter component. The fabrication process in SIFW remained simple and the post acted as an electrical wall for the dielectric material. Commercial EM simulation tools were also carried out to investigate the loss effects on the SIFW filter due to conductor, dielectric, and vias respectively. In that study, the difference comparisons of losses were considered. To consider the dielectric losses in the simulation, two cases of a dielectric loss tangent were studied; the first case when the loss tangent was 0.003 and the second case when the loss tangent was 0. From that, one can see that the dielectric loss was still dominant in this miniature filter. The loss from the conductor was also significant, whereas the vias or radiation loss was negligible. Moreover, the configurations for both a dielectric and cavity (air filling) of the FWG resonator were studied; the air filled case, however, exhibited very good selectivity and performance but with the trade-off of significantly greater dimensions. The idea was not further investigated in terms of the fabrication of the SIFW because of the problem of accurately designing those structures. However, the idea is valid in the case of dielectric filled waveguides.

8.3 Contributions of the thesis

This section aims to summarise the contributions made by this work. The prime objective of this project was to characterize novel cavity resonators for the design of

RF/microwave filters, which can be found in wide applications in wireless communication, radar and other RF/microwave systems and has been achieved. In this thesis, we concerned with improvement and implementation of folded waveguide FWG resonator, as presented in [1] in different manner. Moreover, we evaluated different structures for the realization of microwave cavities with high-Q, the result of which will be a high spurious free range and a reduced footprint. The most important, in this thesis a novel folded waveguide resonator with about a 75 % reduction of the volume from conventional size will be described. For comparison, two types of folded waveguide resonators have been studied, i.e. the square-shaped quarter-wavelength resonator and the newly proposed triangular shape. In addition, demonstrators of a filter application of miniature triangular folded waveguide resonators have been designed and simulated using an EM simulator. Moreover, this includes an improved 4-Pole design using the folded waveguide resonators, and it was proven that the filter size was reduced by 50%.

Furthermore, the main aim was to develop the design techniques for coupled folded waveguide FWG resonator filters in microwave filter applications and to design and assemble the required resonator for the given specifications has been achieved. It involved achieving a high selectivity passband for specific resonant modes, starting with a 1-pole resonator design and optimising with a 4-pole resonator filter design. Experimental results were presented to validate the simulation and to show some useful characteristics. Furthermore, a compact SIFW filter configuration was also proposed. However, more important were probably the suggestions for further improvement of FWG low-cost filters. This included a primary investigation into developing a compact and low-loss bandpass filter using folded-waveguide resonators with a footprint reduction. A slot coupling between adjacent resonators was introduced, which was characterized using full-wave EM simulations and verified experimentally. Two designs of 2-pole folded-waveguide resonator filters of this type were considered, fabricated, tested and proposed.

Among the contributions of this work was the proposal to improve configurations by exploring the advantages and developing a compact dual passband filter using folded-waveguide resonators with a multilayer structure. A new coupling scheme for dual-band operation was realized by using both slot and aperture couplings for the implementation. For the demonstration, a 4-pole dual-band filter of this type was designed, fabricated and tested. Simulations and experimental results were presented to validate the design

and to show the advantages of this type of filter. The proposed new dual passband filter is expected to be attractive for implementation with advanced device technologies. Hence, an improved low cost and compact-size, which can cover a whole waveguide band, has been demonstrated. Further achievement around 75% size reductions was also contributed in this thesis. Stopband improvement could still be one of the advantages of this configuration. In an alternative attempt to reduce the cavity of the FWG filter's dimension, waveguide resonators with planar discontinuities were proposed. With this in mind, two substrate integrated folded-waveguide (SIFW) resonator filters were designed. The proposed SIFW bandpass filter was based on multilayer direct-coupled folded quarter-wavelength resonators, and a 2-Pole filter of this type was demonstrated. Transitions to stripline were implemented, allowing the SIFW to be easily integrated with planar transmission lines. Moreover, another substrate integrated folded-waveguide (SIFW) resonator filter with TZ from the high side band was proposed. The proposed FWG resonator and SIFW filters structures are promising for LTCC and LCP technologies.

8.4 Suggestions for Further Work

The proposed work holds promise for the development of coupled folded waveguide (FWG) resonator filters and this design can be extended to further multi-pole designs, for example, 6-pole, 8-pole etc. Extensions to several cross-couplings could also be one of the interesting points of further research. Several parameters will be taken into account in analyzing filter characteristics in future work, such as group delay, linear phase, and transmission zero including high selectivity and bandwidth, and their profiles. In addition, advanced filter design and dual mode are two interesting areas from which very compact, low loss filters with excellent rejection band characteristics can be obtained. In recent years, several techniques have been proposed for the manufacture of rectangular waveguide RWG circuits [68]. These have included low temperature, co-fired ceramics (LTCC) [41], microwave laminates [40, 69], photoimageable thick-films [70] and Liquid Crystal Polymer (LCP), which is gaining increasing interest as a choice technology in the packaging community due to its superior thermal and electrical properties including low loss, low dielectric constant and low CTE characteristics [71]. Size reduction of circuits by investigating multiple LCP substrates is very attractive area for future work. However, another challenge arises when via-whole groundings are implemented. LCP is a promising material because it

has exceptional properties that make it well suited for use as a substrate material [72, 73]. It is extremely attractive as a high frequency circuit substrate and package material due to its low loss ($\tan\delta \langle$ 0.004) and low dielectric constant (2.9–3) up to mm-wave frequency range. Since these guides are formed from the substrate material they are referred to as substrate integrated waveguides (SIW). Substrate integrated waveguides have clear advantages over RWGs, including low cost, simple integration with planar devices, and size reduction. Another promising technology, particularly for millimetre wave high frequency applications, is micromachining; the author has identified that as part of the future work.

Appendix A

FWG Resonator Filter

A.1 Simulation Results of FWG resonator filter :

This appendix includes all results obtained during simulations and practical measurements for one-pole, two-pole and four-pole cavity resonators.

A.1.1 Approach of extracting external quality factor (Qe)

The cavity design [1] was used to obtain the required external quality factor Qe = 33.26. This involved experimenting with the two varied cavity dimensions: A = 20 mm and B = 20 mm, as shown in Figure A-1. The cutting areas (C) were varied for each varied excitation port position (L).

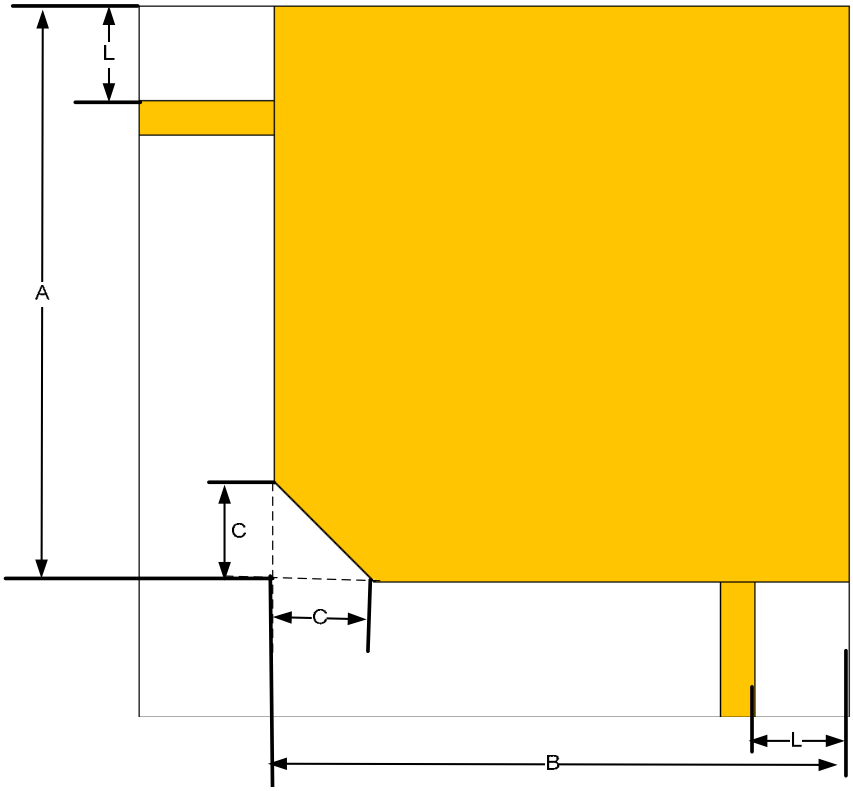

Figure A-1: Layout and dimensions of a 1-pole design.

The desired external quality factor (Q_e) was obtained by changing the position of the excitation port location.

A..1.1.1 Simulation results

Task 2: Excitation port L = 1.8 mm

The following Table A-1 shows the results that were obtained when the length of excitation port L=1.8 mm, with different cutting (C) from the bottom left corner of the separation plate.

Table A-1: Simulation results for L=1.8mm.

Cutting (C) mm	F_1 GHz	F_2 GHz	f_0 GHz	Qe
0	4.57	4.662	4.616	50.17
1	4.608	4.702	4.655	49.52
2	4.684	4.783	4.733	47.80
3	4.785	4.89	4.837	46.06
3.4	4.83	4.939	4.884	44.8
4	4.905	5.019	4.962	43.52
5	5.045	5.168	5.1065	41.51

The following Figure (a) and (b) show the relation between f_0 and Q_e when the length of excitation port is fixed at L = 1.8mm, with different cuttings (C) from the bottom left corner of the separation plate.

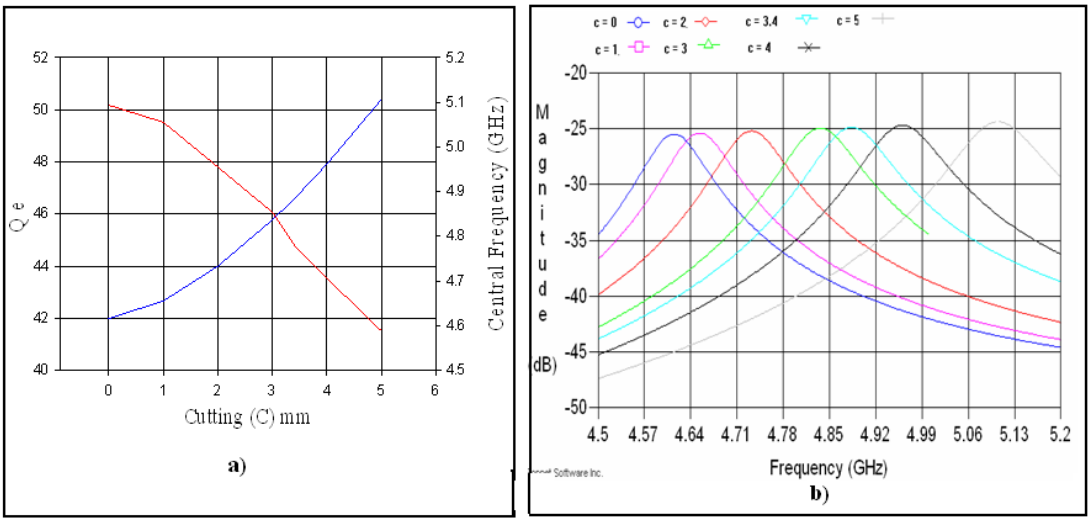

Figure A-2: (a) The values of f_0 and Qe for different C for L = 1.8mm, (b): simulation responses

From the above Figure A-2 (a), it may be seen that when cutting (C) in the corner increases the central frequency, (f_0) increases also, while the external quality factor decreases. From Figure (b), it is clear that the central frequency is shifted to the right and the reason for that is the variation in corner cutting (from 0 to 5mm).

Task 3: Excitation port L L = 1.9 mm:

The following Table A-2 shows the results that were obtained when the length of excitation port L=1.9 mm, with different cutting (C) from the bottom left corner of the separation plate.

Table A-2: Simulation results for L=1.9mm.

Cutting (C) mm	F_1 GHz	F_2 GHz	f_0 GHz	Qe
0	4.569	4.669	4.619	46.19
1	4.606	4.708	4.657	45.65
2	4.683	4.79	4.734	44.25
3	4.784	4.898	4.841	42.46
3.4	4.83	4.947	4.886	41.76
4	4.905	5.027	4.966	40.70
5	5.045	5.177	5.111	38.72

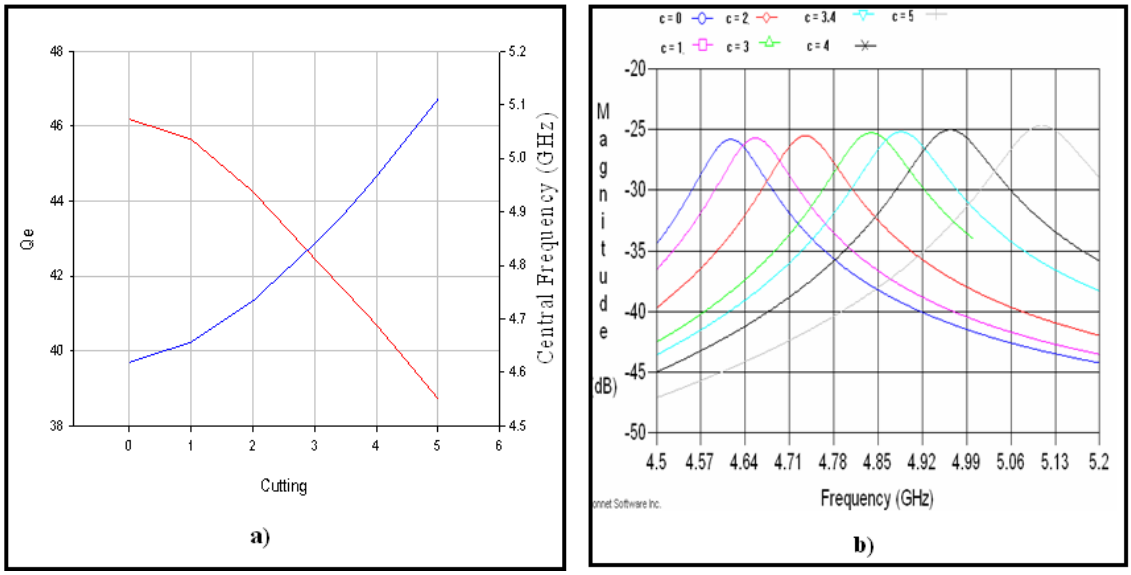

Figure A-3 0: (a) The values of f_0 and Qe for different C , (b): simulation response

From the above Figure A-3 0 (a), it may be seen that when cutting (C) in the corner increases the central frequency, (f_0) increases also, while the external quality factor decreases. From Figure A-3 0 (b) it is clear that the central frequency is shifted to the right and the reason for that is the variation in corner cutting (from 0 to 5mm).

Task 4: Excitation port L L = 2 mm

The following Table A-3 shows the results which were obtained when the length of excitation port L=2 mm, with different cutting (C) from the bottom left corner of the separation plate.

Table A-3: Simulation results for L=2mm.

Cutting (C) mm	F_1 GHz	F_2 GHz	f_0 GHz	Qe
0	4.572	4.68	4.626	42.8
1	4.605	4.715	4.66	42.36
2	4.682	4.797	4.7395	41.21
3	4.782	4.906	4.8445	39.38
3.4	4.824	4.95	4.887	38.78
4	4.904	5.036	4.9705	37.6
5	5.043	5.187	5.115	35.52

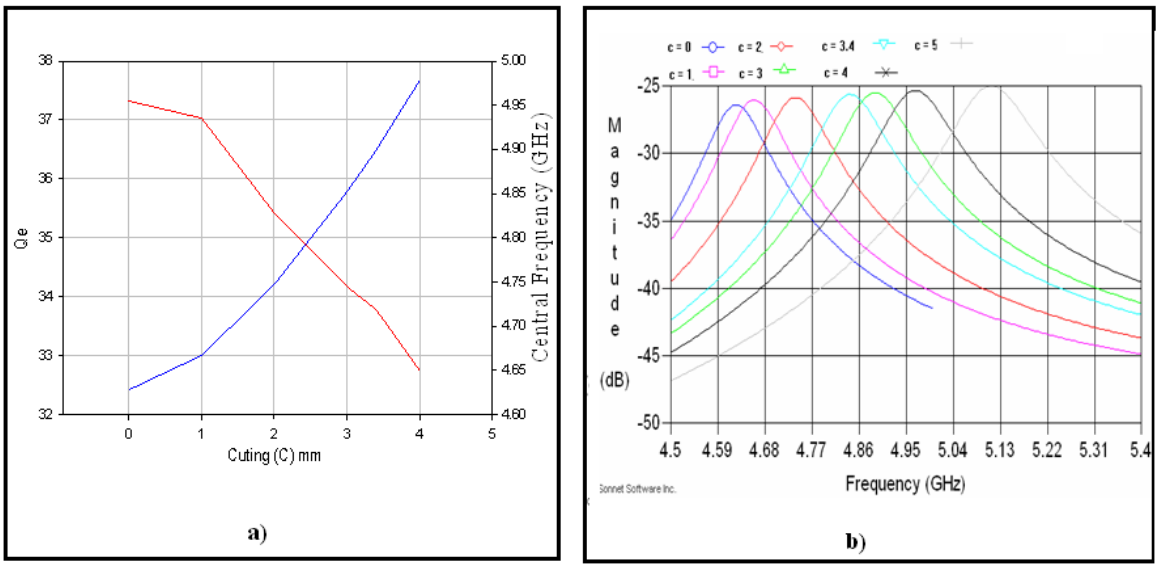

Figure A-4: (a) The values of f_0 and Qe for different C (b) Simulation responses.

From the above Figure (a), it may be seen that when cutting (C) in the corner increases the central frequency, (f_0) increases also, while the external quality factor decreases. From Figure (b) it is clear that the central frequency is shifted to the right and the reason for that is the variation in corner cutting (from 0 to 5mm).

Task 5: Excitation port L L = 2.2 mm

The following Table A-4 shows the results which were obtained when the length of excitation port L=2.2 mm, with different cutting (C) from the bottom left corner of the separation plate.

Table A-4: Simulation results for L=2.2mm.

Cutting (C) mm	F_1 GHz	F_2 GHz	f_0 GHz	Qe
0	4.566	4.69	4.628	37.32
1	4.604	4.730	4.667	37.03
2	4.68	4.814	4.747	35.42
3	4.781	4.923	4.852	34.17
3.4	4.827	4.972	4.899	33.78
4	4.902	5.054	4.978	32.75

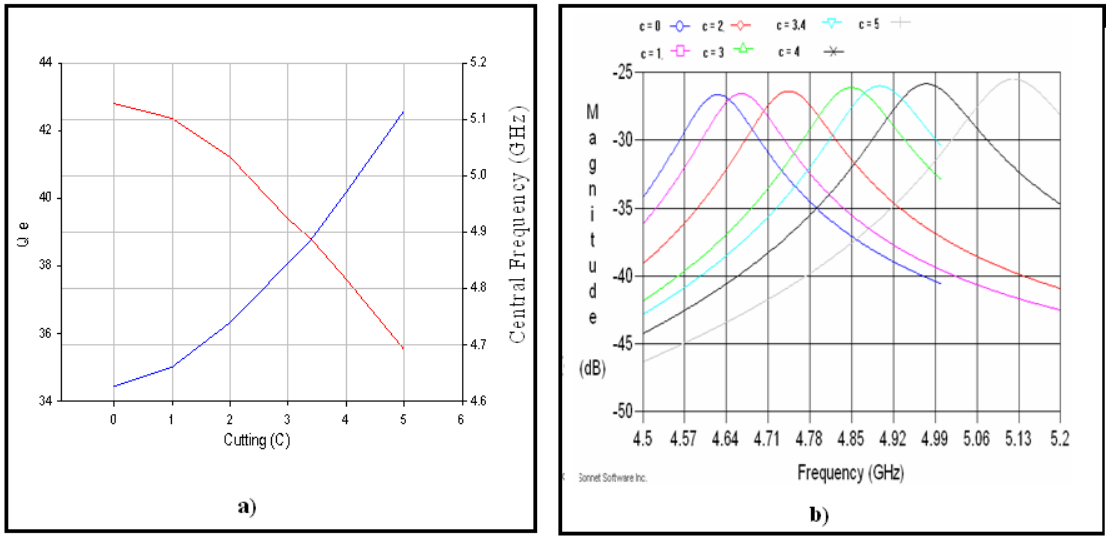

Figure A-5: (a) The values of f_0 and Qe for different C (b) Simulation responses.

From the above Figure A-5 (a), it may be seen that when cutting (C) in the corner increases the central frequency, (f_0) increases also, while the external quality factor decreases. From Figure A-5 (b) it is clear that the central frequency is shifted to the right and the reason for that is the variation in corner cutting (from 0 to 4mm).

Task 6: Excitation port L L = 2.4 mm

The following Table A-5 shows the results which were obtained when the length of excitation port L=2.4 mm, with different cutting (C) from the bottom left corner of the separation plate.

Table A-5: Simulation results for L=2.4mm.

Cutting (C) mm	F_1 GHz	F_2 GHz	f_0 GHz	Qe
0	4.57	4.71	4.64	33.14
1	4.602	4.746	4.674	32.45
2	4.678	4.828	4.753	31.68
2.2	4.696	4.848	4.772	31.39
3	4.78	4.941	4.86	30.18
3.4	4.826	4.992	4.909	29.57
4	4.9015	5.745	4.988	28.83
5	5.043	5.229	5.136	27.91

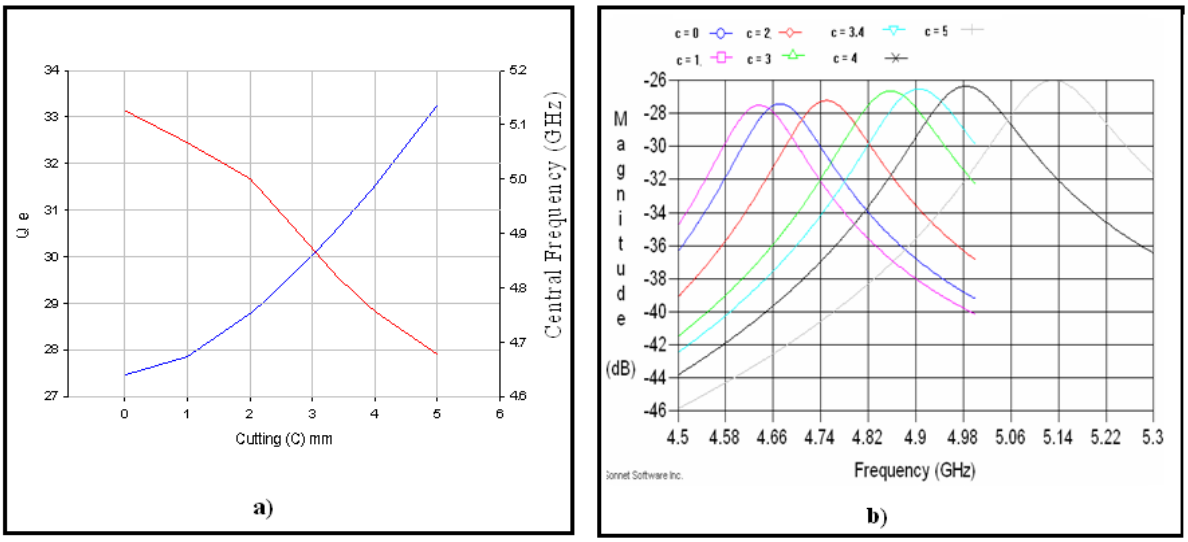

Figure A-6: (a) The values of f_0 and Qe for different C (b): simulation responses

From the above Figure A-6 (a), it may be seen that when cutting (C) in the corner increases the central frequency, (f_0) increases also, while the external quality factor decreases. From Figure A-6 (b), it is clear that the central frequency is shifted to the right and the reason for that is the variation in corner cutting (from 0 to 5mm).

Task 7: Excitation port L L = 2.6 mm

The following Table A-6 shows the results which were obtained when the length of excitation port L=2.6 mm, with different cutting (C) from the bottom left corner of the separation plate.

Table A-6: Simulation results for L=2.6mm.

Cutting (C) mm	F_1 GHz	F_2 GHz	f_0 GHz	Qe
0	4.565	4.72	4.6425	29.95
1	4.605	4.765	4.685	29.28
2	4.68	4.85	4.765	28.03
3	4.78	4.96	4.87	27.05
3.4	4.825	5.01	4.9175	26.58
4	4.9	5.095	4.995	25.61

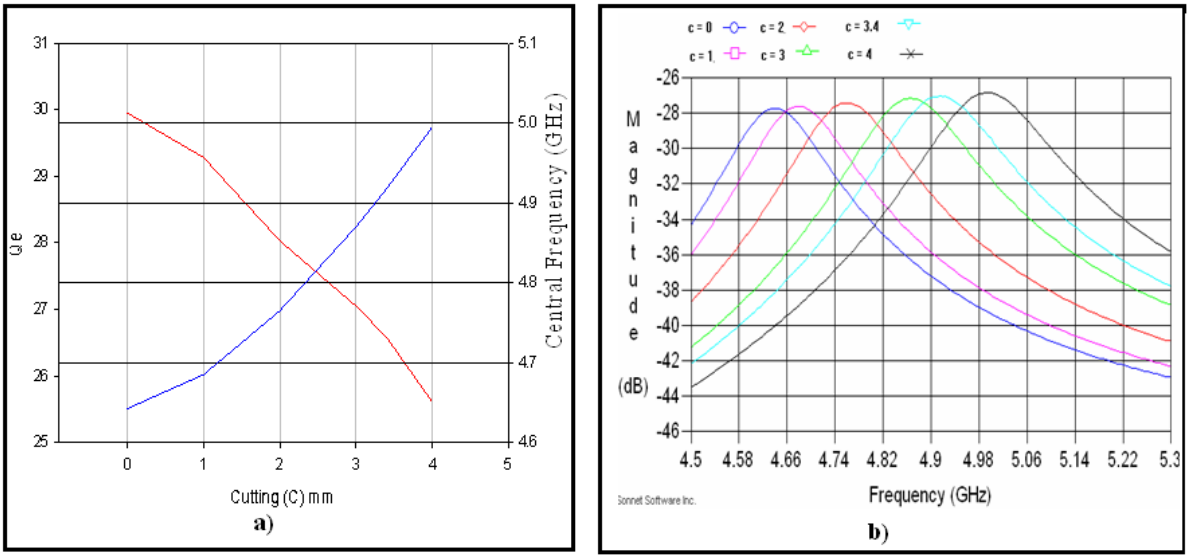

Figure A-7: (a) The values of f_0 and Qe for different C, (b) Simulation responses

From the above Figure A-7 (a), it may be seen that when cutting (C) in the corner increases the central frequency, (f_0) increases also, while the external quality factor decreases. From Figure A-7 (b) it is clear that the central frequency is shifted to the right and the reason for that is the variation in corner cutting (from 0 to 4mm).

Task 8: Excitation port L L = 2.8 mm

The following Table A-7 shows the results which were obtained when the length of excitation port L = 2.8 mm, with different cutting (C) from the bottom left corner of the separation plate.

Table A-7: Simulation results for L=2.8mm.

Cutting (C) mm	F_1 GHz	F_2 GHz	f_0 GHz	Q_e
0	4.565	4.74	4.652	26.5
1	4.6	4.78	4.69	26

2	4.68	4.87	4.775	25.13
3	4.78	4.98	4.88	24.4
3.4	4.826	5.035	4.93	23.58
4	4.905	5.12	5.01	23.3
5	5.045	5.275	5.16	22.4

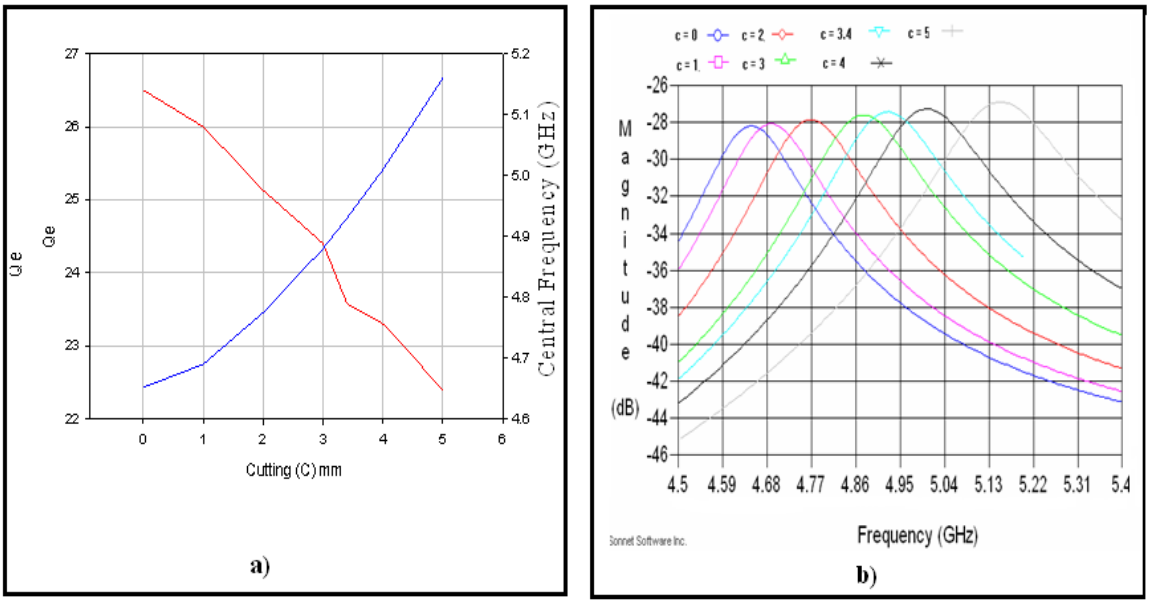

Figure A-8: (a) The values of f_0 and Qe for different C (b) Simulation responses.

From the above Figure A-8 (a), it may be seen that when the cutting (C) in the corner increases the central frequency (f_0) increases also, while the external quality factor decreases. From Figure A-8 (b), it is clear that the central frequency is shifted to the right and reason for that is the variation of the corner (from 0–5).

A.2 Improving of the unloaded quality factor Qu for the folded cavity.

Simulation results

The following sections contain the simulation results for one-pole resonator: that is obtained when the box size is 10.5 x 10.5 x 10 mm. In the first part it is considered with Gold metal for the separation plate, Lossless for the ports and with copper metal for the top and bottom metals and with fixed Height = 10 mm for each half and varying of the separation plate thickness t and the distance between the wall and the separation plate (d). In the second part it is considered with Gold metal for all metals, the separation plate, ports and with copper metal for the top and bottom metals and with fixed Height

= 10 mm for each half and varying of the separation plate thickness (t) and the distance between the wall and the separation plate (d) . The following sections contain the simulation results for one-pole resonator: in the following part it was considered with Gold metal for the separation plate, Lossless for the ports and with fixed Height = 10 mm for each half and varying of the separation plate thickness t with the fixed of the distance between the wall and separation as shown in Figure A-9 and A-10.

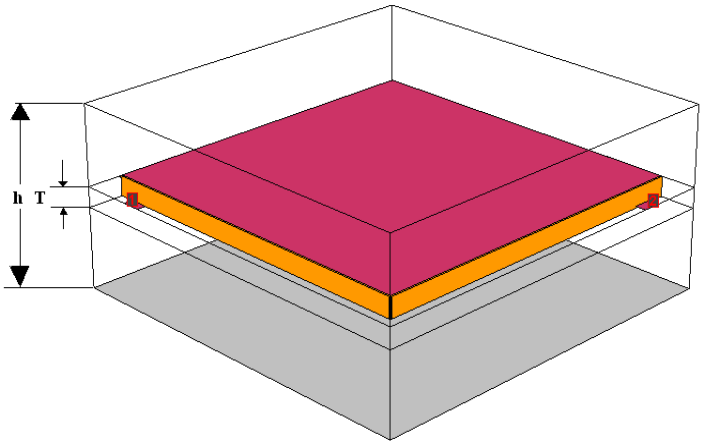

Figure A-9: 3 D for One pole design

Note:

Separation plate is Gold and port is LossLess and the top and bottom metals in the box are copper, we got the following results:-

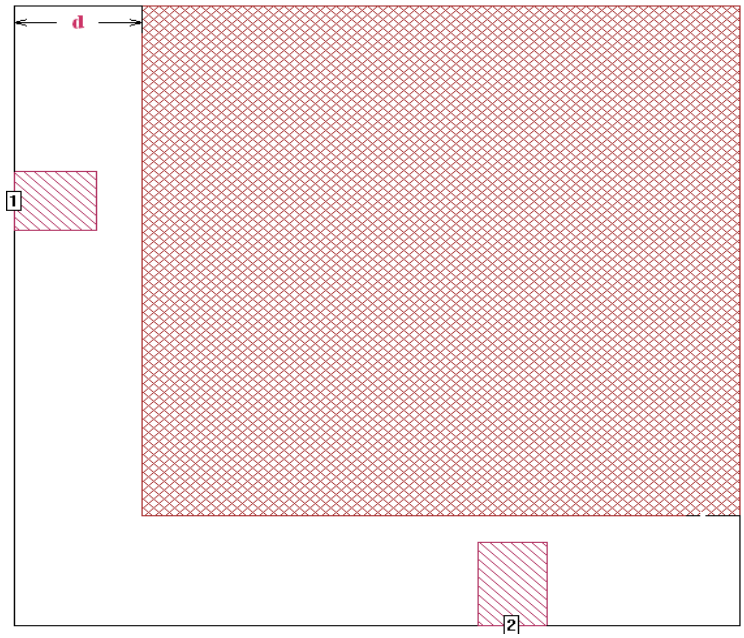

Figure A-10: 2 D for One pole design

In this part it is considered with Gold metal for the separation plate, Lossless for the ports and with copper metal for the top and bottom metals and with fixed Height = 10 mm for each half and varying of the separation plate thickness t and the distance between the wall and the separation plate (d).

Task 1.1:

The following Table A-8 shows the results which were obtained when the length of port one L1 = 2.8 mm, with varied separation plate thicknesses of (t) as shown in Figure 1 and the distance between the wall and separation plate also was fixed as 2.35 mm.

Table A-8 Results for varying (t) when d=2.35mm and L1=2.8mm.

Separation plate Thickness (t mm)	F 0 GHz	Q u (Q L / 1- ⎪ S21 (w0) ⎪)
0.01	13.663	4074
0.02	13.637	3817
0.03	13.637	3717
0.04	13.613	3515
0.05	13.66	3494
0.06	13.6	3379
0.07	13.57	3323
0.08	13.56	3251
0.09	13.55	3178
0.1	13.54	2710
0.5	13.23	2627
1	12.9	2436
1.5	12.66	2372

The conductor is gold but port is LossLess and the top and bottom metals in the box are copper. The following Figures (3) shows the relation between F0 and Qu when the thickness of the separation plate (t) was varied and with port one fixed at L1 = 2.8mm and the distance between the wall and separation plate also was fixed as 2.35 mm.

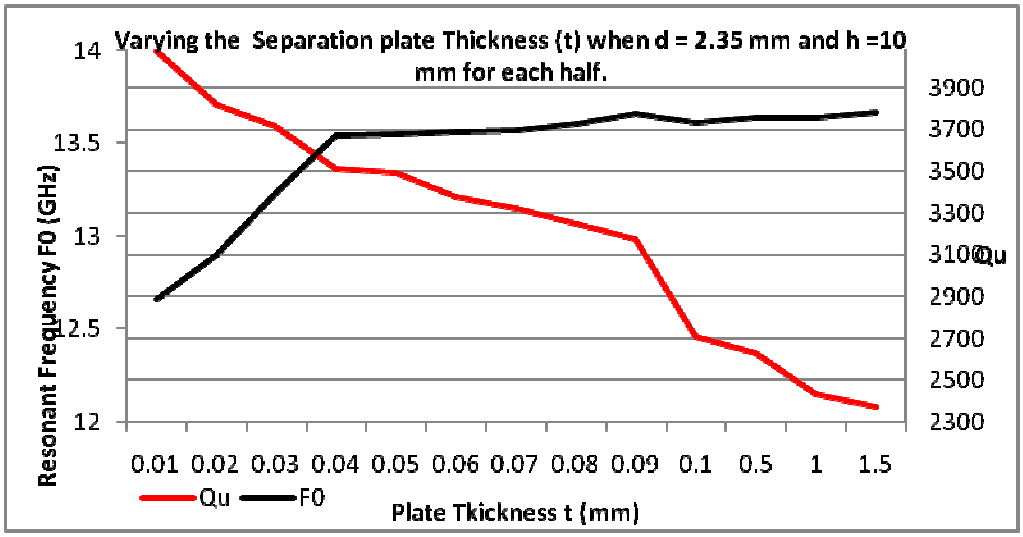

Figure A-11: relation between F0 and Qu when d =2.35 mm and varying of t,

Task 1.2:

The following Table A-9 shows the results which were obtained when the length of port one L1 = 2.8 mm, with varied of the distance (d) between the wall and separation plate as indicated with fixed thicknesses of separation plate (t) as 0.05 mm and the height of each half is 10mm .

Table A-8 : Results for varying (d) when t=0.05mm and L1=2.8mm.

distance (d mm)	F 0 GHz	Q u (Q L / 1- | S21 (w0) |)
0.5	10.738	885
1	11.563	1536
2	13	2821
2.35	13.66	3494
2.5	13.763	3603
3.5	15.29	6307
4	16.013	9144

The following Figures A-12 shows the relation between F0 and Qu when the thickness of the separation plate (t) was fixed = 0.05mm and port one length also fixed at L1 = 2.8mm and the distance between the wall and separation plate was varying.

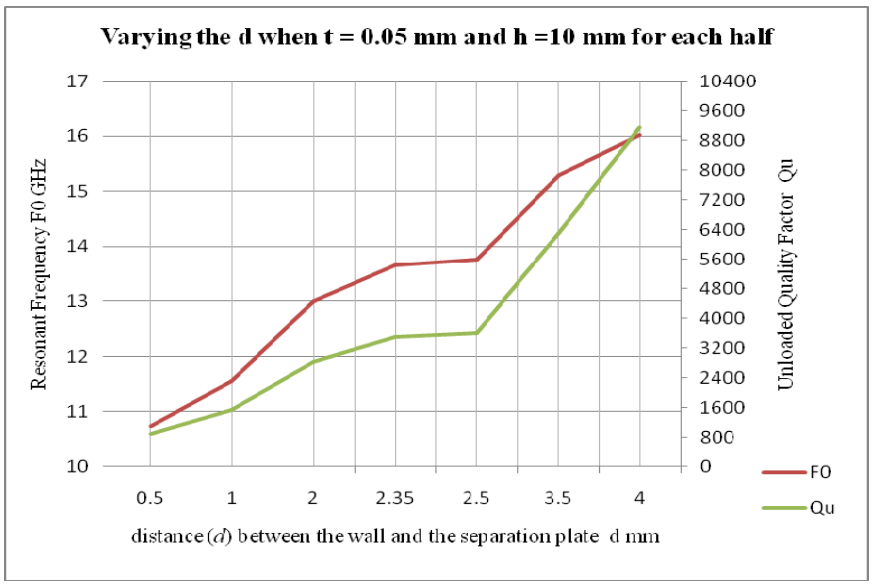

Figure A-12: relation between F0 and Qu when t =0.05 mm and varying of d.

With brass of the separation plate:

2.35	13.59	2191
4	16.015	5987

In the second part it is considered with Gold metal for all metals, the separation plate, ports and with copper metal for the top and bottom metals and with fixed Height = 10 mm for each half and varying of the separation plate thickness (t) and the distance between the wall and the separation plate (d) .

Task 2.1:

The following Table A-10 shows the results which were obtained when the length of port one L1 = 2.8 mm, with varied the distance between the wall and separation plate and with the fixed thickness of separation plate (t) = 0.05mm that is for all metals are Gold metal even ports but copper metal for the top and bottom.

Table A-10 : Results for varying (d) when t=0.05mm and L1=2.8mm.

distance (d mm)	F 0 GHz	Q u = (Q L / 1- | S21 (w0) |)
0.35	10.08	570
0.65	10.5	848
2.35	13.6	1566
2.5	13.8	1626

3.5	14.95	2053
4	15.421	2120

The following Figures A-13 shows the relation between F0 and Qu when the thickness of the separation plate (t) was fixed = 0.05 and with port one fixed at L1 = 2.8mm and varied of the distance between the wall and separation d. That is for all metals are Gold metal even ports but copper metal for the top and bottom.

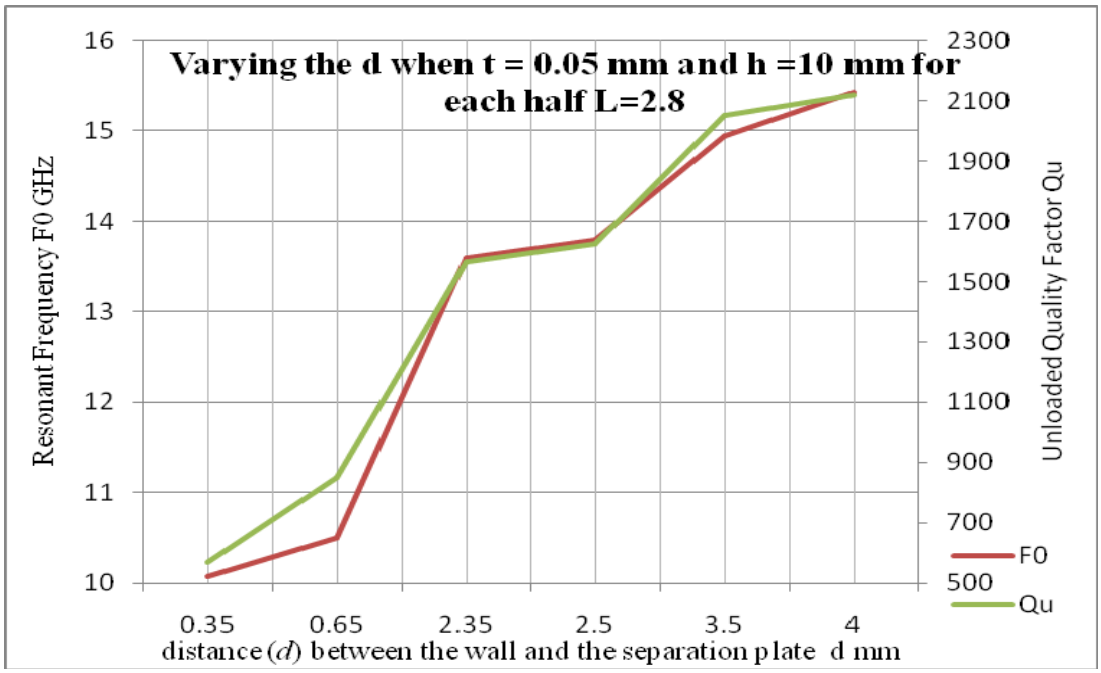

Figure A-13: relation between F0 and Qu when t =0.05 mm and varying of d.

Task 2.2:

The following Table A-11 shows the results which were obtained when the length of port one L1 was varied, with fix distance between the wall and separation plate d = 4mm and with the fixed thickness of separation plate (t) = 0.05mm as well, that is for all metals are Gold metal even ports but copper metal for the top and bottom.

Table A-11 : Results for varying (d) when t=0.05mm and L1=2.8mm.

L (mm)	F0 (GHz)	Qu
0.6	13	2118
0.75	13.078	2527
0.8	13.13	2580
0.85	13.18	2500

0.9	13.19	2307
1	13.36	2457
2.8	15.421	2120

Task 2.3:

The following Table A-12 shows the results which were obtained when the distance between the wall and separation plate is fixed d = 4mm and of port one L1 =0.8mm as well and with varied of the thickness of the separation plate (t). That is for all metals are Gold metal even ports but copper metal for the top and bottom.

Table A-10 : Results for varying (t) when d= 4mm and L1=0.8mm.

Separation plate Thickness (t mm)	F 0 GHz	Q u (Q L / 1- | S21 (w0) |)
0.01	13.145	3050
0.05	13.13	2580
0.08	13.12	2333
0.1	13.11	2230
0.5	13.03	1773
1	12.93	1708

The following Figures A-14 shows the relation between F0 and Qu when the distance between the wall and separation plate is fixed d = 4mm and of port one L1 =0.8mm and with varied of the thickness of the separation plate (t). That is for all metals are Gold metal even ports but copper metal for the top and bottom.

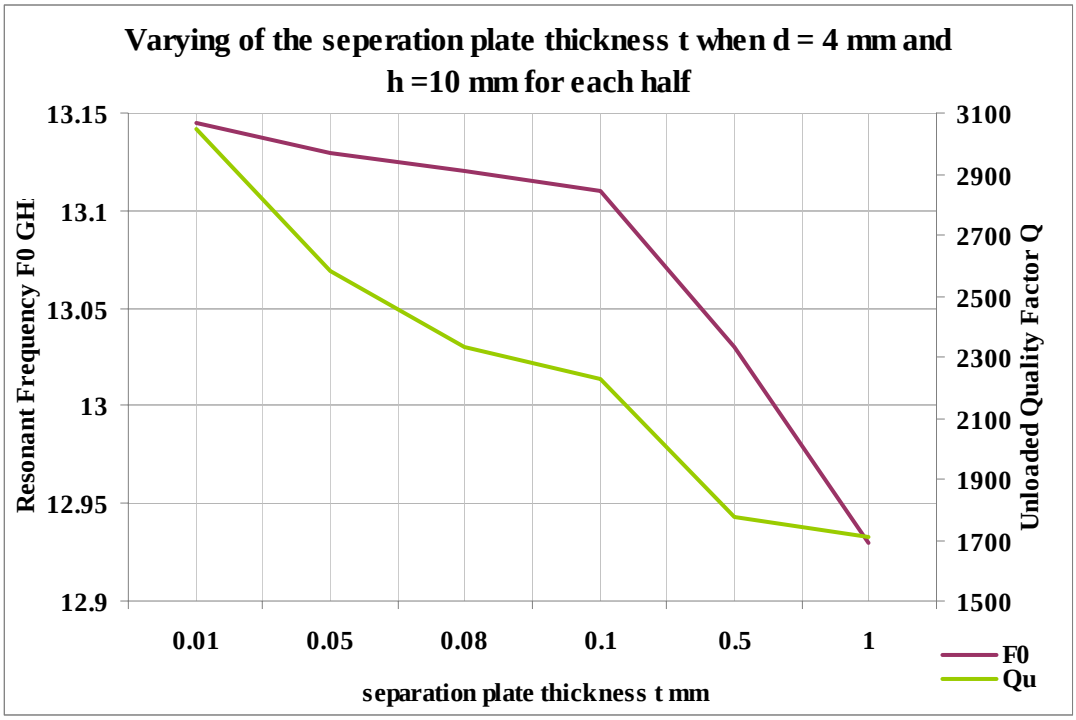

Figure A-14: relation between F0 and Qu when d =4 mm and varying of t.

Task 2.4:

The following Table A-11 shows the results which were obtained when the length of port one L1 = 0.8 mm, with varied the distance between the wall and separation plate and with the fixed thickness of separation plate (t) = 0.01mm that is for all metals are Gold metal even ports but copper metal for the top and bottom.

Table A-11 : Results for varying (d) when t= 0.01mm and L1=0.8mm.

distance (d mm)	F 0 GHz	Q u (Q L / 1- | S21 (w0) |)
0.35	8.6	882
0.65	9.013	1240
2.35	10.49	2300
2.5	11.12	2400
4	13.145	3050

The following Figures A-15 shows the relation between F0 and Qu when the thickness of the separation plate (t) was fixed = 0.01 and with port one fixed at L1 = 0.8mm and varied of the distance between the wall and separation d. That is for all metals are Gold metal even ports but copper metal for the top and bottom.

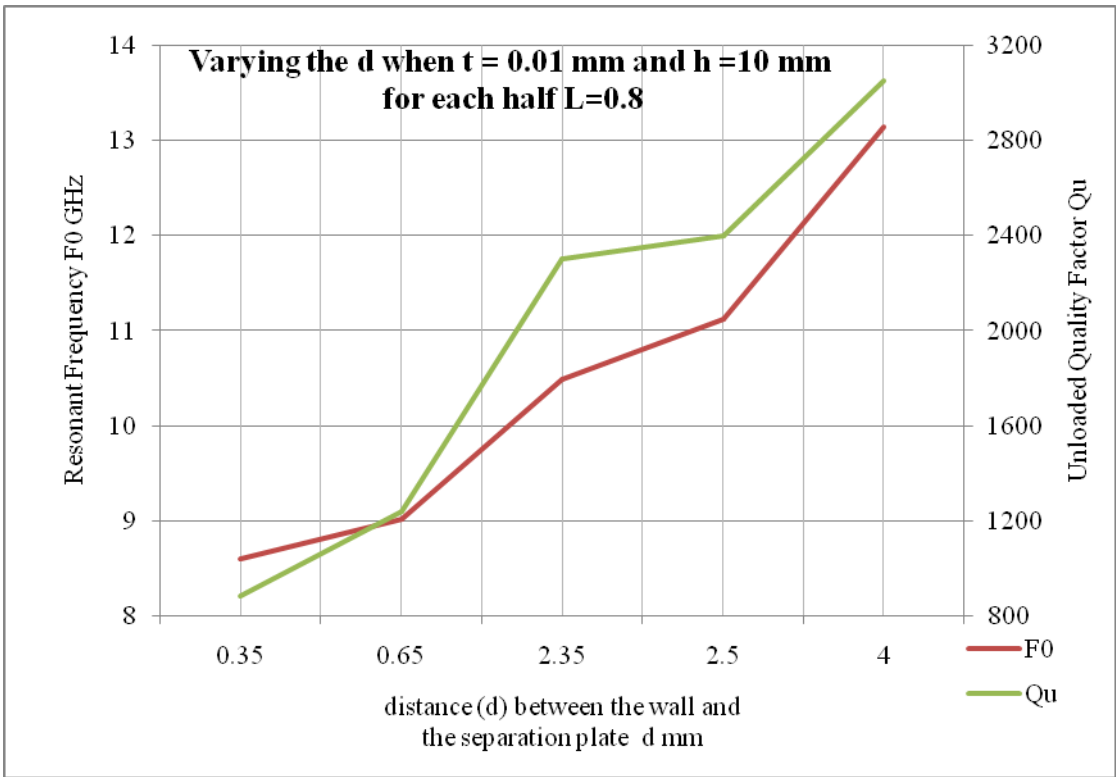

Figure A-15: relation between F0 and Qu when t =0.01 mm and varying of d.

A.3 Two-Pole resonator design

The following table A-12 and graphs are the responses of Two Resonators which have size of, A = 20 mm, B = 20 mm & coupling gap between them is G = 2.7 mm, with different cutting from the edge: -

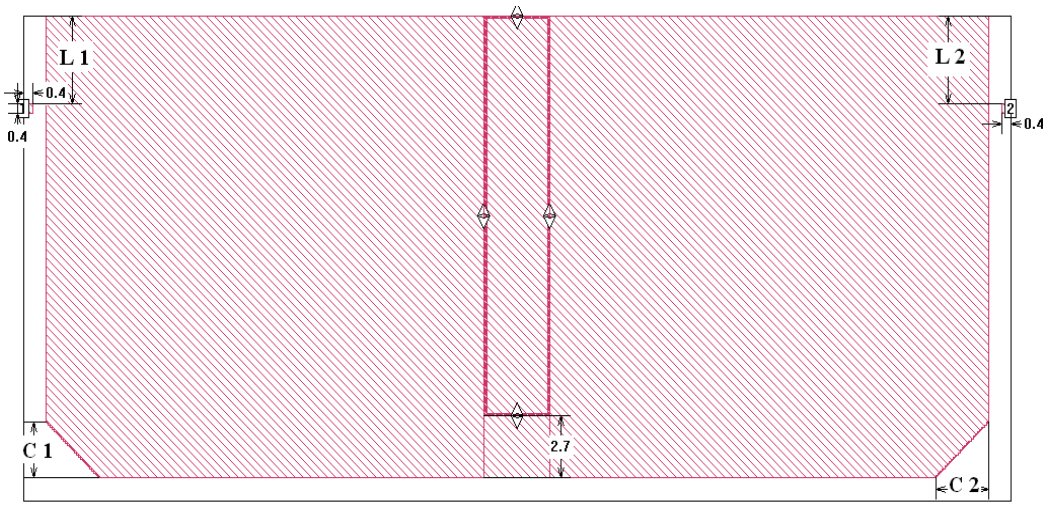

Figure A-16 : The Layout of 2-pole filter when G=2.7mm

Table A-12 : Results for varying (C1 and C2) when G= 2.7mm and.

Cutting edge C (mm)	Fc GHz (central frequency) $\frac{(F_1+F_2)}{2}$	K (Coupling coefficient) $\frac{(F_2-F_1)}{(F_2+F_1)}$	Frequencies
0	4.622	0.0248	**F1 = 4.565 GHz** **F2 = 4.68 GHz**
1	4.652	0.0247	**F1 = 4.595 GHz** **F2 = 4.71 GHz**
2	4.72	0.0275	**F1 = 4.655 GHz** **F2 = 4.785 GHz**
2.2	4.78	0.0083	**F1 = 4.76 GHz** **F2 = 4.8 GHz**
2.3	4.745	0.0273	**F1 = 4.68 GHz** **F2 = 4.81 GHz**

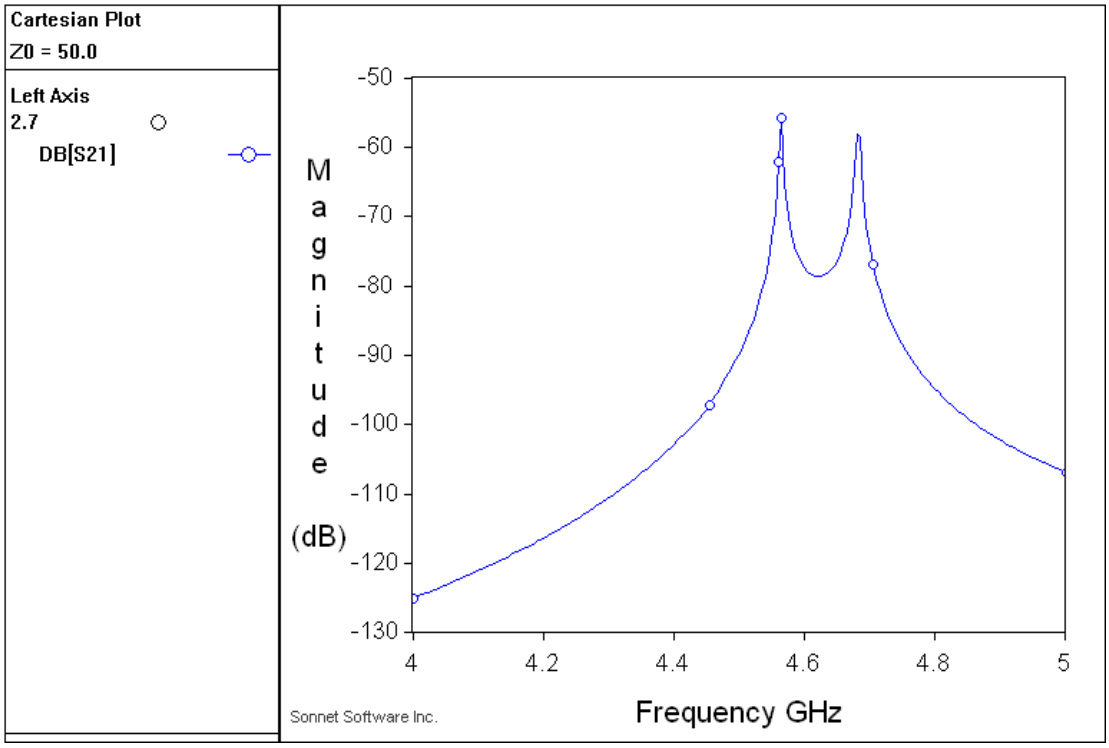

Figure A-17: Two Resonators (20mm X 20mm without Cutting)

Table A-13 : Results for varying (C1 and C2) when G= 2.1mm and.

Cutting edge(C) (mm)	Fc GHz (central frequency)	K (Coupling coefficient)	Frequencies
0	4.645	0.0187	F1 = 4.602 GHz F2 = 4.689 GHz
1	4.679	0.0192	F1 = 4.634 GHz F2 = 4.72 GHz
2	4.744	0.01939	F1 = 4.698 GHz F2 = 4.79 GHz
3	4.831	0.0202	F1 = 4.782 GHz F2 = 4.88 GHz
4	4.938	0.021	F1 = 4.886 GHz F2 = 4.99 GHz

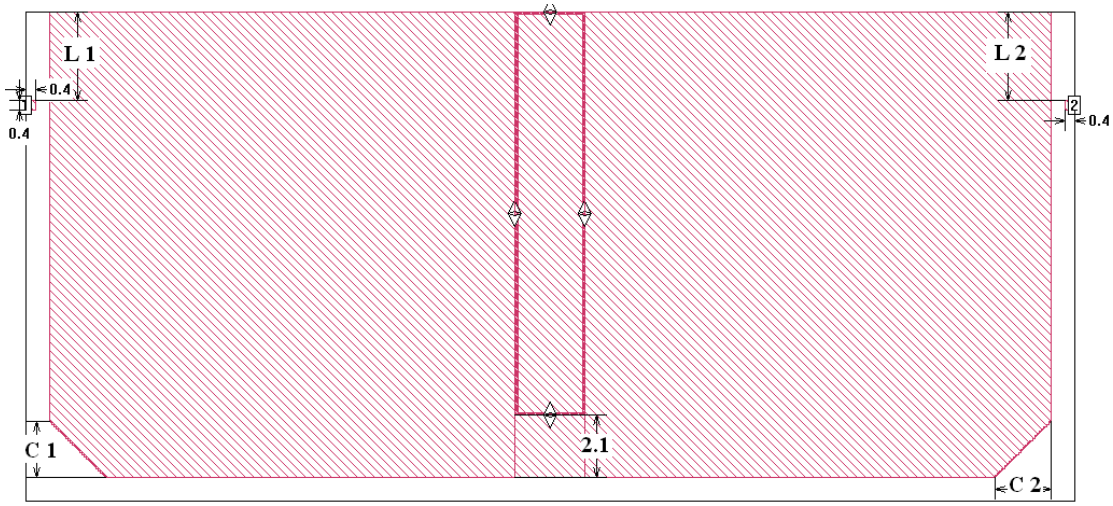

Figure A-18 : The Layout of 2-pole filter when G=2.1

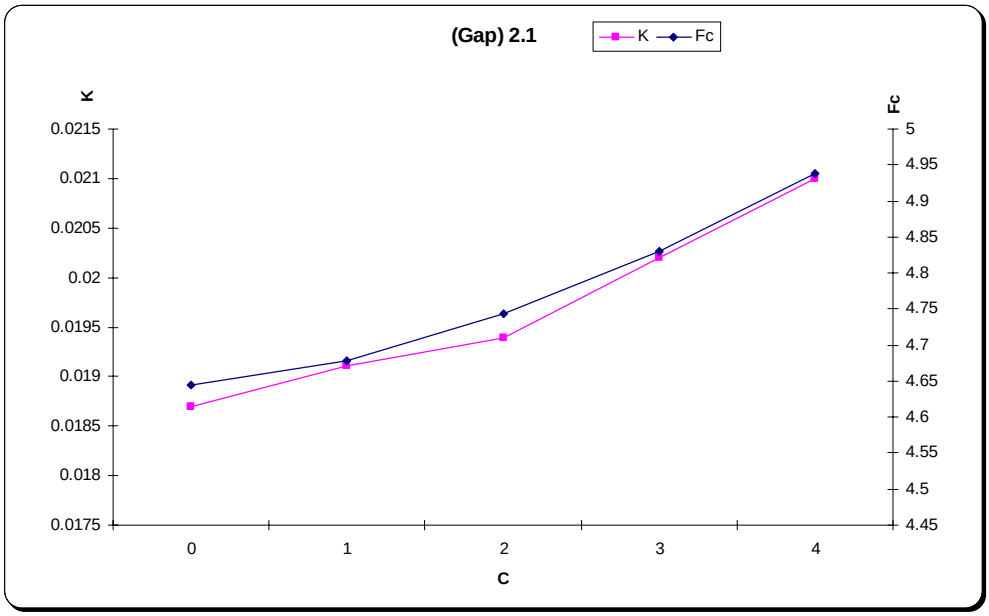

Figure A-19 : The result of 2-pole filter when G=2.1 and C is varied.

The Following responses that shown in Figure A-20 are (*Different L and Same C which is 3 mm*).

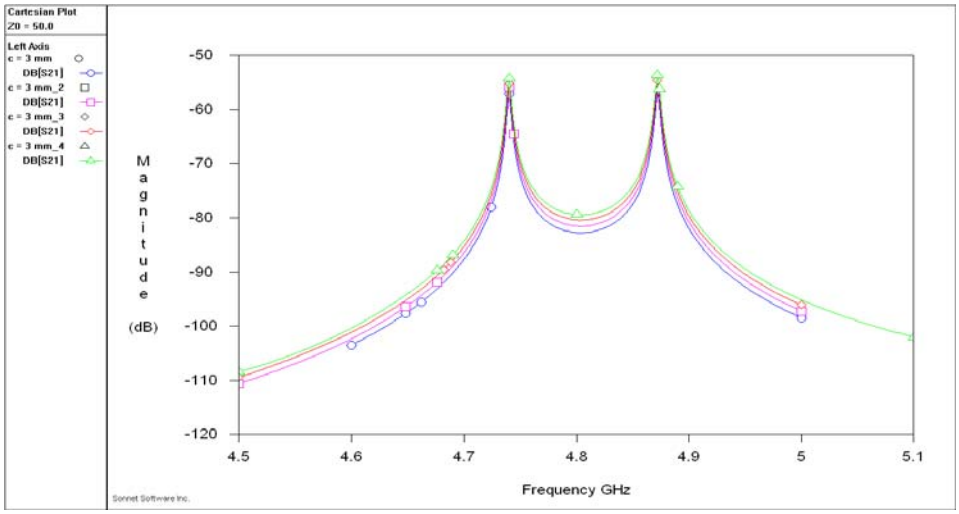

Figure A-20: The responses for different L when C = 3 mm, G = 2.7mm

Figure A-21 depicts the extracted coupling coefficient K and central frequency f_0 against different coupling gap (G). A observation can be obtained for any other given G. From that figure can extract the coupling coefficient K and central frequency f_0 against the different coupling gap G between adjacent resonators for a fixed corner cutting (C) of 3 mm. It was noticed that the coupling coefficient (K) is directly proportional to the

coupling gap length (G), whereas the central frequency f_0 is inversely proportional to the G.

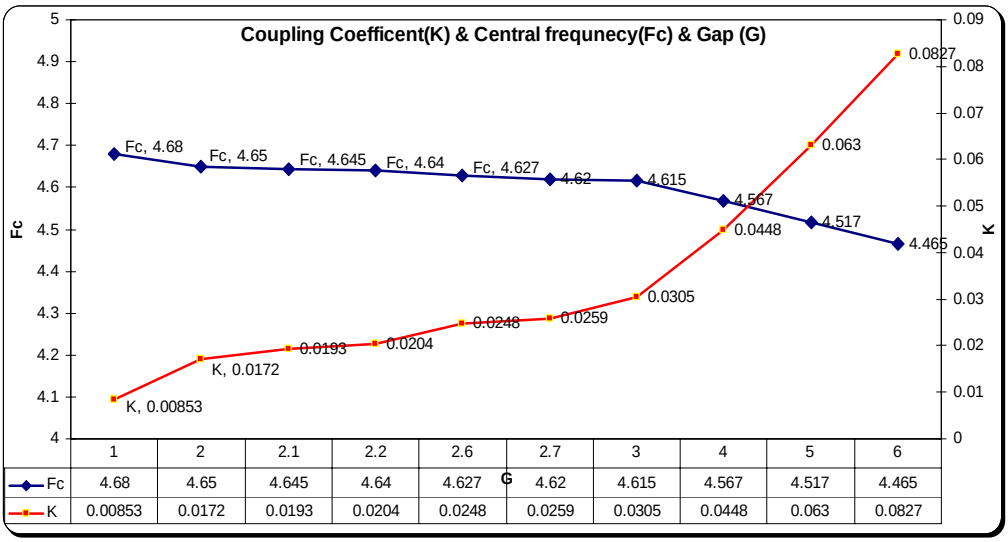

	1	2	2.1	2.2	2.6	2.7	3	4	5	6
Fc	4.68	4.65	4.645	4.64	4.627	4.62	4.615	4.567	4.517	4.465
K	0.00853	0.0172	0.0193	0.0204	0.0248	0.0259	0.0305	0.0448	0.063	0.0827

Figure A-21 : The result of 2-pole filter when G=2.7 and C is varied.

A.4 Four-Pole resonator design

The 4-pole coupled folded waveguide FWG filter containing 4 resonators with couplings between them that is shown in Figure A-22 . This 4-pole resonator filter is composed of three 2-pole resonators.

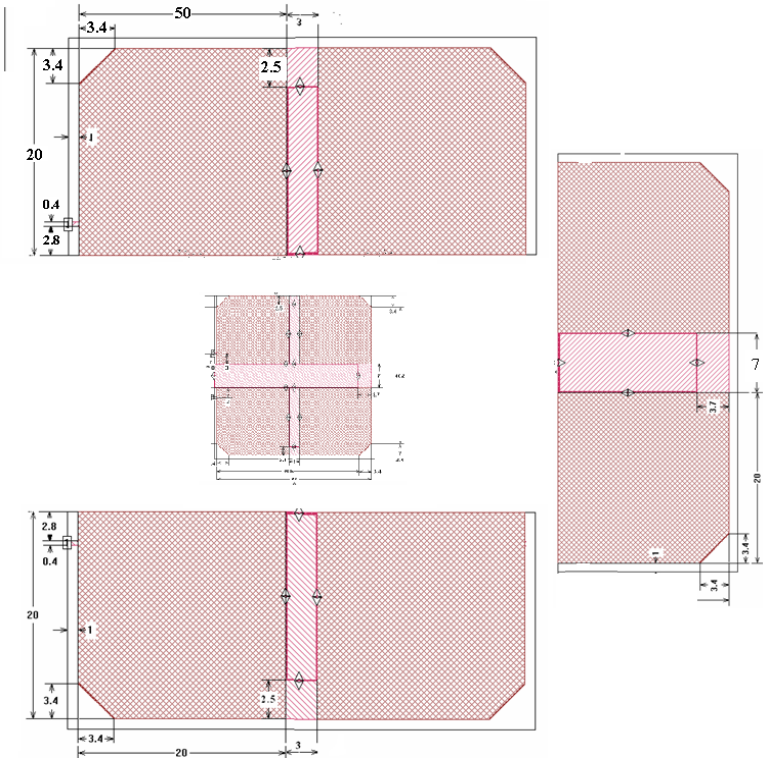

Figure A-22: The Layout of 4-pole filter.

The Following Figure A-23 shows the Simulated and return loss of a compact folded waveguide.

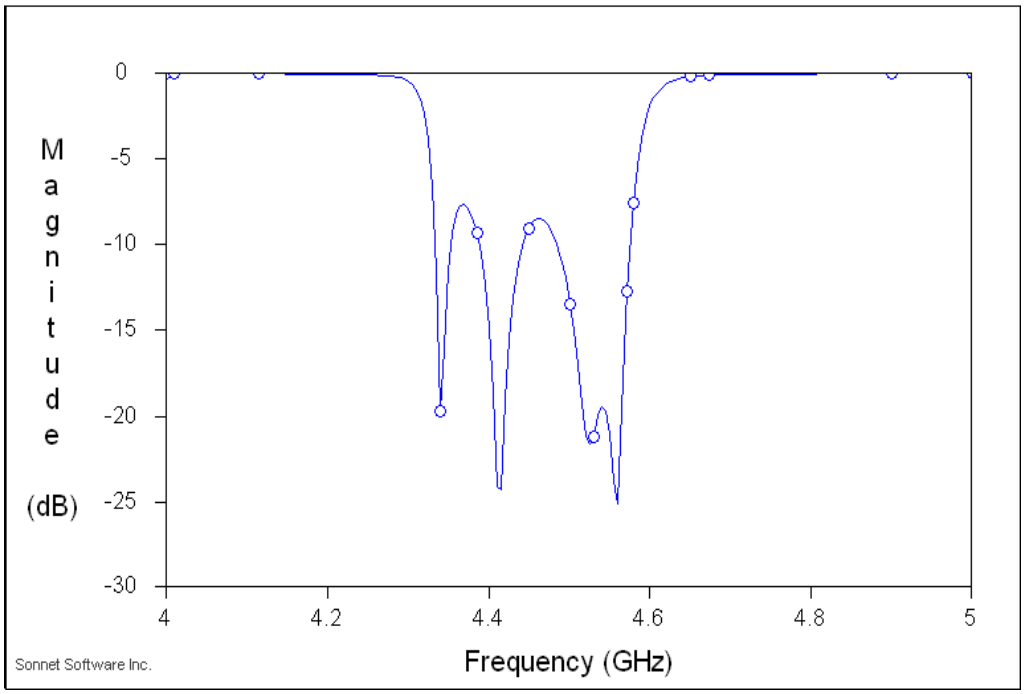

Figure A-23 a) : Simulated and return loss (S11) of 4-pole FWG filter

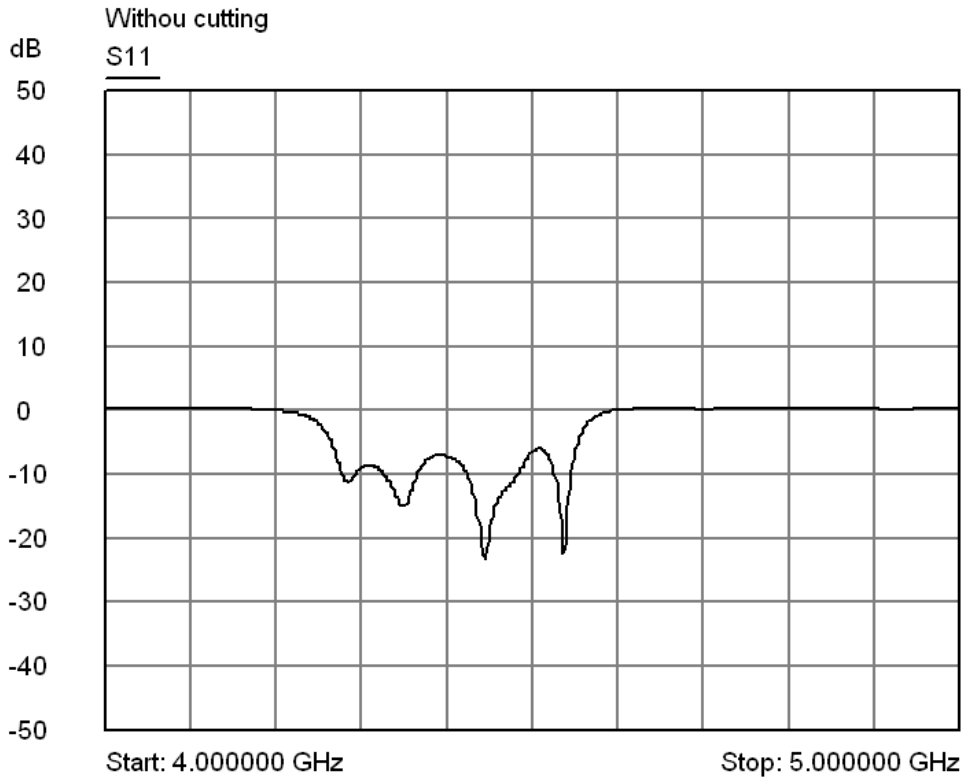

Figure A-23 b): Measured and return loss (S11) of 4-pole FWG filter

The difference between the simulated and the measured return losses (S_{11}) can be seen clearly in the Figure 23 a) and b). The observed difference in the return losses could be avoided by tuning the dimensions of the four-pole cavity. A special design for the cavity using fine tuning of the coupling gap length (G) could achieve the exact performance required. The reasons for the difference in the measured and simulated frequency responses may be the result of one of the following:

- In simulation, the dielectric at the I/O ports was not taken into consideration.

- It could also be owing to the tolerance in the dimensions during the fabrication of the cavity material.

In addition, many losses were neglected in the simulation, which was not the case different in the practical situation. The best measured return losses is in the following figure 29.

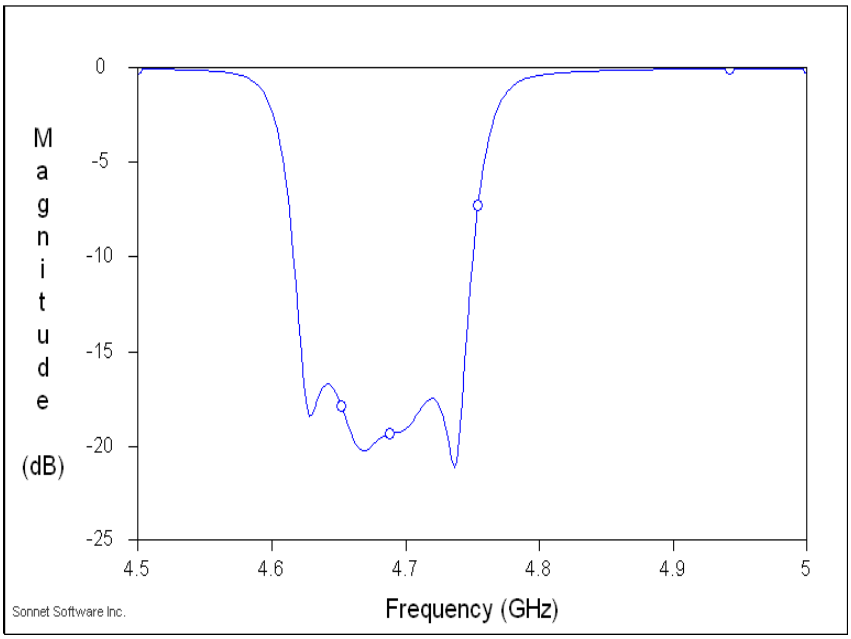

Figure A-24 : Measured and return loss (S11) of 4-pole FWG filter without plate thickness

Appendix B

SIFW Resonator

B.1 Substrate integrated circuit:

One pole resonator of the substrate integrated waveguides (SIW) has been designed in order to attain a Good unloaded quality factor. This has been done by varying many parameter, e.g. Box size, design location, port location and separation plate size. The Ideal will be clear when you read through following:

B.1.1 . Introduction:

In the following part, one-pole resonator design using folded Substrate integrated waveguide structured with Via hole and varying the diameter of the via hole (d) and the distance between the via (p) as shown in the Figure 1 with er = 3.2 and h = 0.762 mm and the tan. Angt = 0.003 as shown in Figure B-1 .

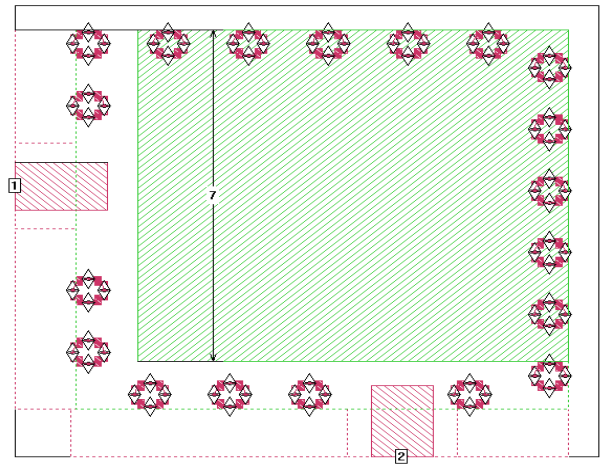

Figure B-1: 2D One pole resonator layout

The following figure B-2 shows the via hole diameter (d) mm and the distance between the Vias (p).

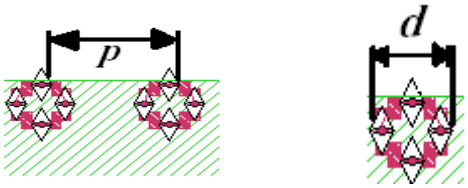

(a) **(b)**

Figure B-2: a) Distance between Via holes. b) Via hole Diameter

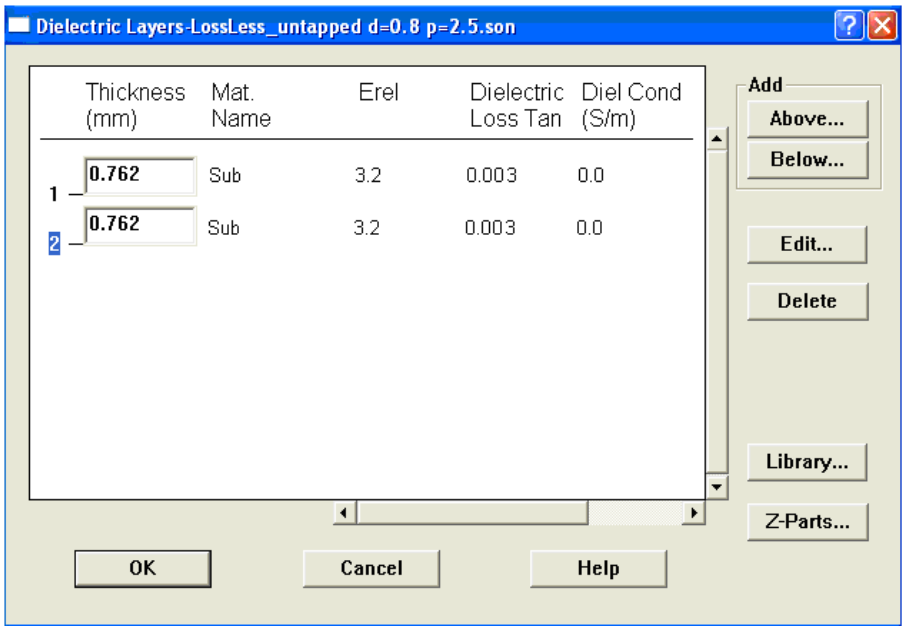

Figure B-3: er = 3.2 and h = 0.762 mm and the tan. Angt = 0.003

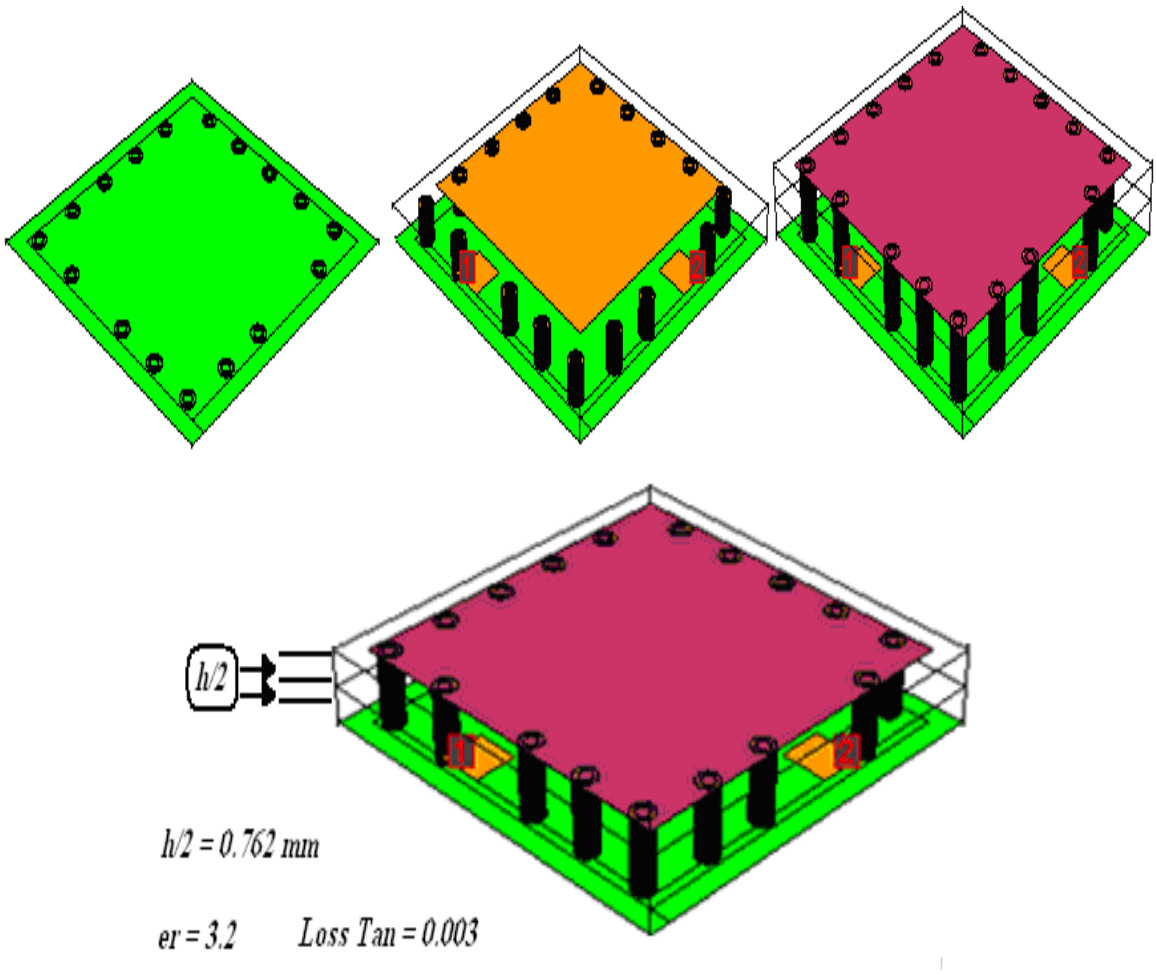

Figure B-4: 3D for One pole resonator layout.

B.1 2. Simulation results :

The following sections contain the simulation results for one-pole resonator design using folded Substrate integrated waveguide structured: In this part; it was considered with Copper metal for top, bottom and separation plate. In the other hand Lossless for the ports and via hole with varying of via hole diameter (d) mm and the distance between the Vias (p) mm.

Task 2.1:

The following Table B-1 shows the results which were obtained when the diameter of via hole d = 0.2 mm and varying the distance between the vais p .

Table B-1 shows the results which were obtained when the diameter of via hole d = 0.2 mm

P mm	F_0 GHz	Q_u

0.4	6.65	280
1	6	245
1.5	5.2	230
2.5	4.5	210

Task 2.2:

The following Table B-2 shows the results which were obtained when the diameter of via hole d = 0.5 mm and varying the distance between the vais p .

Table B-2 shows the results which were obtained when the diameter of via hole d = 0.5

P mm	F_0 GHz	Q_u
0.4	6.1	265
1	5.5	247
1.5	4.8	235
2.5	4	200

Task 2.3:

The following Table B-3 shows the results which were obtained when the diameter of via hole d = 0.8 mm and varying the distance between the vais p.

Table B-3 shows the results which were obtained when the diameter of via hole d = 0.8 mm

P mm	F_0 GHz	Q_u
0.4	6.9	255
1	6.4	235
1.5	5.8	225
2.5	5	204

B.2 3. ALL used metals are Copper :-

The following sections contain the simulation results for one-pole resonator design using folded Substrate integrated waveguide structured: In this part it was considered with Copper metal for all metals that used in the designs. The varying parameters were via hole diameter (d) mm and the distance between the Vias (p).

Task 3.1:

The following Table B-4 shows the results which were obtained when the diameter of via hole d = 0.2 and varying the distance between the vais p.

Table B-4 shows the results which were obtained when the diameter of via hole d = 0.2 mm

P mm	F_0 GHz	Q_u
0.4	6.65	224
1	6	216
1.5	5.2	203
2.5	4.5	189

Task 3.2:

The following Table B-5 shows the results which were obtained when the diameter of via hole d = 0.5 and varying the distance between the vais.

Table B-5 shows the results which were obtained when the diameter of via hole d = 0.5 mm

P mm	F_0 GHz	Q_u
0.4	6.1	214
1	5.5	205
1.5	4.8	195
2.5	4	154

Task 3.3:

The following Table B-6 shows the results which were obtained when the diameter of via hole d = 0.8 and varying the distance between the vais p .

Table B-6 shows the results which were obtained when the diameter of via hole d = 0.5 mm

P mm	F_0 GHz	Q_u
0.4	6.9	226
1	6.4	197
1.5	5.8	185
2.5	5	155

Reference:

[1] J. S. Hong, "Compact folded-waveguide resonators," *Microwave Symposium Digest, 2004 IEEE MTT-S International*, vol. 1, 2004.

[2] J. S. Hong, "Compact folded-waveguide resonators and filters," *Microwaves, Antennas and Propagation, IEE Proceedings-*, vol. 153, pp. 325-329, 2006.

[3] P. Blondy, A. R. Brown, D. Cros, and G. M. Rebeiz, "Low-loss micromachined filters for millimeter-wave communicationsystems," *Microwave Theory and Techniques, IEEE Transactions on*, vol. 46, pp. 2283-2288, 1998.

[4] J. Papapolymerou, J. C. Cheng, J. East, and L. P. B. Katehi, "A micromachined high-Q X-band resonator," *Microwave and Guided Wave Letters, IEEE [see also IEEE Microwave and Wireless Components Letters]*, vol. 7, pp. 168-170, 1997.

[5] T. A. Schwarz and L. P. B. Katehi, "A Micromachined Evanescent Mode Resonator," *European Microwave Conference, 1999. 29th*, vol. 2, 1999.

[6] B. Guillon, D. Cros, P. Pons, K. Grenier, T. Parra, J. L. Cazaux, J. C. Lalaurie, J. Graffeuil, and R. Plana, "Design and realization of high Q millimeter-wave structures throughmicromachining techniques," *Microwave Symposium Digest, 1999 IEEE MTT-S International*, vol. 4, 1999.

[7] D. M. Pozar, "Microwave Engineering, Hoboken," NJ: John Wiley and Sons, 2005.

[8] http://escience.anu.edu.au/lecture/cg/Color/Image/spectrum.gif, (Accessed on 20 Nov. 2006.).

[9] M. Makimoto and S. Yamashita, *Microwave Resonators and Filters for Wireless Communication: Theory, Design, and Application*: Springer, 2001.

[10] W. P. Mason and R. A. Sykes, "The use of coaxiaf and balanced transmission lines in filters and wide band transformers for highradio frequencies:," *Bell Syst. Tech. J.*, vol. 16, pp. 275-302, 1937.

[11] R. M. Fano and A. W. Lawson., *Microwave Transrmssion Circuits* vol. 9, 1948.
.

[12] S. Darlington, "Synthesis of Reactance Four Poles Which Produce Prescribed Insertion Loss Characteristics," *Journ. of Mathematics and Physics*, vol. 18, pp. 257-353, 1939.

[13] M. Makimoto and S. Yamashita, *Microwave Resonators and Filters for Wireless Communication : Theory, Design and Application Publisher*, Springer; 1 edition ed, 2000.

[14] S. Y. Liao, *Microwave Devices & Circuit*, Third ed ed, 1990.

[15] J. P. Christophe A. Tavernier and R. Henderson, "A Hybrid Micromachined High -Q Cavity Resonator at 5.8 GHz," *A. Tavernier1*, 2002.

[16] J. P. Becker and L. P. B. Katehi, "Toward a novel planar circuit compatible silicon micromachinedwaveguide," *Electrical Performance of Electronic Packaging, 1999*, pp. 221-224, 1999.

[17] I. Poole, "Understanding Receiver Selectivity," December 2000.

[18] K. V. Puglia, "A general design procedure for bandpass filters derived from low pass prototype elements," *MICROWAVE JOURNAL*, pp. Part I, 2001.

[19] D.M. Pozar, *Microwave Engineering*, second ed. New York, NY: John Wiley and Sons, Inc, 1998.

[20] U. o. C. Mai, "Waveguide Theory," Group of researchers at the University of Chiang Mai, Thailand, 2005.

[21] D. Filipovic, "Computer Aided Microwave Circuit Design," 2005.

[22] S. B. Cohan, "Microwave Band Pass Filters Containing High Q Dielectric Resonator," *IEEE Trans. Microwave Theory amd Tech.,*, vol. MTT-16, pp. 218-277, 1968.

[23] S. T. Fiedziuzko, "Dual Mode Dielectric Resonator Loaded Cavity Filter," *IEEE Trans. Microwave Theory amd Tech.,*, vol. MTT-30, pp. 311-316, 1982.

[24] C. Kudsia, R. Cameron W. Tang,, "Innovation in Microwave Filters and Multiplexing Network for Communication Satellite System," *IEEE Trans. Microwave Theory amd Tech.,*, vol. 40, pp. 1133-1149, 1992.

[25] J. Yohannan, Joe Jacob, Anil Lonappan and K. T. Mathew,, "Dielectric Properties of Stornatium Sodium Niobate Ceramics Using Microwave Cavity Perturbation Technique,," *Microwave and Optical Technology Letters,*, vol. 39, pp. 112-115, 2003.

[26] S. B. Cohn, "Microwave Bandpass Filters Containing High Q Dielectric Resonators " *IEEE Trans. Microwave Theory amd Tech.,*, vol. MMT-16, 1968.

[27] K. M. Strohm, F. J. Schmuckle, O. Yaglioglu, J. F. Luy, W. Heinrich, D. C. R. Center, and G. Ulm, "3D silicon micromachined RF resonators," *Microwave Symposium Digest, 2003 IEEE MTT-S International*, vol. 3, 2003.

[28] M. Stickel, G.V.E., and P.Kremer, "High-Q bulk micromachined sillicon cavity resonator at Ka-band," *Electronics Letters.*, vol. 37, pp. 433-435., 2001.

[29] C. A. Tavernier, R. M. Henderson, and J. Papapolymerou, "A reduced-size silicon micromachined high-Q resonator at 5.7 GHz," *Microwave Theory and Techniques, IEEE Transactions on*, vol. 50, pp. 2305-2314, 2002.

[30] Sonnet, "em," 10.52 ed. North Syracuse, NY ,USA.: Sonnet Software Inc, 2004.

[31] X. P. Chen, K. Wu, and Z. L. Li, "Dual-Band and Triple-Band Substrate Integrated Waveguide Filters With Chebyshev and Quasi-Elliptic Responses," *Microwave Theory and Techniques, IEEE Transactions on*, vol. 55, pp. 2569-2578, 2007.

[32] J. S. Hong and M. J. Lancaster, *Microstrip filters for RF/microwave applications*: Wiley New York, 2001.

[33] Robert E.Collin ,Foundations for microwave Engineering, Mc Graw hill International Editions, Electrical Engineering series.

[34] L. Accatino, G. Bertin, and M. Mongiardo, "A four-pole dual mode elliptic filter realized in circular cavity without screws," *Microwave Theory and Techniques, IEEE Transactions on*, vol. 44, pp. 2680-2687, 1996.

[35] A. E. Atia and A. E. Williams, "Narrow-Bandpass Waveguide Filters," *Microwave Theory and Techniques, IEEE Transactions on*, vol. 20, pp. 258-265, 1972.

[36] G. Macchiarella, S. Tamiazzo, and D. E. e Inf, "Design techniques for dual-passband filters," *Microwave Theory and Techniques, IEEE Transactions on*, vol. 53, pp. 3265-3271, 2005.

[37] H. W. Yao, C. Wang, and A. K. Zaki, "Quarter wavelength ceramic combline filters," *Microwave Theory and Techniques, IEEE Transactions on*, vol. 44, pp. 2673-2679, 1996.

[38] J. Kocbach and K. Folgero, “Design procedure forwaveguide filters with cross-couplings,” in IEEE MTT-S Int Microwave Symp. Dig., vol. 3, June 2002, pp. 1449–1452.

[39] K. Wu, "Integration and interconnect techniques of planar and non-planarstructures for microwave and millimeter-wave circuits-current statusand future trend," *Microwave Conference, 2001. APMC 2001. 2001 Asia-Pacific*, pp. 411-416, 2001.

[40] D. Deslandes and K. Wu, "Integrated microstrip and rectangular waveguide in planar form," *Microwave and Wireless Components Letters, IEEE [see also IEEE Microwave and Guided Wave Letters]*, vol. 11, pp. 68-70, 2001.

[41] W. Menzel and J. Kassner, "Millimeter-Wave 3D Integration Techniques using LTCC and Related Multilayer Circuits," *European Microwave Conference, 2000. 30th*, pp. 1-4, 2000.

[42] H. Uchimura, T. Takenoshita, and M. Fujii, "Development of a “laminated waveguide”," *Microwave Theory and Techniques, IEEE Transactions on*, vol. 46, pp. 2438-2443, 1998.

[43] M. S. Aftanasar, P. R. Young, and I. D. Robertson, "Rectangular waveguide filters using photoimageable thick-film processing," *Proc. 32nd Eur. Microwave Conf.*

[44] W. Ke, D. Deslandes, and Y. Cassivi, "The substrate integrated circuits - a new concept for high-frequency electronics and optoelectronics," presented at Telecommunications in Modern Satellite, Cable and Broadcasting Service, 2003. TELSIKS 2003. 6th International Conference on, 2003.

[45] D. Deslandes and K. Wu, "Single-substrate integration technique of planar circuits and waveguide filters," *Microwave Theory and Techniques, IEEE Transactions on*, vol. 51, pp. 593-596, 2003.

[46] N. Grigoropoulos, B. Sanz-Izquierdo, and P. R. Young, "Substrate integrated folded waveguides (SIFW) and filters."

[47] Z. C. Hao, W. Hong, X. P. Chen, J. X. Chen, and K. Wu, "A single-layer folded substrate integrated waveguide (SIW) filter," *Microwave Conference* Proceedings, 2005. APMC 2005. Asia-Pacific Conference Proceedings, vol. 1, 2005.

[48] J. A. Curits and S. J. Fiedziuszko, “Miniature dual mode microstrip filters,” in IEEE MTT-S, Dig., 1991, pp. 443-446.

[49] Y. Shih-Jih, R. R. Bonetti, and A. E. Williams, "Generalized dual-plane multicoupled line filters," *Microwave Theory and Techniques, IEEE Transactions on*, vol. 41, pp. 2182-2189, 1993.

[50] A. Bailey, W. Foley, M. Hageman, C. Murray, A. Piloto, K. Sparks, K. Zaki, and N. Grumman, "Miniature LTCC filters for digital receivers," *Microwave Symposium Digest, 1997., IEEE MTT-S International*, vol. 2, 1997.

[51] C. Q. Scrantom, J. C. Lawson, S. E. Inc, and C. A. Costa Mesa, "LTCC technology: where we are and where we're going. II," *Technologies for Wireless Applications, 1999. Digest. 1999 IEEE MTT-S Symposium on*, pp. 193-200, 1999.

[52] J. Lee, M. S. Uhm, and J. H. Park, "Synthesis of a self-equalized dual-passband filter," *Microwave and Wireless Components Letters, IEEE [see also IEEE Microwave and Guided Wave Letters]*, vol. 15, pp. 256-258, 2005.

[53] J. Lee, M. S. Uhm, and J. H. Park, "Synthesis of a dual-passband elliptic filter with equalized group delay," *Wireless Communications and Applied Computational Electromagnetics, 2005. IEEE/ACES International Conference on*, pp. 783-786, 2005.

[54] P. Lenoir, S. Bila, F. Seyfert, D. Baillargeat, and S. Verdeyme, "Synthesis and design of asymmetrical dual-band bandpass filters based on equivalent network simplification," *IEEE Trans. Microw. Theory Tech*, vol. 54, pp. 3090–3097, 2006.

[55] M. L. Chuang, "Concurrent dual band filter using single set of microstrip open-loop resonators," *Electronics Letters*, vol. 41, pp. 1013-1014, 2005.

[56] J. T. Kuo and H. S. Cheng, "Design of quasi-elliptic function filters with a dual-passband response," *Microwave and Wireless Components Letters, IEEE [see also IEEE Microwave and Guided Wave Letters]*, vol. 14, pp. 472-474, 2004.

[57] J. T. Kuo, T. H. Yeh, and C. C. Yeh, "Design of microstrip bandpass filters with a dual-passband response," *Microwave Theory and Techniques, IEEE Transactions on*, vol. 53, pp. 1331-1337, 2005.

[58] R. J. Cameron, M. Yu, Y. Wang, C. Ltd, and U. K. Aylesbury, "Direct-coupled microwave filters with single and dual stopbands," *Microwave Theory and Techniques, IEEE Transactions on*, vol. 53, pp. 3288-3297, 2005.

[59] J. Wang, Y. X. Guo, B. Z. Wang, L. C. Ong, and S. Xiao, "High-selectivity dual-band stepped-impedance bandpass filter," *Electronics Letters*, vol. 42, pp. 538-540, 2006.

[60] H. Miyake, S. Kitazawa, T. Ishizaki, T. Yamada, and Y. Nagatomi, "A miniaturized monolithic dual band filter using ceramic laminationtechnique for dual mode portable telephones," *Microwave Symposium Digest, 1997., IEEE MTT-S International*, vol. 2, 1997.

[61] J. W. Fan, C. H. Liang, and X. W. Dai, "Design of cross-coupled dual-band filter with equal-length split-ring resonators," *Progress In Electromagnetics Research*, pp. 285–293.

[62] K. V. PUGLIA, "A general design procedure for bandpass filters derivedfrom low pass prototype elements," *MICROWAVE JOURNAL*, 2000.

[63] EM, Inc., "Sonnet Software," 11.54 ed, 2007.

[64] S. Amari, U. Rosenberg, and J. Bornemann, "Adaptive synthesis and design of resonator filters with source/load-multiresonator coupling," *Microwave Theory and Techniques, IEEE Transactions on*, vol. 50, pp. 1969-1978, 2002.

[65] R.K. Mongia, I.J. Bahl, P. Bhartia, and J. Hong, *Advanced coupled-line filters in RF and Microwave Coupled-Line Circuits*, 2nd ed: Norwood: Artech House, 2007.

[66] T. Wen-Hua and C. Kai, "Miniaturized dual-mode bandpass filter with harmonic control," *Microwave and Wireless Components Letters, IEEE*, vol. 15, pp. 838-840, 2005.

[67] D. Deslandes and K. Wu, "Design Consideration and Performance Analysis of Substrate Integrated Waveguide Components," *European Microwave Conference, 2002. 32nd*, pp. 1-4, 2002.

[68] Nikolaos Grigoropoulos, Benito Sanz-Izquierdo, and Paul R. Young, "Substrate Integrated Folded Waveguides (SIFW) and Filters," *IEEE MICROWAVE AND WIRELESS COMPONENTS LETTERS*, vol. 15, pp. 829-831, 2005.

[69] T. T. Hiroshi Uchimura, Mikio Fujii,, "Development of a “Laminated Waveguide”," *IEEE TRANSACTIONS ON MICROWAVE THEORY AND TECHNIQUES*, vol. 46, pp. 2438-2443, 1998.

[70] M. S. Aftanasar, P. R. Young, I. D. Robertson, J. Minalgiene, and S.Lucyszyn, "Photoimageable thick-film millimeter-wave metal-pipe rectangular waveguides,," *Electron. Lett.*, vol. 37, pp. 1122–1123,, 2001.

[71] M. F. Davis, S. W. Yoon, S. Pinel, K. Lim, and J. Laskar, "Liquid crystal polymer-based integrated passive development for RF applications," presented at Microwave Symposium Digest, 2003 IEEE MTT-S International, 2003.

[72] D. C. Thompson, O. Tantot, H. Jallageas, G. E. Ponchak, M. M. Tentzeris, and J. Papapolymerou, "Characterization of liquid crystal polymer (LCP) material and transmission lines on LCP substrates from 30 to 110 GHz," *Microwave Theory and Techniques, IEEE Transactions on*, vol. 52, pp. 1343-1352, 2004.

[73] V. Palazzari, S. Pinel, J. Laskar, L. Roselli, and M. M. Tentzeris, "Design of an Asymmetrical Dual-Band WLAN Filter in Liquid Crystal Polymer(LCP) System-On-Package Technology," *IEEE Microwave and Wireless Components Letters*, vol. 15, pp. 165-167, 2005.

[74] N. Marcuvitz, *waveguide handbook*, Peter Pergrinus, London, 1986, Chapter 5